Nevada System of Higher Education

TECHNICAL REPORT

Exceptional Ground Accelerations and Velocities Caused by Earthquakes

Report Document Identifier:
TR-NQ-022-2

Cooperative Agreement # DE-FC28-04RW12232
Project Activity ORD-FY06-022
Final Technical Report Part B (for subtask 2)

REVISION: 0

Author: John G. Anderson

PI: John G. Anderson and James N. Brune

Date Completed: January 17, 2008

Final Technical Report on a Project Sponsored by the US Department of Energy Yucca Mountain Project

Funding provided through Cooperative Agreement with the Nevada System of Higher Education

Project Number ORD-FY06-022.

Nevada Seismological Laboratory and Department of Geological Sciences and Engineering,
Mackay School of Earth Sciences and Engineering,
College of Science,
University of Nevada, Reno, Nevada 89557.
Anderson: 775-784-4265; jga@seismo.unr.edu

1.0 Table of Contents

1.0 Table of Contents iii
1.1 Summary 1
1.2 Acronyms 1
1.3 Acknowledgement 1
1.4 List of Tables 1
1.5 List of Figures 2
2.0 Purpose 6
3.0 Quality Assurance 6
4.0 Assumptions 6
5.0 Software 6
6.0 Attachments 7
7.0 Data Sources and Procedure 7
8.0 Statistics 8
8.1 Statistics of the Chosen Intensity Measure 8
8.2 Time Dependence 9
8.3 Magnitude Dependence 9
8.4 Rank 10
8.5 Normalized Exceedance Rates 12
8.6 Distribution of Peak Values with Magnitude 12
8.7 Dependence on the Mechanism of Faulting 13
8.8 Dependence on Site Conditions 15
8.9 Dependence on Fault-Station Geometry 16
9.0 Causes of Exceptional Motions 17
10.0 How Much Worse? 17
11.0 Conclusions 18
12.0 References 19
13.0 Tables 20
14.0 Figures 30
Appendix A. Earthquake Maps 63
Figure A1. Imperial Valley, May 19, 1940, 04:36:41, M_W 6.90 63
Figure A2. Parkfield, June 28, 1966, 04:26:14, M_W 6.10 64
Figure A3. San Fernando, February 9, 1971, 14:00:41, M_W 6.60 65
Figure A4. Gazli, May 17, 1976, 02:58:40, M 6.80 66
Figure A5. Tabas, Iran, September 16, 1978, 15:35:56, M_W 7.30 67
Figure A6. Imperial Valley, October 15, 1979, 23:16:53, M_W 6.50 68
Figure A7. Victoria, June 9, 1980, 03:28:19, M_W 6.40 69
Figure A8. Westmorland, April 26, 1981, 12:09:28, $M_L$brk 6.30 70
Figure A9. Coalinga, May 2, 1983, 23:42:38, M_W 6.50 70
Figure A10. Coalinga, July 22, 1983, 02:39:54, M_W 6.00 72
Figure A11. Morgan Hill, April 24, 1984, 21:15:18, M_W 6.10 73
Figure A12. Valapraiso, March 3, 1985, 22:47:07, M_W 7.80 74

Figure A13. Michoacan Aftershock, September 21, 1985, 01:37:13, M_W 7.50 75
Figure A14. Nahanni, December 23, 1985, 05:16:00, M_s 6.90 76
Figure A15. North Palm Springs, July 8, 1986, 09:20:44, M_W 6.20 77
Figure A16. Whittier Narrows, October 1, 1987, 14:42:20, M_W 6.10 78
Figure A17. Superstition Hills, November 24, 1987, 13:15:56, $M_L$brk 6.70 79
Figure A18. Loma Prieta, October 18, 1989, 00:04:15, M_W 7.00 80
Figure A19. Manjil, Iran, June 20, 1990, 09:00:10, M_W 7.40 81
Figure A20. Erzican, March 13, 1992, 17:18:40, $M_S$brk 6.90 82
Figure A21. Cape Mendocino, April 25, 1992, 18:06:04, M_W 7.00 83
Figure A22. Landers, June 28, 1992, 11:57:34, M_W 7.30 84
Figure A23. Northridge, January 17, 1994, 12:30:55, M_W 6.70 85
Figure A24. Zanjiran, June 20, 1994, 09:09:02, M_W 5.90 86
Figure A25. Kobe, January 16, 1995, 20:46:52, M_W 6.90 87
Figure A26. East Coast Honshu , May 23, 1996, 09:36:31, M_W 5.00 88
Figure A27. Central Honshu, August 13, 1996, 02:13:00, Mjma 5.00 89
Figure A28. Honshu, December 21, 1996, 01:28:51, mb-GS 5.70 90
Figure A29. South Coast Honshu, March 3, 1997, 14:09:43, M_W 5.00 91
Figure A30. South Coast Honshu, March 16, 1997, 05:51:37, M_W 5.80 92
Figure A31. Kyushu, March 26, 1997, 08:31:47, M_W 6.30 93
Figure A32. Kyushu, May 13, 1997, 05:38:30, M_W 6.20 94
Figure A33. Umbria Marche, Italy foreshock, September 26, 1997, 00:33:16, Mw 5.72 and 09:40:33, Mw 6.04 95
Figure A34. Chamoli, March 28, 1999, 19:05:11, M_W 6.60 96
Figure A35. Karehbas, May 6, 1999, 23:00:53, M_W 5.90 97
Figure A36. Kocaeli, Turkey, August 17, 1999, 00:01:40, M_w-hrv 7.60 98
Figure A37. Southern Honshu, August 20, 1999, 20:33:00, Mjma 5.40 99
Figure A38. Chi-Chi, September 20, 1999, 17:47:16, M_W 7.60 100
Figure A39. Duzce, November 12, 1999, 16:57:27, M_W 7.10 101
Figure A40. South Iceland, June 17, 2000, 15:40:41, M_W 6.57 and 00:51:48, M_W 6.49 102
Figure A41. Japan , July 14, 2000, 16:18:00, Mjma 3.90 103
Figure A42. Yountville, September 3, 2000, 08:36:30, M_W 5.00 104
Figure A43. Western Tottori, October 6, 2000, 04:30:19, M_W 7.10 105
Figure A44. Honshu, October 30, 2000, 16:42:52, Mjma 5.50 106
Figure A45. El Salvador, January 13, 2001, 17:33:32, M_W 7.60 107
Figure A46. Nisqually, February 28, 2001, 18:54:31, M_W 6.80 108
Figure A47. Southern Honshu, March 24, 2001, 06:27:54, M_W 6.40 109
Figure A48. Japan, June 14, 2002, 02:42:00, Mjma 4.90 110
Figure A49. Avaj, Iran, June 22, 2002, 02:58:20, M_W 6.50 111
Figure A50. Denali, Alaska, November 3, 2002, 22:13:00, M_s 7.90 112
Figure A51. Miyagi-Oki, May 26, 2003, 09:24:33, M_W 7.00 113
Figure A52. Tokachi-Oki, September 25, 2003, 19:50:07, M_W 8.00 114
Figure A53. Bam, December 26, 2003, 01:56:56, M_W 6.70 115
Figure A54. Honshu, July 9, 2004, 10:54:00, Mjma 4.40 116

Figure A55. Parkfield, September 28, 2004, 17:15:24, M_W 6.00 117
Figure A56. Niigata-Ken Chuetsu, October 23, 2004, 08:56:00, M_W 6.60 118
Figure A57. Niigata-Ken Chuetsu, October 23, 2004, 09:34:07 M_W 6.30 119
Figure A58. Hokkaido, November 28, 2004, 18:32:00, Mjma 7.10..... 120
Figure A59. Hokkaido, December 14, 2004, 05:56:09, M_W 5.80..... 121
Figure A60. Honshu, August 16, 2005, 02:46:00, Mjma 7.20 122
Figure A61. Anza, June 12, 2005, 15:41:46, M_W 5.20 123
Figure A62. Southern Honshu, March 25, 2007, 00:42:00, Mjma 6.90 124
Figure A63. Southern Honshu, April 15, 2007, 03:19:00, Mjma 5.40 125
Figure A64. Off Southern Shikoku, April 26, 2007, 00:03:00, Mjma 5.30..... 126

1.1 Summary

This project aims to understand the characteristics of the free-field strong-motion records that have yielded the 100 largest peak accelerations and the 100 largest peak velocities recorded to date. The peak is defined as the maximum magnitude of the acceleration or velocity vector during the strong shaking. This compilation includes 35 records with peak acceleration greater than gravity, and 41 records with peak velocities greater than 100 cm/s. The results represent an estimated 150,000 instrument-years of strong-motion recordings. The mean horizontal acceleration or velocity, as used for the NGA ground motion models, is typically 0.76 times the magnitude of this vector peak. Accelerations in the top 100 come from earthquakes as small as magnitude 5, while velocities in the top 100 all come from earthquakes with magnitude 6 or larger. Records are dominated by crustal earthquakes with thrust, oblique-thrust, or strike-slip mechanisms. Normal faulting mechanisms in crustal earthquakes constitute under 5% of the records in the databases searched, and an even smaller percentage of the exceptional records. All NEHRP site categories have contributed exceptional records, in proportions similar to the extent that they are represented in the larger database.

1.2 Acronyms

GMPE	Ground Motion Prediction Equation
NEHRP	National Earthquake Hazard Reduction Program
NGA	New Generation Attenuation
NSHE	Nevada System of Higher Education
PEER	Pacific Earthquake Engineering Research
PGA	Peak Ground Acceleration
PGV	Peak Ground Velocity
PSHA	Probablistic Seismic Hazard Analysis

1.3 Acknowledgement

Justin Flint, Nicholas Hockensmith and Selena Willoughby provided significant assistance in identifying, downloading, and documenting the data. Yuichiro Miyata provided major assistance in map preparation. Rasool Anooshehpoor served as a technical reviewer of the document. This project was supported by the US Department of Energy Yucca Mountain Project, via a Cooperative Agreement with the Nevada System of Higher Education, Project Number ORD-FY06-022.

1.4 List of Tables

Table 1: List of earthquakes and stations included in this study
Table 2: Selected points on the cumulative distribution curves in Figures 2, 3, and 4
Table 3: Top 100 accelerations and velocities
Table 4: Estimate of level of instrumentation effort for selected accelerograph networks

1.5 List of Figures

Figure 1: Locations of earthquakes represented in our data set of exceptional accelerograms. The earthquakes are listed in Table 1.

Figure 2: Distribution of ratios among various peak acceleration intensity measures. The denominator ("Peak Vector") in all cases is the peak magnitude of the 3-component acceleration vector. "Peak Horizontal" is the peak magnitude of the 2-component horizontal acceleration vector. "Peak Component" is the peak acceleration on the largest of the three individual components as recorded. "Mean Horizontal" is the geometrical mean of the peak accelerations of the two horizontal components as recorded. "Peak Vertical" is the peak acceleration on the vertical component. All 255 accelerograms in Table 1 are used to develop this distribution. For records where one of the horizontal components is missing, the peak on that component is treated as equal to zero.

Figure 3: Distribution of ratios among various peak velocity intensity measures. See the caption for an explanation of the variables, which are applied to the velocity rather than acceleration in this figure.

Figure 4: Distribution of angles between the peak 3-component vectors and horizontal. For each 3-component accelerogram, the angle between the acceleration vector and the horizontal is measured at the time when the magnitude of the 3-component acceleration is maximum. The algorithm for velocity is the same. All 255 accelerograms in Table 1 are used to develop this distribution.

Figure 5: Distribution of the ratio of the peak value of the second (generally more northerly) observed horizontal component to the first (generally more easterly) component. The upper figure is for peak acceleration, and the lower is for peak velocity. The pale black line is the best-fitting lognormal distribution for these ratios; the mean (μ) and standard deviation (σ) of the distribution are given in the figure.

Figure 6: Distribution of peak acceleration and peak velocity for the accelerograms listed in Table 1. PGA and PGV are the vector peak values. The "predicted" line is the relationship: $\ln(PGV) = 4.22 + 0.776\ln(PGA)$, where the units of *PGA* are fraction of the acceleration of gravity, and the units of *PGV* are cm/s. This relationship was developed for the PEGASOS project (Abrahamson et al, 2002). The points in this figure represent only the upper-right tip of other compilations of strong-motion data.

Figure 7: Exceptional ground motions over time. Peak acceleration and peak velocity of the records in Table 1, shown as a function of the time that they were recorded.

Figure 8: Exceptional ground motions vs moment magnitude. Peak acceleration and peak velocity for all events in Table 1, shown as a function of the magnitude of the earthquake.

Figure 8. Exceptional ground motions vs moment magnitude. Peak acceleration and peak velocity for all events in Table 1, shown as a function of the magnitude of the earthquake.

Figure 9: Ranking of exceptional records as a function of peak accelerations. The observations are shown as points. The axes are chosen such that data consistent with a power law distribution (Equation 1) of exceptional values would fall on a straight line. The green line, with parameters given in the figure, is the best fit, using an L2 norm, to the data with ranks of 6 to 100.
Figure 10: Ranking of exceptional records as a function of peak velocities. The observations are shown as points. The axes are chosen such that data consistent with a power law distribution (Equation 1) of exceptional values would fall on a straight line. The green line, with parameters given in the figure, is the best fit, using an L2 norm, to the data with ranks of 20 to 100.
Figure 11: Ranking of exceptional records as a function of peak accelerations. The observations are shown as points. The axes are chosen such that data consistent with an exponential distribution (Equation 2) of values would fall on a straight line. The green line, with parameters given in the figure, is the best fit, using an L2 norm, to the data with ranks of 10 to 80.
Figure 12: Ranking of exceptional records as a function of peak velocities. The observations are shown as points. The axes are chosen such that data consistent with an exponential distribution (Equation 2) of exceptional values would fall on a straight line. The green line, with parameters given in the figure, is the best fit, using an L2 norm, to the data with ranks of 5 to 80.
Figure 13: Ranking of exceptional records as a function of peak accelerations. The observations are shown as points. The axes are chosen such that data consistent with an extreme value distribution (Equation 3) of exceptional values would fall on a straight line. The green line, with parameters given in the figure, is the best fitting exponential distribution, using an L2 norm, to the data with ranks of 10 to 100.
Figure 14: Ranking of exceptional records as a function of peak velocities. The observations are shown as points. The axes are chosen such that data consistent with an extreme value distribution (Equation 3) of exceptional values would fall on a straight line. The green line, with parameters given in the figure, is the best fitting exponential distribution, using an L2 norm, to the data with ranks of 10 to 100.
Figure 15: Estimated exceedance rate of peak acceleration per instrument year. The points are obtained by dividing the rank in Figure 9 by the estimate that these data represent about 150,000 instrument-years of data collection effort.
Figure 16: Estimated exceedance rate of peak velocity per instrument year. The points are obtained by dividing the rank in Figure 9 by the estimate that these data represent about 150,000 instrument-years of data collection effort.
Figure 17: Magnitudes of the earthquakes for all of the records included in Table 1. Earthquakes that generated more than one exceptional ground motion record are counted once for each record.
Figure 18: Magnitude distribution of earthquakes causing the top 100 acceleration records, compared with the distribution of magnitudes in the NGA database.

Earthquakes that generated more than one of the top 100 ground motion records are counted once for each record.
Figure 19: Magnitude distribution of earthquakes causing the top 100 velocity records, compared with the distribution of magnitudes in the NGA database. Earthquakes that generated more than one of the top 100 ground motion records are counted once for each record.
Figure 20: Magnitudes of earthquakes causing the top 100 accelerations, displayed by quartile. Earthquakes that generated more than one of the top 100 ground motion records are counted once for each record.
Figure 21: Magnitudes of earthquakes causing the top 100 velocities, displayed by quartile. Earthquakes that generated more than one of the top 100 ground motion records are counted once for each record.
Figure 22: Distribution of focal mechanisms for the earthquake generating each record in Table 1. The mechanism code is as follows: 0) strike-slip faulting in continental crust; 1) normal faulting in continental crust; 2) thrust faulting in continental crust; 3) oblique thrust faulting in continental crust; 4) oblique normal faulting in continental crust; 6) normal faulting associated with the downgoing slab in a subduction zone; 7) thrust faulting in an oceanic subduction zone; and 8) oblique thrust faulting in an oceanic subduction zone. A code of -1 indicates that the mechanism for that record was not available.
Figure 23: Distribution of focal mechanisms of earthquakes causing the top 100 acceleration records, compared with the distribution of focal mechanism in the NGA database. The NGA database does not include subduction zone earthquakes. Therefore, the bars giving the percentage of "Top Crustal Accelerations" is generated for comparison with NGA by renormalizing those top 100 records with mechanisms 0, 1, 2, 3, or 4 to a total of 100%. Mechanism codes are given in the caption to Figure 22. For earthquakes causing more than one record in Table 1, the earthquake is counted once for each record.
Figure 24: Distribution of focal mechanism for the top 100 velocities, compared with the distribution of focal mechanism in the NGA database. See Figure 23 for a detailed explanation.
Figure 25: Focal mechanisms of earthquakes causing the top 100 accelerations, displayed by quartile. See Figure 22 for mechanism codes. For earthquakes causing more than one record in Table 1, the earthquake is counted once for each record.
Figure 26: Focal mechanisms of earthquakes causing the top 100 velocities, displayed by quartile.
Figure 27: Distribution of site categories for all records in Table 1. Site category 1=not available, 2=NEHRP E, 3=NEHRP D, 4=NEHRP C, 5-NEHRP B, 6-NEHRP A. Earthquakes causing more than one record are displayed once for each record.
Figure 28: Distribution of site categories for the top 100 accelerations, compared with the distribution of site categories in the NGA database. See the caption to Figure 27 for a definition of Site Category.

Figure 29: Distribution of site categories for the top 100 velocity records, compared with the distribution of site categories in the NGA database. See the caption to Figure 27 for a definition of Site Category.
Figure 30: Peak acceleration and peak velocity for all records in Table 1, as a function of estimated V_S30. Records for which the value of V_S30 is not available are plotted at $V_S30=0$.
Figure 31: Distribution of average horizontal kappa for all records in Table 1. For each component, κ was calculated as described in the text, and then the average of the horizontal components used to create this histogram. Units of κ are seconds.
Figure 32: Distribution of average horizontal kappa for the top 100 Distribution of average horizontal kappa for the top 100 acceleration records, by quartile. Units of κ are seconds.
Figure 33: Distribution of average horizontal kappa for the top 100 velocity records, by quartile. Units of κ are seconds.

2.0 Purpose

This paper reviews the global set of ground motion recordings from earthquakes, with the object of identifying those records with the largest recorded peak accelerations and peak velocities. The intent is to identify the 100 strongest records in each category. The topic is of general interest for estimating upper bounds on motions that might need to be resisted by the most critical facilities. The study is also motivated by results of a probabilistic seismic hazard analysis for the designated Yucca Mountain High Level Nuclear Repository in southern Nevada, for which the extrapolations to occurrence rates of 10^{-7} per year result in peak accelerations of 5.8 g, and peak velocities of 650 cm/s (DTN: MO0401MWDRPSHA.000; Bechtel SAIC, 2004). These high ground motions have been challenged and criticized as not physically reasonable.

3.0 Quality Assurance

This report is entirely unqualified.

4.0 Assumptions

This report uses unqualified data that has been recovered from hundreds of earthquakes by dozens of different agencies. We assume first that these data are valid records of the ground motion. This requires that the agency that gathered the data carefully digitized and properly calibrated each record, even though it is not possible to qualify the data. For many records that were obtained on analog instruments, we assume that the time base when the records were digitized is the same for all three components.

The site conditions for stations in Japan are documented in tables that give the shear velocity as a function of depth from the surface to 20 m depth. In the US, many models need the average shear velocity to 30 m depth. Thus to use the Japanese information we assume that the shear velocity at 20 m depth is the same as the velocity from 20m to 30 m depth.

5.0 Software

MATLAB v 7.0.1.24704 (R14) Service Pack 1, September 13, 2004, License Number 244191 run under MS Windows environment.

Microsoft Office Excel 2003 (11-8146-8311) SP2 run on MS Windows environment.

Internet Explorer run on MS Windows environment.

Microsoft Office Word 2003 SP2 run on MS Windows environment.

6.0 Attachments

There are no attachments to this report. The scientific notebook that controlled this project is Notebook Number NSHE-UNR-109 Vol. 1, assigned to Task ORD-FY06-022. There is an electronic attachment to the notebook that is being submitted for general use.

7.0 Data Sources and Procedure

Relevant data is recorded on strong-motion accelerographs, which are instruments that are triggered by initial ground motions of a strong earthquake. The first significant strong-motion accelerogram was recorded in March, 1933, during the Long Beach, California earthquake. Since then the global data set has grown to over 30,000 records. Much of the global set of strong-motion data is now accessible over the internet (http://www.cosmos-eq.org/, http://www.k-net.bosai.go.jp/, http://www.kik.bosai.go.jp/, http://www.bhrc.ac.ir/Bhrc/d-stgrmo/D-StGrMo.htm), and the majority of the records used in this study were mined from those sources. Our study uses data from older analog instruments that has been digitized, and from newer equipment where the acceleration is digitized by the instrument and recorded in digital format.

Our search started with a list of strong records compiled by PEER NGA project (Power et al, 2006). This established that the 100 largest accelerations would all be greater than 500 cm/s^2, and that the 100 largest velocities would all be greater than 50 cm/s. Our search of several available databases thus aimed to obtain every accelerogram for which at least one component matches either of those two conditions. This report refers to accelerograms for which at least one component of acceleration exceeds 500 cm/s^2, or for which at least one component of the corresponding velocity exceeds 50 cm/s as an *exceptional* record. Since data is collected as acceleration, and is not necessarily integrated to velocity, our results likely have missed some exceptional velocity records, even though in many cases we endeavored to understand the fault-station geometry and download records that we considered possible to have velocities exceeding 50 cm/s, even though the peak acceleration did not meet our threshold.

In general, the zero-level of an accelerogram must be inferred from the average properties of the time series. Because of noise, in general this "baseline correction" needs to apply a high-pass filter. For much of the data, the agency that operates the instrument has applied an instrument correction and filter. For records that are only available in the uncorrected form, we applied a high-pass 2-pole causal Butterworth filter, with a default corner frequency of 0.1 Hz. Agency corrections may use a larger corner frequency or a filter with more poles, depending on the signal-to-noise level at low frequencies, and in some cases we also used larger corner frequencies for the filters. Peak values will generally depend on how the records are filtered, with peak velocity being more sensitive than peak acceleration. Thus the peaks described here may not agree exactly with other published values for the same records.

Table 1 lists all of the records we obtained. Figure 1 shows locations of the earthquakes that are represented by this data set. There are 255 records identified in Table 1. These time series have been submitted to the Yucca Mountain Record Center (MOL.20071127.0003).

This study defines peak ground acceleration (PGA) and peak ground velocity (PGV) as the maximum magnitude of the three-dimensional acceleration and velocity vectors, after calculating those magnitudes for each point in time in the record. Thus in general the direction of the peak vector is not horizontal.

8.0 Statistics

8.1 Statistics of the Chosen Intensity Measure

Figure 2 begins an exploration of the relationship of the chosen intensity measures and other measures that have been used. Specifically, we consider the relationship of the peak vector to the peak vector in the horizontal plane, the largest of the three components in the recorded orientations, the geometrical mean of the two horizontal components, and the peak on the vertical component. Figure 2 shows the distributions of the ratios of these four intensity measures of acceleration to the peak vector acceleration. Figure 3 shows the equivalent information for peak velocity. Figure 4 shows the distribution of angles between the three-dimensional vector and horizontal. Table 2 lists selected points on these distributions.

Figures 2 - 4 show that in this data set, the peak velocity is more concentrated in the horizontal direction than the peak acceleration vector. This feature also shows up in the distribution of peak vertical amplitudes, where the median for acceleration is about half (0.47) of the three-dimensional peak, while it is about a third (0.30) for velocity. These data also show that for both acceleration and velocity, the peak vector is within 20 degrees of horizontal in the vast majority of cases. The NGA relations use the geometrical mean of the two horizontal components as the intensity measure of an accelerogram. Figures 2 and 3 show that in the selected data, the median value of this parameter is about ¾ (0.76) of the three-dimensional peak for both acceleration and velocity.

Figure 5 shows one other statistic in these data, namely the ratio of the peak value on the second horizontal component to the peak value on the first horizontal. In this data, we aimed to use the convention to report the more east-west of the horizontal components as the first horizontal, and the more north-south component as the second horizontal. But the horizontal axes are in general oriented randomly relative to coordinate axes fixed to the fault, so our naming convention should have no effect on the statistics of this ratio. Because these two peaks can thus be considered as random numbers drawn from the same distribution, the ratios have a median value that is insignificantly different from 1.0, and can be approximated with a lognormal distribution. The standard deviation of this distribution is larger for peak velocity (0.50 in natural log (base *e* units)) than for peak

acceleration (0.39 in natural log units). We believe that the smaller differences in peak acceleration are because this measure is dominated by higher-frequency waves, which are more scattered and randomized than peak velocity.

Figure 6 shows how the values of peak velocity and peak acceleration of each record are distributed. The effects of the search parameters are the dominant features of this plot, as there are practically no records in the data for which both peak acceleration is under 500 cm/s^2 and peak velocity is under 50 cm/s. The points that do fall in this zone represent records that were obtained close to the source, and thus even though we knew the peak acceleration did not meet the search parameters we considered it possible that peak velocity would qualify.

8.2 Time Dependence

Figure 7 shows the values of peak accelerations and peak velocities plotted as a function of the time the earthquake occurred. The first digital strong-motion accelerograms in our data were obtained in 1980, and the percentage of data that is digitally recorded has been increasing since that time. The majority of the records were recorded digitally.

There is not a convincing trend for either the peak acceleration or peak velocity to be increasing over time. While we can certainly expect some additional high readings, these plots suggest that the increasing numbers of instruments that have been recording for the past decade have not had the effect of observing significantly higher values acceleration or velocity than what had been observed over the twenty prior years.

8.3 Magnitude Dependence

Figure 8 shows the magnitude dependence of PGA and PGV. Table 1 and Figure 8 use the moment magnitude for most earthquakes. The differences between moment magnitude and the other magnitude scales, used for a few of the earthquakes, are not large enough to affect the overall trends displayed in Figure 8. The PGA shows little correlation with magnitude – an upper bound for this scatter plot could be a constant. The highest values of the PGV do show a magnitude dependence. These results are predicted from basic physics and earthquake source theory (e.g. Aki and Richards, 1980). In particular, assuming linear wave propagation through the earth, the representation theorem relates peak acceleration at the surface to peak acceleration at the source, and similarly for peak velocity. Simplified source models in Aki and Richards show singularities in the slip velocity at the source, implying that infinite accelerations are possible for a theoretical crack model for failure of a brittle solid, and thus the representation theorem allows infinite accelerations at the station. This reasoning is not limited to large earthquakes. On the other hand, peak velocity at the source is proportional to the stress drop at the source (e.g. Brune, 1970), which is necessarily limited by the strength of the rock. The representation theorem shows that contributions from different parts of the fault can contribute constructively at the station, so the size of the fault may also control the peak velocity. The earthquake magnitude is closely

correlated with the size of the fault rupture (Wells and Coppersmith, 1994). Thus a relationship between peak velocity and magnitude is expected.

The magnitude dependence is explored in more detail later in this report.

8.4 Rank

Table 3 lists the 100 largest accelerations and the 100 largest velocities in the database. Figures 9-14 plot the ranks of the entire set of 255 records as a function of their peak acceleration and peak velocity, on differing axes to compare the distributions of these values with different mathematical shapes. The rank, *R*, is defined as *R*=1 for the largest record, *R*=2 for the second largest, and so forth. Thus for each accelerogram, *R* gives the number of records with PGA or PGV greater than or equal to those statistics.

The largest acceleration in this database is 2381 cm/s^2, recorded on the hanging wall of the thrust fault during the Nahanni earthquake in northern Canada on December 23, 1985 (MS=6.9). These data include 35 records of acceleration greater than gravity. We are aware of one record with a peak acceleration that was probably greater than 2.5 g (FZ16, Parkfield 2004, Shakal et al, 2006), but it is not available at this time. Both the Nahanni and FZ16 records were recorded on analog accelerographs, and the traces go off the edge of the film during an isolated high-frequency spike, so the peak values are uncertain.

The largest velocity is 318 cm/s, recorded on the hanging wall of the thrust fault during the Chi-Chi, Taiwan earthquake on September 20, 1999 (MW=7.6). These data include 41 records with peak velocity exceeding 100 cm/s.

Figures 9 and 10 test whether these values can be fit by a power law distribution with the form:

$$R = \alpha\ A^{-\beta} \tag{1}$$

where *A* represents either PGA or PGV, and α and β are parameters to be determined. Data following this relationship should appear as a linear trend on log-log axes:

$$\log R = \log \alpha - \beta \log A \tag{1A}$$

as in Figures 9 and 10. These figures show fits of a power law to the central portion of the distributions. When these fit lines are extrapolated to higher ranks (ranks closer to one), they predict greater peak accelerations and greater peak velocities than have been observed. Thus the distribution of peak acceleration and peak velocity appears to have a tail that decays more rapidly than a power law.

Figures 11 and 12 test whether these values can be fit by an exponential distribution with the form:

$$R = \alpha e^{-\beta A} \tag{2}$$

In Equation 2, α and β are again parameters to be determined from the data. These figures show fits of an exponential function to the central portion of the distributions. When these fit lines are extrapolated to higher ranks (ranks closer to one), they predict

smaller peak accelerations and smaller peak velocities than have been observed. Thus the distribution of peak acceleration and peak velocity appears to have a tail that does not decay as rapidly as an exponential distribution.

Gumbel (1958) proposed that a double exponential distribution is appropriate to fit the distribution of extreme samples. The experiment that he modeled is somewhat different from the experiment represented by the sample of accelerograms gathered here. The classical Gumbel experiment, applied to strong motion, would take the largest acceleration recorded each year at some individual station. Nevertheless, Figures 13 and 14 test whether these values can be fit by a double exponential (Gumbel) distribution of the form:

$$R = \exp\left[-e^{\alpha+\beta A}\right]. \quad (3)$$

In Equation 3, α and β are again parameters to be determined from the data. These figures show fits of a Gumbel distribution to the central portion of the empirical distributions. When these fit lines are extrapolated to higher ranks (ranks closer to one), they predict smaller peak accelerations and smaller peak velocities than have been observed. Thus the distribution of peak acceleration and peak velocity appears to have a tail that does not decay as rapidly as a Gumbel distribution function.

As the peak acceleration decreases (for higher-ranked records), all three types of distributions diverge from the data at some point. For peak acceleration the divergence from the power law occurs at about 750 cm/s^2. It occurs at about 550 cm/s^2 for the other two distributions. We know that the empirical distribution is incomplete at small amplitudes, and the nature of divergence is consistent with the direction expected from incomplete data. The empirical distribution of peak velocities diverges from all three of the models at about 60 cm/s. Considering that our search criteria are based on the peak amplitude of the largest component, and considering that the ratio of the largest component to the three-dimensional vector amplitude is distributed to values less than one (Figures 2 and 3), it is expected that our database is not complete for some range of PGA above 500 cm/s^2 and for some range of PGV above 50 cm/s. Thus the amplitudes where *R* begins to diverge from any of these distributions are reasonable. As is done in looking at earthquake catalogs, where divergence from the power law is considered to occur at the threshold of completeness, we suggest that Figures 9 and 10 imply that our collection of data is uniformly complete for peak accelerations above 750 cm/s^2 and peak velocity above 60 cm/s.

In the context of probabilistic seismic hazard analysis (PSHA), a general concern is often that the tails of the distribution of accelerations or velocities at a single station, given by a ground motion prediction equation (GMPE) are overestimated and responsible for driving the analyses to extreme motions at very low probabilities. It can be shown that at extremely low probabilities, the exceedance rate of an intensity measure at a single station will have the same dependence as the distribution in a GMPE. If combining multiple stations as is done here were valid, and if the lognormal distribution used in

most GMPE is valid, then we would predict that the empirical distribution would have an exponential tail, as in Figures 11 and 12. The data might be consistent with an exponential distribution provided there is a different set of physics that comes to dominate the peak values above the break in the slope.

8.5 Normalized Exceedance Rates

An interesting question is what is the level of effort that has been involved in collecting the accelerograms listed in Table 1. The measure of effort that we propose is instrument-years. For example, the Guerrero accelerograph network, consisting of 30 instruments that have operated continuously from 1985 through 2006 (and continuing), or for about 21 years, would represent 630 instrument-years of effort. Table 4 considers seven selected networks, from which the data produced were thoroughly searched and that are extensively represented in Table 1, and finds that among these networks there are about 100,000 instrument-years of effort represented. Considering that roughly a quarter of the records in Table 1 are from other networks, one might scale the 100,000 instrument-years effort by 4/3 to account for the instrument effort of the remaining accelerograms. However, considering that there may be some bias caused by preferential reporting of records with high peak values, we guess that scaling by 4/3 is not enough, so we use the estimate that Table 1 represents roughly 150,000 instrument-years of effort.

Starting with this number, we generate Figures 15 and 16 showing the appproximate exceedance rate of these exceptional accelerations and velocities per instrument year. These figures represent a spatial average of the seismic activity, in which most of the points represent relatively active regions. If one wanted to estimate the exceedance rate for a randomly chosen location that is in a region with 1/100 times as much activity as the "average" site in the accelerograph networks represented, we hypothesize that an initial empirical approach might be to multiply these curves by 1/100. There are numerous reasons to object to this simple approximation, of course, but we see no reason why these objections would cause an order-of-magnitude error.

8.6 Distribution of Peak Values with Magnitude

It is, of course, possible to classify the records in Table 1 according to some of the physical characteristics that are believed to have important effects on strong ground motions. We explore three such classifications: magnitude, focal mechanism, and site conditions.

Figures 17-21 expand the consideration of the magnitude distribution of contributing earthquakes. Figure 17 shows a histogram with the number of earthquake records in half-magnitude bins included in Table 1. The modal bin is for magnitude M=6.5. We note that the Gutenberg-Richter distribution predicts numbers of earthquakes increasing rapidly as magnitude decreases, so a modal value at M=6.5 is only possible if there is a decreasing probability of smaller earthquakes generating an exceptional record.

Figures 18 and 19 compare the distributions of magnitudes of the top 100 accelerations and top 100 velocities in Table 1 with the distributions of magnitudes in the NGA database. The NGA database made an effort to be complete for crustal earthquakes in North America, Europe, and southern Asia (excluding Japan). Thus it can be considered to be fairly representative of the complete set of crustal earthquakes, and without doubt is the best choice of any data set if one must be chosen to represent the larger body of strong-motion records. Figure 18 shows that earthquakes with $M \geq 6.25$ are represented much more strongly in the top 100 records than in the NGA database. This tendency for the top 100 records to have larger magnitudes is expressed much more strongly for peak velocity, in Figure 19. About 55% of the NGA data falls in a magnitude bin for magnitude 5, 5.5, or 6, but only about 9% of the exceptional observations come from earthquakes in any of those ranges.

Figures 20 and 21 show the magnitudes of the top 100 accelerations and velocities in Table 1, separated by quartiles. Within these quartiles, we are not convinced that one can see any significant trends, as the few points are not sufficient to overcome the randomness in the statistics of small numbers.

8.7 Dependence on the Mechanism of Faulting

We have broadly classified these earthquakes into several categories, expanding on the classification used by PEER for the NGA database. Those categories, and the number of seismograms in the top 100 and in our complete database of 255 records, are as follows:

0) strike-slip faulting in continental crust (73);
1) normal faulting in continental crust (2),
2) thrust faulting in continental crust (60),
3) oblique thrust faulting in continental crust (54),
4) oblique normal faulting in continental crust (0),
6) normal faulting associated with the downgoing slab in a subduction zone (15),
7) thrust faulting in an oceanic subduction zone (33), and
8) oblique thrust faulting in an oceanic subduction zone (3).

Mechanisms for the earthquakes that caused 15 smaller records are not available from the Harvard CMT catalog. The numbers of records in these different categories are displayed in Figure 22.

Figure 22 shows that the overwhelming majority of the exceptional records are associated with thrust, oblique-thrust, or strike-slip faulting in the continental crust. Thus to the extent that strong-motion instruments are distributed in areas that are representative of the seismic hazard as a whole, continental thrust faults are the most likely to cause exceptional velocities and accelerations, and crustal strike-slip earthquakes are second, with other categories of faulting, in particular faulting related to subduction zones, much less represented.

To interpret this distribution of exceptional records, we again normalize by the rates of earthquakes in each category that are represented in the NGA strong-motion database. These comparisons are shown in Figure 23 for peak acceleration, and in Figure 24 for peak velocity. These figures contain two normalizations based on the exceptional data set. Besides the normalization over all the mechanism categories, it shows the subset of shallow earthquakes in continental crust. This subset of crustal events is the most appropriate to compare with the distribution of NGA mechanisms.

Figure 23 shows that the number of top 100 accelerations is comparable from strike-slip and from thrust earthquakes, while the number of oblique-thrust earthquakes contributing is about half as large. In relative terms, strike-slip is over-represented, while the number of records from crustal thrust earthquakes is under-represented, compared with the numbers in the NGA database. Figure 24 shows that a comparable number of exceptional velocities have been observed from earthquakes crustal strike-slip, oblique thrust, and thrust mechanisms. Compared with NGA, strike-slip earthquakes are slightly over-represented in the top 100 velocities, while the number of oblique thrust events is significantly overrepresented, and the number of thrust mechanisms is underrepresented. These results are somewhat surprising, since thrust earthquakes are often considered the source of stronger shaking than strike-slip earthquakes.

The limitations of the NGA database might be important in evaluating whether thrust mechanisms are actually less likely to cause exceptional motions. Because the NGA database does not include earthquakes from Japan, and because Japanese earthquakes are more likely to have a thrust mechanism than a strike-slip mechanism, thrust mechanisms may be underrepresented in the NGA database compared to the exceptional motions database. If that is the case, the anomalies associated with Figures 23 and 24 become even more striking.

Our overall impression is that subduction zone earthquakes (category 8) are significantly more common in the overall strong-motion database than in the list of exceptional records in Table 1. Normal faulting at 50-100 km depth in subduction zones (Category 7) similarly is perhaps surprisingly well represented among the highest-ranking acceleration records, considering the earthquake depth. There are quite a few earthquakes of this type, including records from Nisqually, Mexico, and Japan, represented in the searched strong-motion database. Both of these mechanisms are more represented at high values of peak acceleration than peak velocity. This is perhaps somewhat surprising, especially since the searched dataset include records from three subduction earthquakes with M>8 (Chile, Guerrero, Hokkaido) with very large mean slips capable of generating high velocities if the stress drop is sufficient.

Normal and oblique-normal mechanisms are very sparsely represented in the NGA database, so it is not surprising that there are few records from these mechanisms in either the top 100 accelerations or velocities. Only two records from these categories are in our selected dataset; the largest of these is M_w~6.0. However, considering Figures 23 and 24,

there is the suggestion that these mechanisms might be considered underrepresented even after adjusting for the sparsity of such records.

Figures 25 and 26 show the mechanisms in the quartiles of the top acceleration and velocity categories. As with the magnitude dependence, we do not think these figures reveal any significant trends.

8.8 Dependence on Site Conditions

The near-surface geology is also well-known to have a significant effect on the amplitudes of strong ground motions. Figure 27 therefore shows the distribution of site categories in Table 1, associated with the NEHRP classifications. Figures 28 and 29 compare the site classifications of the top 100 accelerations and velocities with the site classifications of the NGA database.

The source of the data for V_s30 is either the NGA flatfile (published on their web site at http://peer.berkeley.edu/products/rep_nga_models.html) or data on site conditions for California Strong Motion Instrumentation Program, K-net and KiK-net, given on their respective web sites (http://www.consrv.ca.gov/CGS/smip/about.htm, http://www.k-net.bosai.go.jp/, http://www.kik.bosai.go.jp/, respectively). For the K-net stations, most sites have profiles of V_s to a depth of 20 m. In estimating Vs30, we assumed that the shear velocity at the greatest depth given extends to 30 m. On average, this will result in the estimates of V_s30 for these stations biased slightly low, because the velocity is more likely to increase somewhat than to remain constant. When data is available to 20 m depth, the true value is at most 50% greater than the estimate obtained by this procedure: this extreme can only occur if the velocity from 20-30 meters is so large that the travel time through this depth range is negligible compared to the travel time from 0-20 m. Thus usually the bias will be much smaller than 50%, and we conclude that for our purposes the uncertainty is not important. The NGA database assigns a value of V30 for every station, often based on its geology. However, for stations in this study that are outside of the NGA study, we did not assign an estimate for V_s30 other than the procedure described here for Japan. This is the explanation for many unknown sites in Table 1 while there are none in the NGA.

In Figures 28 and 29, to first order the site conditions in this study have the same distribution as in the NGA study. The most notable possible difference is that two of the highest peak accelerations are observed on NEHRP A sites, while in NGA the fraction of sites in NEHRP A is much smaller than 2%. We consider the statistical basis too small to draw a conclusion.

Figure 30 shows the PGA and PGV observations as a function of the value of V_s30 where known for each site. We see no evidence of dependence of PGA on V_s30 in Figure 4. The site with V_s30=2016 m/s is Pacoima Dam, which had an exceptional record during both the San Fernando and Northridge earthquakes. It might be surprising to some that an acceleration of over 1500 cm/s^2 has been observed on a site with V_s30 as low as 200

m/s, as very soft sediments are presumed to not transmit the strains that will cause such high accelerations. This is recorded during the 1979 Imperial Valley earthquake at station El Centro Array #6, in which the peak acceleration occurs on the vertical component and is dominated by P-waves. S-waves arriving 3 seconds later cause obvious nonlinear site response on the accelerogram.

There is perhaps some hint that the upper bound of PGV decreases as V_s30 increases. However, the data is so sparse for high values of Vs30 that we have no confidence in such a trend. The three points plotted at V_s30=1433 m/s were recorded at the K-net station MYG011 (Oshika) from earthquakes with hypocentral depths from 42-71 km. Models of peak acceleration in Japan (e.g. Si and Midorikawa, 2000) find that deep earthquakes tend to have higher motions than shallow earthquakes at the same hypocentral distance, consistent with the high values observed here. But because of the large hypocentral and presumed fault distances, these points can not be considered to constrain an upper bound on PGV.

Another parameter that is at least in part related to the site condition is kappa (κ). This was defined by Anderson and Hough (1984) from the slope of the Fourier spectrum of acceleration, which they modeled as $\sim \exp(-\pi\kappa f)$. Anderson and Hough (1984) and Anderson (1986) presented evidence that that κ is dominantly controlled by attenuation in the region and especially in the shallow crust below the station. However, Purvance and Anderson (2003) also demonstrated that there is a source contribution to κ.

Following the procedure of Anderson and Hough (1984), the value of κ was estimated for each horizontal component over the frequency band from 5-20 Hz, for a 30-second window starting 10 seconds before the peak velocity. Figure 31 shows the distribution of the average of the two horizontal components for the 255 records in the database. The mode of this larger data set has κ=0.02 s. This is perhaps a surprisingly small value, as most published values of κ for the western US are greater.

Figure 32 compares the distribution in Figure 31 with the values of the top 100 accelerations, by quartile. The top quartile of records have a distribution that is skewed towards smaller values than the full distribution. Figure 33 is the equivalent of Figure 32 for peak velocity. In this case, the top quartile of the records have a distribution that is skewed towards larger values than the full distribution. Since κ is measuring the relative amplitudes of high frequencies in the accelerograms, this shows that the records with the highest peak accelerations tend to be rich in high frequency energy. Conversely the records with the highest peak velocities tend to be relatively depleted in high frequency energy.

8.9 Dependence on Fault-Station Geometry

Appendix A contains a map for many of the earthquakes in Table 1. The maps show the earthquake epicenter, the locations of the stations in Table 1 that recorded the earthquake,

and the locations of aftershocks. The default catalog of aftershocks is the USGS global earthquake catalog (searchable at http://neic.usgs.gov/neis/epic/epic_global.html). If a regional catalog was located the aftershocks from that catalog were substituted for the global file. The aftershock distribution may be an indication of the extent of fault rupture, particularly in locations where the catalog is well constrained. The information in Appendix A was supplemented by a review of literature about the earthquakes.

Perusing Appendix A, we conclude that most of the exceptional records were obtained in a location close to the fault. Indeed, virtually all of the top 25 accelerations and top 25 velocities can be identified as being located on the hanging wall of a thrust fault, being located in a forward directivity direction from the hypocenter, or both.

The exceptional peak accelerations are caused by the Miyagi-Oki earthquake, which occurred at 70 km depth below some stations.

9.0 Causes of Exceptional Motions

From the review above, we conclude that 100 most exceptional accelerations and velocities can be seen on all types of site conditions. Most of the highest values are associated with forward directivity, with a location on the hanging wall of a thrust fault, or sometimes both. The exceptions to this generalization are high stress-drop earthquakes at 40-80 km depth. Since the earthquakes that have been located in the vicinity of Yucca Mountain are nearly all shallower than 15 km, these deep earthquakes are not relevant to the seismicity at Yucca Mountain.

10.0 How Much Worse?

An important question is how near the observations compiled here are to the "upper limit", to the extent that such limit might exist. This is a difficult question. In the discussion of Figure 7, it was noted that the upper bound of the peak observations has not been increasing rapidly with time, in spite of the substantial increase in the number of instruments. This might be taken as weak evidence that the ground motions that have been recorded are near the upper limit of what occurs during earthquakes.

On the other hand, Midorikawa (1994) has compiled a summary of cases where rocks or other objects have been thrown by an earthquake for distances of up to four meters. None of the records in this compilation are capable of throwing objects. Thus by the intensity measure of throwing an object, the ground motion can be stronger. It is recommended that this phenomenon be carefully investigated in order to understand the implications for strong motions. We could also note that objects that are potentially thrown by exceptional motions are abundant everyplace. Thus the number of "instrument-years" represented by these objects is enormous compared with the instrumentation program summarized in Table 4. It is recommended that the information about the frequency of objects being thrown or not thrown be considered as a part of the analysis of the ground motions necessary to throw objects.

11.0 Conclusions

This project defines exceptional ground motions as those for which either peak acceleration exceeds 500 cm/s^2 or peak velocity exceeds 50 cm/s. A global review of strong motions uncovered 255 time histories in this category. Based on an estimate that the data represent roughly 150,000 instrument years, records in this category have occurred at a rate of roughly once for every 600 instrument years. Of these, 35 records have peak acceleration greater than gravity and 41 records have peak velocity greater than 100 cm/s.

Earthquakes with magnitudes as small as 5 are included in this compilation. Some earthquakes this small qualify to be included in the 100 largest accelerations, but the 100 largest velocities all originate with earthquakes with magnitudes of 6.5 or larger. The data are dominated by records from shallow crustal earthquakes with thrust, oblique-thrust, or strike-slip focal mechanisms. Earthquakes with a normal faulting mechanism are not well represented in the larger data set of accelerograms, from which these records were identified. Thus it would be inappropriate to conclude that normal faulting mechanisms are unlikely to cause exceptional motions. There is a hint that hard sites (NEHRP category A) might be more strongly represented in the set of exceptional records than it is in the larger data base, but other than that, all NEHRP site categories are represented in roughly the same proportion as in the larger data set. The distribution of values of kappa among the exceptional records peaks at kappa = 0.02 sec. Records with the highest peak accelerations (> gravity) tend to have smaller values of kappa. Records with the highest peak accelerations tend to have smaller values of kappa.

One can speculate on how these results might apply to Yucca Mountain. The geological deformation rates at Yucca Mountain are probably about two orders of magnitude smaller than they are at the "average" station contributing data to this study. Thus scaling the exceedance rate downwards by two orders of magnitude would suggest that accelerations of 2g, or velocities of 200 cm/s might have an exceedance rate of 10^{-7} per year. There are however flaws with that line of reasoning. The most prominent one is that the highest acceleration in the database, from Nahanni, comes from aftershock monitoring in a region with an even smaller deformation rate. It could be possible that regions with small deformation rates have higher stress drops and higher ground motions than the average.

Perhaps the more important conclusion is that the highest peak accelerations and peak velocities recorded to date are far below the values predicted by the probabilistic seismic hazard analysis for Yucca Mountain.

12.0 References

Aki, K. and P. G. Richards (1980). Quantitative Seismology Theory and Methods, Volume I and II, W. H. Freeman and Company, San Francisco.

Anderson, J. G. (1986). Implication of attenuation for studies of the earthquake source, in *Earthquake Source Mechanics, Maurice Ewing Series 6*, S. Das, J. Boatright, and C. H. Scholz (Editors), American Geophysical Union, Washington, D.C., 311–318.

ANDERSON, J. G. and S. E. HOUGH (1984). A model for the shape of the Fourier amplitude spectrum of acceleration at high frequencies**,** Bulletin of the Seismological Society of America, Oct 1984; 74: 1969 - 1993.

Bechtel SAIC (2004). Technical Basis Document No. 14: Low Probability Seismic Events. Revision 1, 306 pages.

Brune, J. N. (1970). Tectonic stress and the spectra of seismic shear waves for earthquakes, *J. Geophys. Res.* **75,**4997 –5009.

Gumbel, E. J. (1958). Statistics of Extremes, Columbia University Press, New York, 375 pages.

Midorikawa, S. (1994). Case histories of upthrow of objects during earthquakes (in Japanese), JISHIN (Journal of the Seismological Society of Japan) 47, 333-340.

Power, M., B. Chiou, N. Abrahamson, and C. Roblee (2006). The next generation of ground motion attenuation models (NGA) project: An overview. Proc. Eighth National Conf. Earthquake Engineering, Paper No. 22.

Matthew D. Purvance and John G. Anderson (2003). A Comprehensive Study of the Observed Spectral Decay in Strong-Motion Accelerations Recorded in Guerrero, Mexico**,** Bulletin of the Seismological Society of America, Apr 2003; 93: 600 - 611.

Shakal, A. F., H. R. Haddadi, and M. J. Huang (2006). Note on the Very-High-Acceleration Fault Zone 16 Record from the 2004 Parkfield Earthquake, Bulletin of the Seismological Society of America, 96, S119 - S128.

Si, H. and Midorikawa, S., 2000, New Attenuation relations for peak ground acceleration and velocity considering effects of fault type and site condition, Proceedings of Twelfth World Conference on Earthquake Engineering, paper#532.

Wells, D. G. and K. J. Coppersmith (1994). New empirical relationships among magnitude, rupture length, rupture width, rupture area, and surface displacement, Bull. Seism. Soc. Am. 84, 974-1002.

13.0 Tables

Table 1. List of earthquakes and stations included in this study.

Earthquake Name	Date	Time	Magnitude	Magnitude Type	Latitude	Longitude	Depth (km)	Mechanism	Station	Latitude	Longitude	Preferred NEHRP V_S30	Preferred V_S30 (m/s)	File Name
Imperial Valley 1940	5/19/1940	4:36:41	6.90	MW	32.73	-115.5	8.8	0	El Centro	32.794	-115.549	D	213.4	avcnto1940.dat
Parkfield	6/28/1966	4:26:14	6.10	Mw	36	-120.5	10	0	Cholome 2wa	35.733	-120.29	D	184.8	avcholame0.dat
San Fernando	2/9/1971	14:00:41	6.60	Mw	34.44	-118.41	13	2	Pacoima Dam	34.334	-118.396	A	2016.1	avsanfer00.dat
Gazli	5/17/1976	2:58:40	6.80		40.465	63.462	18.2	2	Karakyr	40.35	63.47	C	659.6	avkarakyr0.dat
Iran	9/16/1978	15:35:56	7.30	MW	33.37	57.02	11	2	Tabas	33.6	56.92	B	766.8	avtabas000.dat
Imperial Valley 1979	10/15/1979	23:16:53	6.50	Mw	32.6435	-115.3088	9.96	0	El Centro Array #4	32.864	-115.5	D	208.9	avcentro40.dat
Imperial Valley 1979	10/15/1979	23:16:53	6.50	Mw	32.6435	-115.3088	9.96	0	El Centro Array #5	32.855	-115.47	D	205.6	avcentro50.dat
Imperial Valley 1979	10/15/1979	23:16:53	6.50	Mw	32.6435	-115.3088	9.96	0	El Centro Array #6	32.839	-115.49	D	203.2	avcentro60.dat
Imperial Valley 1979	10/15/1979	23:16:53	6.50	Mw	32.6435	-115.3088	9.96	0	El Centro Array #7	32.829	-115.5	D	210.5	avcentro70.dat
Imperial Valley 1979	10/15/1979	23:16:53	6.50	Mw	32.6435	-115.3088	9.96	0	Differential Array	32.796	-115.535	D	202.3	avdiffar00.dat
Imperial Valley 1979	10/15/1979	23:16:53	6.50	Mw	32.6435	-115.3088	9.96	0	Bonds Corner	32.6932	-115.3382	D	223.0	avimperial.dat
Imperial Valley 1979	10/15/1979	23:16:53	6.50	Mw	32.6435	-115.3088	9.96	0	El Centro Array #8	32.811	-115.53	D	206.1	avimpvall0.dat
Imperial Valley 1979	10/15/1979	23:16:53	6.50	Mw	32.6435	-115.3088	9.96	0	EC Meloland Overpass	32.773	-115.448	D	186.2	avoverpass.dat
Imperial Valley	10/15/1979	23:16:53	6.50	Mw	32.6435	-115.3088	9.96	0	Westmorland	33.037	-115.623	D	193.7	avwmorland.dat
Imperial Valley	10/15/1979	23:16:53	6.50	Mw	32.6435	-115.3088	9.96	0	Agrarias	32.621	-115.301	D	274.5	avagrarias.dat
Victoria	6/9/1980	3:28:19	6.40	Mw	32.185	-115.076	11	0	Victoria	32.29	-115.1	D	274.5	avvictoria.dat
Victoria	6/9/1980	3:28:19	6.40	Mw	32.185	-115.076	11	0	Cerro Prieto	32.421	-115.301	C	659.6	avceprieto.dat
Westmorland	4/26/1981	12:09:28	6.30	MLbrk	33.33	-115.65	6	0	Westmorland	33.037	-115.623	D	193.7	avwmorln81.dat
Coalinga	5/2/1983	23:42:38	6.50	Mw	36.233	-120.31	4.6	2	Pleasant Valley P.P. yard	36.308	-120.249	D	257.4	avppyard00.dat
Coalinga aftershock	5/9/1983	2:49:11	5.20	MLGS	36.23	-120.31	12	2	Anticline Ridge	36.233	-120.333	C	376.1	avanticlin.dat
Coalinga	7/22/1983	2:39:54	6.00	Mw	36.241	-120.409	7.4	2	Oil City	36.229	-120.36	C	376.1	avoilcity0.dat
Coalinga	7/22/1983	2:39:54	6.00	Mw	36.241	-120.409	7.4	2	Transmitter Hill	36.249	-120.343	C	376.1	avtranhill.dat
Coalinga	7/25/1983	22:31:39	5.30	Mw	36.229	-120.398	8.4	2	Old Chp	36.151	-120.353	D	338.5	avoldchp00.dat
Morgan Hill	4/24/1984	21:15:18	6.10	Mw	37.306	-121.695	8.5	0	Coyote Lake Dam	37.118	-121.55	C	597.1	avmorgan00.dat
Valapraiso	3/3/1985	22:47:07	7.80	Mw	-33.135	-71.871	33	7	Melipilla	-33.68	-71.22		-1	avmelipill.dat
Valapraiso	3/3/1985	22:47:07	7.80	Mw	-33.135	-71.871	33	7	Llolleo	-32.635	-71.63		-1	avllolleo1.dat
Valapraiso	3/3/1985	22:47:07	7.80	Mw	-33.135	-71.871	33	7	San Isidro				-1	avsnisidro.dat
Michoacan Aftershock	9/21/1985	1:37:13	7.50	Mw	17.8	-101.65	30	7	Paraiso	17.343	-100.225		-1	avparaiso1.dat
Nahanni	12/23/1985	5:16:00	6.90	Ms	62.222	-124.239	6	2	Site 1	62.199	-124.338	C	659.6	avnahanni0.dat
Nahanni	12/23/1985	5:16:00	6.90	Ms	62.222	-124.239	6	2	Site 2	62.227	-124.168	C	659.6	avnahanni2.dat
North Palm Springs	7/8/1986	9:20:44	6.20	Mw	33.533	-116.578	14.1	3	Desert Hot Springs	33.962	-116.509	D	345.4	avnorth000.dat
North Palm Springs	7/8/1986	9:20:44	6.20	Mw	34	-116.6117	11	3	North Palm Springs Post Office	33.924	-116.543	D	345.4	avnps00000.dat
North Palm Springs	7/8/1986	9:20:44	6.20	Mw	34	-116.6117	11	3	Whitewater Canyon - WWTrout Farm	33.989	-116.655	D	345.4	avwwt00000.dat
North Palm Springs	7/8/1986	9:20:44	6.20	Mw	34	-116.6117	11	3	Devers Substation	33.932	-116.579		-1	avdevers00.dat
Whittier Narrows	10/1/1987	14:42:20	6.10	Mw	34.0493	-118.081	14.6	3	Tarzana	34.16	-118.534	D	257.2	avwhittier.dat
Whittier Narrows	10/1/1987	14:42:20	6.10	Mw	34.0493	-118.081	14.6	3	Whittier Narrows Dam Upstream	34.002	-118.053	D	298.7	avwhitndam.dat
Superstition Hills	11/24/1987	13:15:56	6.70	MLbrk	33.01	-115.84	2	0	Parachute Test Site	32.93	-115.7	D	348.7	avparachut.dat
Superstition Hills	11/24/1987	13:16:00	6.70	MLbrk	33.01	-115.84	2	0	Superstition Mtn. Camera	32.955	-115.823	C	362.4	avsuphill0.dat
Loma Prieta	10/18/1989	0:04:15	7.00	Mw	37.0407	-121.8829	17.48	3	BRAN			C	376.1	avbran0000.dat
Loma Prieta	10/18/1989	0:04:15	7.00	Mw	37.0407	-121.8829	17.48	3	Corralitos	37.046	-121.803	C	462.2	avcorra000.dat
Loma Prieta	10/18/1989	0:04:15	7.00	Mw	37.0407	-121.8829	17.48	3	Capitola	36.974	-121.952	D	288.6	avcapitola.dat
Loma Prieta	10/18/1989	0:04:15	7.00	Mw	37.0407	-121.8829	17.48	3	Gilroy Array #3	36.987	-121.536	D	349.9	avgilroya3.dat
Loma Prieta	10/18/1989	0:04:15	7.00	Mw	37.0407	-121.8829	17.48	3	Los Gatos Lexington Dam	37.202	-121.949	B	1070.3	avgatos000.dat
Loma Prieta	10/18/1989	0:04:15	7.00	Mw	37.0407	-121.8829	17.48	3	Hollister South Pine	36.848	-121.397	C	370.8	avholli000.dat

Earthquake Name	Date	Time	Magnitude	Magnitude Type	Latitude	Longitude	Depth (km)	Mechanism	Station	Latitude	Longitude	Preferred NEHRP V_S30	Preferred V_S30 (m/s)	File Name
Loma Prieta	10/18/1989	0:04:15	7.00	Mw	37.0407	-121.8829	17.48	3	LGPC			C	477.7	avlgpc0000.dat
Loma Prieta	10/18/1989	0:04:15	7.00	Mw	37.0407	-121.8829	17.48	3	Redwood Highway	37.52	-122.25	E	133.1	avred00000.dat
Loma Prieta	10/18/1989	0:04:15	7.00	Mw	37.0407	-121.8829	17.48	3	WAHO			C	376.1	avwaho0000.dat
Loma Prieta	10/18/1989	0:05:00	7.00	Mw	37.0407	-121.8829	17.48	3	Saratoga	37.255	-122.031	C	370.8	avsaratoga.dat
Manjil, Iran	6/20/1990	9:00:10	7.40	Mw	36.95	49.52	18	0	Abbar	36.92	48.97	C	724.0	avabbar000.dat
Manjil, Iran	6/20/1990	9:00:10	7.40	Mw	36.95	49.52	18	0	Abhar	36.15	49.22	D	274.5	avabhar000.dat
Erzican	3/13/1992	17:18:40	6.90	MSbrk	39.705	39.587	9	0	Erzincan			D	274.5	averzincan.dat
Cape Mendocino	4/25/1992	18:06:04	7.00	Mw	40.3338	-124.2294	21	2	Cape Mendocino, Petrolia	40.348	-124.352	D	311.8	avcape0000.dat
Cape Mendocino	4/25/1992	18:06:14	7.00	Mw	40.3338	-124.2294	9.6	2	Petrolia Gen Store 1	40.325	-124.287	C	712.8	avgen10000.dat
Cape Mendocino	4/26/1992	7:41:00	6.60	Ms	40.282	-124.244	10	2	Petrolia Gen Store 2	40.325	-124.287	C	712.8	avgen20000.dat
Landers	6/28/1992	11:57:34	7.30	Mw	34.201	-116.436	7	0	Lucerne	34.5675	-116.6122	C	684.9	avlanders0.dat
Big Bear	6/28/1992	15:05:36	6.40	Mw	34.21	-116.826	13	0	Big Bear Lake	34.238	-116.935	D	338.5	avbigbear0.dat
Northridge	1/17/1994	12:30:55	6.70	Mw	34.2057	-118.5539	17.5	2	Arleta Fire Station	34.236	-118.439	D	297.7	avarletafs.dat
Northridge	1/17/1994	12:30:55	6.70	Mw	34.2057	-118.5539	17.5	2	Beverly Hills 12520 Mullholand Dr.	34.127	-118.405	C	545.7	avbevhill0.dat
Northridge	1/17/1994	12:30:55	6.70	Mw	34.2057	-118.5539	17.5	2	Castaic Old Ridge Route	34.56	-118.64	C	450.3	avcastaic0.dat
Northridge	1/17/1994	12:30:55	6.70	Mw	34.2057	-118.5539	17.5	2	Canoga Park	34.2119	-118.6056	D	267.5	avcanogapk.dat
Northridge	1/17/1994	12:30:55	6.70	Mw	34.2057	-118.5539	17.5	2	Jensen F.P. Generator	34.313	-118.498	C	525.8	avjengen00.dat
Northridge	1/17/1994	12:30:55	6.70	Mw	34.2057	-118.5539	17.5	2	Jensen F.P. Administration Bldg	34.312	-118.496	C	373.1	avjenplan0.dat
Northridge	1/17/1994	12:30:55	6.70	Mw	34.2057	-118.5539	17.5	2	LA Dam	34.294	-118.483	C	629.0	avladam000.dat
Northridge	1/17/1994	12:30:55	6.70	Mw	34.2057	-118.5539	17.5	2	14145 Mullholand Dr.	34.132	-118.439	D	355.8	avmulholl0.dat
Northridge	1/17/1994	12:30:55	6.70	Mw	34.2057	-118.5539	17.5	2	Newhall F.S.	34.39	-118.53	D	269.1	avnewhall0.dat
Northridge	1/17/1994	12:30:55	6.70	Mw	34.2057	-118.5539	17.5	2	Pacoima Dam	34.334	-118.396	A	2016.1	avpacoi000.dat
Northridge	1/17/1994	12:30:55	6.70	Mw	34.2057	-118.5539	17.5	2	Pardee			D	345.4	avpardee00.dat
Northridge	1/17/1994	12:30:55	6.70	Mw	34.2057	-118.5539	17.5	2	West Pico Canyon Road	34.391	-118.621	D	285.9	avpico0000.dat
Northridge	1/17/1994	12:30:55	6.70	Mw	34.2057	-118.5539	17.5	2	Rinaldi Receiving Station	34.281	-118.478	D	282.3	avrinaldi0.dat
Northridge	1/17/1994	12:30:55	6.70	Mw	34.2057	-118.5539	17.5	2	Santa Monica City Hall	34.011	-118.49	D	336.2	avsanta000.dat
Northridge	1/17/1994	12:30:55	6.70	Mw	34.2057	-118.5539	17.5	2	17645 Saticoy St., Northridge	34.2089	-118.5172	D	280.9	avsaticoy1.dat
Northridge	1/17/1994	12:30:55	6.70	Mw	34.2057	-118.5539	17.5	2	Sepulvelda VA Hospital	34.249	-118.478	C	380.1	avsepul000.dat
Northridge	1/17/1994	12:30:55	6.70	Mw	34.2057	-118.5539	17.5	2	Simi Valley	34.264	-118.666	C	557.4	avsimi0000.dat
Northridge	1/17/1994	12:30:55	6.70	Mw	34.2057	-118.5539	17.5	2	Sylmar Valve Hall Floor - Converter Station East	34.312	-118.481	C	370.5	avsylmar00.dat
Northridge	1/17/1994	12:30:55	6.70	Mw	34.2057	-118.5539	17.5	2	Sylmar Converter Stn Valve Group 1-6 (East)	34.312	-118.481	C	370.52	avsylmarc6.dat
Northridge	1/17/1994	12:30:55	6.70	Mw	34.2057	-118.5539	17.5	2	Sylmar Converter Stn Valve Group 7	34.311	-118.49	D	251.24	avscsvalv7.dat
Northridge	1/17/1994	12:30:55	6.70	Mw	34.2057	-118.5539	17.5	2	Sylmar County Hospital (Olive View)	34.326	-118.444	C	440.54	avhospital.dat
Northridge	1/17/1994	12:30:55	6.70	Mw	34.2057	-118.5539	17.5	2	Tarzana	34.16	-118.534	D	257.21	avtarz0000.dat
Northridge aftershock	1/29/1994	11:20:35	5.10	Mw	34.31	-118.58		-1	Brown's Canyon	34.307	-118.603		-1	avbrwnscyn.dat
Zanjiran	6/20/1994	9:09:02	5.90	Mw	29.06	52.44		0	Zanjiran	29.07	52.62		-1	avzanjiran.dat
Zanjiran	6/20/1994	9:09:02	5.90	Mw	29.06	52.44		0	Maymand	28.87	52.75		-1	avmaymand1.dat
Kobe	1/16/1995	20:46:52	6.90	Mw	34.5948	135.0121	17.9	0	KJMA	34.6833	135.18	D	312.0	avkjma0000.dat
Kobe	1/16/1995	20:46:52	6.90	Mw	34.5948	135.0121	17.9	0	Takatori	34.649	135.139	D	256.0	avtaka0000.dat
Kobe	1/16/1995	20:46:52	6.90	Mw	34.5948	135.0121	17.9	0	Takarazuka	34.809	135.344	D	312.0	avtakar000.dat
Kobe	1/16/1995	20:46:52	6.90	Mw	34.5948	135.0121	17.9	0	Port Island, Kobe	34.67	135.201	D	198.0	avkobeport.dat
East Coast Honshu	5/23/1996	9:36:31	5.00	Mw	38.7	142.3	39	-1	MYG011 Oshika	38.29	141.508	B	1433	avoshika00.dat
Central Honshu	8/13/1996	2:13:00	5.00	Mjma	38.803	140.597	10	-1	MYG005 Naruko	38.7992	140.597	D+	337	avmyg005w1.dat
Honshu	12/21/1996	1:28:51	5.70	mb-GS	36.03	139.77	44	7	TCG009 Imaichi	36.73	139.72	D	248	avimaichi0.dat
South Coast Honshu	3/3/1997	14:09:43	5.00	Mw	35	139.2	3	-1	SZO002 Itoh	34.962	139.106	D+	281	avitoh0000.dat
South Coast Honshu	3/16/1997	5:51:37	5.80	Mw	34.9	137.5	39	6	AIC010 Tsukude	34.973	137.427	E+	173	avtsuk0000.dat
Kyushu	3/26/1997	8:31:47	6.30	Mw	32	130.4	8	0	KGS002 Izumi	32.087	130.356	C	442	avizumi000.dat
Kyushu	3/26/1997	8:31:47	6.30	Mw	32	130.4	8	0	KGS005 Miyanojoh	31.897	130.454	C-	356	avkgs005w1.dat
Kyushu	5/13/1997	5:38:30	6.20	Mw	32	130.3	8	0	KGS005 Miyanojoh	31.897	130.454	C-	356	avmiyan000.dat
Kyushu	5/13/1997	5:38:30	6.20	Mw	32	130.3	8	0	KGS002 Izumi	32.0909	130.3532	C	442	avkgs002k1.dat
Umbria Marche, Italy foreshock	9/26/1997	0:33:16	5.72	Mw	43.023	12.862	7	1	0593 Nocera Umbra	43.113	12.785		-1	av593umbra.dat
Umbria Marche, Italy	9/26/1997	9:40:33	6.04	Mw	43.031	12.862	6	1	0594 Nocera Umbra	43.113	12.785		-1	av594umbra.dat

Earthquake Name	Date	Time	Magnitude	Magnitude Type	Latitude	Longitude	Depth (km)	Mechanism	Station	Latitude	Longitude	Preferred NEHRP V_S30	Preferred V_S30 (m/s)	File Name
Chamoli	3/28/1999	19:05:11	6.60	Mw	30.512	79.403	15	2	Gopeshwar	30.4	79.33		-1	avgope0000.dat
Karehbas	5/6/1999	23:00:53	5.90	Mw	29.18	52.54	17	0	Balaadeh	29.28	51.93		-1	avbalaa000.dat
Kocaeli, Turkey	8/17/1999	0:01:40	7.60	Mw-hrv	40.702	29.987	17	0	Yarimca	40.7639	29.762	D	297.0	avyarimca0.dat
Kocaeli, Turkey	8/17/1999	0:01:40	7.60	Mw-hrv	40.702	29.987	17	0	Sakarya	40.7639	29.762	C	471.0	avturkey00.dat
Kocaeli, Turkey	8/17/1999	0:01:40	7.60	Mw-hrv	40.702	29.987	17	0	Duzce	40.843	31.151	D	276.0	avduzce000.dat
Southern Honshu	8/20/1999	20:33:00	5.40	Mjma	34.053	135.464	70	6	WKY005	33.8938	135.4883	D+	338	avwky005w1.dat
Chi-Chi	9/20/1999	17:47:16	7.60	Mw	23.8603	120.7995	33	3	CHY006	23.5815	120.552	C	438.2	avchy006a0.dat
Chi-Chi	9/20/1999	17:47:16	7.60	Mw	23.8603	120.7995	33	3	CHY024	23.757	120.6062	C	427.7	avchy02400.dat
Chi-Chi	9/20/1999	17:47:16	7.60	Mw	23.8603	120.7995	33	3	CHY028	23.632	120.6052	C	542.6	avchy02800.dat
Chi-Chi	9/20/1999	17:47:16	7.60	Mw	23.8603	120.7995	33	3	CHY080	23.5972	120.6777	C	553.4	avchy08000.dat
Chi-Chi	9/20/1999	17:47:16	7.60	Mw	23.8603	120.7995	33	3	CHY101	23.6862	120.5622	D	258.9	avchy101a0.dat
Chi-Chi	9/20/1999	17:47:16	7.60	Mw	23.8603	120.7995	33	3	CHY104	23.6695	120.4648	D	223.2	avchy104a0.dat
Chi-Chi	9/20/1999	17:47:16	7.60	Mw	23.8603	120.7995	33	3	NSY	24.4162	120.7607	C	599.6	avnsya0000.dat
Chi-Chi	9/20/1999	17:47:16	7.60	Mw	23.8603	120.7995	33	3	TCU036	24.4488	120.6963	D	272.6	avtcu03600.dat
Chi-Chi	9/20/1999	17:47:16	7.60	Mw	23.8603	120.7995	33	3	TCU039	24.04917	120.7837	C	540.7	avtcu03900.dat
Chi-Chi	9/20/1999	17:47:16	7.60	Mw	23.8603	120.7995	33	3	TCU040	24.4497	120.6455	C	362.0	avtcu04000.dat
Chi-Chi	9/20/1999	17:47:16	7.60	Mw	23.8603	120.7995	33	3	TCU049	24.179	120.6902	C	487.3	avtcu04900.dat
Chi-Chi	9/20/1999	17:47:16	7.60	Mw	23.8603	120.7995	33	3	TCU052	24.198	120.7393	C	393.2	avtcu05200.dat
Chi-Chi	9/20/1999	17:47:16	7.60	Mw	23.8603	120.7995	33	3	TCU055	24.1392	120.6643	D	272.6	avtcu05500.dat
Chi-Chi	9/20/1999	17:47:16	7.60	Mw	23.8603	120.7995	33	3	TCU059	24.2687	120.5637	D	272.6	avtcu05900.dat
Chi-Chi	9/20/1999	17:47:16	7.60	Mw	23.8603	120.7995	33	3	TCU063	24.1083	120.6158	D	272.6	avtcu06300.dat
Chi-Chi	9/20/1999	17:47:16	7.60	Mw	23.8603	120.7995	33	3	TCU065	24.0588	120.6912	D	305.9	avtcu06500.dat
Chi-Chi	9/20/1999	17:47:16	7.60	Mw	23.8603	120.7995	33	3	TCU067	24.0912	120.72	C	433.6	avtcu06700.dat
Chi-Chi	9/20/1999	17:47:16	7.60	Mw	23.8603	120.7995	33	3	TCU068	24.2772	120.7658	C	487.3	avtcu06800.dat
Chi-Chi	9/20/1999	17:47:16	7.60	Mw	23.8603	120.7995	33	3	TCU070	24.196	120.5403	C	401.3	avtcu07000.dat
Chi-Chi	9/20/1999	17:47:16	7.60	Mw	23.8603	120.7995	33	3	TCU071	23.9855	120.7883	C	624.9	avtcu07100.dat
Chi-Chi	9/20/1999	17:47:16	7.60	Mw	23.8603	120.7995	33	3	TCU072	20.0407	120.8488	C	468.1	avtcu07200.dat
Chi-Chi	9/20/1999	17:47:16	7.60	Mw	23.8603	120.7995	33	3	TCU074	23.9622	120.9618	C	468.1	avtcu07400.dat
Chi-Chi	9/20/1999	17:47:16	7.60	Mw	23.8603	120.7995	33	3	TCU075	23.9827	120.6778	C	549.4	avtcu07500.dat
Chi-Chi	9/20/1999	17:47:16	7.60	Mw	23.8603	120.7995	33	3	TCU076	23.9077	120.6757	C	573.0	avtcu07600.dat
Chi-Chi	9/20/1999	17:47:16	7.60	Mw	23.8603	120.7995	33	3	TCU079	23.8395	120.8942	C	364.0	avtcu07900.dat
Chi-Chi	9/20/1999	17:47:16	7.60	Mw	23.8603	120.7995	33	3	TCU082	24.1475	120.676	C	472.8	avtcu08200.dat
Chi-Chi	9/20/1999	17:47:16	7.60	Mw	23.8603	120.7995	33	3	TCU084	23.883	120.8998	C	553.4	avtcu08400.dat
Chi-Chi	9/20/1999	17:47:16	7.60	Mw	23.8603	120.7995	33	3	TCU087	24.3482	120.7733	C	473.9	avtcu08700.dat
Chi-Chi	9/20/1999	17:47:16	7.60	Mw	23.8603	120.7995	33	3	TCU095	24.6917	121.0135	C	446.6	avtcu09500.dat
Chi-Chi	9/20/1999	17:47:16	7.60	Mw	23.8603	120.7995	33	3	TCU101	24.242	120.7092	D	272.6	avtcu10100.dat
Chi-Chi	9/20/1999	17:47:16	7.60	Mw	23.8603	120.7995	33	3	TCU102	24.2493	120.7208	C	714.3	avtcu10200.dat
Chi-Chi	9/20/1999	17:47:16	7.60	Mw	23.8603	120.7995	33	3	TCU103	24.3098	120.7072	C	494.1	avtcu10300.dat
Chi-Chi	9/20/1999	17:47:16	7.60	Mw	23.8603	120.7995	33	3	TCU109	24.0848	120.5713	C	473.9	avtcu10900.dat
Chi-Chi	9/20/1999	17:47:16	7.60	Mw	23.8603	120.7995	33	3	TCU117	24.1335	120.4598	D	215.0	avtcu11700.dat
Chi-Chi	9/20/1999	17:47:16	7.60	Mw	23.8603	120.7995	33	3	TCU128	24.4162	120.7607	C	599.6	avtcu12800.dat
Chi-Chi	9/20/1999	17:47:16	7.60	Mw	23.8603	120.7995	33	3	TCU129	23.8783	120.6843	C	664.4	avtcu12900.dat
Chi-Chi	9/20/1999	17:47:16	7.60	Mw	23.8603	120.7995	33	3	WGK	23.6862	120.5622	D	258.9	avwgka0000.dat
Chi-Chi	9/20/1999	17:47:16	7.60	Mw	23.8603	120.7995	33	3	WNT	23.8783	120.6843	C	664.4	avwnt00000.dat
Duzce	11/12/1999	16:57:27	7.10	MW	40.93	31.25	18	0	Bolu	40.746	31.607	D	326.0	avbolu0000.dat
Duzce	11/12/1999	16:57:27	7.10	MW	40.93	31.25	18	0	Duzce	40.843	31.151	D	276.0	avduzce011.dat
Duzce	11/12/1999	16:57:27	7.10	MW	40.93	31.25	18	0	Lamont 375	40.743	30.876	C	424.8	avlamont37.dat
Duzce	11/12/1999	16:57:27	7.10	MW	40.93	31.25	18	0	IRIGM 496	40.742	30.873		-1	avIRI496ms.dat
Duzce Aftershock 1	11/12/1999	17:16:50	4.80	mbGS	40.76	31.02	10	-1	IRIGM 496	40.742	30.873		-1	avduzcf496.dat
Duzce Aftershock 1	11/12/1999	17:16:50	4.80	mbGS	40.76	31.02	10	-1	IRIGM 492	40.743	30.876		-1	avduzcf492.dat
Duzce Aftershock 2	11/12/1999	17:17:56	5.50	mbGS	40.78	31.12	10	-1	IRIGM 496	40.742	30.873		-1	avduzc496b.dat
South Iceland	6/17/2000	15:40:41	6.57	MW	63.97	-20.36	15	0	004674 Flagbjarnarholt	63.991	-20.264		-1	av4674flag.dat
South Iceland	6/17/2000	15:40:41	6.57	MW	63.97	-20.36	15	0	006263 Kaldarholt	64.004	-20.474		-1	av6263kard.dat
South Iceland Aftershock	6/21/2000	0:51:48	6.49	MW	63.97	-20.71		0	006334 Solheimar	64.065	-20.642		-1	av6334solh.dat
South Iceland Aftershock	6/21/2000	0:51:48	6.49	MW	63.97	-20.71		0	006349 Thjorsarbru	63.931	-20.649		-1	av6349tbru.dat
South Iceland Aftershock	6/21/2000	0:51:48	6.49	MW	63.97	-20.71		0	006332 Thjorsartun	63.928	-20.648		-1	av6332ttun.dat
Japan	7/14/2000	16:18:00	3.90	Mjma	34.408	139.227	6	-1	TKY010 Niijima	34.3775	139.2557	D	259	avtky010d1.dat
Yountville	9/3/2000	8:36:30	5.00	Mw	38.377	-122.414	9.4	0	Napa	38.33	-122.318	D	271.4	avyount000.dat
Western Tottori	10/6/2000	4:30:19	7.10	Mw	35.275	133.3937	11	0	TTRH02 Hino	35.2281	133.3937	D	310	avttrh02t2.dat

Earthquake Name	Date	Time	Magnitude	Magnitude Type	Latitude	Longitude	Depth (km)	Mechanism	Station	Latitude	Longitude	Preferred NEHRP V_S30	Preferred V_S30 (m/s)	File Name
Western Tottori	10/6/2000	4:30:19	7.10	Mw	35.275	133.3937	11	0	SMNH02 Nita	35.2203	133.0882	C	503	avsmnh02t2.dat
Western Tottori	10/6/2000	4:30:19	7.10	Mw	35.275	133.3937	11	0	HRS001 Takano	35.0337	132.9018	C-	354	avhrs001d1.dat
Western Tottori	10/6/2000	4:30:19	7.10	Mw	35.275	133.3937	11	0	HRS002 Tohjoh	34.8951	133.2755	C-	352	avhrs002d1.dat
Western Tottori	10/6/2000	4:30:19	7.10	Mw	35.275	133.3937	11	0	HRS005 Yuki	34.777	133.345	C	440	avhrs005t2.dat
Western Tottori	10/6/2000	4:30:19	7.10	Mw	35.275	133.3937	11	0	OKY004 Niimi	34.9579	133.5018	C	411	avoky004t2.dat
Western Tottori	10/6/2000	4:30:19	7.10	Mw	35.275	133.3937	11	0	SMN003 Yokota	35.1795	133.0929	C-	341	avsmn003t2.dat
Western Tottori	10/6/2000	4:30:19	7.10	Mw	35.275	133.3937	11	0	SMNH01 Hakuta	35.2931	133.263	C	464	avsmnh01t2.dat
Western Tottori	10/6/2000	4:30:19	7.10	Mw	35.275	133.3937	11	0	TTR007 Kohfu	35.2826	133.4876	C	404	avttr007t2.dat
Western Tottori	10/6/2000	4:30:19	7.10	Mw	35.275	133.3937	11	0	TTR009 Nichinan	35.1629	133.3063	C	423	avttr009t2.dat
Honshu	10/30/2000	16:42:52	5.50	Mjma	34.283	136.345	44	8	MIEH05 Owase	34.0606	136.1717	C	590	avmieh05t2.dat
El Salvador	1/13/2001	17:33:32	7.60	Mw	13.049	-88.66	60	6	Santa Tecla	13.675	-89.3		-1	avsantatec.dat
El Salvador	1/13/2001	17:33:32	7.60	Mw	13.049	-88.66	60	6	Armenia, Sonsonate	13.744	-89.501		-1	avsonsonat.dat
El Salvador	1/13/2001	17:33:32	7.60	Mw	13.049	-88.66	60	6	Puerto La Libertad, La Libertad	13.486	-89.327		-1	avlibertad.dat
El Salvador	1/13/2001	17:33:32	7.60	Mw	13.049	-88.66	60	6	San Pedro Nonualco, La Paz	13.602	-88.927		-1	avnonualco.dat
El Salvador	1/13/2001	17:33:32	7.60	Mw	13.049	-88.66	60	6	Santiago de Maria				-1	avsdemaria.dat
Nisqually	2/28/2001	18:54:31	6.80	Mw	47.167	-122.733	52.4	6	Seattle	47.5842	-122.3331		-1	avnisqua00.dat
Southern Honshu	3/24/2001	6:27:54	6.40	Mw	34.12	132.708	51	6	Mistugi	34.515	133.1401		-1	avmits0000.dat
Southern Honshu	3/24/2001	6:27:54	6.40	Mw	34.12	132.708	51	6	EHM003 Tohyo	33.9266	133.0843	D	237	avehm003e1.dat
Southern Honshu	3/24/2001	6:27:54	6.40	Mw	34.12	132.708	51	6	EHMH05 Tobe	33.7079	132.8057	C	362	avtobe0000.dat
Southern Honshu	3/24/2001	6:27:54	6.40	Mw	34.12	132.708	51	6	HRS009 Yuki	34.4926	132.2794	C	473	avhrs009e1.dat
Southern Honshu	3/24/2001	6:27:54	6.40	Mw	34.12	132.708	51	6	HRS017 Mihara	34.404	133.0832	C	408	avhrs017e1.dat
Southern Honshu	3/24/2001	6:27:54	6.40	Mw	34.12	132.708	51	6	HRS019 Kure	34.2485	132.5647	D	204	avhrs019e1.dat
Southern Honshu	3/24/2001	6:27:54	6.40	Mw	34.12	132.708	51	6	HRSH01 MIHARA	34.3704	133.0259	C	403	avhrsh01h1.dat
Japan	6/14/2002	2:42:00	4.90	Mjma	36.215	139.977	57	-1	IBR013 Hokota	36.1587	140.4892	D	265	avibr013e1.dat
Avaj, Iran	6/22/2002	2:58:20	6.50	Mw	35.82	48.97	5	2	Avaj	35.58	49.22			avavaj0000.dat
Denali, Alaska	11/3/2002	22:13:00	7.90	Ms	63.23	-144.89	15	0	Taps Pump Station #10	63.4239	-145.7658	D	329.4	avdenalia0.dat
Miyagi-Oki	5/26/2003	9:24:33	7.00	Mw	38.805	141.682	71	7	IWT007 Kamaishi	39.2701	141.8561	E	141	aviwt007g1.dat
Miyagi-Oki	5/26/2003	9:24:33	7.00	Mw	38.805	141.682	71	7	IWT012 Kitakami	39.3209	141.1378	C	384	aviwt012g1.dat
Miyagi-Oki	5/26/2003	9:24:33	7.00	Mw	38.805	141.682	71	7	IWTH05 Fujisawa	38.8625	141.3547	C	429	avfuji0000.dat
Miyagi-Oki	5/26/2003	9:24:33	7.00	Mw	38.805	141.682	71	7	IWTH26 Ichinoseki-E	38.9661	141.0047	C	371	avichino00.dat
Miyagi-Oki	5/26/2003	9:24:33	7.00	Mw	38.805	141.682	71	7	IWTH02 Tamayama	39.8222	141.3861	C	390.0	avtamay000.dat
Miyagi-Oki	5/26/2003	9:24:33	7.00	Mw	38.805	141.682	71	7	IWTH04 Sumita	39.1781	141.3944	C	456.0	avsumita00.dat
Miyagi-Oki	5/26/2003	9:24:33	7.00	Mw	38.805	141.682	71	7	IWTH21 Yamada	39.4706	141.9372	C	527.0	avyamada00.dat
Miyagi-Oki	5/26/2003	9:24:33	7.00	Mw	38.805	141.682	71	7	IWTH23 Kamaishi	39.2717	141.8267	B	923.0	aviwth23m1.dat
Miyagi-Oki	5/26/2003	9:24:33	7.00	Mw	38.805	141.682	71	7	IWTH27 Rikuzentakata	39.0278	141.5356	C	670.0	avrikuz000.dat
Miyagi-Oki	5/26/2003	9:24:33	7.00	Mw	38.805	141.682	71	7	MYG002 Utatsu	38.7262	141.5109	C	469	avmyg002g1.dat
Miyagi-Oki	5/26/2003	9:24:33	7.00	Mw	38.805	141.682	71	7	MYG003 Tohwa	38.7348	141.3106	C	476	avmyg003g1.dat
Miyagi-Oki	5/26/2003	9:24:33	7.00	Mw	38.805	141.682	71	7	MYG011 Oshika	38.2972	141.5043	B	1433	avmyg011g1.dat
Miyagi-Oki	5/26/2003	9:24:33	7.00	Mw	38.805	141.682	71	7	MYGH03 Karakuwa	38.9189	141.6422	B	951	avkarak000.dat
Miyagi-Oki	5/26/2003	9:24:33	7.00	Mw	38.805	141.682	71	7	MYGH04 Touwa	38.7831	141.3289	B	850	avtouwa000.dat
Miyagi-Oki	5/26/2003	9:24:33	7.00	Mw	38.805	141.682	71	7	MYGH05 Onoda	38.5764	140.7839	D	305	avonoda000.dat
Tokachi-Oki	9/25/2003	19:50:07	8.00	Mw	41.778	144.078	42	7	HKD066 Shibetsu	43.6619	145.1307	E	126	avhkd066g1.dat
Tokachi-Oki	9/25/2003	19:50:07	8.00	Mw	41.778	144.078	42	7	HKD075 Hamanaka	43.0767	145.1296	D	266	avhkd075g1.dat
Tokachi-Oki	9/25/2003	19:50:07	8.00	Mw	41.778	144.078	42	7	HKD086 Chokubetsu	42.8526	143.8636	D	201	avhkd08600.dat
Tokachi-Oki	9/25/2003	19:50:07	8.00	Mw	41.778	144.078	42	7	HKD092 Ikeda	42.9283	143.4483	D	236	avhkd092g1.dat
Tokachi-Oki	9/25/2003	19:50:07	8.00	Mw	41.778	144.078	42	7	KSRH10 Hamanaka	43.0741	145.1336	D	242	avhama0000.dat
Tokachi-Oki	9/25/2003	19:50:07	8.00	Mw	41.778	144.078	42	7	HKD100 Hiroo	42.2838	143.3158	D	236	avhiroo000.dat
Tokachi-Oki	9/25/2003	19:50:07	8.00	Mw	41.778	144.078	42	7	KSRH03 Shibecha	43.3822	144.6319	D	250	avshibech0.dat
Tokachi-Oki	9/25/2003	19:50:07	8.00	Mw	41.778	144.078	42	7	NMRH02 Shibetsu S	43.6747	144.9658	D	315	avnmrh02t1.dat
Tokachi-Oki	9/25/2003	19:50:07	8.00	Mw	41.778	144.078	42	7	KSRH07 Tsurui-S	43.1333	144.3314	D	250	avksrh07t1.dat
Tokachi-Oki	9/25/2003	21:08:00	7.00	Mw	41.8	143.512	33	7	HKD109 Urakawa	42.1652	142.7711	D	231	avuraka000.dat
Bam	12/26/2003	1:56:56	6.70	Mw	29.09	58.35	7	0	Bam	29.09	58.35		-1	avbam00000.dat
Honshu	7/9/2004	10:54:00	4.40	Mjma	39.915	141.033	9	-1	IWT021	39.9203	141.082	D	247	aviwt021i1.dat
Parkfield 2004	9/28/2004	17:15:24	6.00	Mw	35.815	-120.374	7.9	0	CHOLAME 2WA	35.733	-120.29		-1	avchalome0.dat
Parkfield 2004	9/28/2004	17:15:24	6.00	Mw	35.815	-120.374	7.9	0	Fault Zone 1	35.758	-120.307		-1	avfz100000.dat
Parkfield 2004	9/28/2004	17:15:24	6.00	Mw	35.815	-120.374	7.9	0	Fault Zone 14	35.908	-120.458		-1	avfz140000.dat
Parkfield 2004	9/28/2004	17:15:24	6.00	Mw	35.815	-120.374	7.9	0	Fault Zone 11	35.896	-120.398		-1	avfltzne11.dat

Earthquake Name	Date	Time	Magnitude	Magnitude Type	Latitude	Longitude	Depth (km)	Mechanism	Station	Latitude	Longitude	Preferred NEHRP V_S30	Preferred V_S30 (m/s)	File Name
Parkfield 2004	9/28/2004	17:15:24	6.00	Mw	35.815	-120.374	7.9	0	Cholame 3E	35.77	-120.247		-1	avcholam3e.dat
Parkfield 2004	9/28/2004	17:15:24	6.00	Mw	35.815	-120.374	7.9	0	Vinyard Canyon 2W	35.927	-120.509		-1	avvinyrd2w.dat
Parkfield 2004	9/28/2004	17:15:24	6.00	Mw	35.815	-120.374	7.9	0	Fault Zone 8	35.878	-120.381		-1	avfltzone8.dat
Parkfield 2004	9/28/2004	17:15:24	6.00	Mw	35.815	-120.374	7.9	0	Stone Corral 1E	35.788	-120.294		-1	avcorral1e.dat
Parkfield 2004	9/28/2004	17:15:24	6.00	Mw	35.815	-120.374	7.9	0	Cholame 3W	35.726	-120.296		-1	avcholam3w.dat
Parkfield 2004	9/28/2004	17:15:24	6.00	Mw	35.815	-120.374	7.9	0	Cholame 4W	35.7171	-120.305		-1	avcholam4w.dat
Parkfield 2004	9/28/2004	17:15:24	6.00	Mw	35.815	-120.374	7.9	0	Gold Hill 3W	35.796	-120.411		-1	avgldhll3w.dat
Parkfield 2004	9/28/2004	17:15:24	6.00	Mw	35.815	-120.374	7.9	0	Joaquin Canyon	35.9397	-120.4319		-1	avjoaquinc.dat
Parkfield 2004	9/28/2004	17:15:24	6.00	Mw	35.815	-120.374	7.9	0	Slack Canyon	36.034	-120.59		-1	avslack000.dat
Niigata-Ken Chuetsu	10/23/2004	8:56:00	6.60	Mw	37.229	138.773	15.8	2	NIGH11 Kawanishi	37.1697	138.7472	C	375	avkawa0000.dat
Niigata-Ken Chuetsu	10/23/2004	8:56:00	6.60	Mw	37.229	138.773	15.8	2	NIGH01 NAGAOKA	37.4242	138.87		-1	avnigh01n1.dat
Niigata-Ken Chuetsu	10/23/2004	8:56:00	6.60	Mw	37.229	138.773	15.8	2	Kawaguchi				-1	avkawaguch.dat
Niigata-Ken Chuetsu	10/23/2004	8:56:00	6.60	Mw	37.229	138.773	15.8	2	NIG020 Koide	37.2302	138.9652	D+	351	avkoide080.dat
Niigata-Ken Chuetsu	10/23/2004	8:56:00	6.60	Mw	37.229	138.773	15.8	2	NIG028 Nagaoka-Shisho	37.4231	138.8894		-1	avnaga0000.dat
Niigata-Ken Chuetsu	10/23/2004	8:56:00	6.60	Mw	37.229	138.773	15.8	2	NIG019 Ojiya	37.3027	138.793	D	292	avojiya000.dat
Niigata-Ken Chuetsu	10/23/2004	8:56:00	6.60	Mw	37.229	138.773	15.8	2	NIG021 Tohkamachi	37.125	138.75	C	419	avtohk0000.dat
Niigata-Ken Chuetsu	10/23/2004	8:56:00	6.60	Mw	37.229	138.773	15.8	2	NIG017 Nagaoka	37.4416	138.8431	D	268	avnig017n1.dat
Niigata-Ken Chuetsu aftershock 1	10/23/2004	9:03:00	6.30	Mjma	37.35	138.985	9	2	NIGH01 Nagaoka	37.4242	138.87		-1	avnigh01n2.dat
Niigata-Ken Chuetsu aftershock 2	10/23/2004	9:07:00	5.70	Mjma	37.348	138.864	15	-1	NIG019 Ojiya	37.3027	138.793	D	292	avnig019n3.dat
Niigata-Ken Chuetsu aftershock 3	10/23/2004	9:34:07	6.30	Mw	37.28	138.787	22.2	2	NIG020 Koide	37.2302	138.9652	D+	351	avkoide090.dat
Niigata-Ken Chuetsu aftershock 3	10/23/2004	9:34:07	6.30	Mw	37.28	138.787	22.2	2	NIG021 Tohkamachi	37.125	138.75	C	419	avnig021n4.dat
Niigata-Ken Chuetsu aftershock 3	10/23/2004	9:34:07	6.30	Mw	37.28	138.787	22.2	2	NIG019 Ojiya	37.3027	138.793	D	292	avnig019n4.dat
Niigata-Ken Chuetsu aftershock 3	10/23/2004	9:34:07	6.30	Mw	37.28	138.787	22.2	2	NIG024 Yasuduka	37.1268	138.444	D+	340	avnig024n4.dat
Niigata-Ken Chuetsu aftershock 3	10/23/2004	9:34:07	6.30	Mw	37.28	138.787	22.2	2	NIGH11 Kawanishi	37.1697	138.7472	C	375	avnigh11n4.dat
Niigata-Ken Chuetsu aftershock 3	10/23/2004	9:34:07	6.30	Mw	37.28	138.787	22.2	2	NIGH12 Yunotani	37.2208	138.9853	C	553	avnigh12n4.dat
Niigata-Ken Chuetsu aftershock 4	10/27/2004	1:40:00	6.10	Mjma	37.291	139.032	12	2	NIG020 Koide	37.2302	138.9652	D+	351	avnig020n5.dat
Hokkaido	11/28/2004	18:32:00	7.10	Mjma	42.946	145.274	48	8	HKD074 Nosappu	43.368	145.8026	D	275	avhkd074h1.dat
Hokkaido	11/28/2004	18:32:00	7.10	Mjma	42.946	145.274	48	8	KSRH06 TSURUI-E	43.2175	144.4325		326	avksrh06h1.dat
Hokkaido	12/14/2004	5:56:09	5.80	Mw	44.108	141.753	10	2	Minatomachi	44.1463	141.668		-1	avminato00.dat
Niigata-Ken Chuetsu aftershock 5	1/18/2005	12:50:00	4.70	Mjma	37.373	138.994	8	-1	NIG028 Nagaoka-Shisho	37.4261	138.8862		-1	avnig028n6.dat
Honshu	8/16/2005	2:46:00	7.20	Mjma	38.15	142.278	42	7	MYG002	38.7262	141.519	C	469	avmyg002m1.dat
Honshu	8/16/2005	2:46:00	7.20	Mjma	38.15	142.278	42	7	MYG004	38.7292	142.278	C	430	avmyg004m1.dat
Honshu	8/16/2005	2:46:00	7.20	Mjma	38.15	142.278	42	7	MYG011	38.3052	141.5044	B	1433	avmyg011m1.dat
Anza	6/12/2005	15:41:46	5.20	Mw	33.533	-116.578	14.1	0	Santa Rosa	33.568	-116.51		-1	avsantaros.dat
Southern Honshu (~Fukui)	3/25/2007	0:42:00	6.90	Mjma	37.22	136.685	11	2	ISK003	37.3919	136.9083	D	292	avisk003i1.dat
Southern Honshu (~Fukui)	3/25/2007	0:42:00	6.90	Mjma	37.22	136.685	11	2	ISK004	37.308	137.147	D+	325	avisk004i1.dat
Southern Honshu (~Fukui)	3/25/2007	0:42:00	6.90	Mjma	37.22	136.685	11	2	ISK005	37.2307	136.9039	D+	323	avisk005i1.dat
Southern Honshu (~Fukui)	3/25/2007	0:42:00	6.90	Mjma	37.22	136.685	11	2	ISK006	37.1602	136.6897	C	406	avisk006i1.dat
Off Southern Honshu	4/15/2007	3:19:00	5.40	Mjma	34.787	136.41	16	-1	MIEH10 GEINOU	34.8194	136.4275	C	422	avmieh10m1.dat
Off Southern Honshu	4/15/2007	3:19:00	5.40	Mjma	34.787	136.41	16	-1	MIE004	34.8569	136.4493	C	404	avmie004m1.dat
Off Southern Shikoku	4/26/2007	0:03:00	5.30	Mjma	33.888	133.583	39	-1	KOC008	33.7758	133.3465	B	818	avkoc008k1.dat
Kashiwazaki, Niigata, Japan	7/16/2007	1:13:28	6.60	Mw	37.5	138.6	10	2	NIG018 Kashiwazaki	37.3724	138.5579	D	180	avnig018m1.dat
Kashiwazaki, Niigata, Japan	7/16/2007	1:13:28	6.60	Mw	37.5	138.6	10	2	NIG019 Ojiya	37.3027	138.793	D	292	avnig019m1.dat

Table 2. Selected Points on the Cumulative Distribution Curves in Figures 2, 3, and 4.

Paramter	**Peak Acceleration**	**Peak Velocity**
Peak Vertical / Three-Dimensional Peak: Median	.47	.30
Peak Vertical / Three-Dimensional Peak: 10th Percentile	.24	.17
Geometric Mean of Horizontals / Three-Dimensional Peak: Median	.76	.76
Geometric Mean of Horizontals / Three-Dimensional Peak: 10th Percentile	.64	0.62
Largest Peak on Any Component / Three-Dimensional Peak: Median	.93	.94
Largest Peak on Any Component / Three-Dimensional Peak: 10th Percentile	.82	.79
Peak Rotated Horizontal / Three-Dimensional Peak: Median	.99	.995
Peak Rotated Horizontal / Three-Dimensional Peak: 10th Percentile	.84	.96
Angle Between Three-Dimensional Peak and Horizontal: 90th Percentile	35	12
Angle Between Three-Dimensional Peak and Horizontal: Median	1.5	-1.6
Angle Between Three-Dimensional Peak and Horizontal: 10th Percentile	-15	-14

Table 3. Top 100 accelerations and velocities

A. Top 100 accelerations

Rank	Earthquake Name	Date	Time	Magnitude	Magnitude Type	Earthquake Loatitude	Earthquake Longitude	Depth (km)	Mechanism	Station	Station Latitude	Station Longitude	Preferred NEHRP Vs30	Preferred V_s30 (m/s)	PGA 3D-Vec. (cm/s^2)	PGV 3D-Vec. (cm/s)
1	Nahanni	12/23/1985	5:16:00	6.90	Ms	62.222	-124.239	6	2	Site 1	62.199	-124.338	C	659.6	2380.6	52.27
2	Northridge	1/17/1994	12:30:55	6.70	Mw	34.2057	-118.5539	17.5	2	Tarzana	34.16	-118.534	D	257.21	1970.7	109.88
3	Cape Mendocino	4/25/1992	18:06:04	7.00	Mw	40.3338	-124.2294	21	2	Cape Mendocino, Petrolia	40.348	-124.352	D	311.8	1843.5	138.15
4	Niigata-Ken Chuetsu	10/23/2004	8:56:00	6.60	Mw	37.229	138.773	15.8	2	Kawaguchi				-1	1839.3	144.63
5	Imperial Valley 1979	10/15/1979	23:16:53	6.50	Mw	32.6435	-115.3088	9.96	0	El Centro Array #6	32.839	-115.49	D	203.2	1777.9	111.09
6	Niigata-Ken Chuetsu	10/23/2004	8:56:00	6.60	Mw	37.229	138.773	15.8	2	NIG021 Tohkamachi	37.125	138.75	C	419	1765.7	74.10
7	Northridge	1/17/1994	12:30:55	6.70	Mw	34.2057	-118.5539	17.5	2	Pacoima Dam	34.334	-118.396	A	2016.1	1743.4	111.05
8	Miyagi-Oki	5/26/2003	9:24:33	7.00	Mw	38.805	141.682	71	7	MYG011 Oshika	38.2972	141.5043	B	1433	1586.7	60.52
9	Niigata-Ken Chuetsu	10/23/2004	8:56:00	6.60	Mw	37.229	138.773	15.8	2	NIG019 Ojiya	37.3027	138.793	D	292	1533.3	136.60
10	Gazli	5/17/1976	2:58:40	6.80		40.465	63.462	18.2	2	Karakyr	40.35	63.47	C	659.6	1429.5	76.86
11	San Fernando	2/9/1971	14:00:41	6.60	Mw	34.44	-118.41	13	2	Pacoima Dam	34.334	-118.396	A	2016.1	1389.6	125.10
12	Miyagi-Oki	5/26/2003	9:24:33	7.00	Mw	38.805	141.682	71	7	IWTH04 Sumita	39.1781	141.3944	C	456.0	1311.7	40.54
13	Parkfield 2004	9/28/2004	17:15:24	6.00	Mw	35.815	-120.374	7.9	0	Fault Zone 14	35.908	-120.458		-1	1287.1	88.50
14	Victoria	6/9/1980	3:28:19	6.40	Mw	32.185	-115.076	11	0	Victoria	32.29	-115.1	D	274.5	1280.0	111.95
15	North Palm Springs	7/8/1986	9:20:44	6.20	Mw	34	-116.6117	11	3	Devers Substation	33.932	-116.579		-1	1269.0	107.43
16	Chi-Chi	9/20/1999	17:47:16	7.60	Mw	23.8603	120.7995	33	3	CHY080	23.5972	120.6777	C	553.4	1254.2	128.06
17	Coalinga	7/22/1983	2:39:54	6.00	Mw	36.241	-120.409	7.4	2	Transmitter Hill	36.249	-120.343	C	376.1	1250.1	65.81
18	Hokkaido	12/14/2004	5:56:09	5.80	Mw	44.108	141.753	10	2	Minatomachi	44.1463	141.668		-1	1206.8	70.86
19	Iran	9/16/1978	15:35:56	7.30	MW	33.37	57.02	11	2	Tabas	33.6	56.92	B	766.8	1201.5	36.51
20	El Salvador	1/13/2001	17:33:32	7.60	Mw	13.049	-88.66	60	6	Puerto La Libertad, La Libertad	13.486	-89.327		-1	1200.3	55.36
21	Morgan Hill	4/24/1984	21:15:18	6.10	Mw	37.306	-121.695	8.5	0	Coyote Lake Dam	37.118	-121.55	C	597.1	1193.5	77.25
22	Loma Prieta	10/18/1989	0:04:15	7.00	Mw	37.0407	-121.8829	17.48	3	LGPC			C	477.7	1134.3	117.89
23	Bam	12/26/2003	1:56:56	6.70	Mw	29.09	58.35	7	0	Bam	29.09	58.35		-1	1133.6	122.46

Rank	Earthquake Name	Date	Time	Magnitude	Magnitude Type	Earthquake Loatitude	Earthquake Longitude	Depth (km)	Mechanism	Station	Station Latitude	Station Longitude	Preferred NEHRP Vs30	Preferred V_s30 (m/s)	PGA 3D-Vec. (cm/s^2)	PGV 3D-Vec. (cm/s)
24	Zanjiran	6/20/1994	9:09:02	5.90	Mw	29.06	52.44		0	Zanjiran	29.07	52.62		-1	1119.2	42.68
25	Northridge	1/17/1994	12:30:55	6.70	Mw	34.2057	-118.5539	17.5	2	Jensen F.P. Generator	34.313	-118.498	C	525.8	1114.9	98.91
26	Duzce Aftershock 1	11/12/1999	17:16:50	4.80	mbGS	40.76	31.02	10	-1	IRIGM 496	40.742	30.873		-1	1105.8	37.96
27	Western Tottori	10/6/2000	4:30:19	7.10	Mw	35.275	133.3937	11	0	TTRH02 Hino	35.2281	133.3937	D	310	1104.5	125.36
28	Miyagi-Oki	5/26/2003	9:24:33	7.00	Mw	38.805	141.682	71	7	IWTH27 Rikuzentakata	39.0278	141.5356	C	670.0	1099.7	17.52
29	Duzce	11/12/1999	16:57:27	7.10	MW	40.93	31.25	18	0	IRIGM 496	40.742	30.873		-1	1071.2	50.95
30	Miyagi-Oki	5/26/2003	9:24:33	7.00	Mw	38.805	141.682	71	7	IWT007 Kamaishi	39.2701	141.8561	E	141	1061.6	25.07
31	Northridge	1/17/1994	12:30:55	6.70	Mw	34.2057	-118.5539	17.5	2	Rinaldi Receiving Station	34.281	-118.478	D	282.3	1035.5	160.48
32	Chi-Chi	9/20/1999	17:47:16	7.60	Mw	23.8603	120.7995	33	3	TCU084	23.883	120.8998	C	553.4	1034.0	124.10
33	Chi-Chi	9/20/1999	17:47:16	7.60	Mw	23.8603	120.7995	33	3	TCU129	23.8783	120.6843	C	664.4	1002.9	71.43
34	Niigata-Ken Chuetsu aftershock 3	10/23/2004	9:34:07	6.30	Mw	37.28	138.787	22.2	2	NIG021 Tohkamachi	37.125	138.75	C	419	993.7	57.70
35	Tokachi-Oki	9/25/2003	19:50:07	8.00	Mw	41.778	144.078	42	7	HKD100 Hiroo	42.2838	143.3158	D	236	992.2	52.12
36	Southern Honshu (~Fukui)	3/25/2007	0:42:00	6.90	Mjma	37.22	136.685	11	2	ISK006	37.1602	136.6897	C	406	975.8	57.24
37	Duzce	11/12/1999	16:57:27	7.10	MW	40.93	31.25	18	0	Lamont 375	40.743	30.876	C	424.8	971.7	35.72
38	Anza	6/12/2005	15:41:46	5.20	Mw	33.533	-116.578	14.1	0	Santa Rosa	33.568	-116.51		-1	959.9	17.32
39	Coalinga	7/22/1983	2:39:54	6.00	Mw	36.241	-120.409	7.4	2	Oil City	36.229	-120.36	C	376.1	958.8	47.56
40	Kyushu	5/13/1997	5:38:30	6.20	Mw	32	130.3	8	0	KGS005 Miyanojoh	31.897	130.454	C-	356	958.2	47.46
41	Northridge	1/17/1994	12:30:55	6.70	Mw	34.2057	-118.5539	17.5	2	Sepulvelda VA Hospital	34.249	-118.478	C	380.1	949.6	80.26
42	Miyagi-Oki	5/26/2003	9:24:33	7.00	Mw	38.805	141.682	71	7	MYG002 Utatsu	38.7262	141.5109	C	469	948.8	22.96
43	Chi-Chi	9/20/1999	17:47:16	7.60	Mw	23.8603	120.7995	33	3	WNT	23.8783	120.6843	C	664.4	946.7	66.45
44	Southern Honshu (~Fukui)	3/25/2007	0:42:00	6.90	Mjma	37.22	136.685	11	2	ISK005	37.2307	136.9039	D+	323	945.5	102.53
45	Parkfield 2004	9/28/2004	17:15:24	6.00	Mw	35.815	-120.374	7.9	0	Fault Zone 11	35.896	-120.398		-1	940.6	28.71
46	Imperial Valley	10/15/1979	23:16:53	6.50	Mw	32.6435	-115.3088	9.96	0	Agrarias	32.621	-115.301	D	274.5	939.4	46.63
47	Niigata-Ken Chuetsu	10/23/2004	8:56:00	6.60	Mw	37.229	138.773	15.8	2	NIG028 Nagaoka-Shisho	37.4231	138.8894		-1	913.2	67.22
48	Parkfield 2004	9/28/2004	17:15:24	6.00	Mw	35.815	-120.374	7.9	0	Stone Corral 1E	35.788	-120.294		-1	912.7	43.61
49	El Salvador	1/13/2001	17:33:32	7.60	Mw	13.049	-88.66	60	6	Santiago de Maria				-1	911.5	41.00
50	Chi-Chi	9/20/1999	17:47:16	7.60	Mw	23.8603	120.7995	33	3	TCU079	23.8395	120.8942	C	364.0	908.6	50.24
51	Kyushu	3/26/1997	8:31:47	6.30	Mw	32	130.4	8	0	KGS002 Izumi	32.087	130.356	C	442	903.9	16.63
52	Duzce	11/12/1999	16:57:27	7.10	MW	40.93	31.25	18	0	Bolu	40.746	31.607	D	326.0	901.5	64.19
53	Hokkaido	11/28/2004	18:32:00	7.10	Mjma	42.946	145.274	48	8	KSRH06 TSURUI-E	43.2175	144.4325		326	886.5	31.75
54	Kobe	1/16/1995	20:46:52	6.90	Mw	34.5948	135.0121	17.9	0	KJMA	34.6833	135.18	D	312.0	884.0	99.78
55	Northridge	1/17/1994	12:30:55	6.70	Mw	34.2057	-118.5539	17.5	2	Newhall F.S.	34.39	-118.53	D	269.1	878.6	121.71
56	Western Tottori	10/6/2000	4:30:19	7.10	Mw	35.275	133.3937	11	0	OKY004 Niimi	34.9579	133.5018	C	411	878.2	26.42
57	Valapraiso	3/3/1985	22:47:07	7.80	Mw	-33.135	-71.871	33	7	Llolleo	-32.635	-71.63		-1	878.2	43.25
58	Miyagi-Oki	5/26/2003	9:24:33	7.00	Mw	38.805	141.682	71	7	MYGH03 Karakuwa	38.9189	141.6422	B	951	874.1	14.50
59	Northridge	1/17/1994	12:30:55	6.70	Mw	34.2057	-118.5539	17.5	2	Sylmar Valve Hall Floor - Converter Station East	34.312	-118.481	C	370.5	872.2	122.56
60	El Salvador	1/13/2001	17:33:32	7.60	Mw	13.049	-88.66	60	6	Santa Tecla	13.675	-89.3		-1	868.6	60.48
61	South Iceland	6/17/2000	15:40:41	6.57	MW	63.97	-20.36	15	0	006263 Kaldarholt	64.004	-20.474		-1	868.5	45.07
62	Northridge	1/17/1994	12:30:55	6.70	Mw	34.2057	-118.5539	17.5	2	Santa Monica City Hall	34.011	-118.49	D	336.2	866.4	43.29
63	Off Southern Honshu	4/15/2007	3:19:00	5.40	Mjma	34.787	136.41	16	-1	MIEH10 GEINOU	34.8194	136.4275	C	422	862.4	27.54
64	Parkfield 2004	9/28/2004	17:15:24	6.00	Mw	35.815	-120.374	7.9	0	Fault Zone 1	35.758	-120.307		-1	861.3	82.30
65	Nisqually	2/28/2001	18:54:31	6.80	Mw	47.167	-122.733	52.4	6	Seattle	47.5842	-122.3331		-1	859.2	42.30
66	Miyagi-Oki	5/26/2003	9:24:33	7.00	Mw	38.805	141.682	71	7	IWTH02 Tamayama	39.8222	141.3861	C	390.0	855.1	19.59
67	Niigata-Ken Chuetsu	10/23/2004	8:56:00	6.60	Mw	37.229	138.773	15.8	2	NIGH01 NAGAOKA	37.4242	138.87		-1	855.0	69.77
68	Southern Honshu	3/24/2001	6:27:54	6.40	Mw	34.12	132.708	51	6	HRS009 Yuki	34.4926	132.2794	C	473	851.2	31.23
69	Kashiwazaki, Niigata, Japan	7/16/2007	1:13:28	6.60	Mw	37.5	138.6	10	2	NIG018 Kashiwazaki	37.3724	138.5579	D	180	849.5	152.11
70	Miyagi-Oki	5/26/2003	9:24:33	7.00	Mw	38.805	141.682	71	7	IWTH21 Yamada	39.4706	141.9372	C	527.0	848.6	24.22

Rank	Earthquake Name	Date	Time	Magnitude	Magnitude Type	Earthquake Loatitude	Earthquake Longitude	Depth (km)	Mechanism	Station	Station Latitude	Station Longitude	Preferred NEHRP Vs30	Preferred V_s30 (m/s)	PGA 3D-Vec. (cm/s^2)	PGV 3D-Vec. (cm/s)
71	Western Tottori	10/6/2000	4:30:19	7.10	Mw	35.275	133.3937	11	0	SMNH01 Hakuta	35.2931	133.263	C	464	843.1	43.63
72	South Iceland Aftershock	6/21/2000	0:51:48	6.49	MW	63.97	-20.71		0	006349 Thjorsarbru	63.931	-20.649		-1	833.7	104.09
73	Northridge	1/17/1994	12:30:55	6.70	Mw	34.2057	-118.5539	17.5	2	Sylmar County Hospital (Olive View)	34.326	-118.444	C	440.54	827.4	131.19
74	Niigata-Ken Chuetsu aftershock 3	10/23/2004	9:34:07	6.30	Mw	37.28	138.787	22.2	2	NIG019 Ojiya	37.3027	138.793	D	292	826.5	71.61
75	Niigata-Ken Chuetsu aftershock 1	10/23/2004	9:03:00	6.30	Mjma	37.35	138.985	9	2	NIGH01 Nagaoka	37.4242	138.87		-1	826.3	41.86
76	Valapraiso	3/3/1985	22:47:07	7.80	Mw	-33.135	-71.871	33	7	San Isidro				-1	823.0	45.80
77	Chi-Chi	9/20/1999	17:47:16	7.60	Mw	23.8603	120.7995	33	3	TCU071	23.9855	120.7883	C	624.9	820.4	71.43
78	Northridge	1/17/1994	12:30:55	6.70	Mw	34.2057	-118.5539	17.5	2	17645 Saticoy St., Northridge	34.2089	-118.5172	D	280.9	812.7	62.72
79	Chi-Chi	9/20/1999	17:47:16	7.60	Mw	23.8603	120.7995	33	3	CHY028	23.632	120.6052	C	542.6	812.1	80.17
80	Tokachi-Oki	9/25/2003	19:50:07	8.00	Mw	41.778	144.078	42	7	HKD086 Chokubetsu	42.8526	143.8636	D	201	810.8	80.87
81	Duzce Aftershock 2	11/12/1999	17:17:56	5.50	mbGS	40.78	31.12	10	-1	IRIGM 496	40.742	30.873		-1	810.2	33.88
82	Landers	6/28/1992	11:57:34	7.30	Mw	34.201	-116.436	7	0	Lucerne	34.5675	-116.6122	C	684.9	807.5	147.49
83	Northridge aftershock	1/29/1994	11:20:35	5.10	Mw	34.31	-118.58		-1	Brown's Canyon	34.307	-118.603		-1	803.9	39.59
84	Western Tottori	10/6/2000	4:30:19	7.10	Mw	35.275	133.3937	11	0	TTR007 Kohfu	35.2826	133.4876	C	404	797.8	42.45
85	Northridge	1/17/1994	12:30:55	6.70	Mw	34.2057	-118.5539	17.5	2	Simi Valley	34.264	-118.666	C	557.4	796.2	68.31
86	Chi-Chi	9/20/1999	17:47:16	7.60	Mw	23.8603	120.7995	33	3	TCU065	24.0588	120.6912	D	305.9	795.8	151.42
87	Northridge	1/17/1994	12:30:55	6.70	Mw	34.2057	-118.5539	17.5	2	Sylmar Converter Stn Valve Group 7	34.311	-118.49	D	251.24	786.2	134.93
88	Parkfield 2004	9/28/2004	17:15:24	6.00	Mw	35.815	-120.374	7.9	0	Joaquin Canyon	35.9397	-120.4319		-1	781.9	32.82
89	Off Southern Honshu	4/15/2007	3:19:00	5.40	Mjma	34.787	136.41	16	-1	MIE004	34.8569	136.4493	C	404	781.8	35.19
90	Imperial Valley 1979	10/15/1979	23:16:53	6.50	Mw	32.6435	-115.3088	9.96	0	Bonds Corner	32.6932	-115.3382	D	223.0	781.1	53.13
91	North Palm Springs	7/8/1986	9:20:44	6.20	Mw	34	-116.6117	11	3	North Palm Springs Post Office	33.924	-116.543	D	345.4	769.0	74.27
92	Kyushu	5/13/1997	5:38:30	6.20	Mw	32	130.3	8	0	KGS002 Izumi	32.0909	130.3532	C	442	763.4	23.05
93	Manjil, Iran	6/20/1990	9:00:10	7.40	Mw	36.95	49.52	18	0	Abbar	36.92	48.97	C	724.0	762.8	101.55
94	Niigata-Ken Chuetsu aftershock 3	10/23/2004	9:34:07	6.30	Mw	37.28	138.787	22.2	2	NIGH11 Kawanishi	37.1697	138.7472	C	375	761.6	47.36
95	Kobe	1/16/1995	20:46:52	6.90	Mw	34.5948	135.0121	17.9	0	Takarazuka	34.809	135.344	D	312.0	756.5	89.50
96	Western Tottori	10/6/2000	4:30:19	7.10	Mw	35.275	133.3937	11	0	TTR009 Nichinan	35.1629	133.3063	C	423	745.7	41.59
97	Imperial Valley 1979	10/15/1979	23:16:53	6.50	Mw	32.6435	-115.3088	9.96	0	Differential Array	32.796	-115.535	D	202.3	742.7	74.39
98	Parkfield 2004	9/28/2004	17:15:24	6.00	Mw	35.815	-120.374	7.9	0	Cholame 3E	35.77	-120.247		-1	741.6	34.77
99	Umbria Marche, Italy	9/26/1997	9:40:33	6.04	Mw	43.031	12.862	6	1	0594 Nocera Umbra	43.113	12.785		-1	737.0	40.73
100	Michoacan Aftershock	9/21/1985	1:37:13	7.50	Mw	17.8	-101.65	30	7	Paraiso	17.343	-100.225		-1	736.1	12.43

B. Top 100 velocities

Rank	Earthquake Name	Date	Time	Magnitude	Magnitude Type	Earthquake Loatitude	Earthquake Longitude	Depth (km)	Mechanism	Station	Station Latitude	Station Longitude	Preferred NEHRP Vs30	Preferred V_s30 (m/s)	PGA 3D-Vec. (cm/s^2)	PGV 3D-Vec. (cm/s)
1	Chi-Chi	9/20/1999	17:47:16	7.60	Mw	23.8603	120.7995	33	3	TCU068	24.2772	120.7658	C	487.3	583.5	317.57
2	Chi-Chi	9/20/1999	17:47:16	7.60	Mw	23.8603	120.7995	33	3	TCU052	24.198	120.7393	C	393.2	502.2	200.45
3	Kobe	1/16/1995	20:46:52	6.90	Mw	34.5948	135.0121	17.9	0	Takatori	34.649	135.139	D	256.0	688.1	169.72
4	Northridge	1/17/1994	12:30:55	6.70	Mw	34.2057	-118.5539	17.5	2	Rinaldi Receiving Station	34.281	-118.478	D	282.3	1035.5	160.48
5	Kashiwazaki, Niigata, Japan	7/16/2007	1:13:28	6.60	Mw	37.5	138.6	10	2	NIG018 Kashiwazaki	37.3724	138.5579	D	180	849.5	152.11
6	Chi-Chi	9/20/1999	17:47:16	7.60	Mw	23.8603	120.7995	33	3	TCU065	24.0588	120.6912	D	305.9	795.8	151.42
7	Landers	6/28/1992	11:57:34	7.30	Mw	34.201	-116.436	7	0	Lucerne	34.5675	-116.6122	C	684.9	807.5	147.49
8	Niigata-Ken Chuetsu	10/23/2004	8:56:00	6.60	Mw	37.229	138.773	15.8	2	Kawaguchi				-1	1839.3	144.63
9	Cape Mendocino	4/25/1992	18:06:04	7.00	Mw	40.3338	-124.2294	21	2	Cape Mendocino,	40.348	-124.352	D	311.8	1843.5	138.15

Rank	Earthquake Name	Date	Time	Magnitude	Magnitude Type	Earthquake Loatitude	Earthquake Longitude	Depth (km)	Mechanism	Station	Station Latitude	Station Longitude	Preferred NEHRP Vs30	Preferred V_s30 (m/s)	PGA 3D-Vec. (cm/s^2)	PGV 3D-Vec. (cm/s)
										Petrolia						
10	Niigata-Ken Chuetsu	10/23/2004	8:56:00	6.60	Mw	37.229	138.773	15.8	2	NIG019 Ojiya	37.3027	138.793	D	292	1533.3	136.60
11	Northridge	1/17/1994	12:30:55	6.70	Mw	34.2057	-118.5539	17.5	2	Sylmar Converter Stn Valve Group 7	34.311	-118.49	D	251.24	786.2	134.93
12	Northridge	1/17/1994	12:30:55	6.70	Mw	34.2057	-118.5539	17.5	2	Sylmar County Hospital (Olive View)	34.326	-118.444	C	440.54	827.4	131.19
13	Chi-Chi	9/20/1999	17:47:16	7.60	Mw	23.8603	120.7995	33	3	CHY080	23.5972	120.6777	C	553.4	1254.2	128.06
14	Western Tottori	10/6/2000	4:30:19	7.10	Mw	35.275	133.3937	11	0	TTRH02 Hino	35.2281	133.3937	D	310	1104.5	125.36
15	San Fernando	2/9/1971	14:00:41	6.60	Mw	34.44	-118.41	13	2	Pacoima Dam	34.334	-118.396	A	2016.1	1389.6	125.10
16	Chi-Chi	9/20/1999	17:47:16	7.60	Mw	23.8603	120.7995	33	3	TCU084	23.883	120.8998	C	553.4	1034.0	124.10
17	Northridge	1/17/1994	12:30:55	6.70	Mw	34.2057	-118.5539	17.5	2	Sylmar Converter Stn Valve Group 1-6 (East)	34.312	-118.481	C	370.52	684.9	123.74
18	Northridge	1/17/1994	12:30:55	6.70	Mw	34.2057	-118.5539	17.5	2	Sylmar Valve Hall Floor - Converter Station East	34.312	-118.481	C	370.5	872.2	122.56
19	Bam	12/26/2003	1:56:56	6.70	Mw	29.09	58.35	7	0	Bam	29.09	58.35		-1	1133.6	122.46
20	Northridge	1/17/1994	12:30:55	6.70	Mw	34.2057	-118.5539	17.5	2	Newhall F.S.	34.39	-118.53	D	269.1	878.6	121.71
21	Loma Prieta	10/18/1989	0:04:15	7.00	Mw	37.0407	-121.8829	17.48	3	Los Gatos Lexington Dam	37.202	-121.949	B	1070.3	462.5	121.50
22	Superstition Hills	11/24/1987	13:16:00	6.70	MLbrk	33.01	-115.84	2	0	Superstition Mtn. Camera	32.955	-115.823	C	362.4	206.6	120.79
23	Northridge	1/17/1994	12:30:55	6.70	Mw	34.2057	-118.5539	17.5	2	West Pico Canyon Road	34.391	-118.621	D	285.9	414.1	118.49
24	Loma Prieta	10/18/1989	0:04:15	7.00	Mw	37.0407	-121.8829	17.48	3	LGPC			C	477.7	1134.3	117.89
25	Northridge	1/17/1994	12:30:55	6.70	Mw	34.2057	-118.5539	17.5	2	Jensen F.P. Administration Bldg	34.312	-118.496	C	373.1	621.9	116.86
26	Chi-Chi	9/20/1999	17:47:16	7.60	Mw	23.8603	120.7995	33	3	TCU102	24.2493	120.7208	C	714.3	308.2	115.47
27	Superstition Hills	11/24/1987	13:15:56	6.70	MLbrk	33.01	-115.84	2	0	Parachute Test Site	32.93	-115.7	D	348.7	556.3	114.67
28	Chi-Chi	9/20/1999	17:47:16	7.60	Mw	23.8603	120.7995	33	3	TCU075	23.9827	120.6778	C	549.4	331.5	113.01
29	Victoria	6/9/1980	3:28:19	6.40	Mw	32.185	-115.076	11	0	Victoria	32.29	-115.1	D	274.5	1280.0	111.95
30	Imperial Valley 1979	10/15/1979	23:16:53	6.50	Mw	32.6435	-115.3088	9.96	0	El Centro Array #6	32.839	-115.49	D	203.2	1777.9	111.09
31	Northridge	1/17/1994	12:30:55	6.70	Mw	34.2057	-118.5539	17.5	2	Pacoima Dam	34.334	-118.396	A	2016.1	1743.4	111.05
32	Northridge	1/17/1994	12:30:55	6.70	Mw	34.2057	-118.5539	17.5	2	Tarzana	34.16	-118.534	D	257.21	1970.7	109.88
33	Chi-Chi	9/20/1999	17:47:16	7.60	Mw	23.8603	120.7995	33	3	CHY101	23.6862	120.5622	D	258.9	508.9	109.87
34	North Palm Springs	7/8/1986	9:20:44	6.20	Mw	34	-116.6117	11	3	Devers Substation	33.932	-116.579		-1	1269.0	107.43
35	South Iceland Aftershock	6/21/2000	0:51:48	6.49	MW	63.97	-20.71		0	006334 Solheimar	64.065	-20.642		-1	727.9	107.03
36	Imperial Valley 1979	10/15/1979	23:16:53	6.50	Mw	32.6435	-115.3088	9.96	0	EC Meloland Overpass	32.773	-115.448	D	186.2	434.3	104.26
37	South Iceland Aftershock	6/21/2000	0:51:48	6.49	MW	63.97	-20.71		0	006349 Thjorsarbru	63.931	-20.649		-1	833.7	104.09
38	Denali, Alaska	11/3/2002	22:13:00	7.90	Ms	63.23	-144.89	15	0	Taps Pump Station #10	63.4239	-145.7658	D	329.4	399.0	103.93
39	Southern Honshu (~Fukui)	3/25/2007	0:42:00	6.90	Mjma	37.22	136.685	11	2	ISK005	37.2307	136.9039	D+	323	945.5	102.53
40	Manjil, Iran	6/20/1990	9:00:10	7.40	Mw	36.95	49.52	18	0	Abbar	36.92	48.97	C	724.0	762.8	101.55
41	Kobe	1/16/1995	20:46:52	6.90	Mw	34.5948	135.0121	17.9	0	KJMA	34.6833	135.18	D	312.0	884.0	99.78
42	Northridge	1/17/1994	12:30:55	6.70	Mw	34.2057	-118.5539	17.5	2	Jensen F.P. Generator	34.313	-118.498	C	525.8	1114.9	98.91
43	Cape Mendocino	4/25/1992	18:06:14	7.00	Mw	40.3338	-124.2294	9.6	2	Petrolia Gen Store 1	40.325	-124.287	C	712.8	697.2	98.79
44	Erzican	3/13/1992	17:18:40	6.90	MSbrk	39.705	39.587	9	0	Erzincan			D	274.5	540.8	95.54
45	Chi-Chi	9/20/1999	17:47:16	7.60	Mw	23.8603	120.7995	33	3	TCU067	24.0912	120.72	C	433.6	560.2	93.67
46	Chi-Chi	9/20/1999	17:47:16	7.60	Mw	23.8603	120.7995	33	3	TCU103	24.3098	120.7072	C	494.1	192.7	90.64
47	Kobe	1/16/1995	20:46:52	6.90	Mw	34.5948	135.0121	17.9	0	Takarazuka	34.809	135.344	D	312.0	756.5	89.50
48	Imperial Valley 1979	10/15/1979	23:16:53	6.50	Mw	32.6435	-115.3088	9.96	0	El Centro Array #5	32.855	-115.47	D	205.6	570.5	88.89
49	Parkfield 2004	9/28/2004	17:15:24	6.00	Mw	35.815	-120.374	7.9	0	Fault Zone 14	35.908	-120.458		-1	1287.1	88.50
50	Northridge	1/17/1994	12:30:55	6.70	Mw	34.2057	-118.5539	17.5	2	14145 Mullholand Dr.	34.132	-118.439	D	355.8	532.2	87.72
51	Imperial Valley 1979	10/15/1979	23:16:53	6.50	Mw	32.6435	-115.3088	9.96	0	El Centro Array #7	32.829	-115.5	D	210.5	623.9	87.48

Rank	Earthquake Name	Date	Time	Magnitude	Magnitude Type	Earthquake Loatitude	Earthquake Longitude	Depth (km)	Mechanism	Station	Station Latitude	Station Longitude	Preferred NEHRP Vs30	Preferred V_s30 (m/s)	PGA 3D-Vec. (cm/s^2)	PGV 3D-Vec. (cm/s)
52	Kocaeli, Turkey	8/17/1999	0:01:40	7.60	Mw-hrv	40.702	29.987	17	0	Yarimca	40.7639	29.762	D	297.0	377.1	87.30
53	Duzce	11/12/1999	16:57:27	7.10	MW	40.93	31.25	18	0	Duzce	40.843	31.151	D	276.0	534.8	86.86
54	Chi-Chi	9/20/1999	17:47:16	7.60	Mw	23.8603	120.7995	33	3	TCU063	24.1083	120.6158	D	272.6	200.0	86.37
55	South Iceland Aftershock	6/21/2000	0:51:48	6.49	MW	63.97	-20.71		0	006332 Thjorsartun	63.928	-20.648		-1	704.1	86.27
56	Kobe	1/16/1995	20:46:52	6.90	Mw	34.5948	135.0121	17.9	0	Port Island, Kobe	34.67	135.201	D	198.0	552.5	85.63
57	Chi-Chi	9/20/1999	17:47:16	7.60	Mw	23.8603	120.7995	33	3	TCU101	24.242	120.7092	D	272.6	266.3	85.61
58	Chi-Chi	9/20/1999	17:47:16	7.60	Mw	23.8603	120.7995	33	3	TCU076	23.9077	120.6757	C	573.0	461.8	82.76
59	Chi-Chi	9/20/1999	17:47:16	7.60	Mw	23.8603	120.7995	33	3	WGK	23.6862	120.5622	D	258.9	500.2	82.74
60	Parkfield 2004	9/28/2004	17:15:24	6.00	Mw	35.815	-120.374	7.9	0	Fault Zone 1	35.758	-120.307		-1	861.3	82.30
61	Tokachi-Oki	9/25/2003	19:50:07	8.00	Mw	41.778	144.078	42	7	HKD086 Chokubetsu	42.8526	143.8636	D	201	810.8	80.87
62	Northridge	1/17/1994	12:30:55	6.70	Mw	34.2057	-118.5539	17.5	2	Sepulvelda VA Hospital	34.249	-118.478	C	380.1	949.6	80.26
63	Chi-Chi	9/20/1999	17:47:16	7.60	Mw	23.8603	120.7995	33	3	CHY028	23.632	120.6052	C	542.6	812.1	80.17
64	Chi-Chi	9/20/1999	17:47:16	7.60	Mw	23.8603	120.7995	33	3	TCU128	24.4162	120.7607	C	599.6	199.7	80.13
65	Chi-Chi	9/20/1999	17:47:16	7.60	Mw	23.8603	120.7995	33	3	TCU039	24.04917	120.7837	C	540.7	220.2	79.73
66	Chi-Chi	9/20/1999	17:47:16	7.60	Mw	23.8603	120.7995	33	3	TCU074	23.9622	120.9618	C	468.1	608.4	79.06
67	Imperial Valley 1979	10/15/1979	23:16:53	6.50	Mw	32.6435	-115.3088	9.96	0	El Centro Array #4	32.864	-115.5	D	208.9	546.0	77.83
68	Tokachi-Oki	9/25/2003	19:50:07	8.00	Mw	41.778	144.078	42	7	HKD066 Shibetsu	43.6619	145.1307	E	126	578.0	77.73
69	Morgan Hill	4/24/1984	21:15:18	6.10	Mw	37.306	-121.695	8.5	0	Coyote Lake Dam	37.118	-121.55	C	597.1	1193.5	77.25
70	Gazli	5/17/1976	2:58:40	6.80		40.465	63.462	18.2	2	Karakyr	40.35	63.47	C	659.6	1429.5	76.86
71	Imperial Valley 1979	10/15/1979	23:16:53	6.50	Mw	32.6435	-115.3088	9.96	0	El Centro Array #8	32.811	-115.53	D	206.1	635.0	76.14
72	Northridge	1/17/1994	12:30:55	6.70	Mw	34.2057	-118.5539	17.5	2	Pardee			D	345.4	703.5	75.60
73	Parkfield	6/28/1966	4:26:14	6.10	Mw	36	-120.5	10	0	Cholome 2wa	35.733	-120.29	D	184.8	473.4	75.34
74	Northridge	1/17/1994	12:30:55	6.70	Mw	34.2057	-118.5539	17.5	2	LA Dam	34.294	-118.483	C	629.0	337.7	75.06
75	Loma Prieta	10/18/1989	0:05:00	7.00	Mw	37.0407	-121.8829	17.48	3	Saratoga	37.255	-122.031	C	370.8	408.2	74.66
76	Coalinga	5/2/1983	23:42:38	6.50	Mw	36.233	-120.31	4.6	2	Pleasant Valley P.P. yard	36.308	-120.249	D	257.4	608.4	74.58
77	Imperial Valley 1979	10/15/1979	23:16:53	6.50	Mw	32.6435	-115.3088	9.96	0	Differential Array	32.796	-115.535	D	202.3	742.7	74.39
78	North Palm Springs	7/8/1986	9:20:44	6.20	Mw	34	-116.6117	11	3	North Palm Springs Post Office	33.924	-116.543	D	345.4	769.0	74.27
79	Niigata-Ken Chuetsu	10/23/2004	8:56:00	6.60	Mw	37.229	138.773	15.8	2	NIG021 Tohkamachi	37.125	138.75	C	419	1765.7	74.10
80	Chi-Chi	9/20/1999	17:47:16	7.60	Mw	23.8603	120.7995	33	3	TCU072	20.0407	120.8488	C	468.1	476.0	73.27
81	Niigata-Ken Chuetsu aftershock 3	10/23/2004	9:34:07	6.30	Mw	37.28	138.787	22.2	2	NIG019 Ojiya	37.3027	138.793	D	292	826.5	71.61
82	Chi-Chi	9/20/1999	17:47:16	7.60	Mw	23.8603	120.7995	33	3	TCU129	23.8783	120.6843	C	664.4	1002.9	71.43
83	Chi-Chi	9/20/1999	17:47:16	7.60	Mw	23.8603	120.7995	33	3	TCU071	23.9855	120.7883	C	624.9	820.4	71.43
84	Hokkaido	12/14/2004	5:56:09	5.80	Mw	44.108	141.753	10	2	Minatomachi	44.1463	141.668		-1	1206.8	70.86
85	Niigata-Ken Chuetsu	10/23/2004	8:56:00	6.60	Mw	37.229	138.773	15.8	2	NIGH01 NAGAOKA	37.4242	138.87		-1	855.0	69.77
86	Kocaeli, Turkey	8/17/1999	0:01:40	7.60	Mw-hrv	40.702	29.987	17	0	Sakarya	40.7639	29.762	C	471.0	436.6	68.68
87	Niigata-Ken Chuetsu	10/23/2004	8:56:00	6.60	Mw	37.229	138.773	15.8	2	NIGH11 Kawanishi	37.1697	138.7472	C	375	647.5	68.50
88	Northridge	1/17/1994	12:30:55	6.70	Mw	34.2057	-118.5539	17.5	2	Simi Valley	34.264	-118.666	C	557.4	796.2	68.31
89	Chi-Chi	9/20/1999	17:47:16	7.60	Mw	23.8603	120.7995	33	3	TCU055	24.1392	120.6643	D	272.6	294.7	68.06
90	Chi-Chi	9/20/1999	17:47:16	7.60	Mw	23.8603	120.7995	33	3	CHY006	23.5815	120.552	C	438.2	424.8	67.77
91	Chi-Chi	9/20/1999	17:47:16	7.60	Mw	23.8603	120.7995	33	3	TCU049	24.179	120.6902	C	487.3	325.6	67.76
92	Niigata-Ken Chuetsu	10/23/2004	8:56:00	6.60	Mw	37.229	138.773	15.8	2	NIG028 Nagaoka-Shisho	37.4231	138.8894		-1	913.2	67.22
93	Chi-Chi	9/20/1999	17:47:16	7.60	Mw	23.8603	120.7995	33	3	TCU036	24.4488	120.6963	D	272.6	141.7	67.16
94	Chi-Chi	9/20/1999	17:47:16	7.60	Mw	23.8603	120.7995	33	3	TCU087	24.3482	120.7733	C	473.9	140.5	66.99
95	Chi-Chi	9/20/1999	17:47:16	7.60	Mw	23.8603	120.7995	33	3	WNT	23.8783	120.6843	C	664.4	946.7	66.45
96	Chi-Chi	9/20/1999	17:47:16	7.60	Mw	23.8603	120.7995	33	3	CHY024	23.757	120.6062	C	427.7	310.7	66.44
97	Coalinga	7/22/1983	2:39:54	6.00	Mw	36.241	-120.409	7.4	2	Transmitter Hill	36.249	-120.343	C	376.1	1250.1	65.81
98	El Salvador	1/13/2001	17:33:32	7.60	Mw	13.049	-88.66	60	6	Armenia, Sonsonate	13.744	-89.501		-1	611.2	65.14
99	Northridge	1/17/1994	12:30:55	6.70	Mw	34.2057	-118.5539	17.5	2	Canoga Park	34.2119	-118.6056	D	267.5	473.6	65.08
100	Parkfield 2004	9/28/2004	17:15:24	6.00	Mw	35.815	-120.374	7.9	0	CHOLAME 2WA	35.733	-120.29		-1	598.5	64.73

Table 4. Estimate of Level of Instrumentation Effort for Selected Accelerograph Networks

Strong Motion Network	Number of Instruments	Year Installed	Present	Years	Inst-Years	Assumptions
USGS	700	1980	2007.5	27.5	19250	assumed built on timetable similar to CSMIP
USGS	300	2000	2007.5	7.5	2250	estimate last 300 in ANSS
CSMIP	650	1980	2007.5	27.5	17875	established 1972, assumed complete 1990
Guerrero	30	1986	2007.5	21.5	645	Some instruments installed 1985 - use average installation date
K-Net	1000	1996.5	2007.5	11	11000	Estimated start date from earliest records on web
Kik-Net	680	2000.5	2007.5	7	4276	Precise calculation
Taiwan	708	1994	2007.5	13.5	9558	Estimated start date, from dates of early earthquakes
Iran	1094	1982	2007.5	25.5	27897	start in 1973, assume complete in 1990
Turkey	114	1973	2007.5	34.5	3933	From info in web site: http://angora.deprem.gov.tr/TKYHAKKen.htm, July 2007
Turkey	20	2001	2007.5	6.5	130	ditto
Total					**96814**	

14.0 Figures

Figure 1. Earthquake Locations

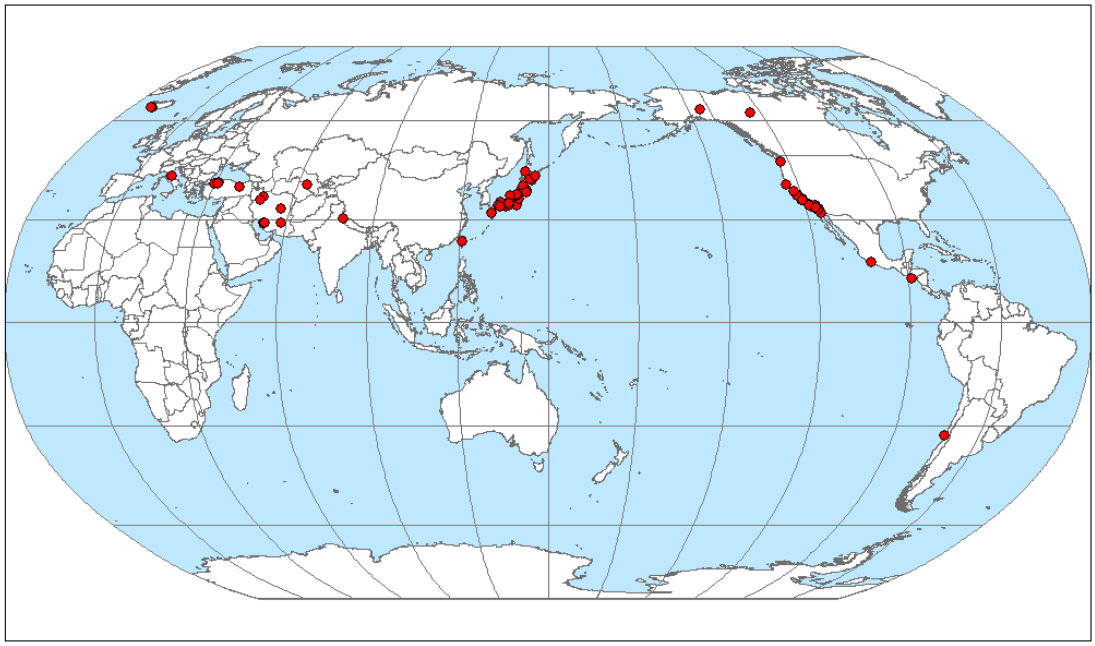

Figure 1. Locations of earthquakes represented in the data set of exceptional accelerograms. The earthquakes are listed in Table 1.

Figure 2. Distribution of Ratios among Various Peak Acceleration Intensity Measures

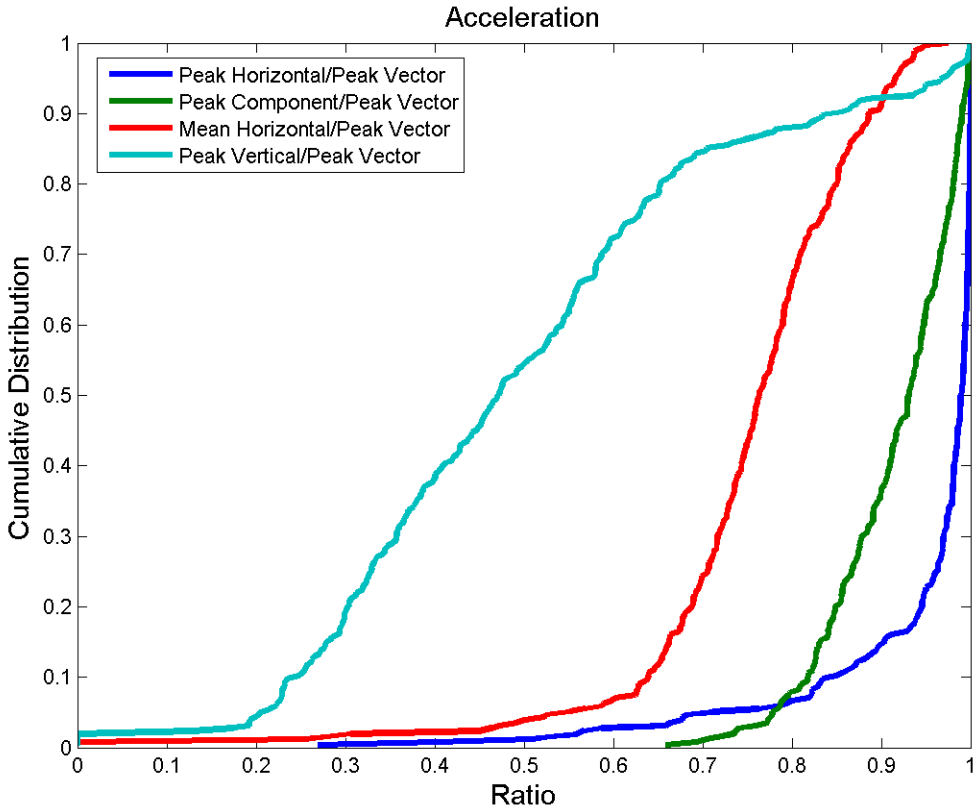

Figure 2. Distribution of ratios among various peak acceleration intensity measures. The denominator ("Peak Vector") in all cases is the peak magnitude of the 3-component acceleration vector. "Peak Horizontal" is the peak magnitude of the 2-component horizontal acceleration vector. "Peak Component" is the peak acceleration on the largest of the three individual components as recorded. "Mean Horizontal" is the geometrical mean of the peak accelerations of the two horizontal components as recorded. "Peak Vertical" is the peak acceleration on the vertical component. All 255 accelerograms in Table 1 are used to develop this distribution. For records where one of the horizontal components is missing, the peak on that component is treated as equal to zero. The figure is generated by the script **j10s1.m** in directory *C:\Task_22\Analysis\Statistics-1*. The file name is *C:\Task_22\Analysis\Statistics-1\J4_4.png*.

Figure 3. Distribution of Ratios among Various Peak Velocity Intensity Measures

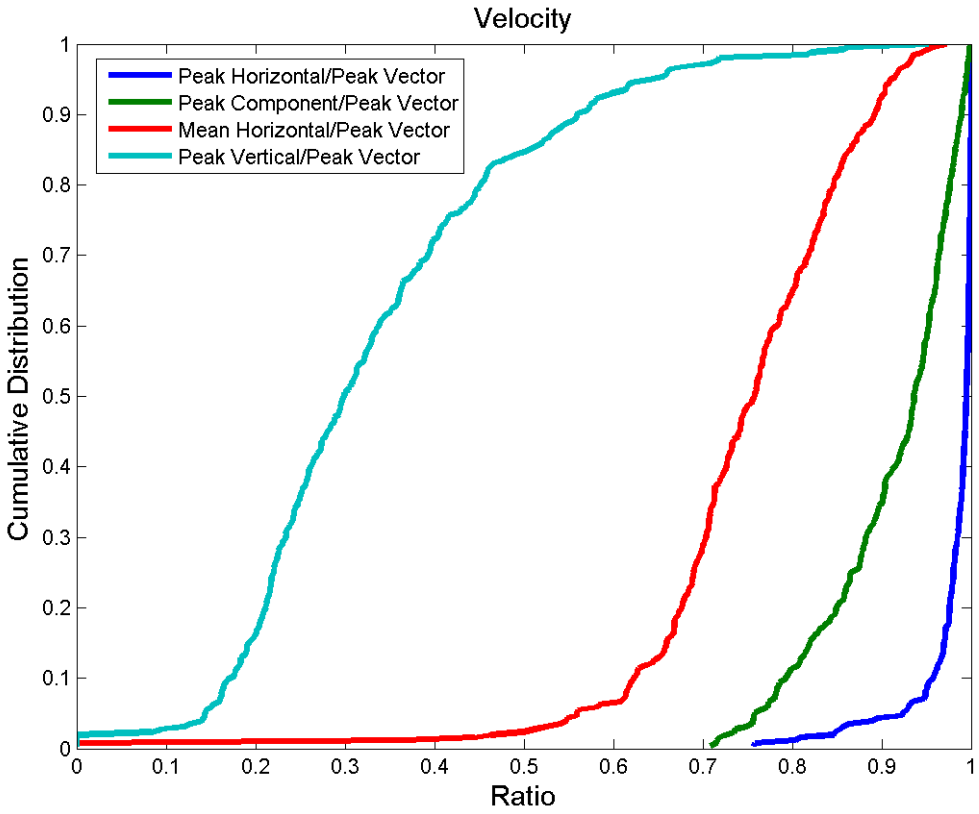

Figure 3. Distribution of ratios among various peak velocity intensity measures. See the caption for an explanation of the variables, which are applied to the velocity rather than acceleration in this figure. The figure is generated by the script **j10s1.m** in directory *C:\Task_22\Analysis\Statistics-1*. The file name is *C:\Task_22\Analysis\Statistics-1\J4_5.png*.

Figure 4. Distribution of Angles between the Peak 3-Component Vectors and Horizontal

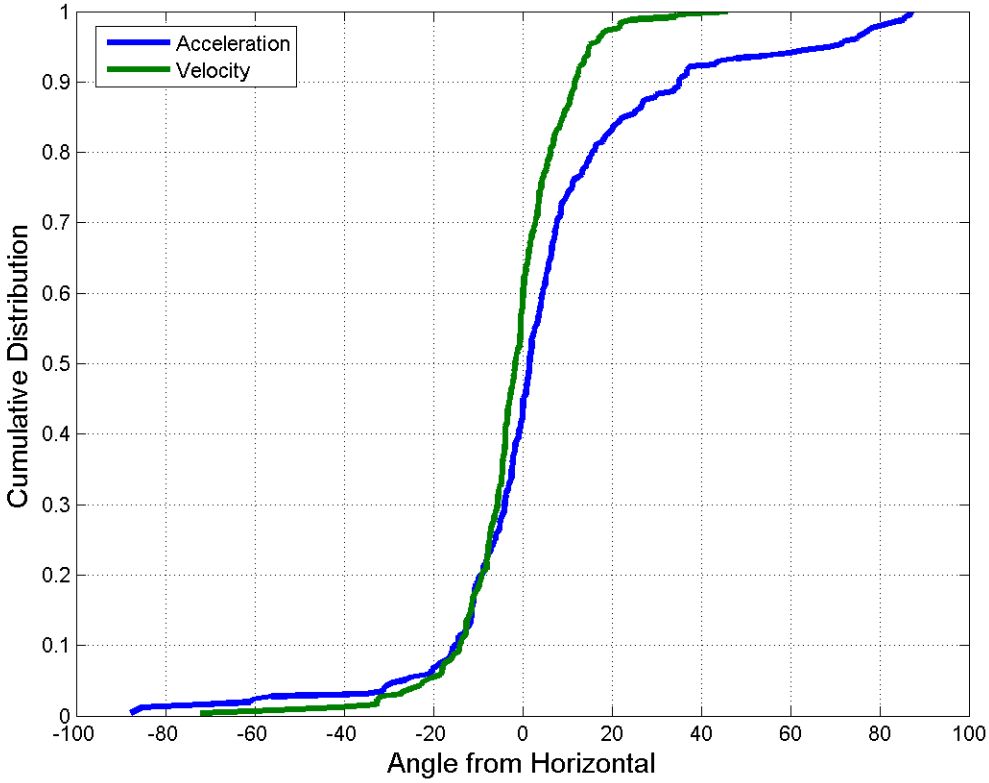

Figure 4. Distribution of angles between the peak 3-component vectors and horizontal. For each 3-component accelerogram, the angle between the acceleration vector and the horizontal is measured at the time when the magnitude of the 3-component acceleration is maximum. The algorithm for velocity is the same. All 255 accelerograms in Table 1 are used to develop this distribution. The figure is generated by the script **j10s1.m** in directory *C:\Task_22\Analysis\Statistics-1*. The file name is *C:\Task_22\Analysis\Statistics-1\J4_7.png*.

Figure 5. Distribution of Ratio of the Two Observed Horizontal Components

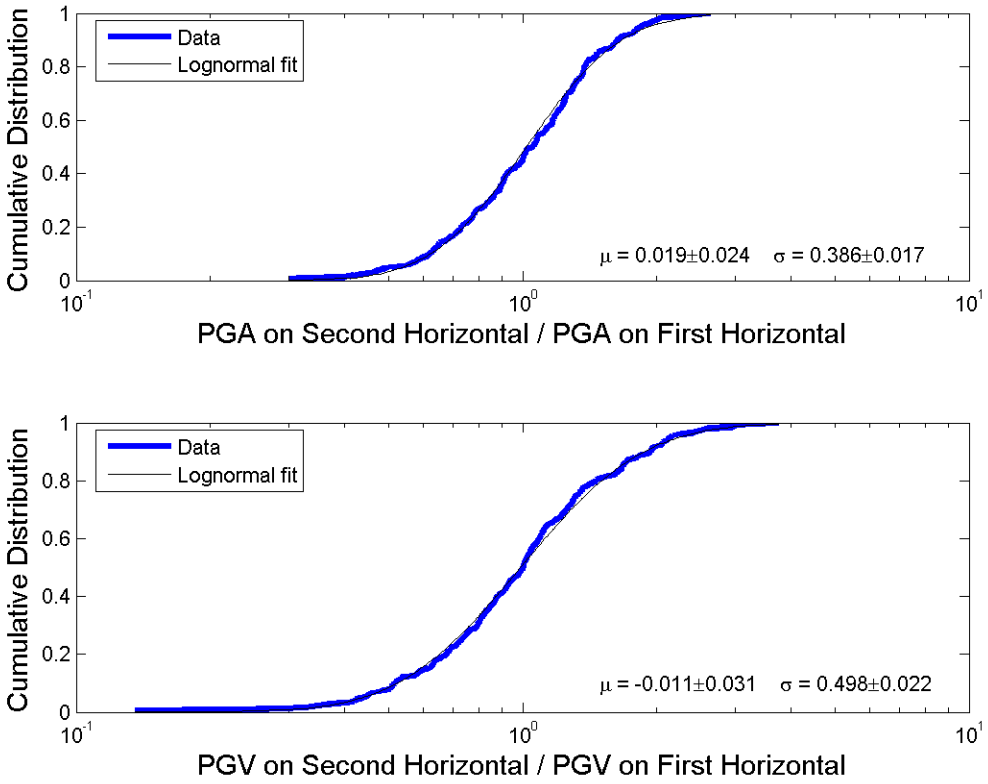

Figure 5. Distribution of the ratio of the peak value of the second (generally more northerly) observed horizontal component to the first (generally more easterly) component. The upper figure is for peak acceleration, and the lower is for peak velocity. The pale black line is the best-fitting lognormal distribution for these ratios; the mean (μ) and standard deviation (σ) of the distribution are given in the figure. The figure is generated by the script **j10s1.m** in directory *C:\Task_22\Analysis\Statistics-1*. The file name is *C:\Task_22\Analysis\Statistics-1\J4_10.png*.

Figure 6. Distribution of Peak Acceleration and Peak Velocity in the Selected Data

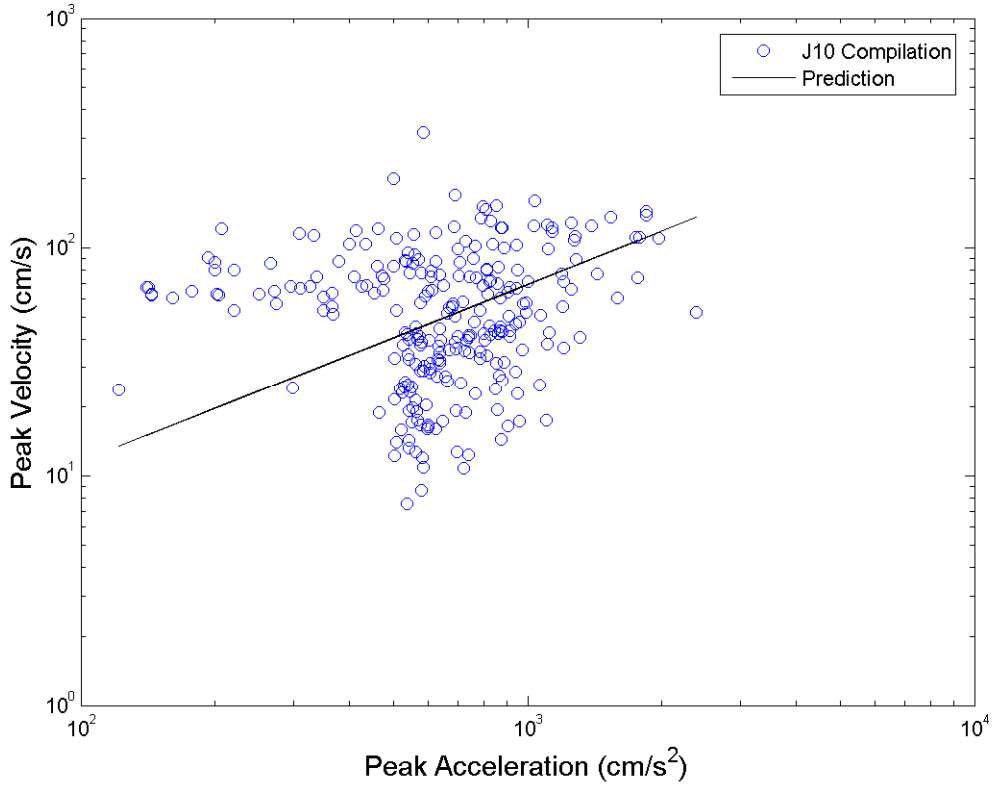

Figure 6. Distribution of peak acceleration and peak velocity for the accelerograms listed in Table 1. PGA and PGV are the vector peak values. The "predicted" line is the relationship: $\ln(PGV) = 4.22 + 0.776\ln(PGA)$, where the units of *PGA* are fraction of the acceleration of gravity, and the units of *PGV* are cm/s. This relationship was developed for the PEGASOS project (Abrahamson et al, 2002). The points in this figure represent only the upper-right tip of other compilations of strong-motion data. Figure 6 is generated by the script **j10s1.m** in directory *C:\Task_22\Analysis\Statistics-1*. The file name is *C:\Task_22\Analysis\Statistics-1\J4_5.png*.

Figure 7. Exceptional ground motions over time

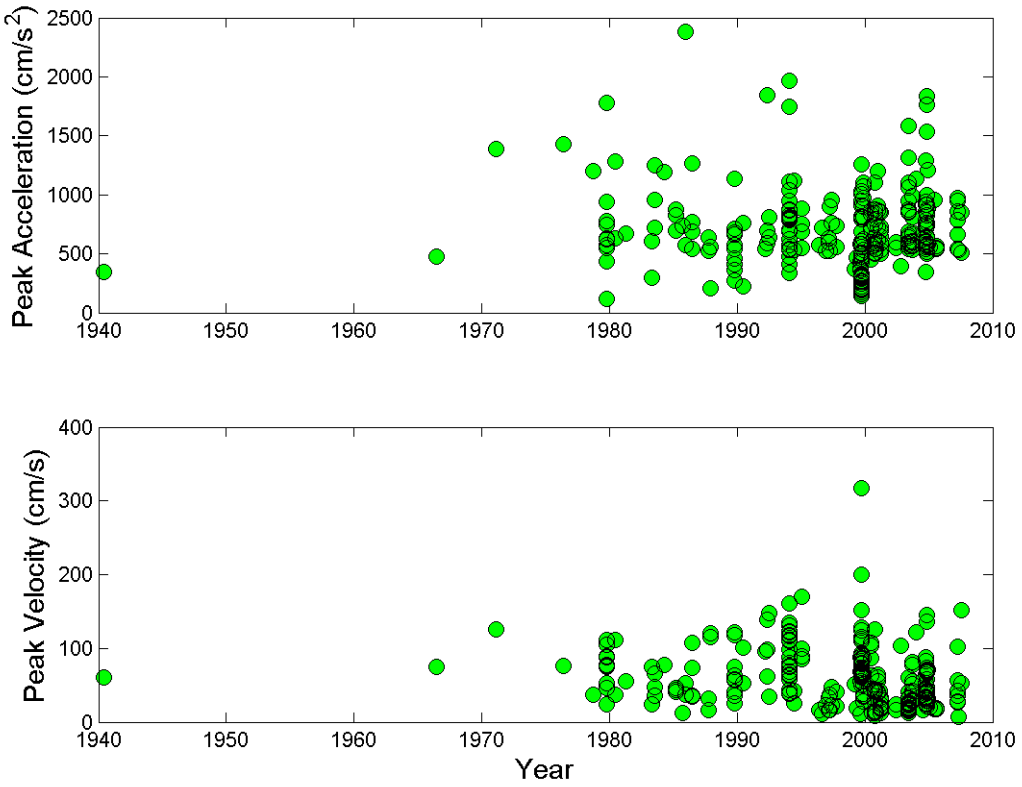

Figure 7. Exceptional ground motions over time. Peak acceleration and peak velocity of the records in Table 1, shown as a function of the time that they were recorded. This figure is generated by the script **j10s1.m** in directory *C:\Task_22\Analysis\Statistics-1*. The file name is *C:\Task_22\Analysis\Statistics-1\J4_1.png*.

Figure 8. Exceptional Ground Motions vs Moment Magnitude

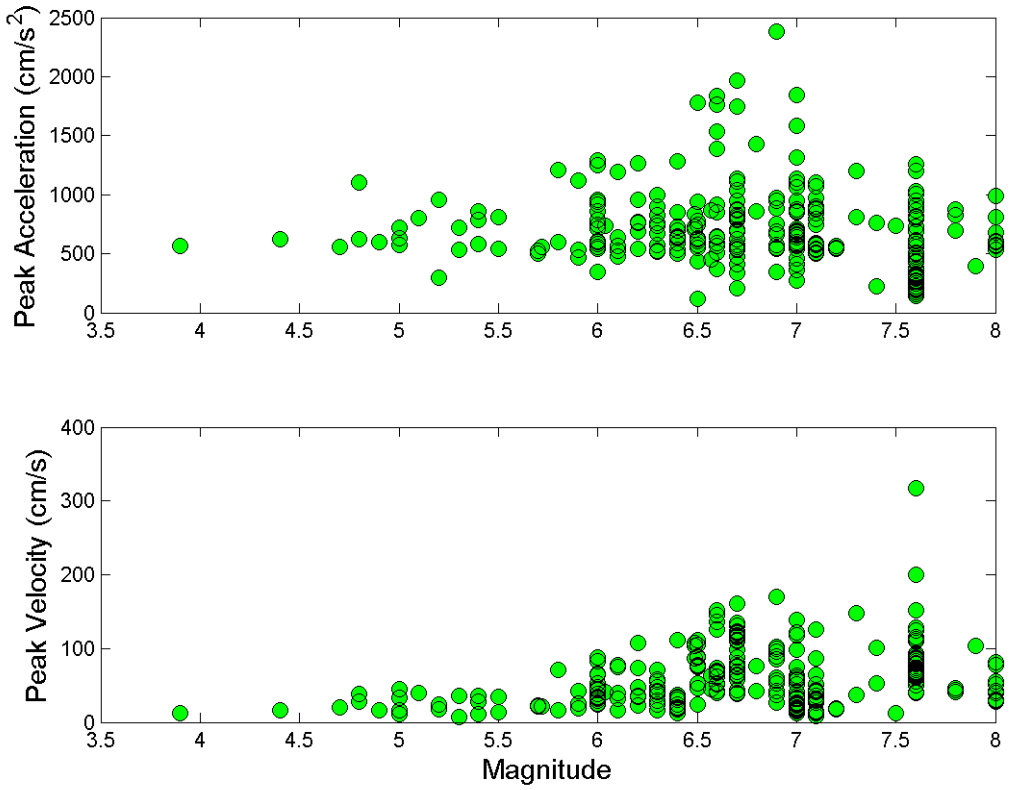

Figure 8. Exceptional ground motions vs moment magnitude. Peak acceleration and peak velocity for all events in Table 1, shown as a function of the magnitude of the earthquake. This figure is generated by the script **j10s1.m** in directory *C:\Task_22\Analysis\Statistics-1*. The file name is *C:\Task_22\Analysis\Statistics-1\J4_5.png*.

Figure 9. Rank of Peak Acceleration, Displayed as a Power Law

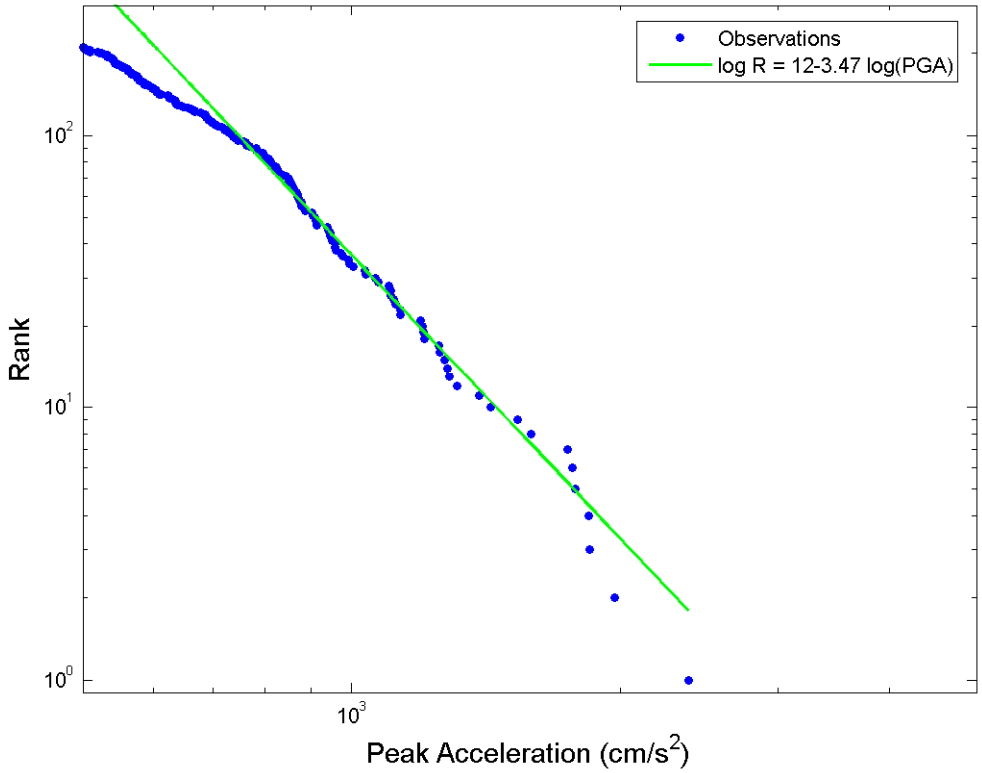

Figure 9. Ranking of exceptional records as a function of peak accelerations. The observations are shown as points. The axes are chosen such that data consistent with a power law distribution (Equation 1) of exceptional values would fall on a straight line. The green line, with parameters given in the figure, is the best power-law fit, using an L2 norm, to the data with ranks of 6 to 100. This figure is generated by the Matlab script **j10s2.m** in directory *C:\Task_22\Analysis\Statistics-1*. The file name is *C:\Task_22\Analysis\Statistics-1\J5_01.png*.

Figure 10. Rank of Peak Velocity, Displayed as a Power Law

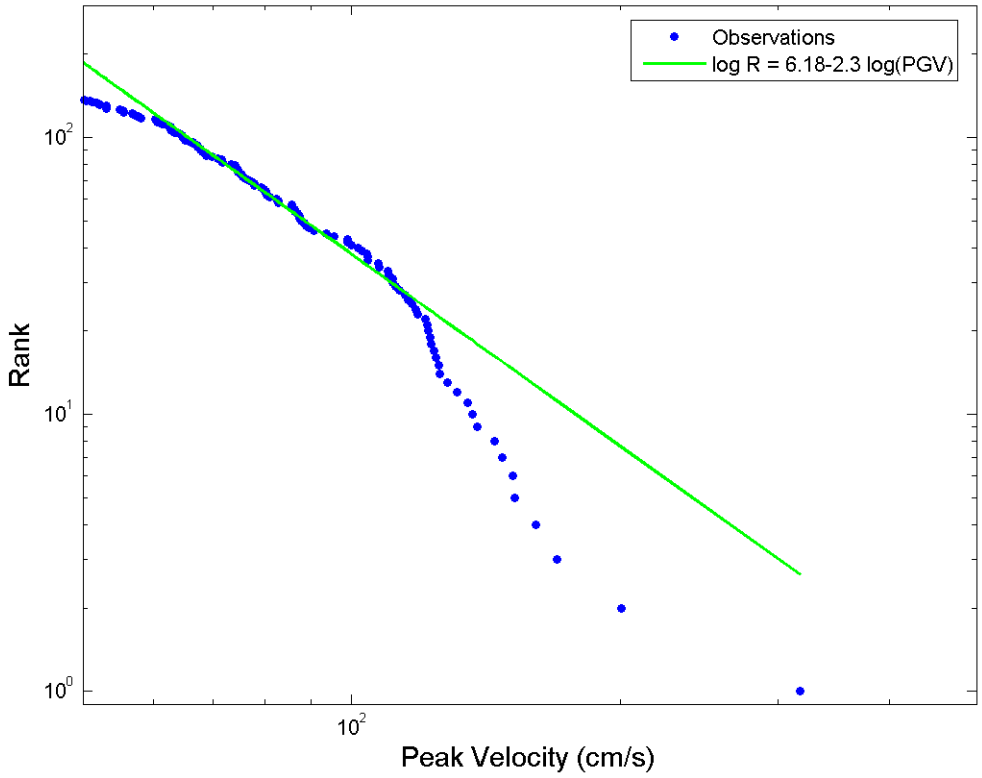

Figure 10. Ranking of exceptional records as a function of peak velocities. The observations are shown as points. The axes are chosen such that data consistent with a power law distribution (Equation 1) of exceptional values would fall on a straight line. The green line, with parameters given in the figure, is the best power law fit, using an L2 norm, to the data with ranks of 20 to 100. This figure is generated by the script **j10s2.m** in directory *C:\Task_22\Analysis\Statistics-1*. The file name is *C:\Task_22\Analysis\Statistics-1\J5_02.png*.

Figure 11. Rank of Peak Acceleration, Displayed as an Exponential Law

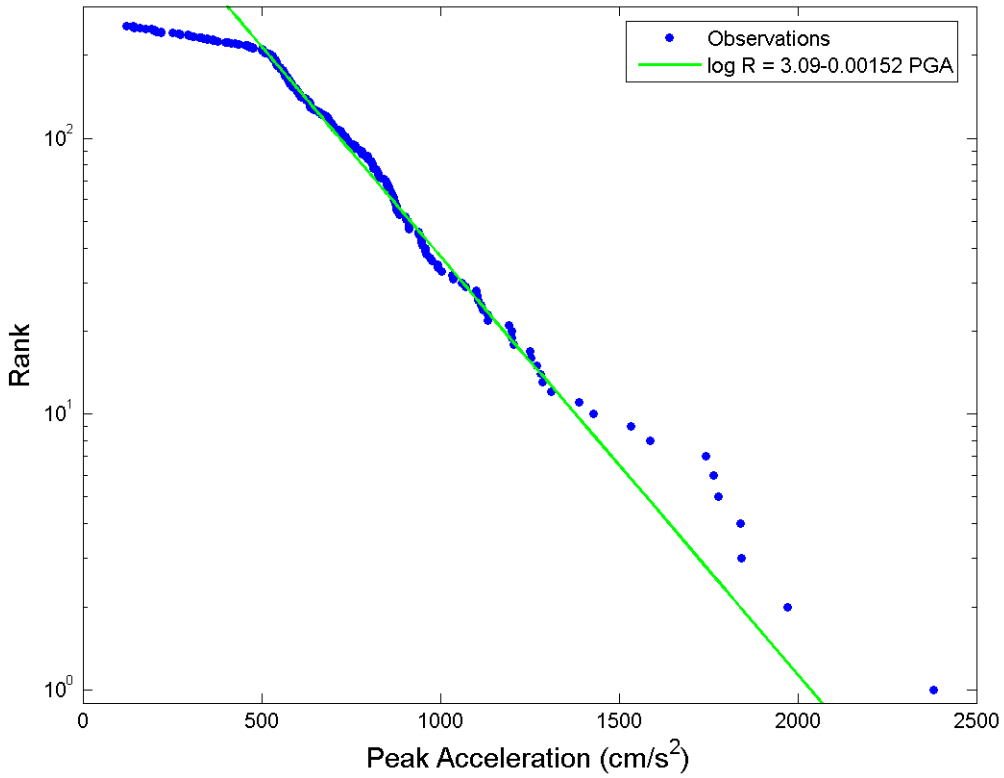

Figure 11. Ranking of exceptional records as a function of peak accelerations. The observations are shown as points. The axes are chosen such that data consistent with an exponential distribution (Equation 2) of exceptional values would fall on a straight line. The green line, with parameters given in the figure, is the best fitting exponential distribution, using an L2 norm, to the data with ranks of 10 to 80. This figure is generated by the script **j10s2.m** in directory *C:\Task_22\Analysis\Statistics-1*. The file name is *C:\Task_22\Analysis\Statistics-1\J5_03.png*.

Figure 12. Rank of Peak Velocity, Displayed as an Exponential Law

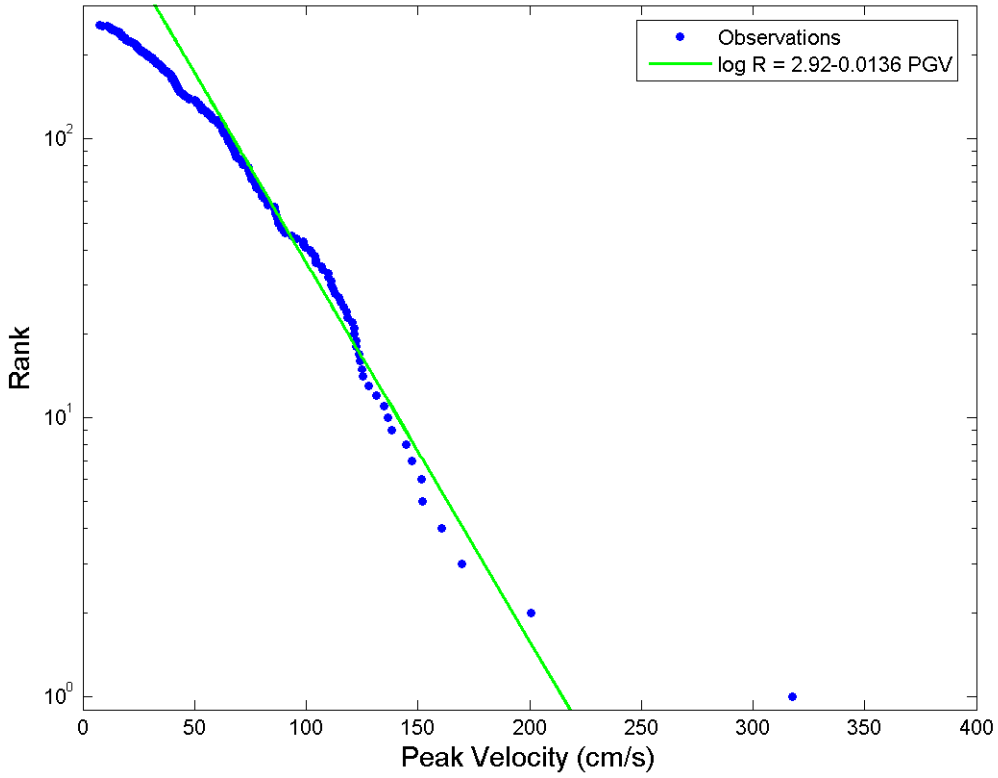

Figure 12. Ranking of exceptional records as a function of peak velocities. The observations are shown as points. The axes are chosen such that data consistent with an exponential distribution (Equation 2) of exceptional values would fall on a straight line. The green line, with parameters given in the figure, is the best fitting exponential distribution, using an L2 norm, to the data with ranks of 5 to 80. This figure is generated by the script **j10s2.m** in directory *C:\Task_22\Analysis\Statistics-1*. The file name is *C:\Task_22\Analysis\Statistics-1\J5_04.png*.

Figure 13. Rank of Peak Acceleration, Displayed as an Extreme Value Distribution

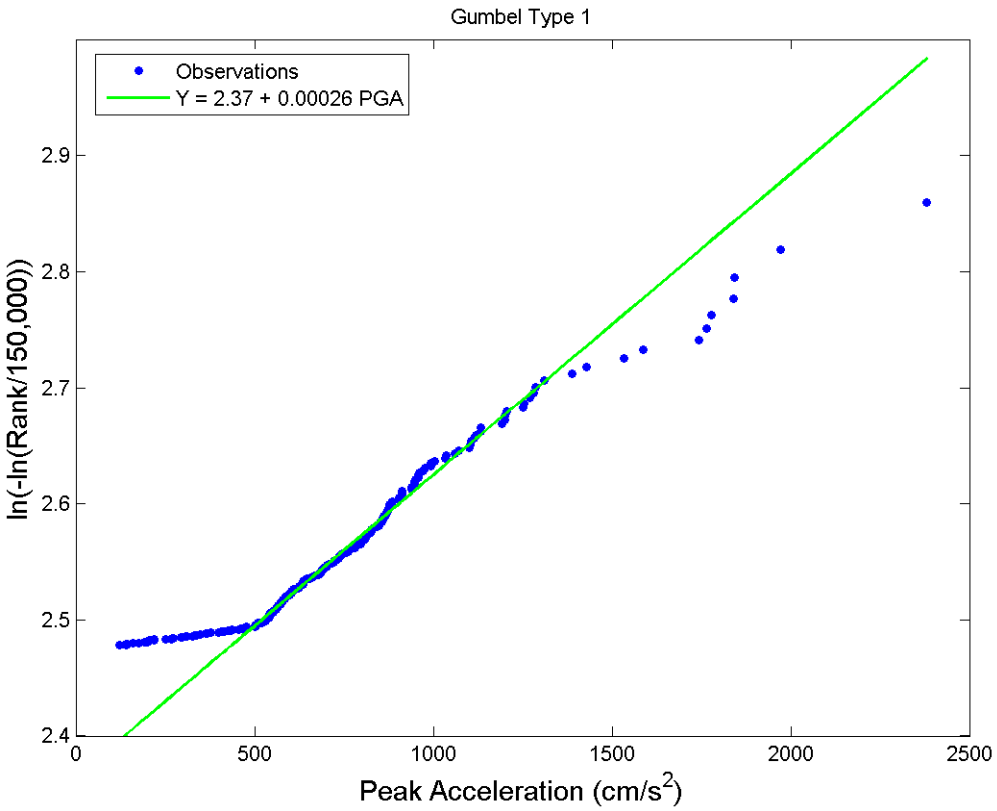

Figure 13. Ranking of exceptional records as a function of peak accelerations. The observations are shown as points. The axes are chosen such that data consistent with an extreme value distribution (Equation 3) of exceptional values would fall on a straight line. The green line, with parameters given in the figure, is the best fitting exponential distribution, using an L2 norm, to the data with ranks of 10 to 100. This figure is generated by the script **j10s2.m** in directory *C:\Task_22\Analysis\Statistics-1*. The file name is *C:\Task_22\Analysis\Statistics-1\J5_05.png*.

Figure 14. Rank of Peak Velocity, Displayed as an Extreme Value Distribution

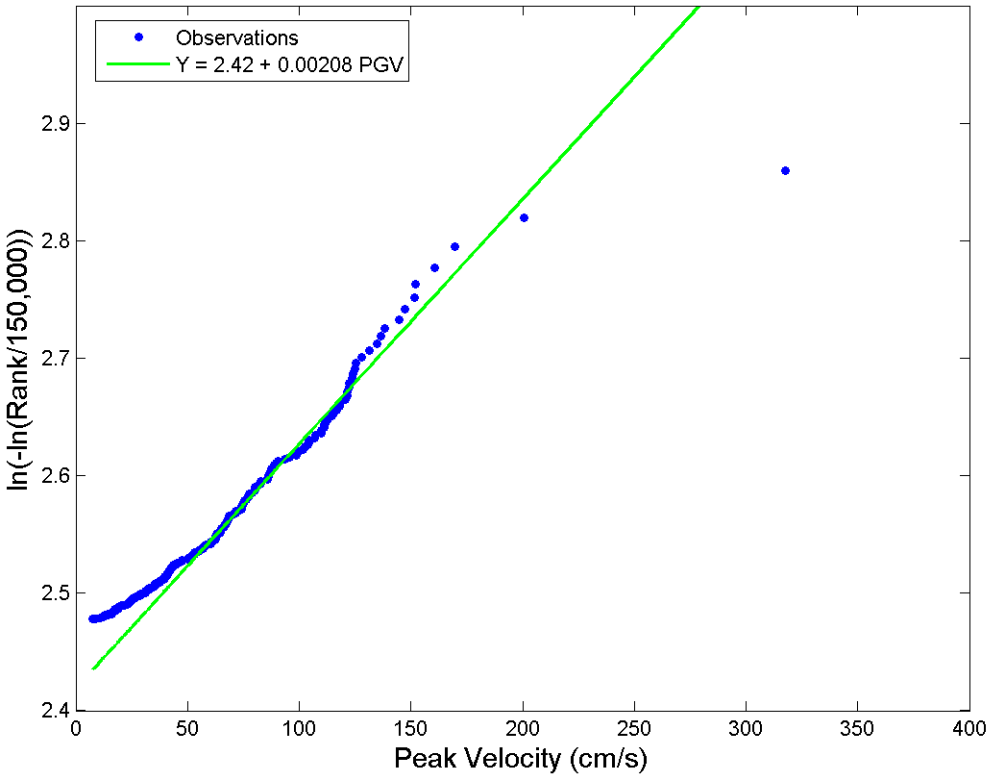

Figure 14. Ranking of exceptional records as a function of peak velocities. The observations are shown as points. The axes are chosen such that data consistent with an extreme value distribution (Equation 3) of exceptional values would fall on a straight line. The green line, with parameters given in the figure, is the best fitting exponential distribution, using an L2 norm, to the data with ranks of 10 to 100. This figure is generated by the script **j10s2.m** in directory *C:\Task_22\Analysis\Statistics-1*. The file name is *C:\Task_22\Analysis\Statistics-1\J5_06.png*.

Figure 15. Estimated Exceedance Rate of Peak Acceleration Per Instrument Year

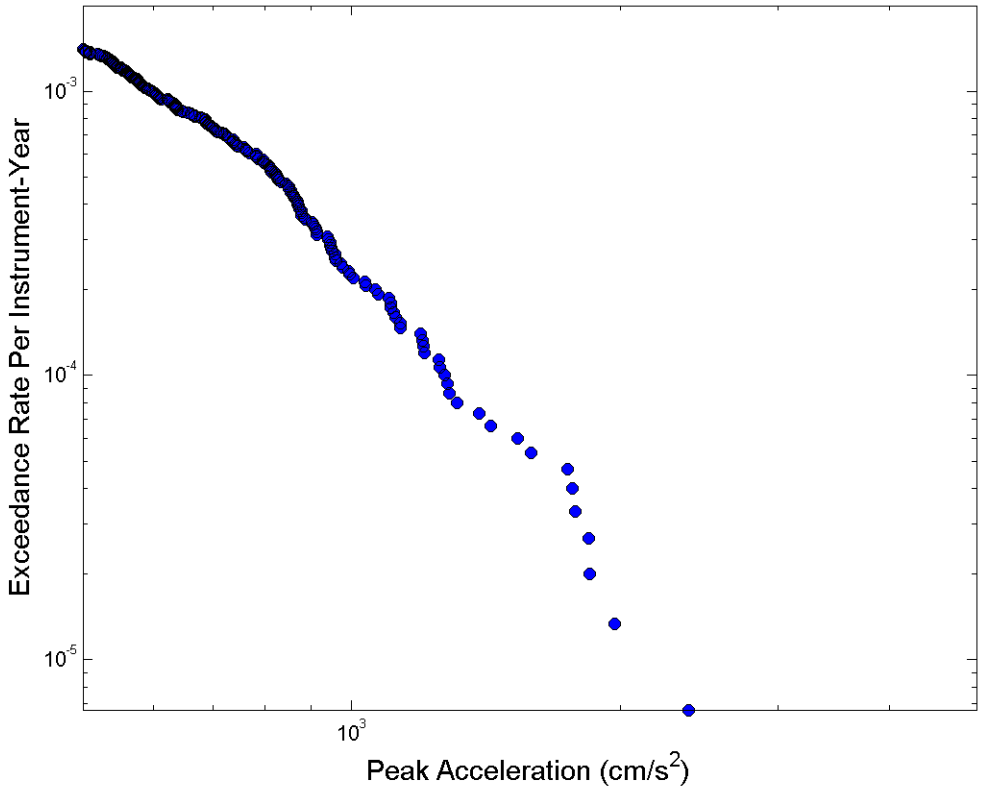

Figure 15. Estimated exceedance rate of peak acceleration per instrument year. The points are obtained by dividing the rank in Figure 9 by the estimate that these data represent about 150,000 instrument-years of data collection effort. This figure is generated by the script **j10s2.m** in directory *C:\Task_22\Analysis\Statistics-1*. The file name is *C:\Task_22\Analysis\Statistics-1\J5_07.png*.

Figure 16. Estimated Exceedance Rate of Peak Velocity Per Instrument Year

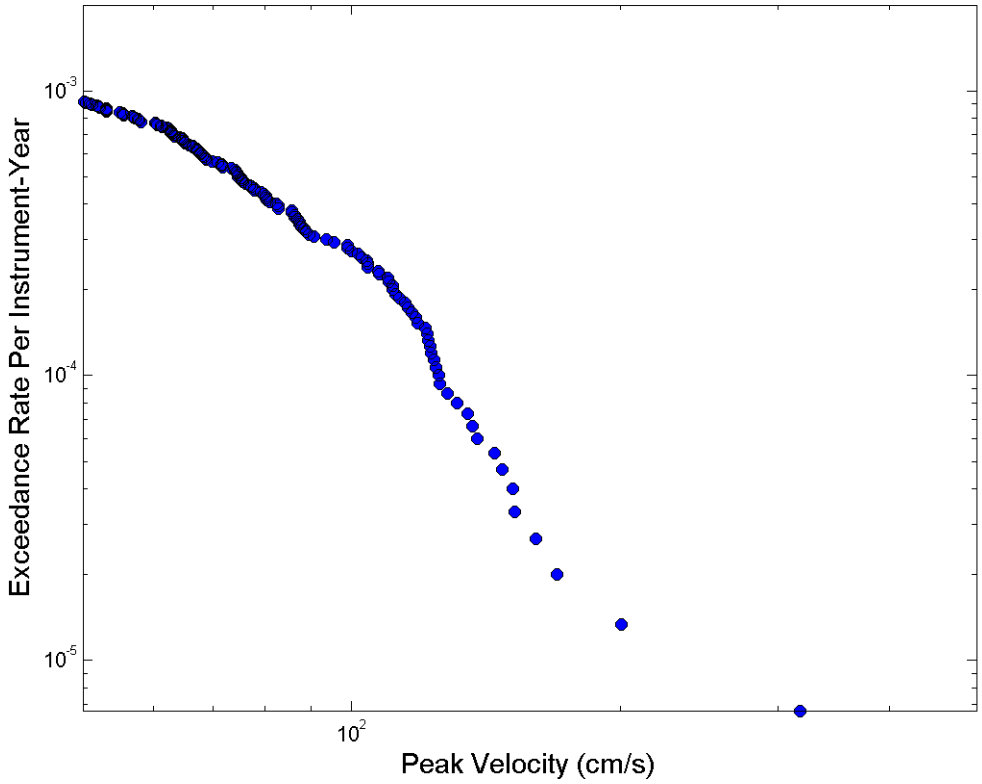

Figure 16. Estimated exceedance rate of peak velocity per instrument year. The points are obtained by dividing the rank in Figure 9 by the estimate that these data represent about 150,000 instrument-years of data collection effort. This figure is generated by the script **j10s2.m** in directory *C:\Task_22\Analysis\Statistics-1*. The file name is *C:\Task_22\Analysis\Statistics-1\J5_08.png*.

Figure 17. Distribution of Magnitudes for All Included Earthquakes

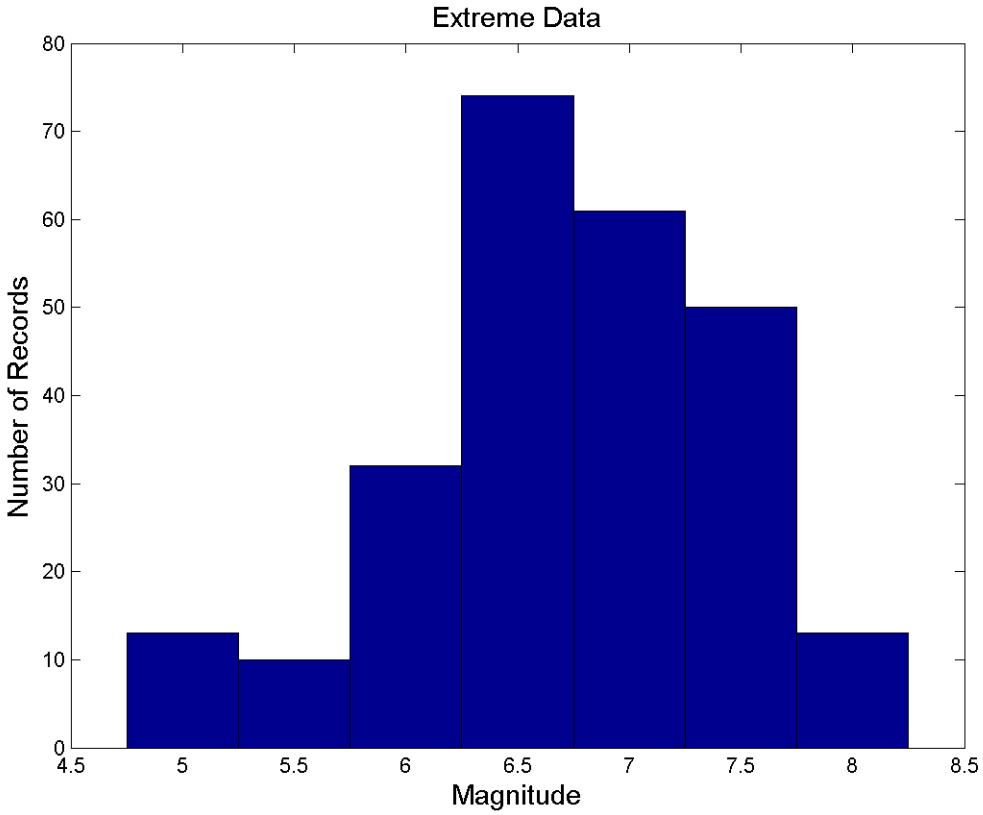

Figure 17. Magnitudes of the earthquakes for all of the records included in Table 1. Earthquakes that generated more than one exceptional ground motion record are counted once for each record. This figure is generated by the Matlab script **j11sa.m** in directory *C:\Task_22\Analysis\Statistics-2*. The file name of this figure is *C:\Task_22\Analysis\Statistics-2\J11sa_08.png*.

Figure 18. Magnitude Distribution of Earthquakes Causing the Top 100 Accelerations, Compared With the Distribution of Magnitude in the NGA Database

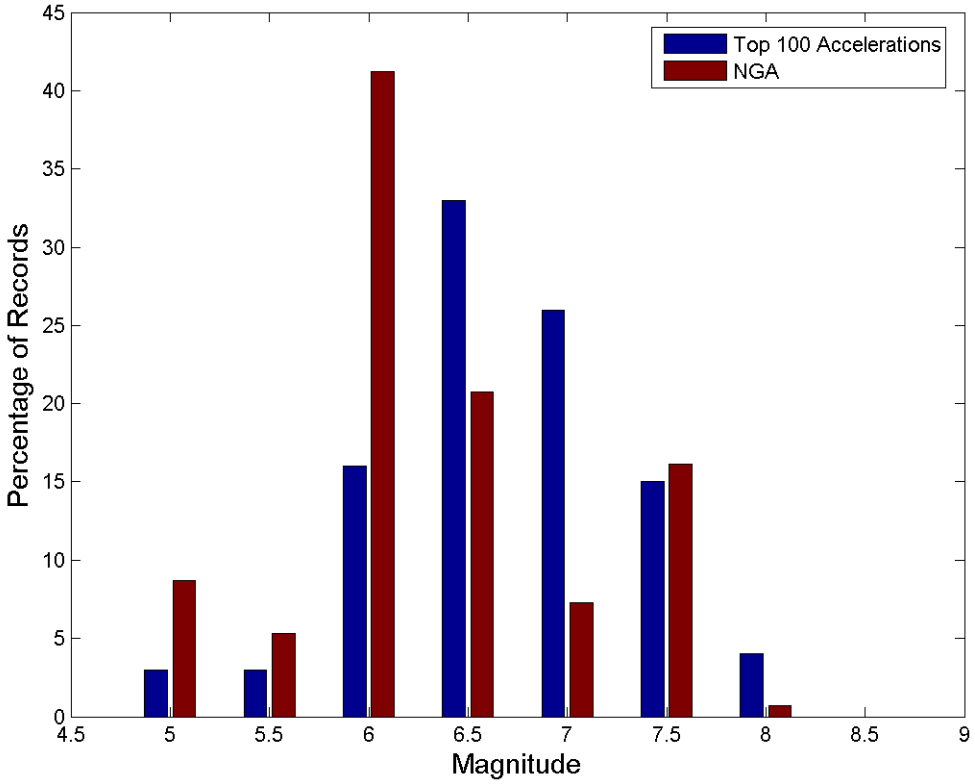

Figure 18. Magnitude distribution of earthquakes causing the top 100 acceleration records, compared with the distribution of magnitudes in the NGA database. Earthquakes that generated more than one of the top 100 ground motion records are counted once for each record. This figure is generated by the Matlab script **j11sa.m** in directory *C:\Task_22\Analysis\Statistics-2*. The file name of this figure is *C:\Task_22\Analysis\Statistics-2\J11sa_08a.png*.

Figure 19. Magnitude Distribution of Earthquakes Causing the Top 100 Velocities, Compared With the Distribution of Magnitude in the NGA Database

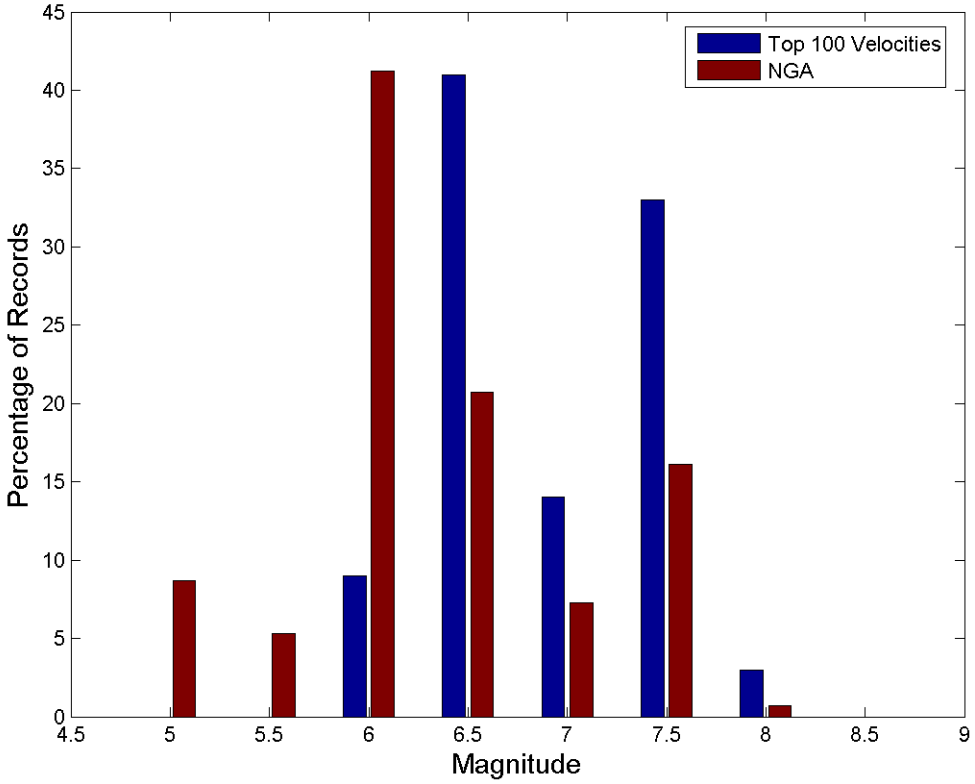

Figure 19. Magnitude distribution of earthquakes causing the top 100 velocity records, compared with the distribution of magnitudes in the NGA database. Earthquakes that generated more than one of the top 100 ground motion records are counted once for each record. Figure 19 is generated by the Matlab script **j11sv.m** in directory *C:\Task_22\Analysis\Statistics-2*. The file name of this figure is *C:\Task_22\Analysis\Statistics-2\J11sv_08a.png*.

Figure 20. Magnitudes of Earthquakes Causing the Top 100 Accelerations, Displayed by Quartile

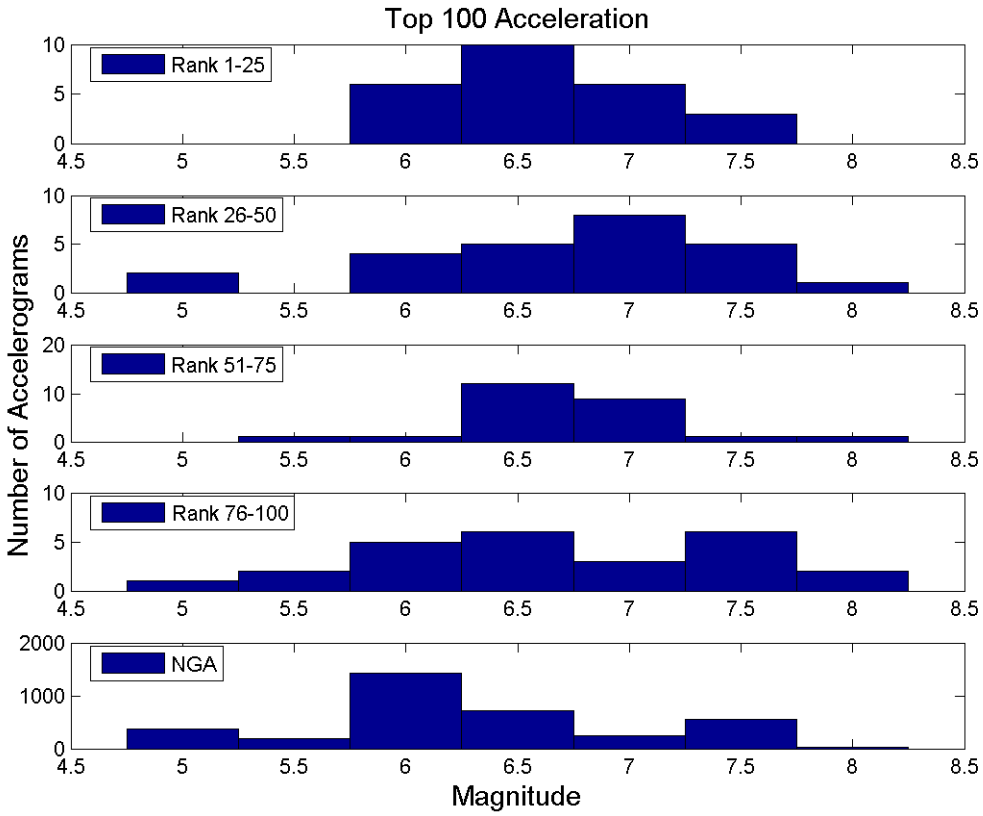

Figure 20. Magnitudes of earthquakes causing the top 100 accelerations, displayed by quartile. Earthquakes that generated more than one of the top 100 ground motion records are counted once for each record. This figure is generated by the Matlab script **j11sa.m** in directory *C:\Task_22\Analysis\Statistics-2*. The file name of this figure is *C:\Task_22\Analysis\Statistics-2\J11sa_10.png*.

Figure 21. Magnitudes of Earthquakes Causing the Top 100 Velocities, Displayed by Quartile

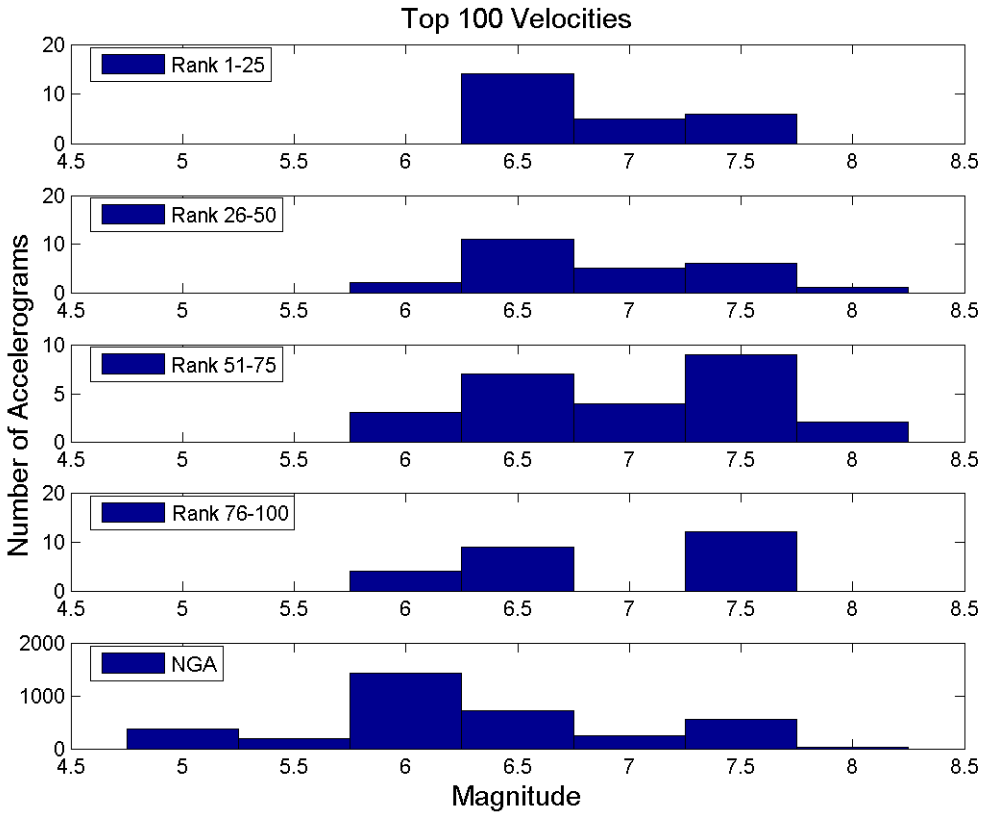

Figure 21. Magnitudes of earthquakes causing the top 100 velocities, displayed by quartile. Earthquakes that generated more than one of the top 100 ground motion records are counted once for each record. This figure is generated by the Matlab script **j11sv.m** in directory *C:\Task_22\Analysis\Statistics-2*. The file name of this figure is *C:\Task_22\Analysis\Statistics-2\J11sv_10.png*.

Figure 22. Distribution of Focal Mechanisms for All Included Earthquakes

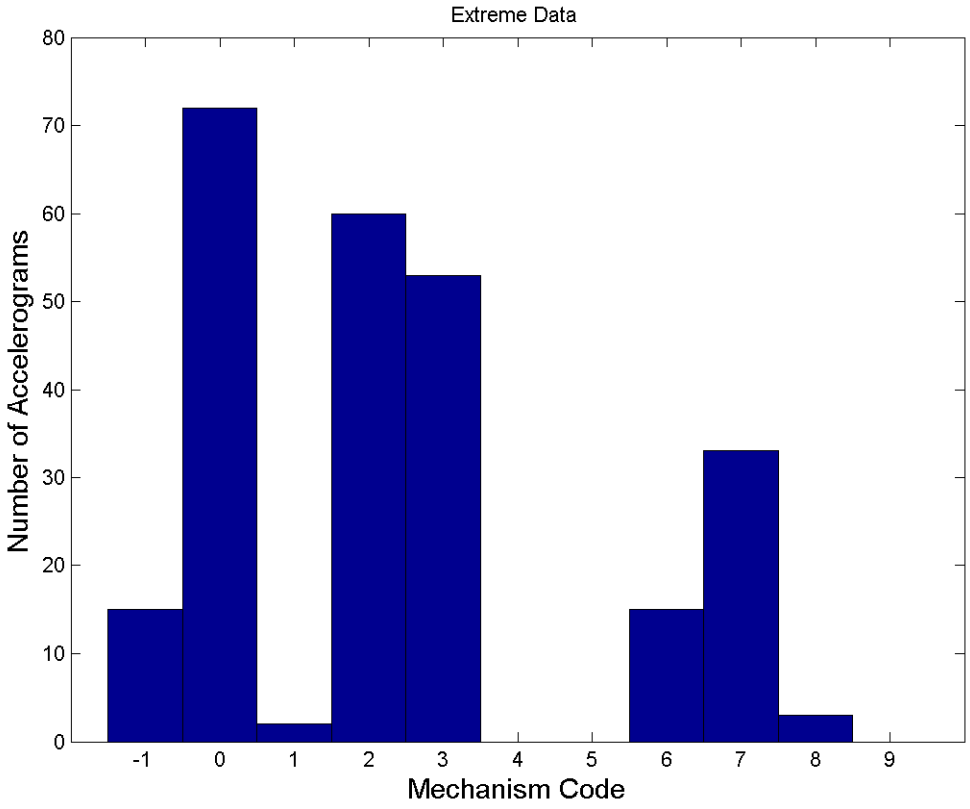

Figure 22. Distribution of focal mechanisms for the earthquake generating each record in Table 1. The mechanism code is as follows: 0) strike-slip faulting in continental crust; 1) normal faulting in continental crust; 2) thrust faulting in continental crust; 3) oblique thrust faulting in continental crust; 4) oblique normal faulting in continental crust; 6) normal faulting associated with the downgoing slab in a subduction zone; 7) thrust faulting in an oceanic subduction zone; and 8) oblique thrust faulting in an oceanic subduction zone. A code of -1 indicates that the mechanism for that record was not available. For earthquakes causing more than one record in Table 1, the earthquake is counted once for each record. This is generated by the Matlab script **j11sa.m** in directory *C:\Task_22\Analysis\Statistics-2*. The file name of this figure is *C:\Task_22\Analysis\Statistics-2\J11sa_01.png*.

Figure 23. Distribution of Focal Mechanism for the Top 100 Acceleration Records, Compared With the Distribution of Focal Mechanism in the NGA Database

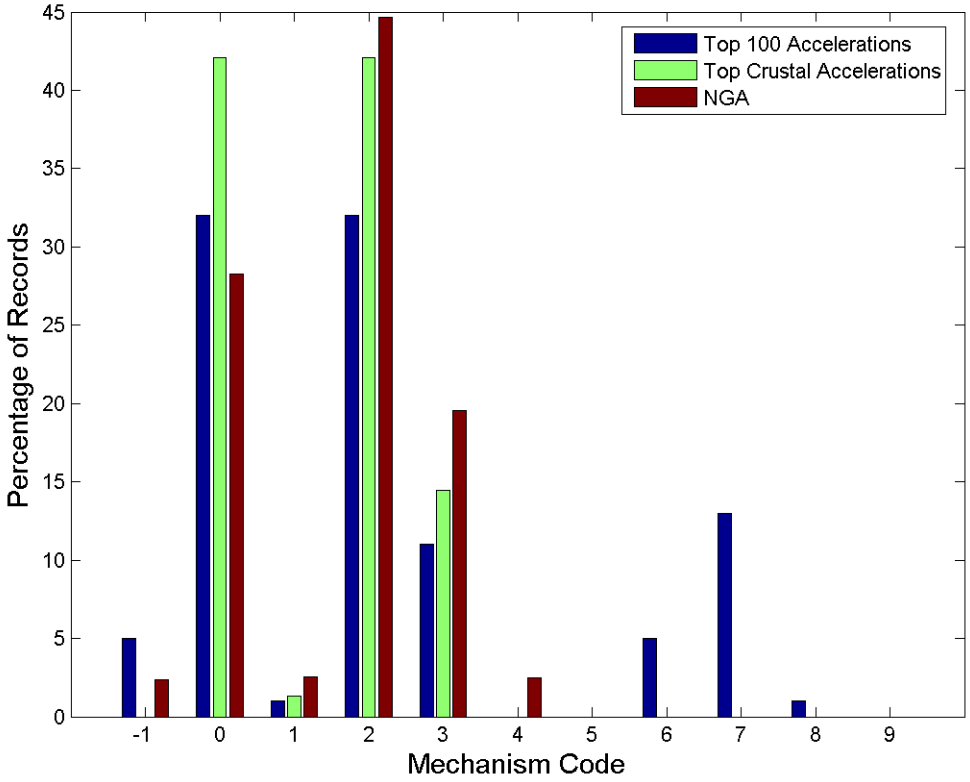

Figure 23. Distribution of focal mechanisms of earthquakes causing the top 100 acceleration records, compared with the distribution of focal mechanism in the NGA database. The NGA database does not include subduction zone earthquakes. Therefore, the bars giving the percentage of "Top Crustal Accelerations" is generated for comparison with NGA by renormalizing those top 100 records with mechanisms 0, 1, 2, 3, or 4 to a total of 100%. Mechanism codes are given in the caption to Figure 22. For earthquakes causing more than one record in Table 1, the earthquake is counted once for each record. This figure is generated by the Matlab script **j11sa.m** in directory *C:\Task_22\Analysis\Statistics-2*. The file name of this figure is *C:\Task_22\Analysis\Statistics-2\J11sa_01a.png*.

Figure 24. Distribution of Focal Mechanism for the Top 100 Velocities, Compared With the Distribution of Focal Mechanism in the NGA Database

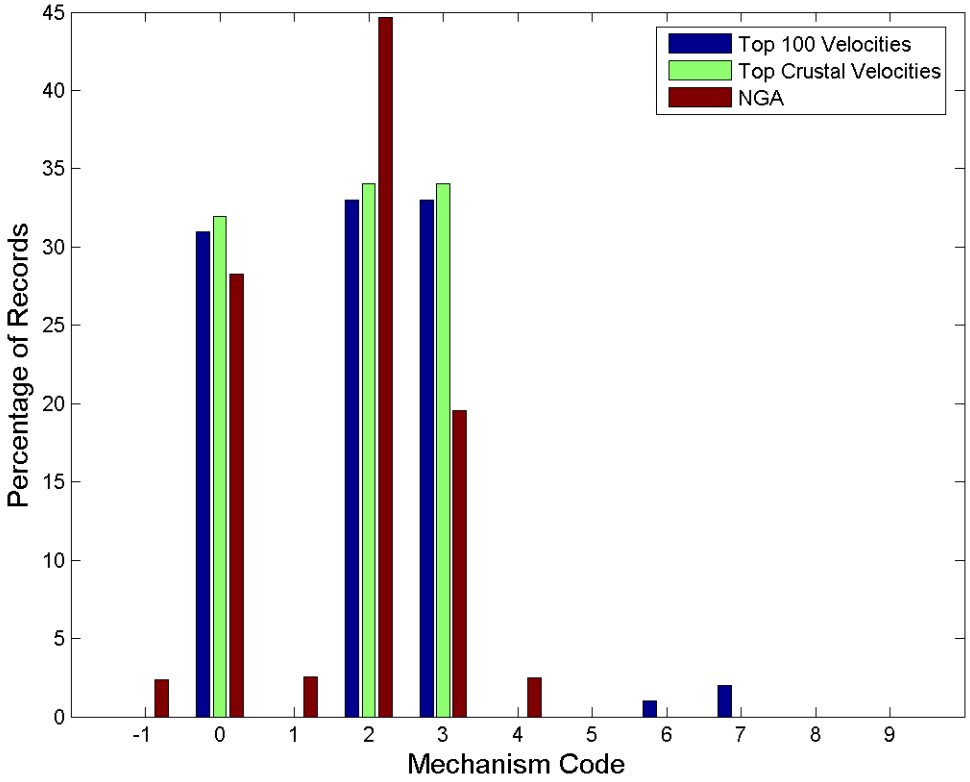

Figure 24. Distribution of focal mechanisms of earthquakes causing the top 100 velocity records, compared with the distribution of focal mechanism in the NGA database. See Figure 23 for a detailed explanation. This figure is generated by the Matlab script **j11sv.m** in directory *C:\Task_22\Analysis\Statistics-2*. The file name of this figure is *C:\Task_22\Analysis\Statistics-2\J11sv_01a.png*.

Figure 25. Focal Mechanisms of Earthquakes Causing the Top 100 Acceleration Records, Displayed by Quartile

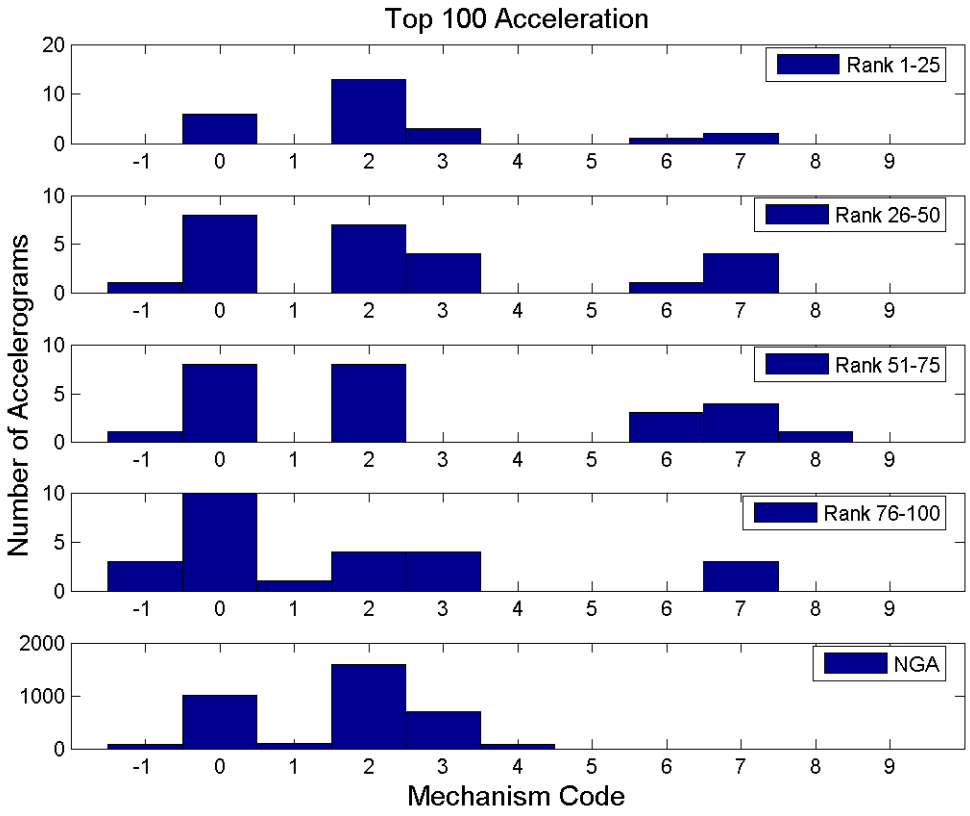

Figure 25. Focal mechanisms of earthquakes causing the top 100 acceleration records, displayed by quartile. See Figure 22 for mechanism codes. For earthquakes causing more than one record in Table 1, the earthquake is counted once for each record. This figure is generated by the Matlab script **j11sa.m** in directory *C:\Task_22\Analysis\Statistics-2*. The file name of this figure is *C:\Task_22\Analysis\Statistics-2\J11sa_03.png*.

Figure 26. Focal Mechanisms of Earthquakes Causing the Top 100 Velocity Records, Displayed by Quartile

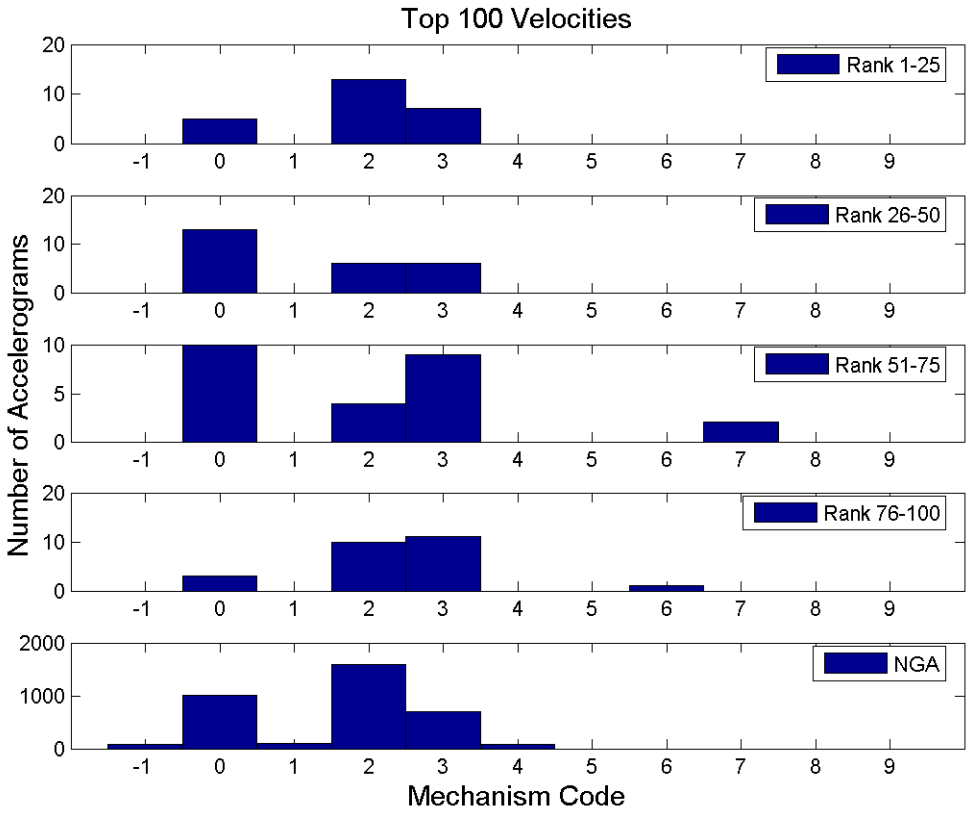

Figure 26. Focal mechanisms of earthquakes causing the top 100 velocity records, displayed by quartile. See Figure 25 for additional details. This figure is generated by the Matlab script **j11sv.m** in directory *C:\Task_22\Analysis\Statistics-2*. The file name of this figure is *C:\Task_22\Analysis\Statistics-2\J11sv_03.png*.

Figure 27. Distribution of Site Categories for All Included Records.

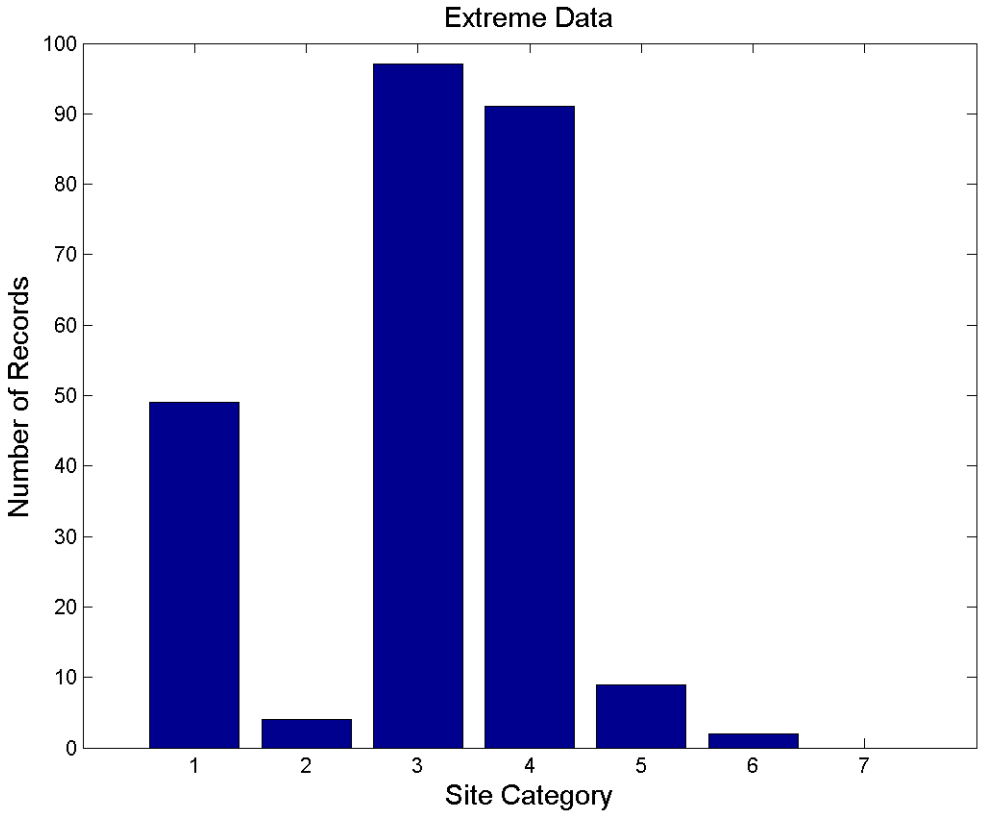

Figure 27. Distribution of site categories for all records in Table 1. Site category 1=not available, 2=NEHRP E, 3=NEHRP D, 4=NEHRP C, 5-NEHRP B, 6-NEHRP A. Earthquakes causing more than one record are displayed once for each record. This figure is generated by the Matlab script **j11sa.m** in directory *C:\Task_22\Analysis\Statistics-2*. The file name of this figure is *C:\Task_22\Analysis\Statistics-2\J11sa_04.png*.

Figure 28. Distribution of Site Categories for the Top 100 Acceleration Records, Compared with the Distribution of Site Categories in the NGA Database.

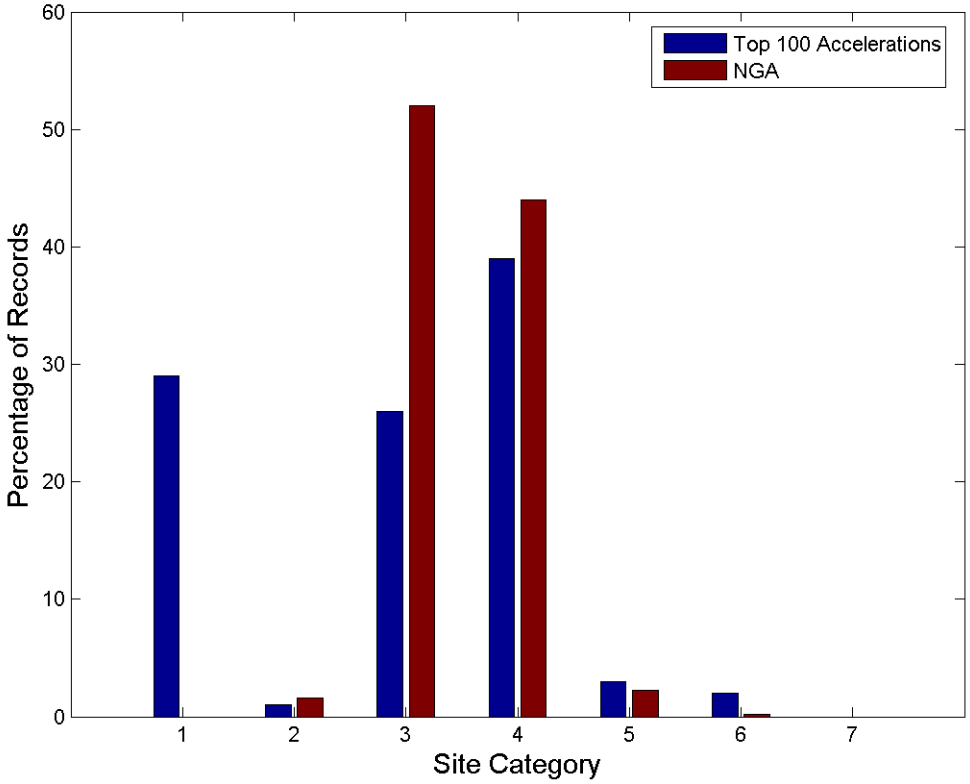

Figure 28. Distribution of site categories for the top 100 acceleration records, compared with the distribution of site categories in the NGA database. See the caption to Figure 27 for a definition of Site Category. This figure is generated by the Matlab script **j11sa.m** in directory *C:\Task_22\Analysis\Statistics-2*. The file name of this figure is *C:\Task_22\Analysis\Statistics-2\J11sa_04a.png*.

Figure 29. Distribution of Site Categories for the Top 100 Velocity Records, Compared with the Distribution of Site Categories in the NGA Database.

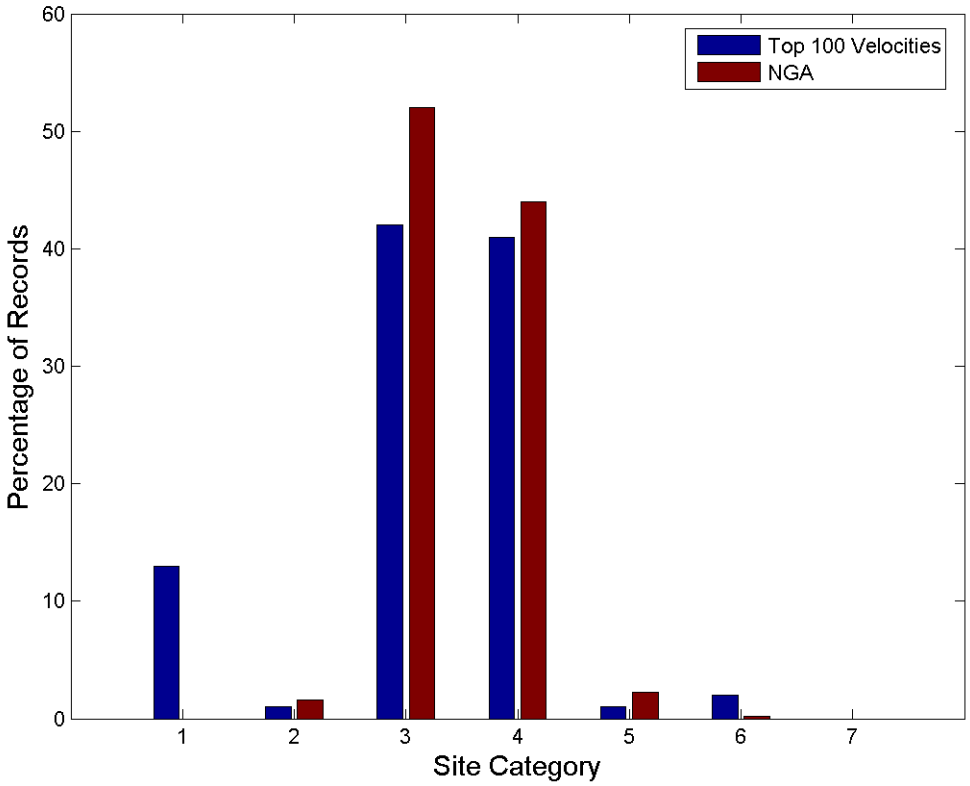

Figure 29. Distribution of site categories for the top 100 velocity records, compared with the distribution of site categories in the NGA database. See the caption to Figure 27 for a definition of Site Category. This figure is generated by the Matlab script **j11sv.m** in directory *C:\Task_22\Analysis\Statistics-2*. The file name of this figure is *C:\Task_22\Analysis\Statistics-2\J11sv_04a.png*.

Figure 30. Peak Acceleration and Peak Velocity for all Included Data, as a Function of Estimated V30

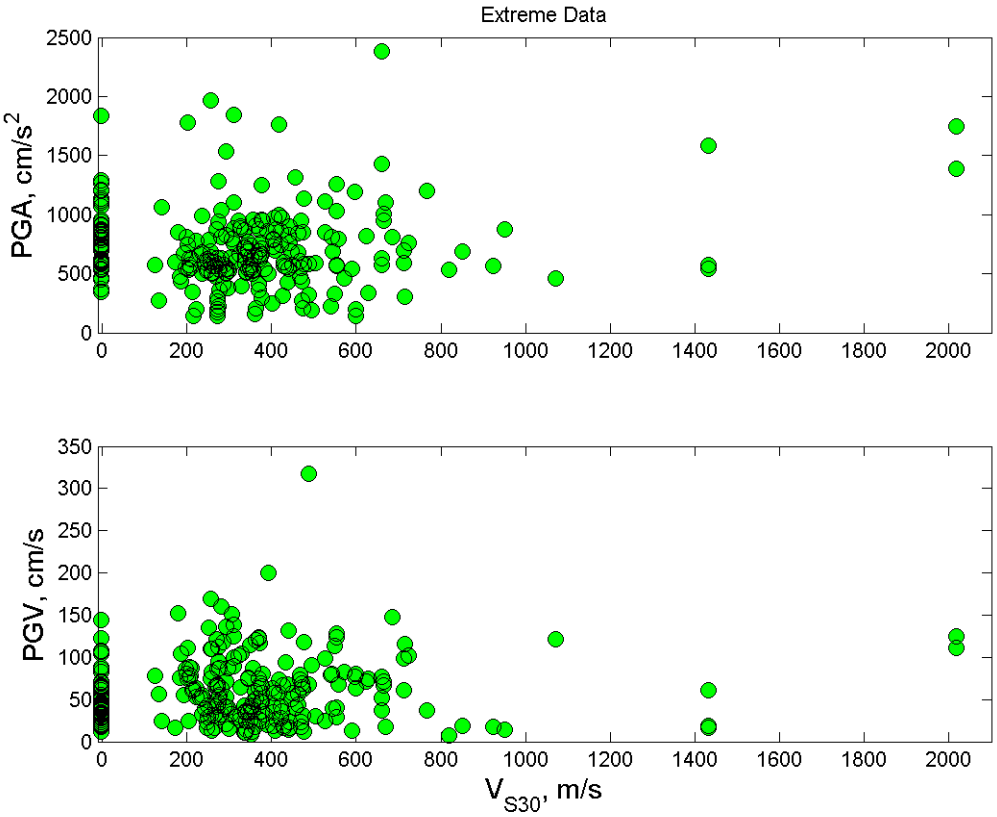

Figure 30. Peak acceleration and peak velocity for all records in Table 1, as a function of estimated V_S30. Records for which the value of V_S30 is not available are plotted at V_S30=0. This figure is generated by the Matlab script **j11sa.m** in directory *C:\Task_22\Analysis\Statistics-2*. The file name of this figure is *C:\Task_22\Analysis\Statistics-2\J11sa_07.png*.

Figure 31. Distribution of Average Horizontal Kappa for All Records in Table 1.

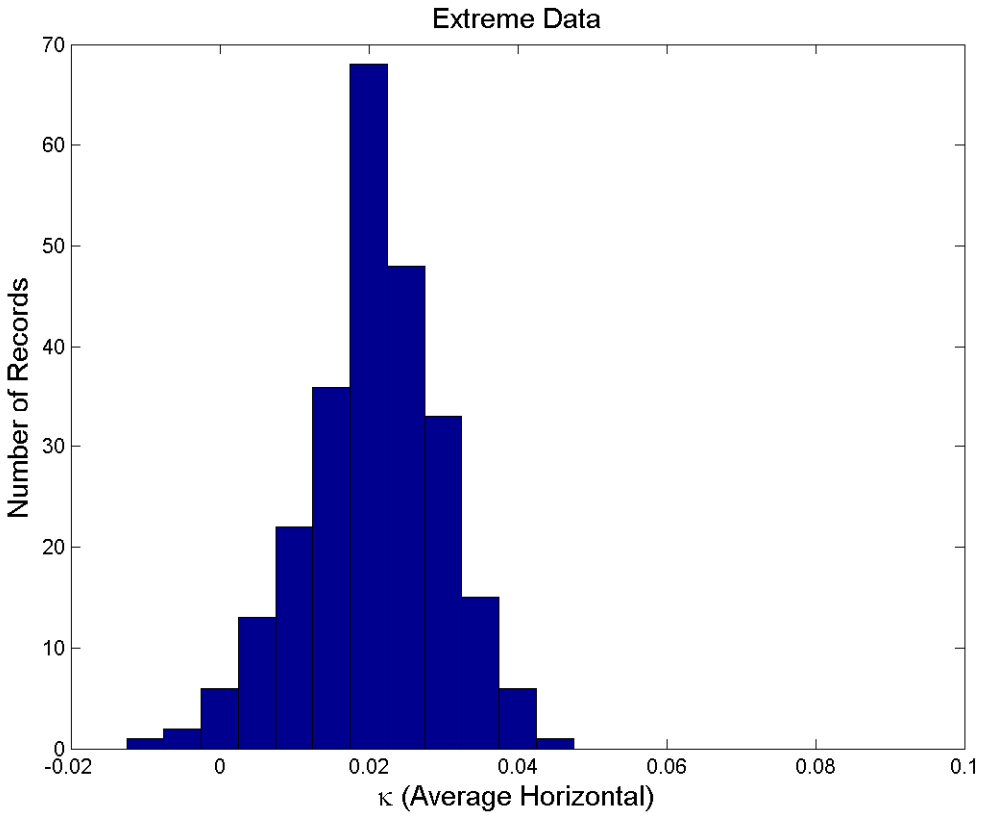

Figure 31. Distribution of average horizontal kappa for all records in Table 1. For each component, κ was calculated as described in the text, and then the average of the horizontal components used to create this histogram. Units of κ are seconds. This figure is generated by the Matlab script **j11sa.m** in directory *C:\Task_22\Analysis\Statistics-2*. The file name of this figure is *C:\Task_22\Analysis\Statistics-2\J11sa_13.png*.

Figure 32. Distribution of Average Horizontal Kappa for the Top 100 Acceleration Records, by Quartile.

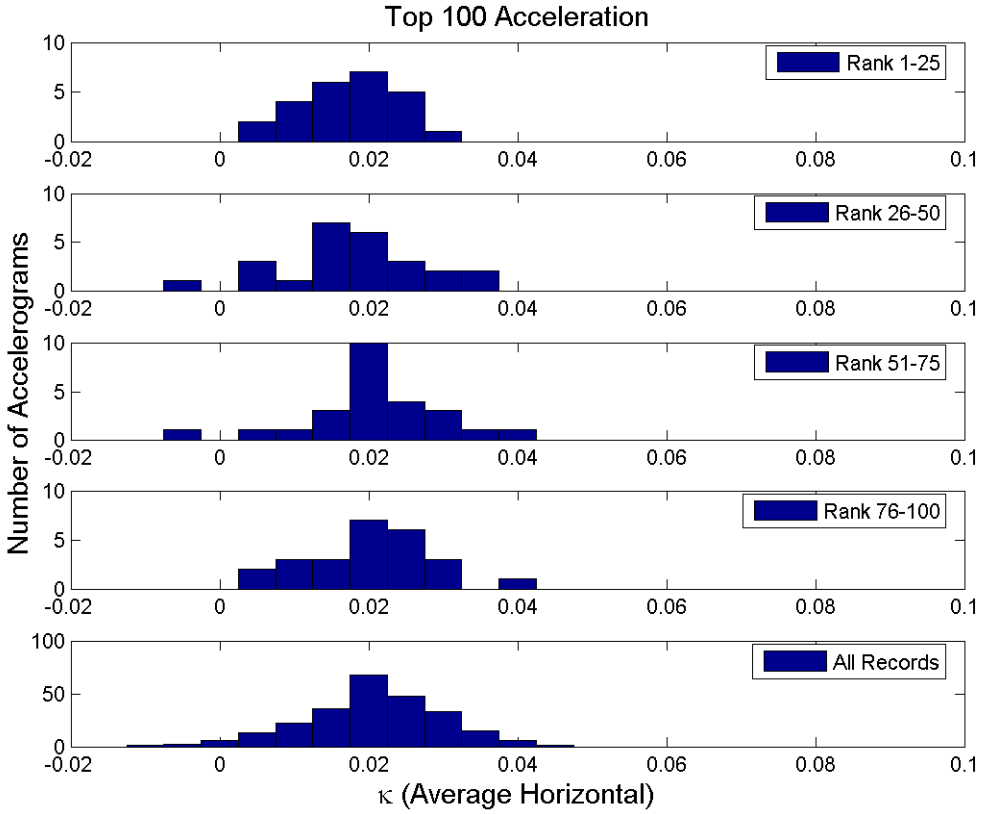

Figure 32. Distribution of average horizontal kappa for the top 100 acceleration records, by quartile. Units of κ are seconds. This figure is generated by the Matlab script **j11sa.m** in directory *C:\Task_22\Analysis\Statistics-2*. The file name of this figure is *C:\Task_22\Analysis\Statistics-2\J11sa_14.png*.

Figure 33. Distribution of Average Horizontal Kappa for the Top 100 Velocitie Records, by Quartile.

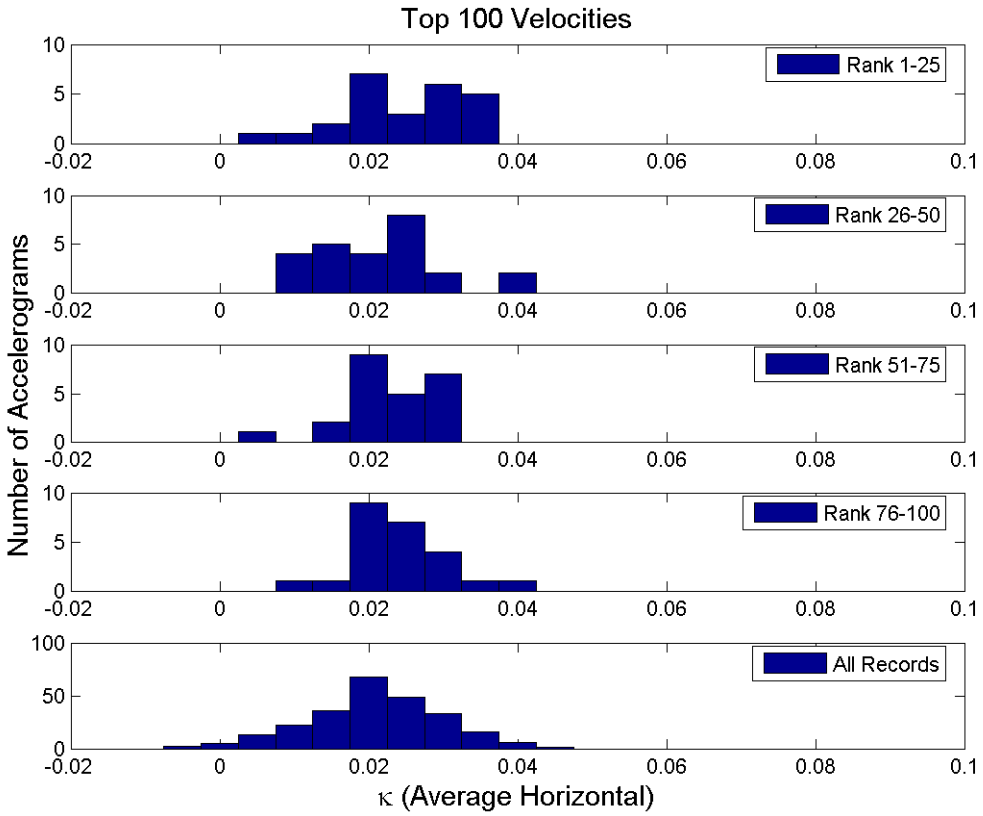

Figure 33. Distribution of average horizontal kappa for the top 100 velocity records, by quartile. Units of κ are seconds. This figure is generated by the Matlab script **j11sv.m** in directory *C:\Task_22\Analysis\Statistics-2*. The file name of this figure is *C:\Task_22\Analysis\Statistics-2\J11sv_14.png*.

Appendix A. Earthquake Maps

Figure A1. Imperial Valley, May 19, 1940, 04:36:41, M_W 6.90

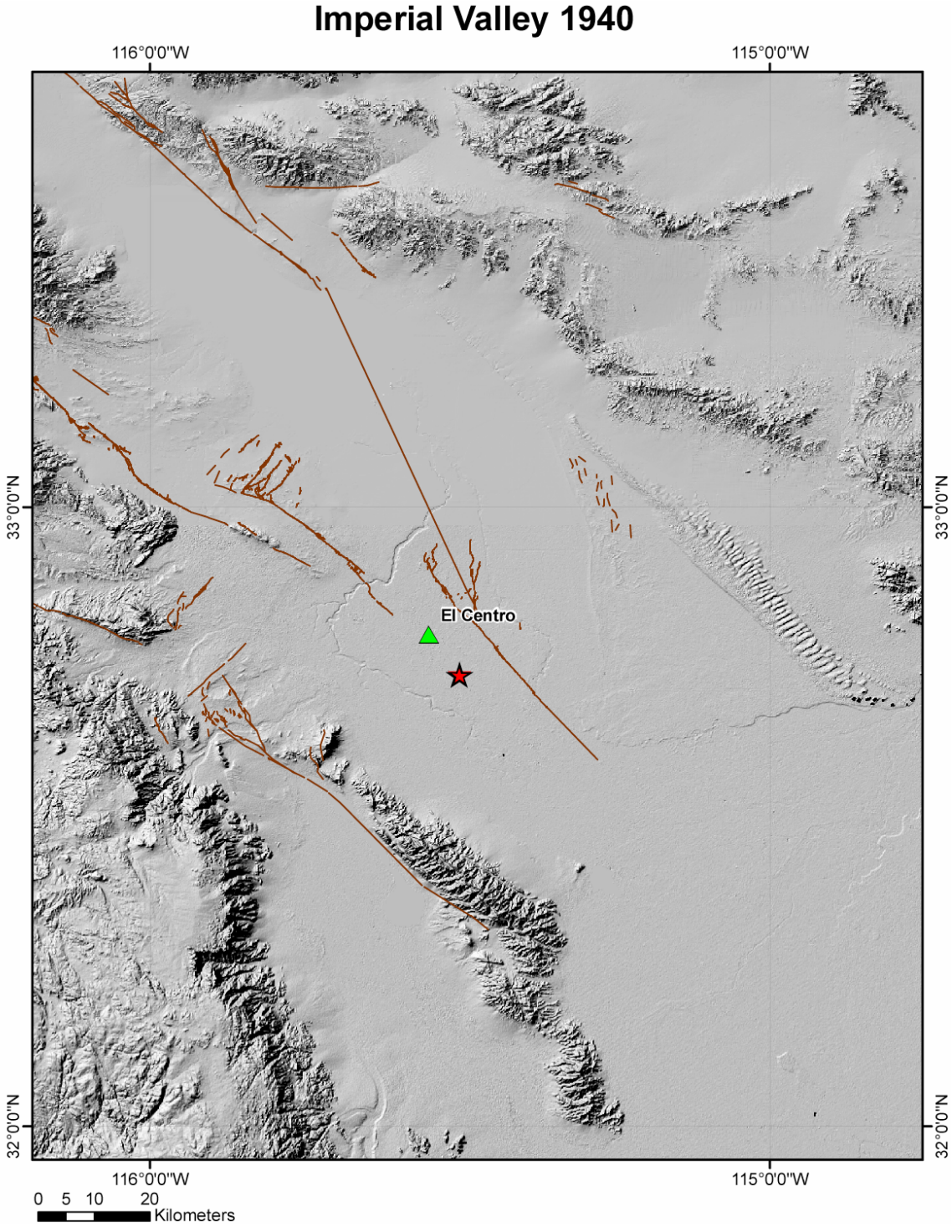

Figure A2. Parkfield, June 28, 1966, 04:26:14, M_W 6.10

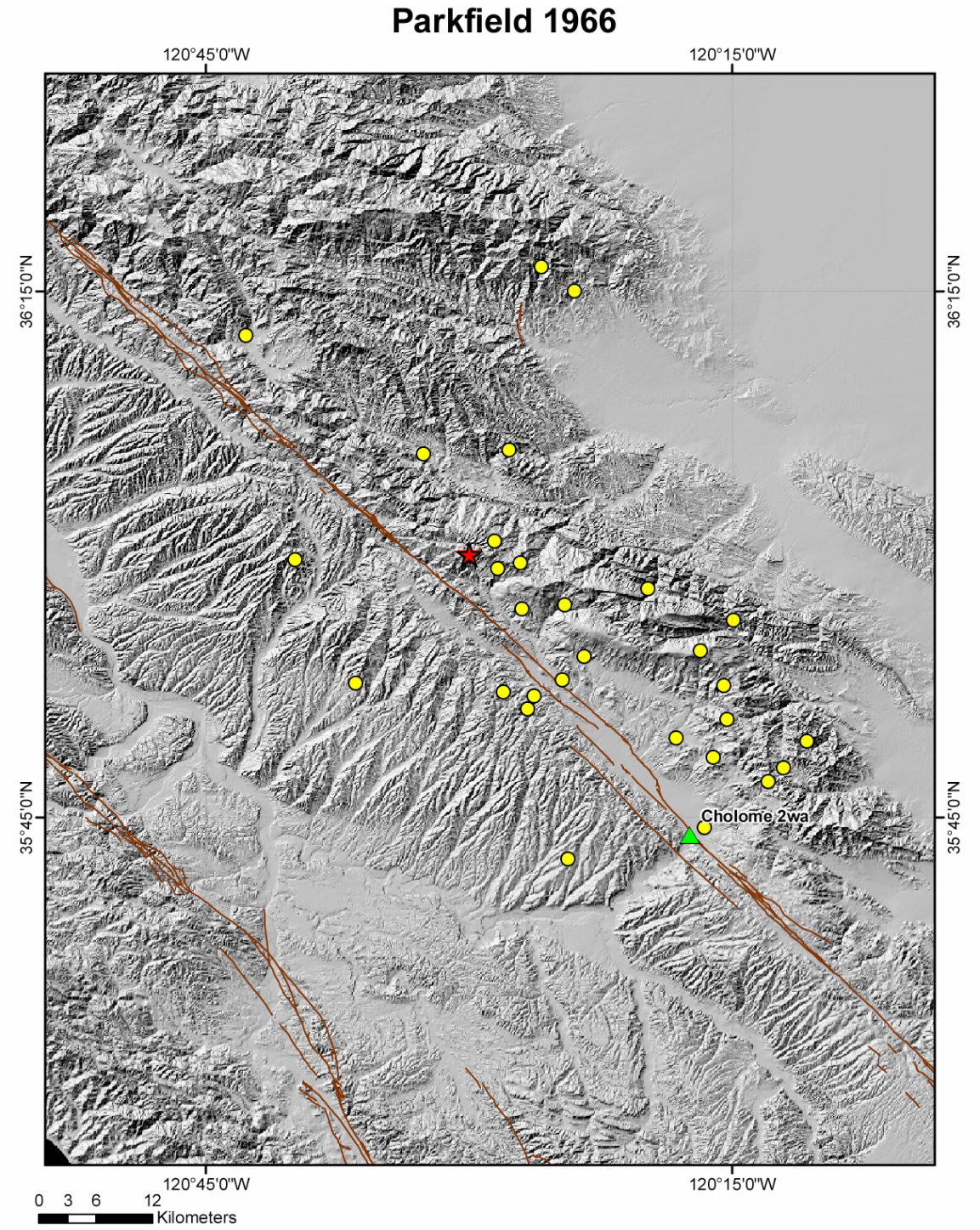

Figure A3. San Fernando, February 9, 1971, 14:00:41, M_W 6.60

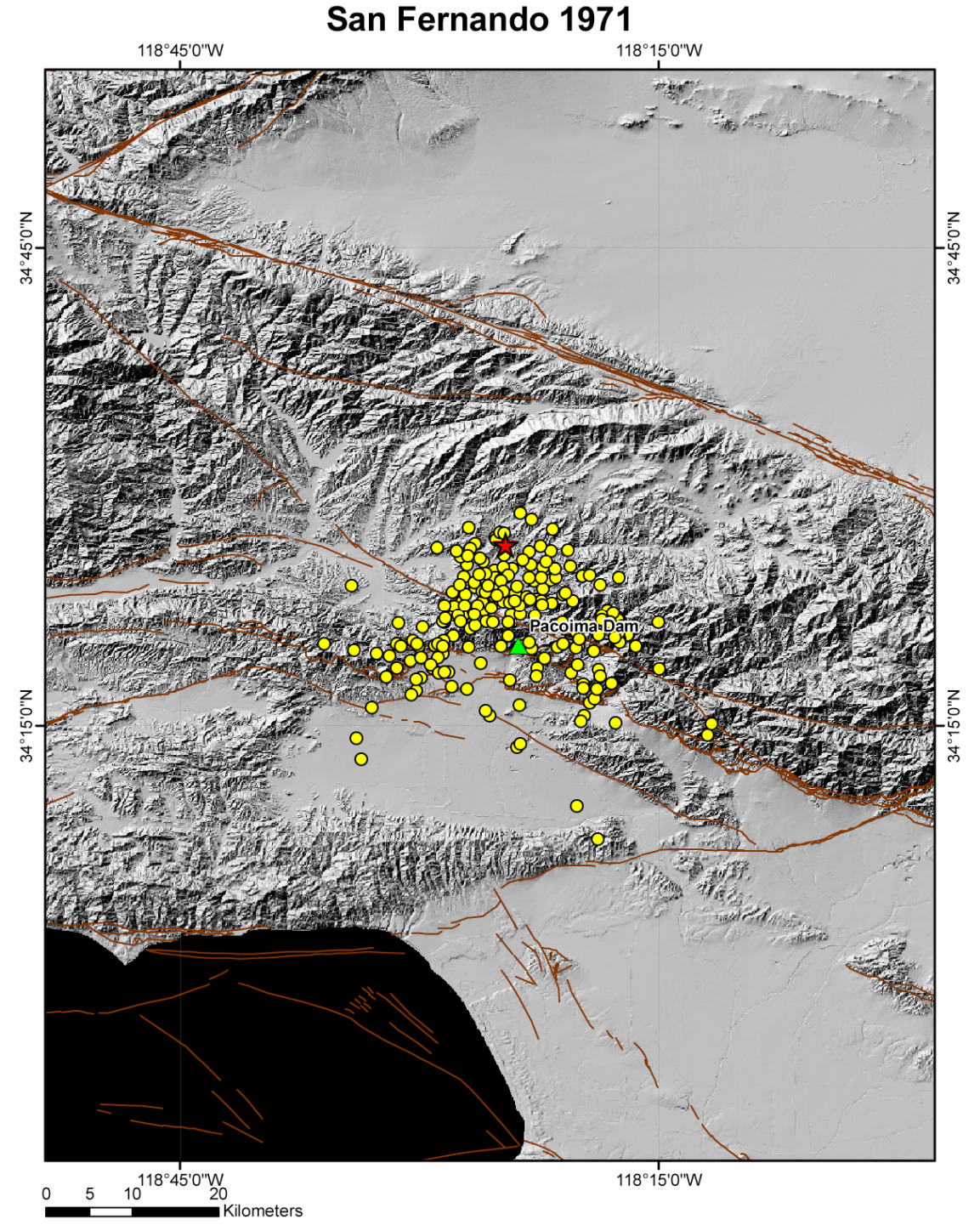

Figure A4. Gazli, May 17, 1976, 02:58:40, M 6.80

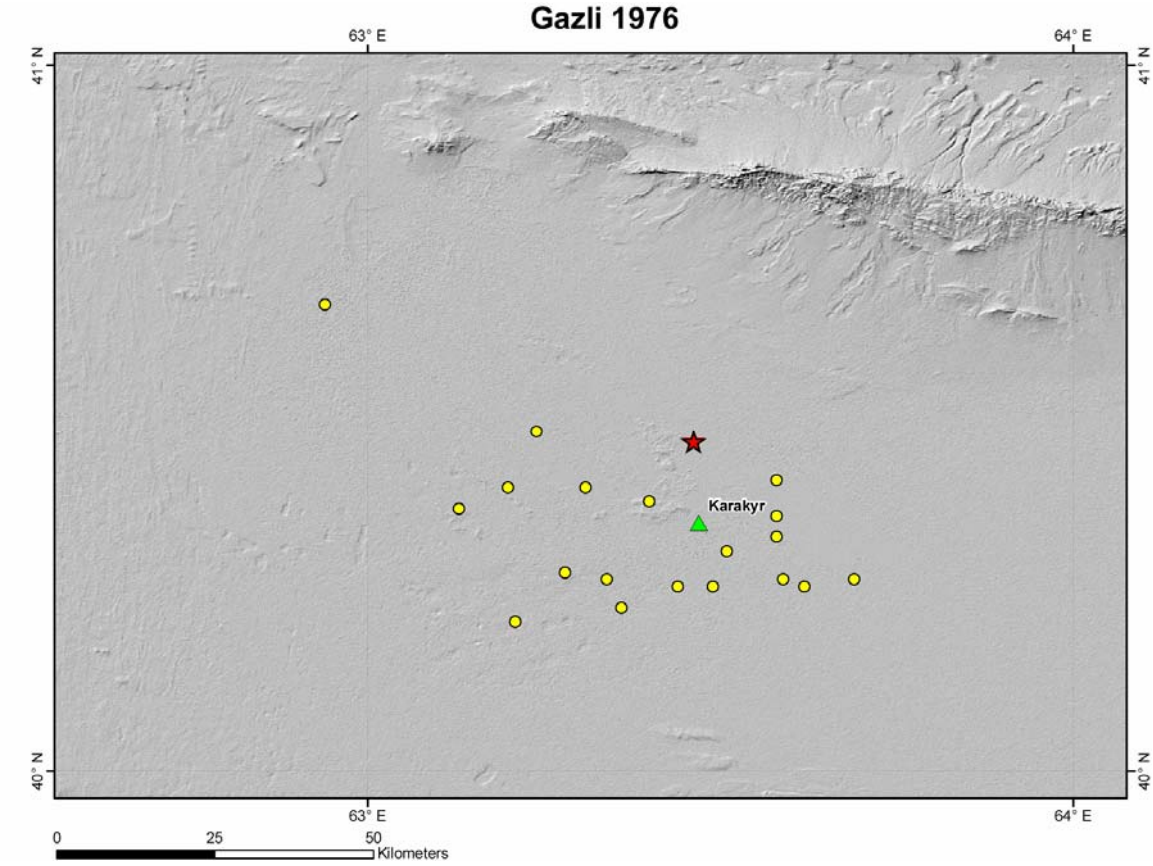

Figure A5. Tabas, Iran, September 16, 1978, 15:35:56, M_W 7.30

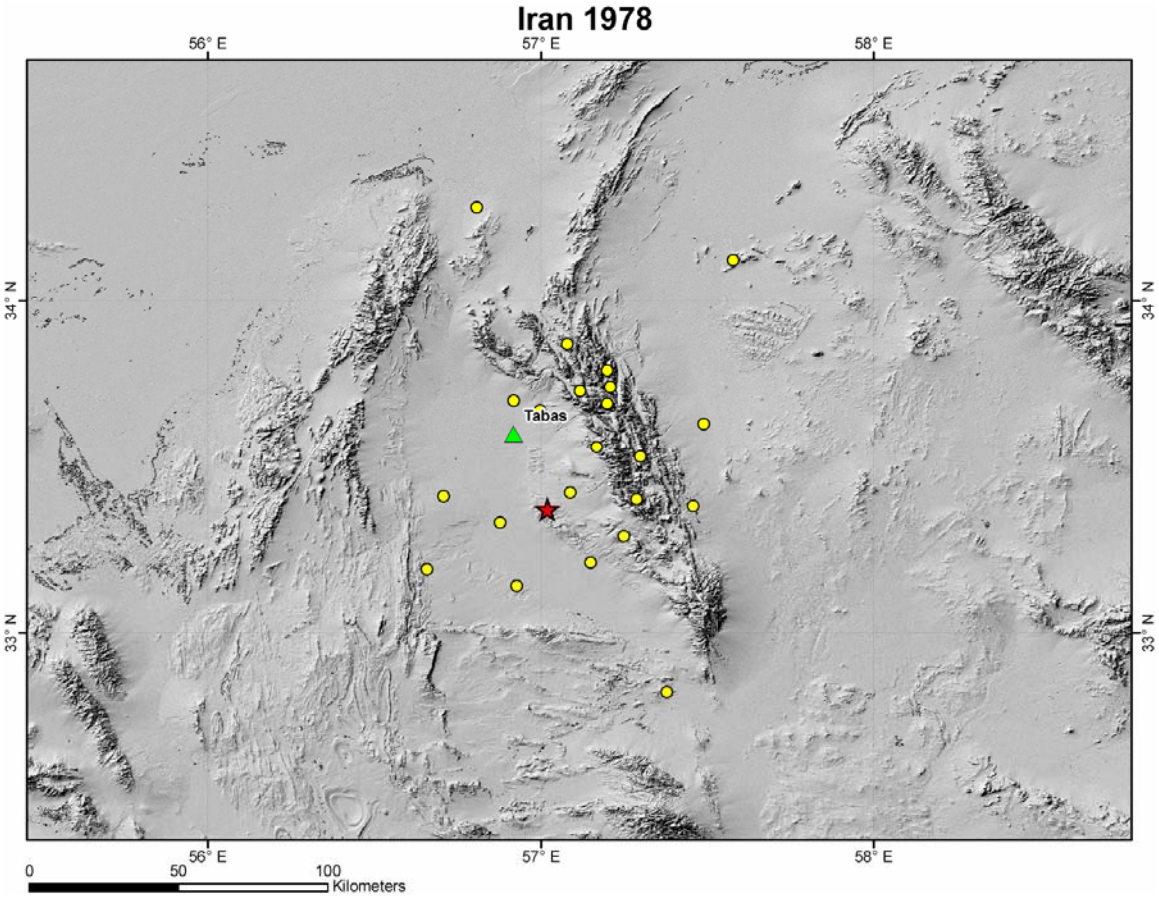

Figure A6. Imperial Valley, October 15, 1979, 23:16:53, M_W 6.50

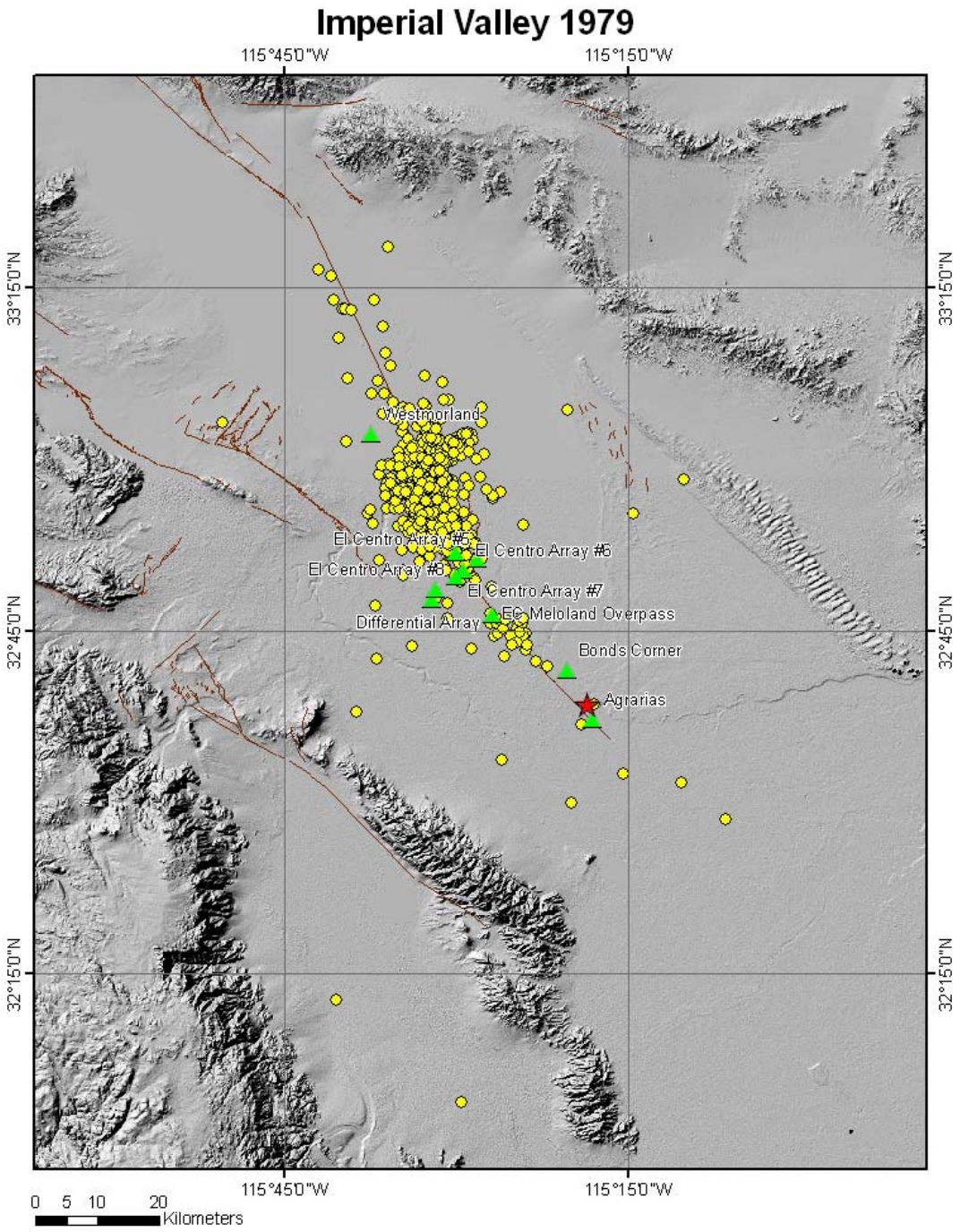

Figure A7. Victoria, June 9, 1980, 03:28:19, M_W 6.40

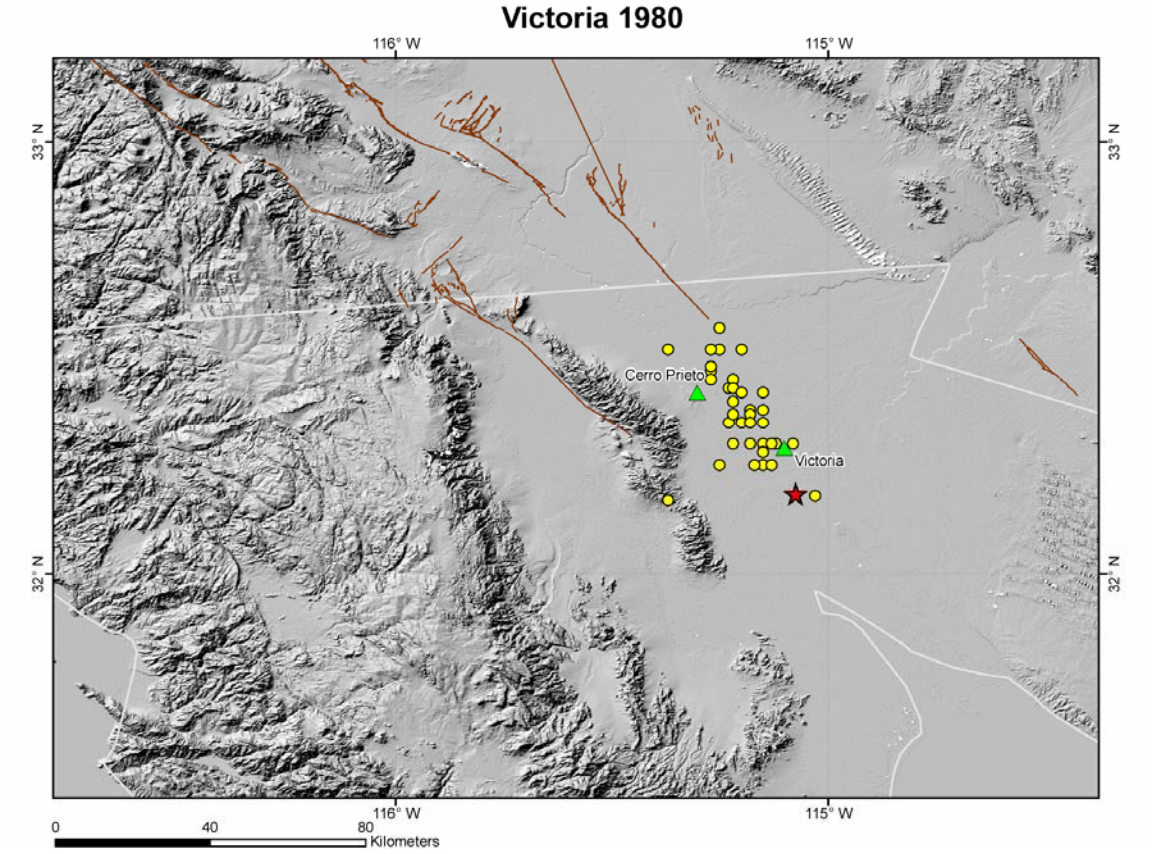

Figure A8. Westmorland, April 26, 1981, 12:09:28, $M_L$brk 6.30

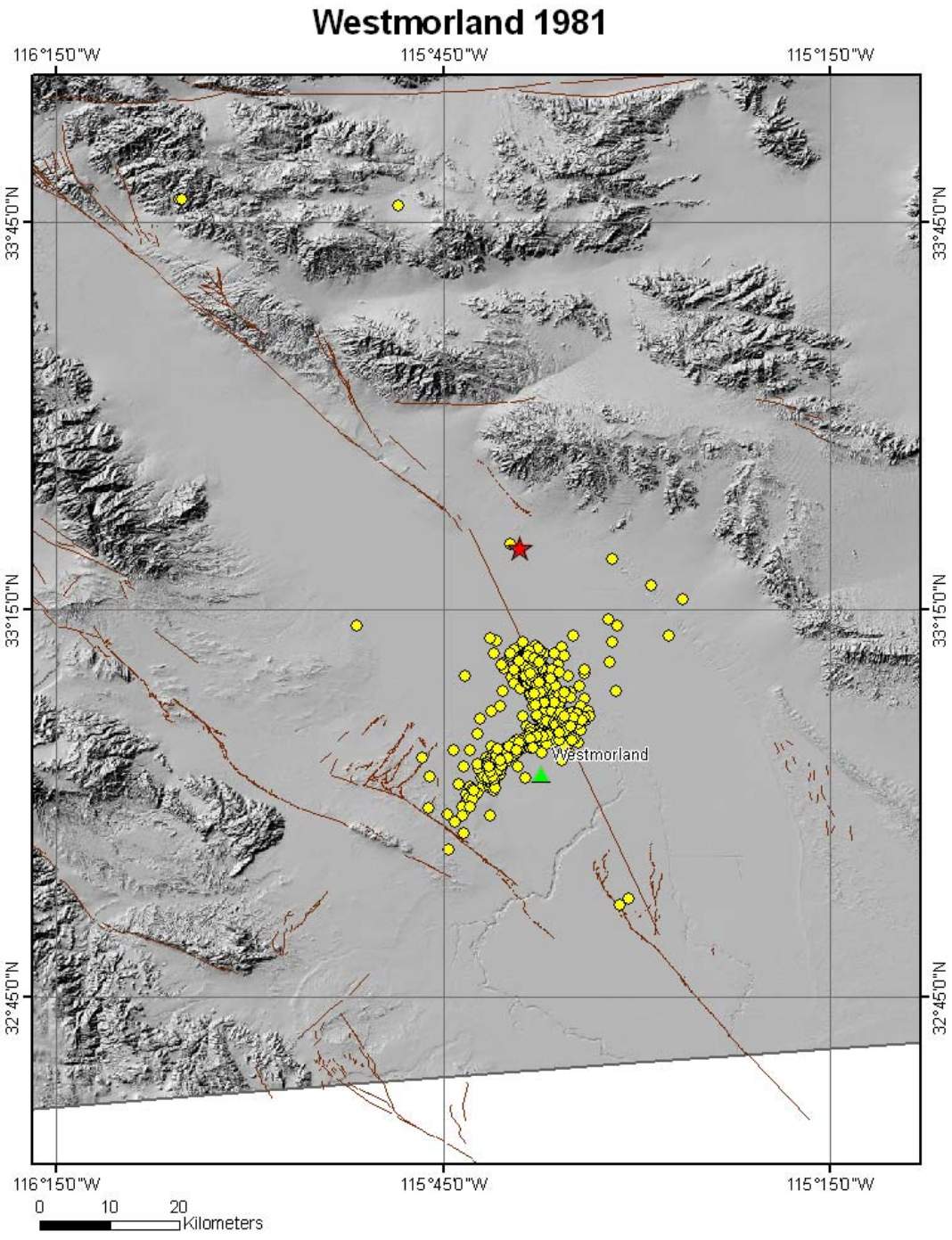

Figure A9. Coalinga, May 2, 1983, 23:42:38, M_W 6.50

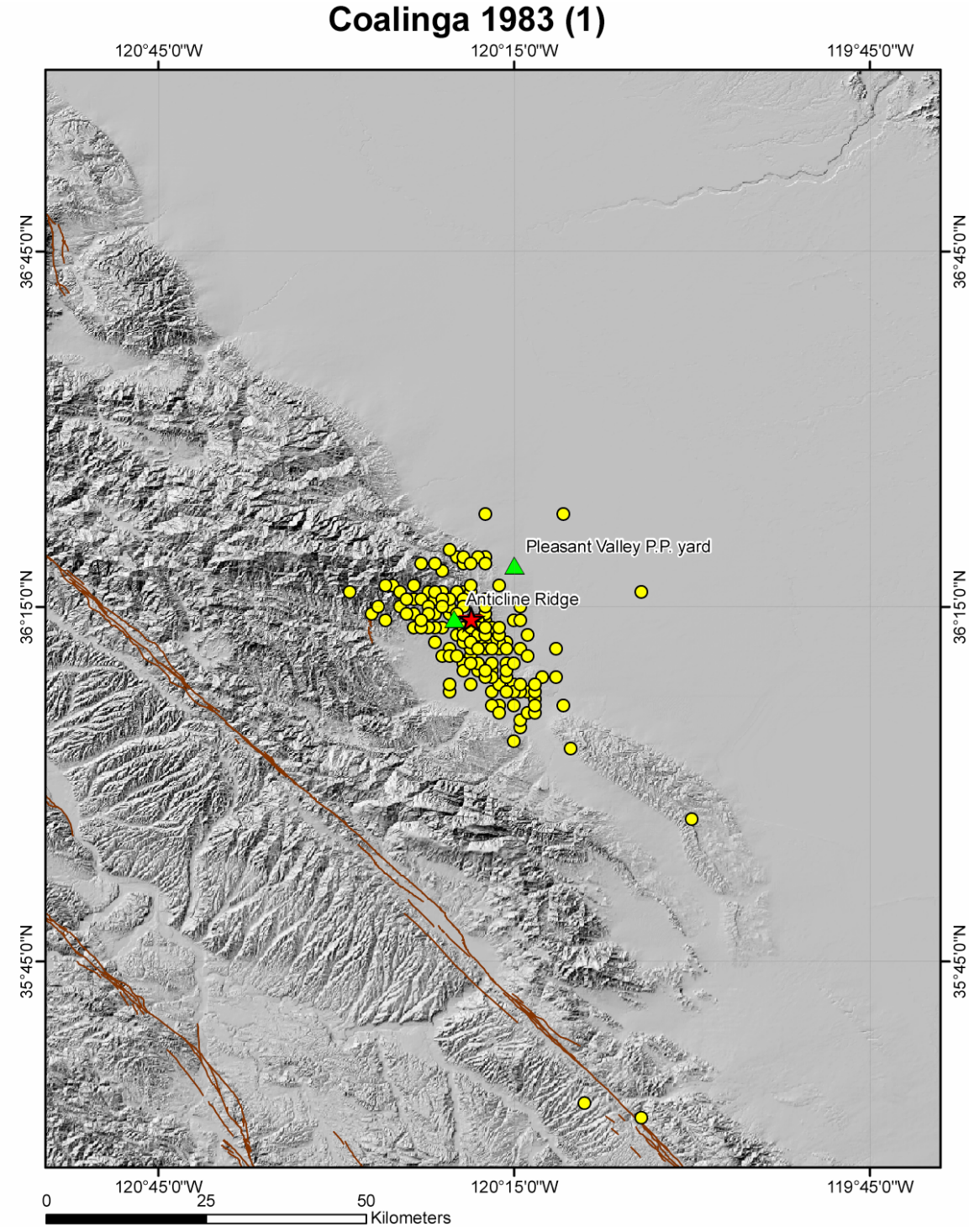
Coalinga 1983 (1)
120°45'0"W
120°15'0"W
119°45'0"W
36°45'0"N
36°15'0"N
35°45'0"N
Pleasant Valley P.P. yard
Anticline Ridge
0
25
50
Kilometers

Figure A10. Coalinga, July 22, 1983, 02:39:54, M_W 6.00

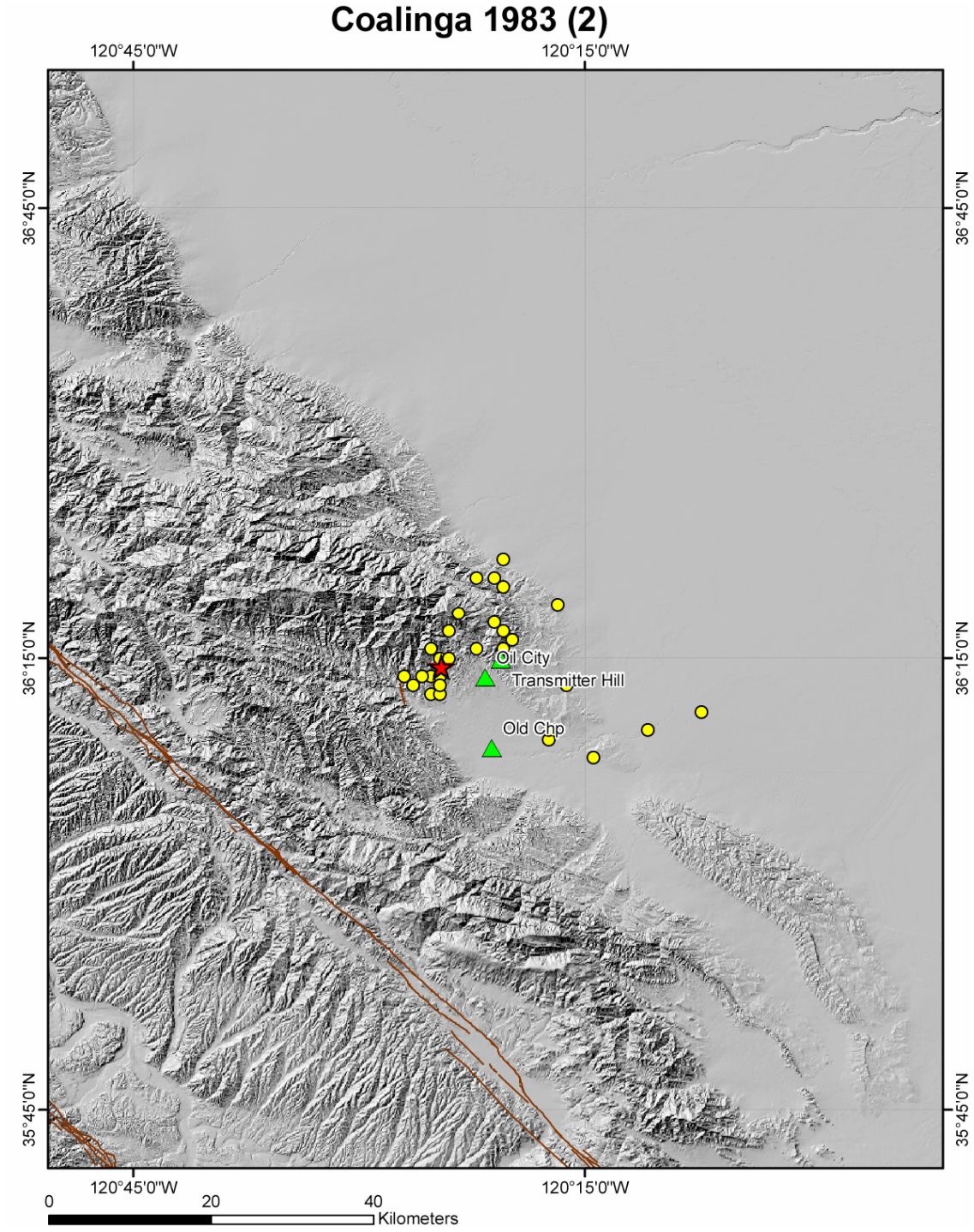

Figure A11. Morgan Hill, April 24, 1984, 21:15:18, M_W 6.10

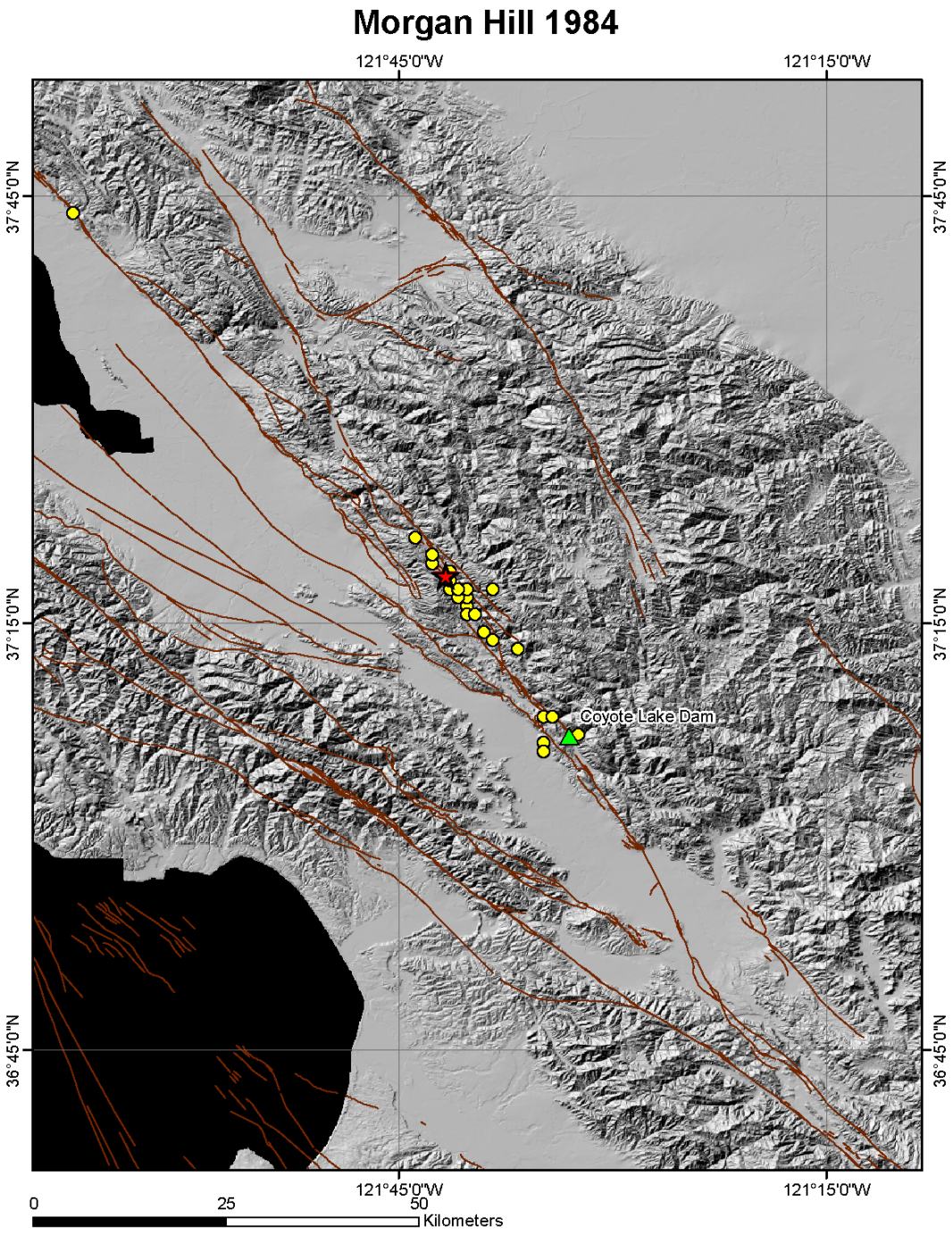

Figure A12. Valapraiso, March 3, 1985, 22:47:07, M_W 7.80

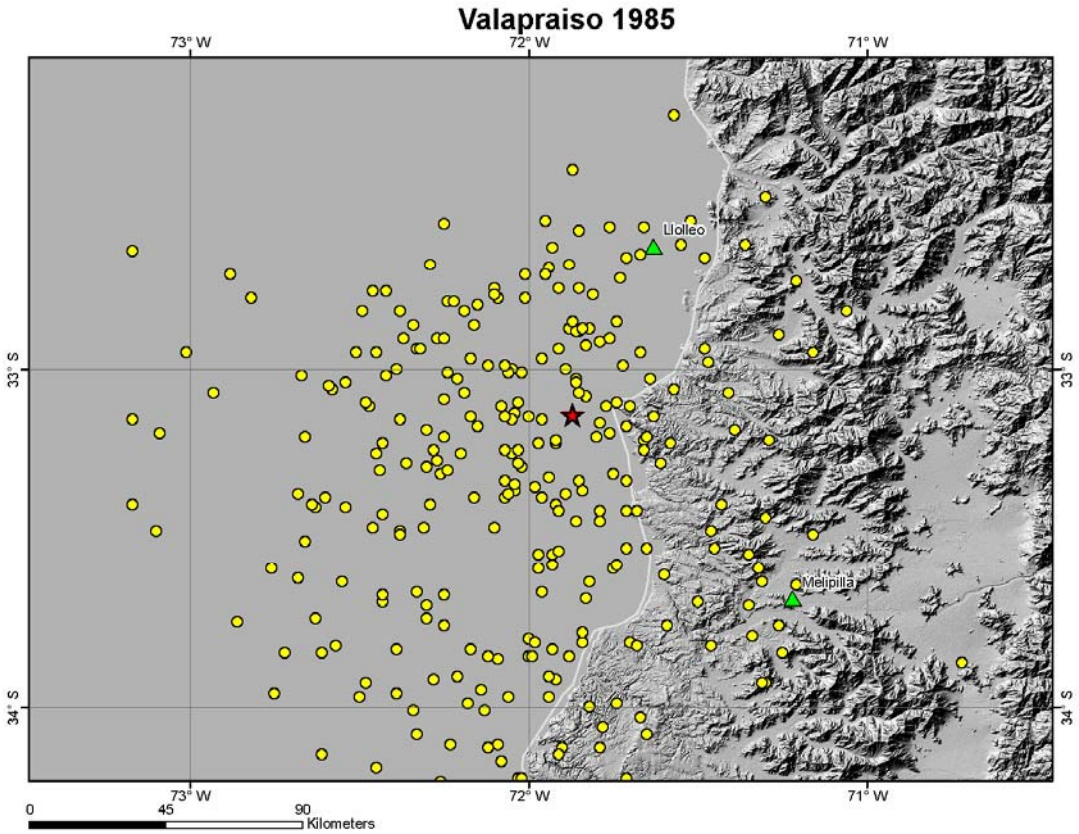

Figure A13. Michoacan Aftershock, September 21, 1985, 01:37:13, M_W 7.50

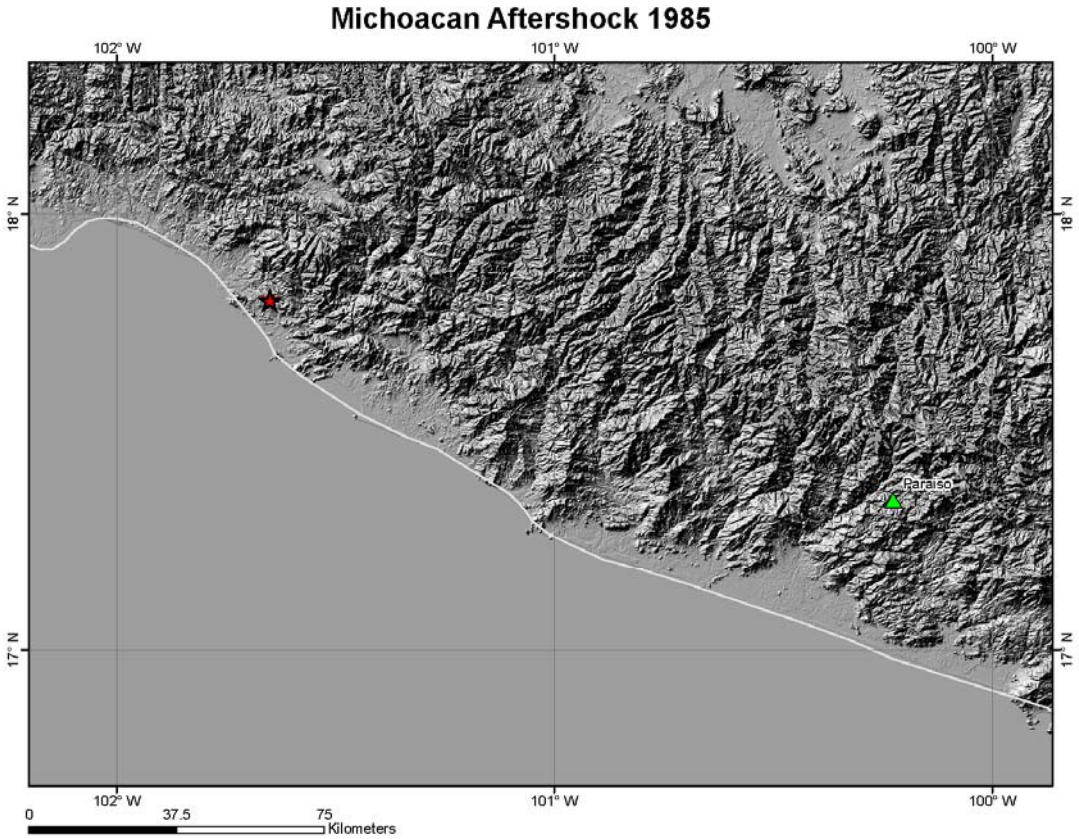

Figure A14. Nahanni, December 23, 1985, 05:16:00, M_S 6.90

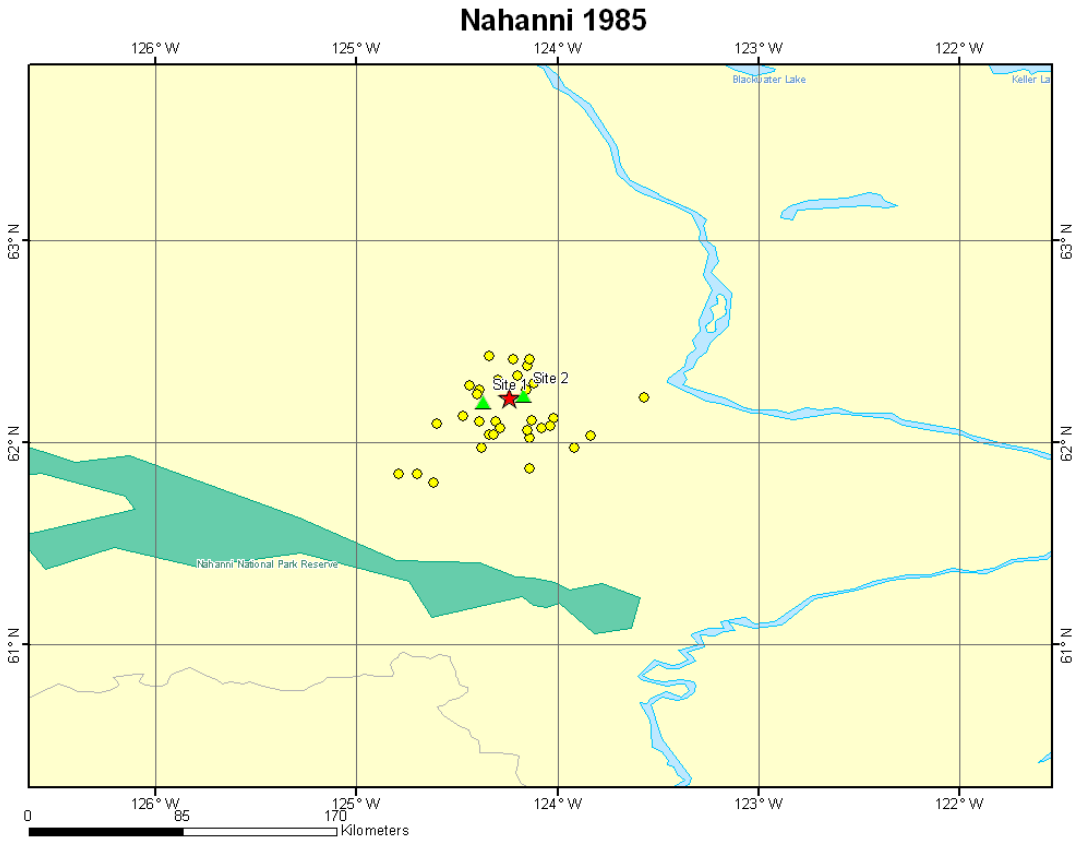

Figure A15. North Palm Springs, July 8, 1986, 09:20:44, M_W 6.20

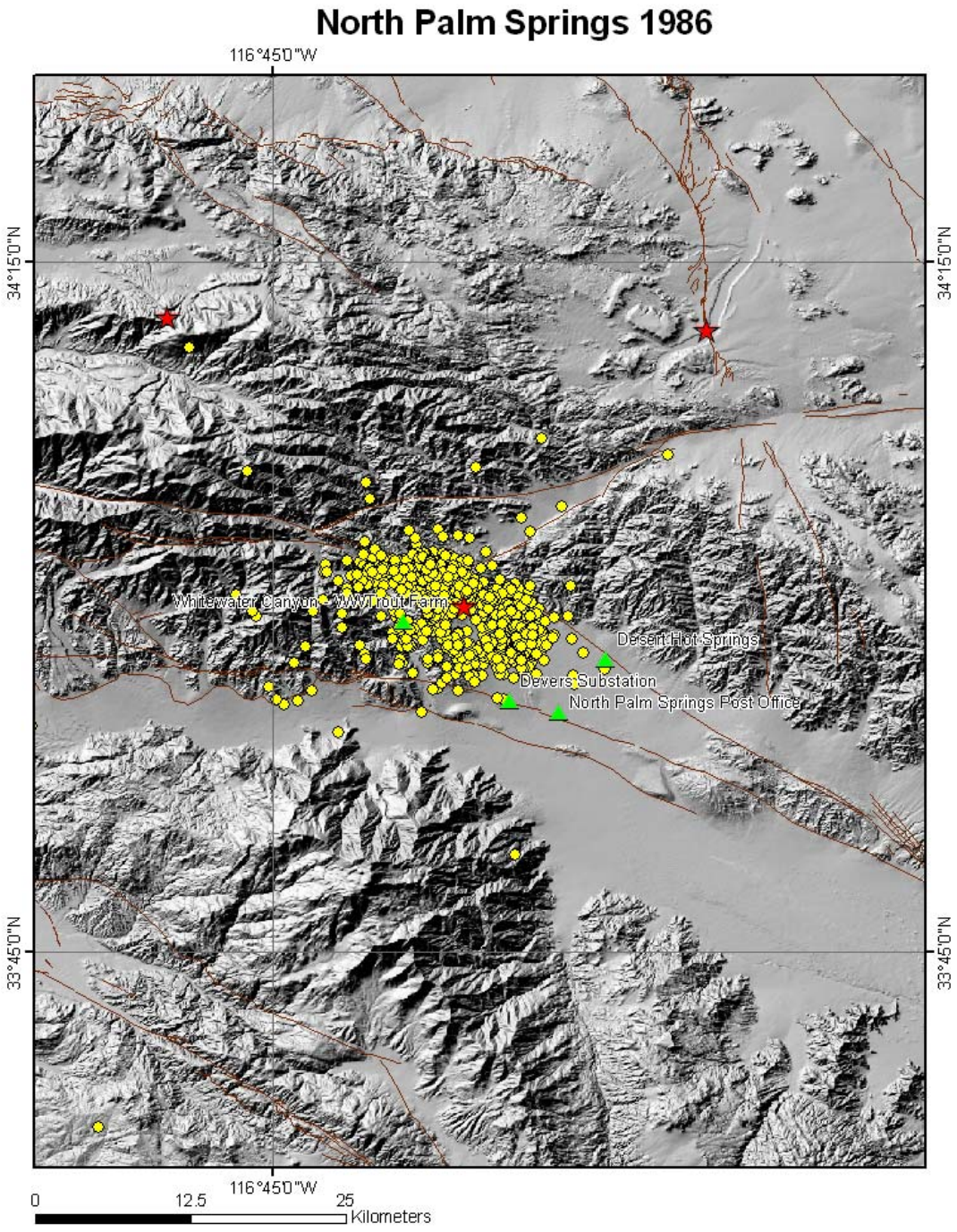

Figure A16. Whittier Narrows, October 1, 1987, 14:42:20, M_W 6.10

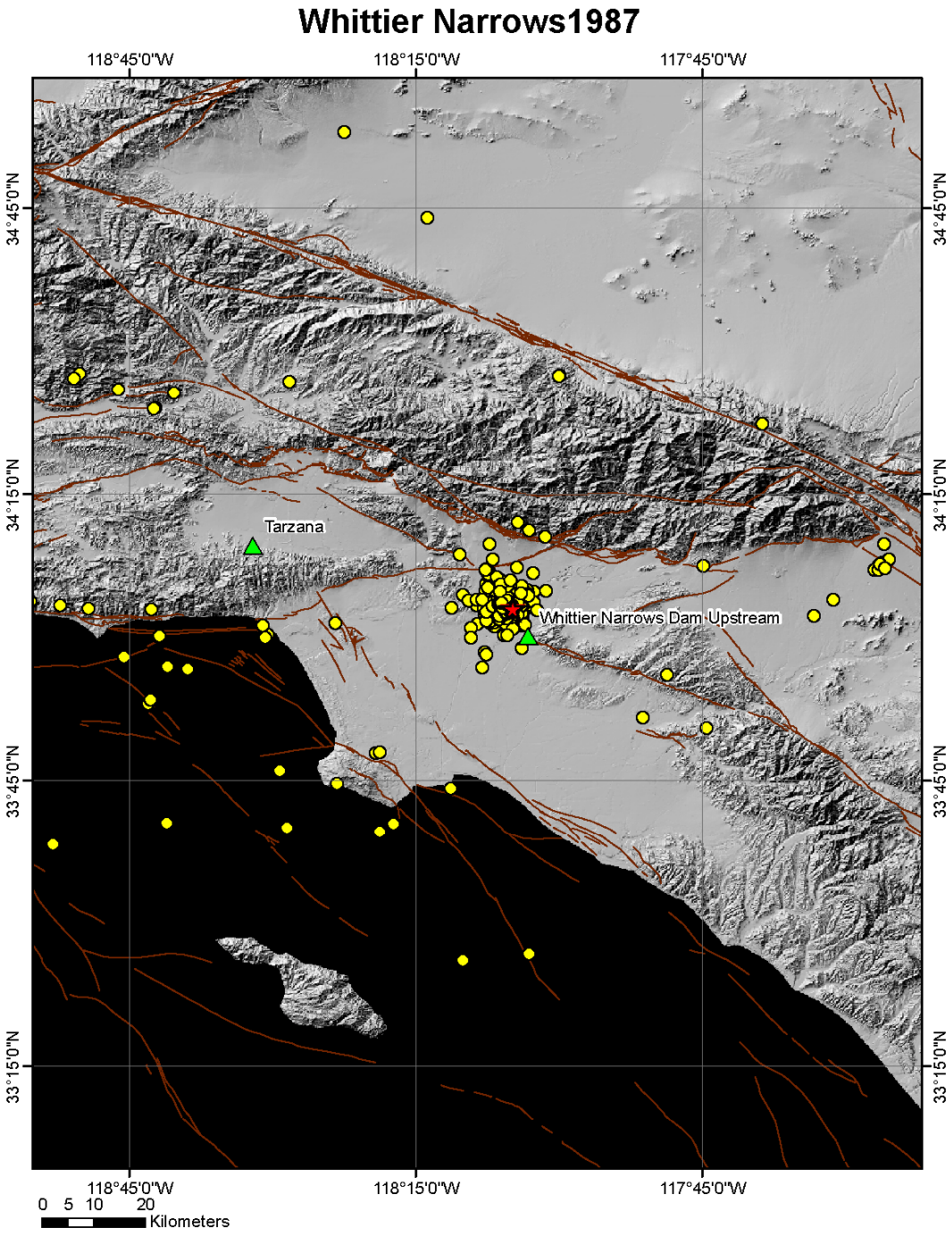

Figure A17. Superstition Hills, November 24, 1987, 13:15:56, $M_L$brk 6.70

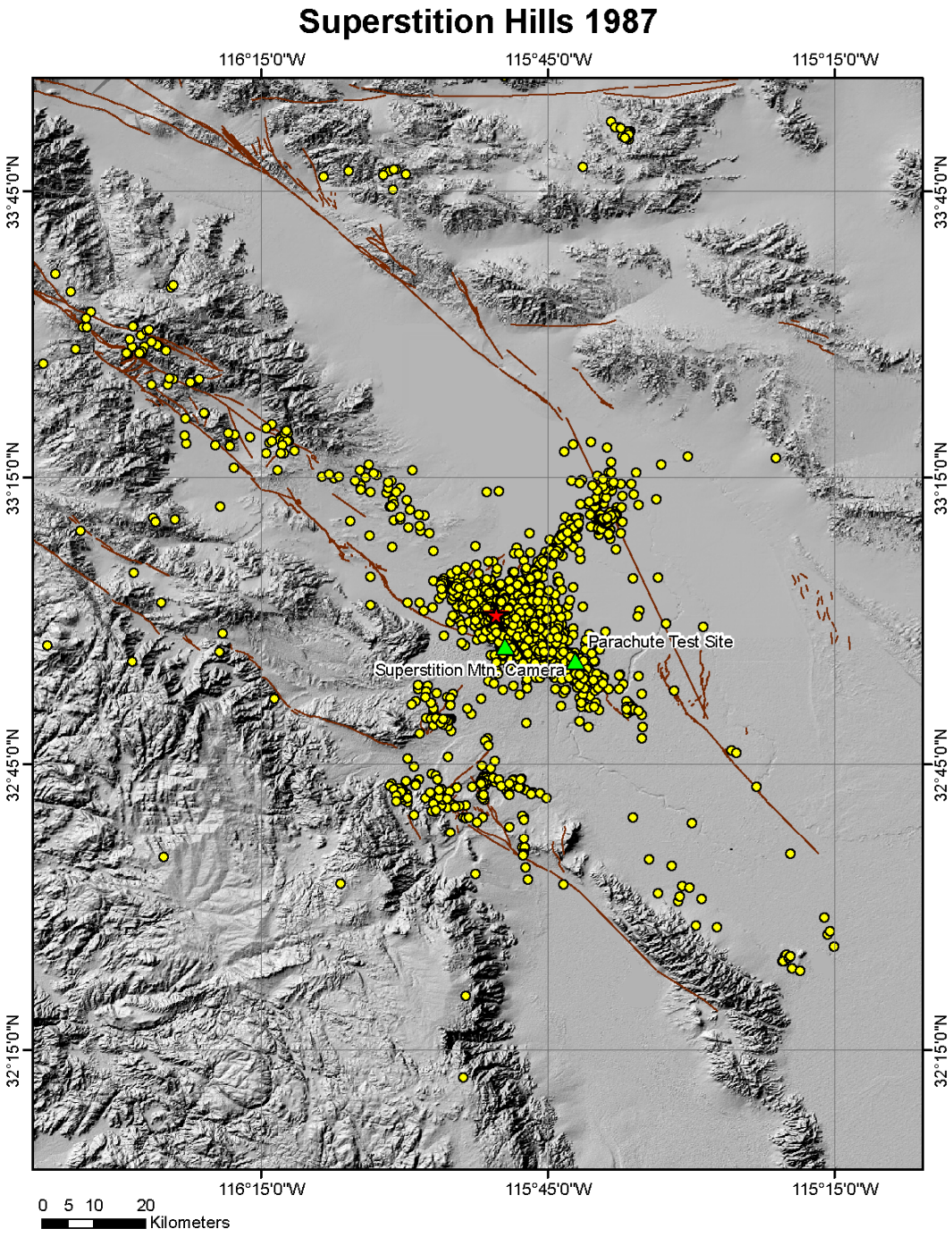

Figure A18. Loma Prieta, October 18, 1989, 00:04:15, M_W 7.00

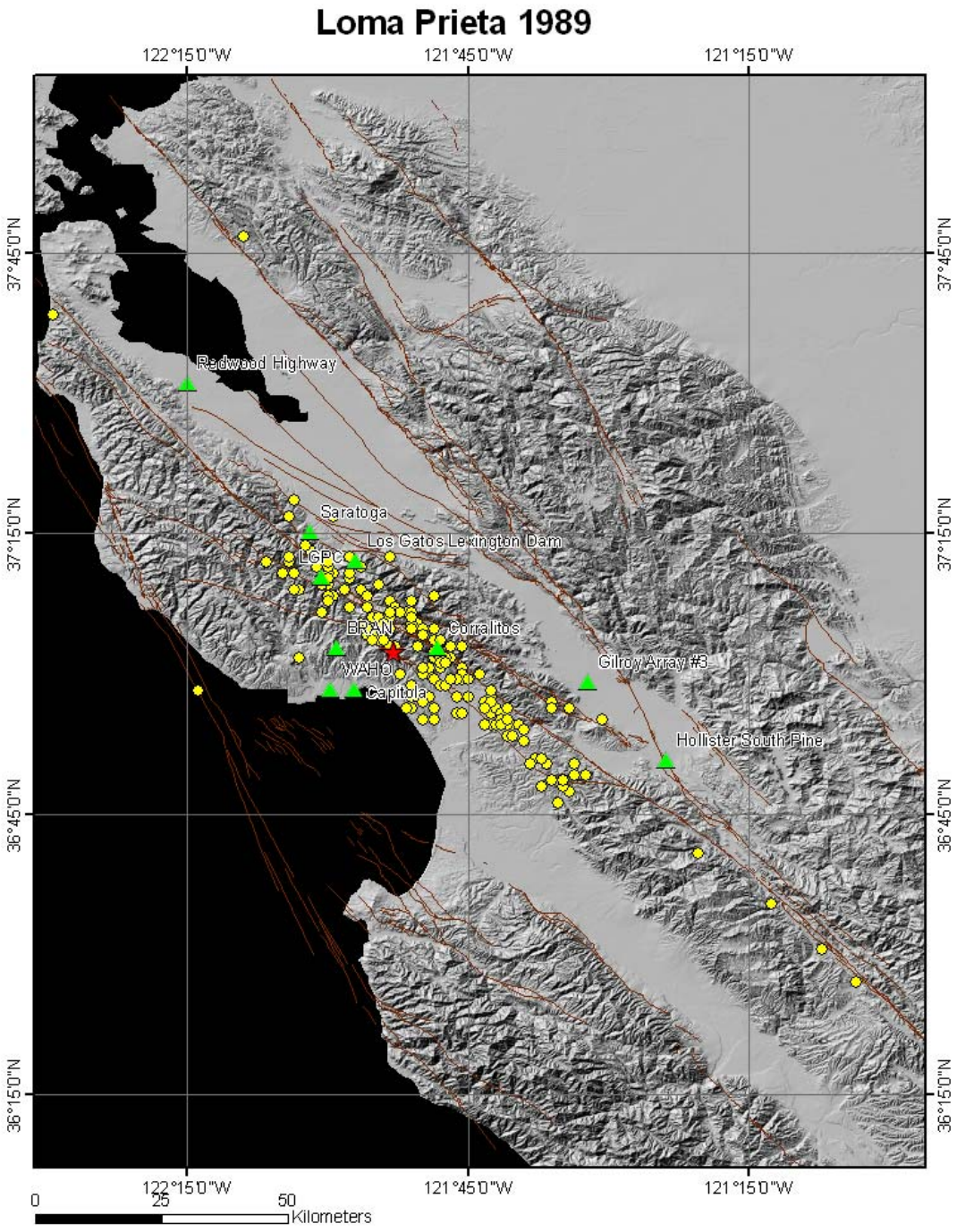

Figure A19. Manjil, Iran, June 20, 1990, 09:00:10, M_W 7.40

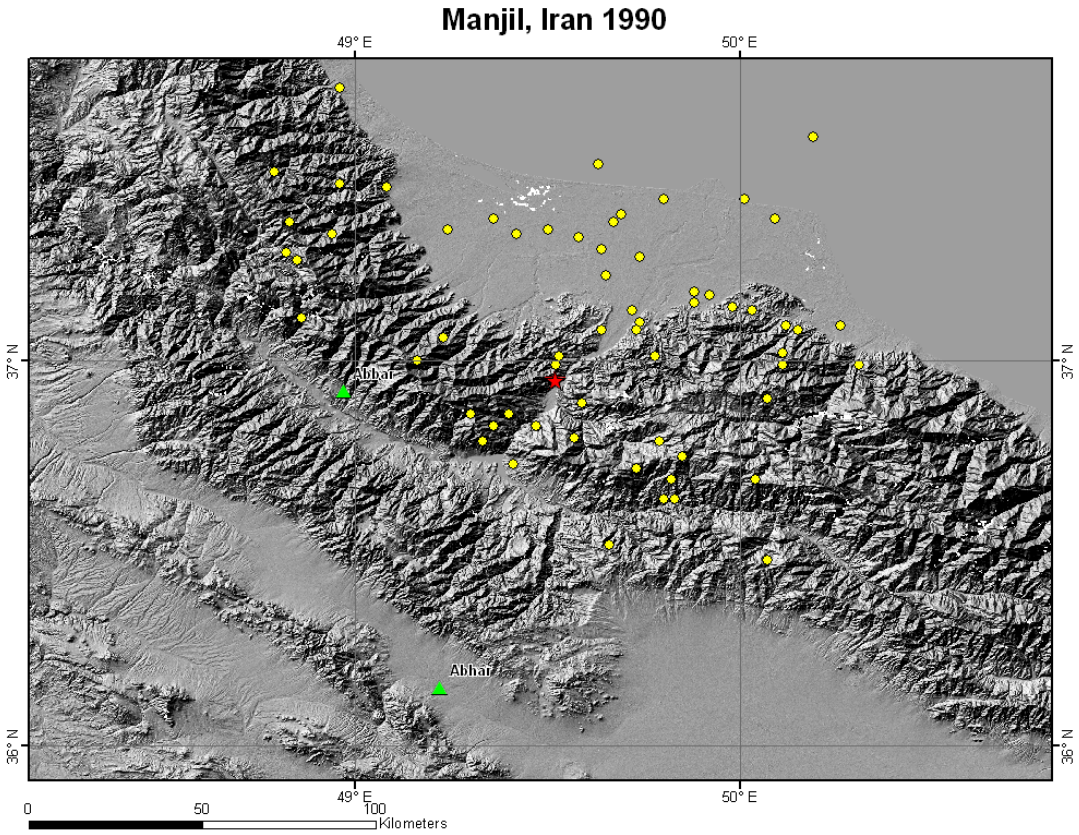

Figure A20. Erzican, March 13, 1992, 17:18:40, $M_S$brk 6.90

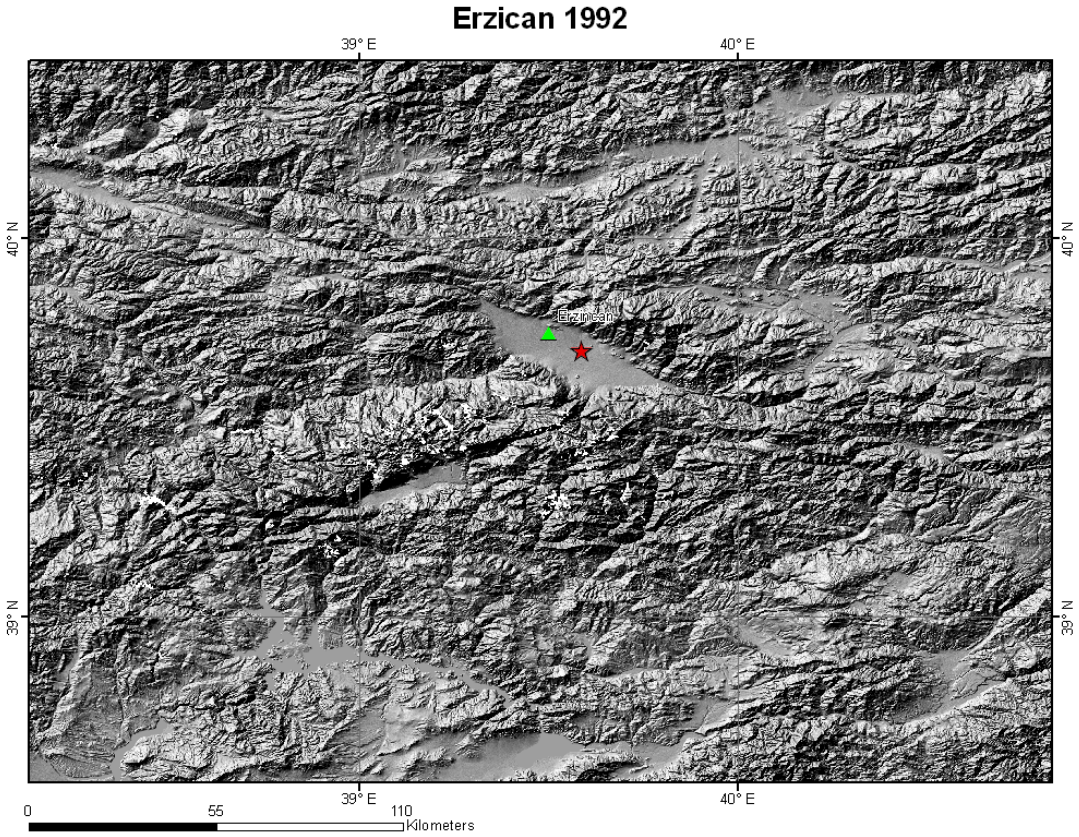

Figure A21. Cape Mendocino, April 25, 1992, 18:06:04, M_W 7.00

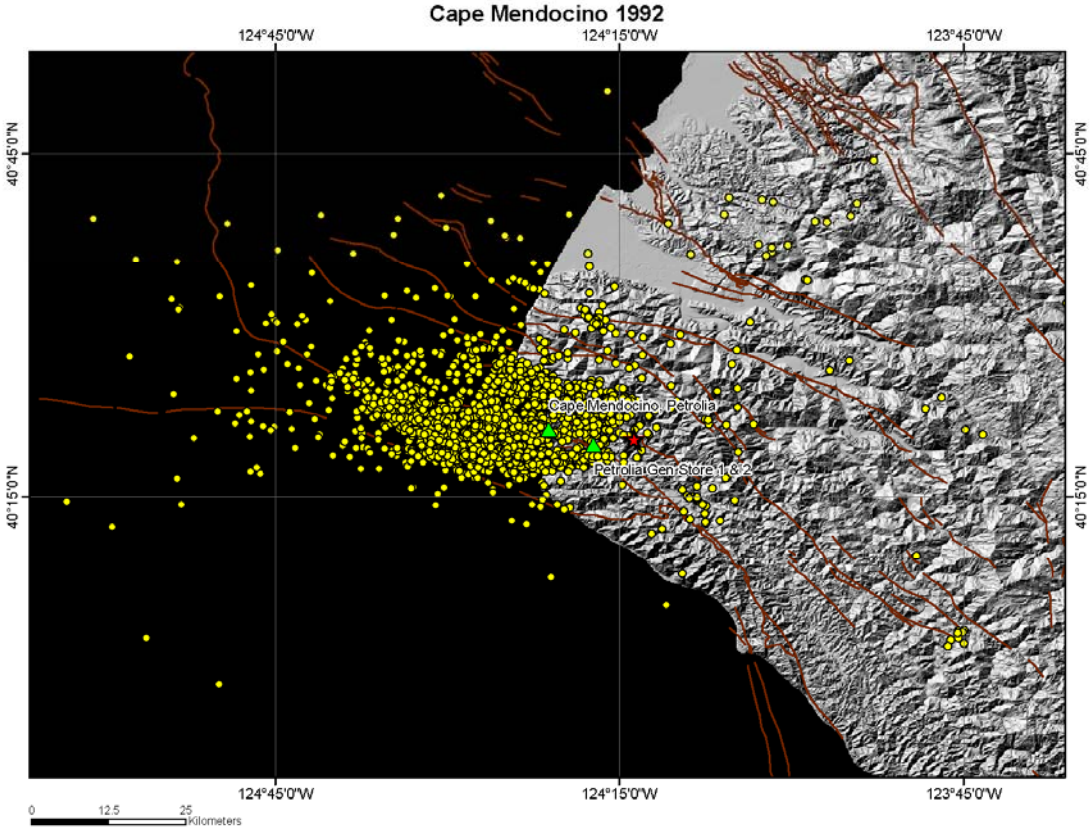

Figure A22. Landers, June 28, 1992, 11:57:34, M_W 7.30

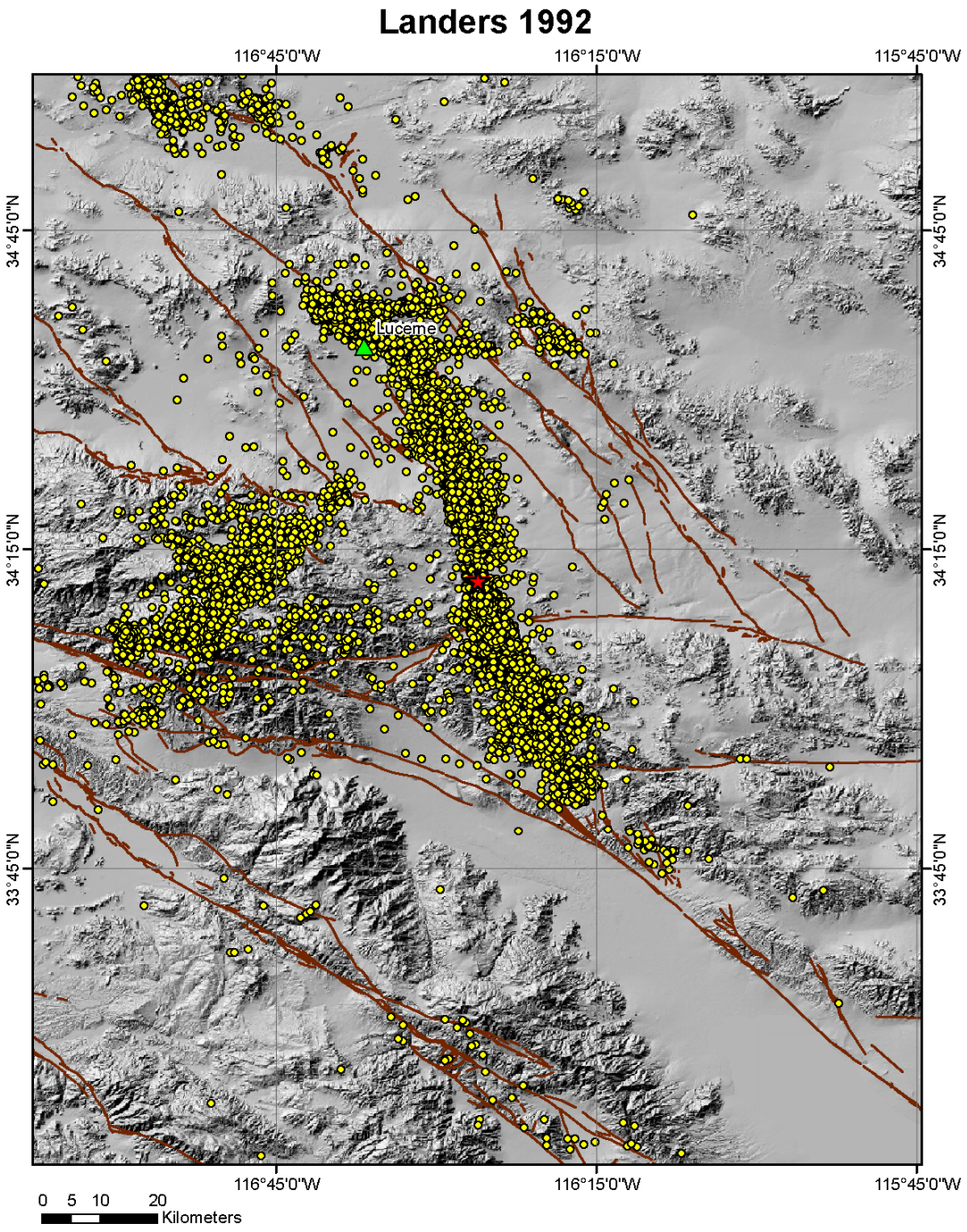

Figure A23. Northridge, January 17, 1994, 12:30:55, M_W 6.70

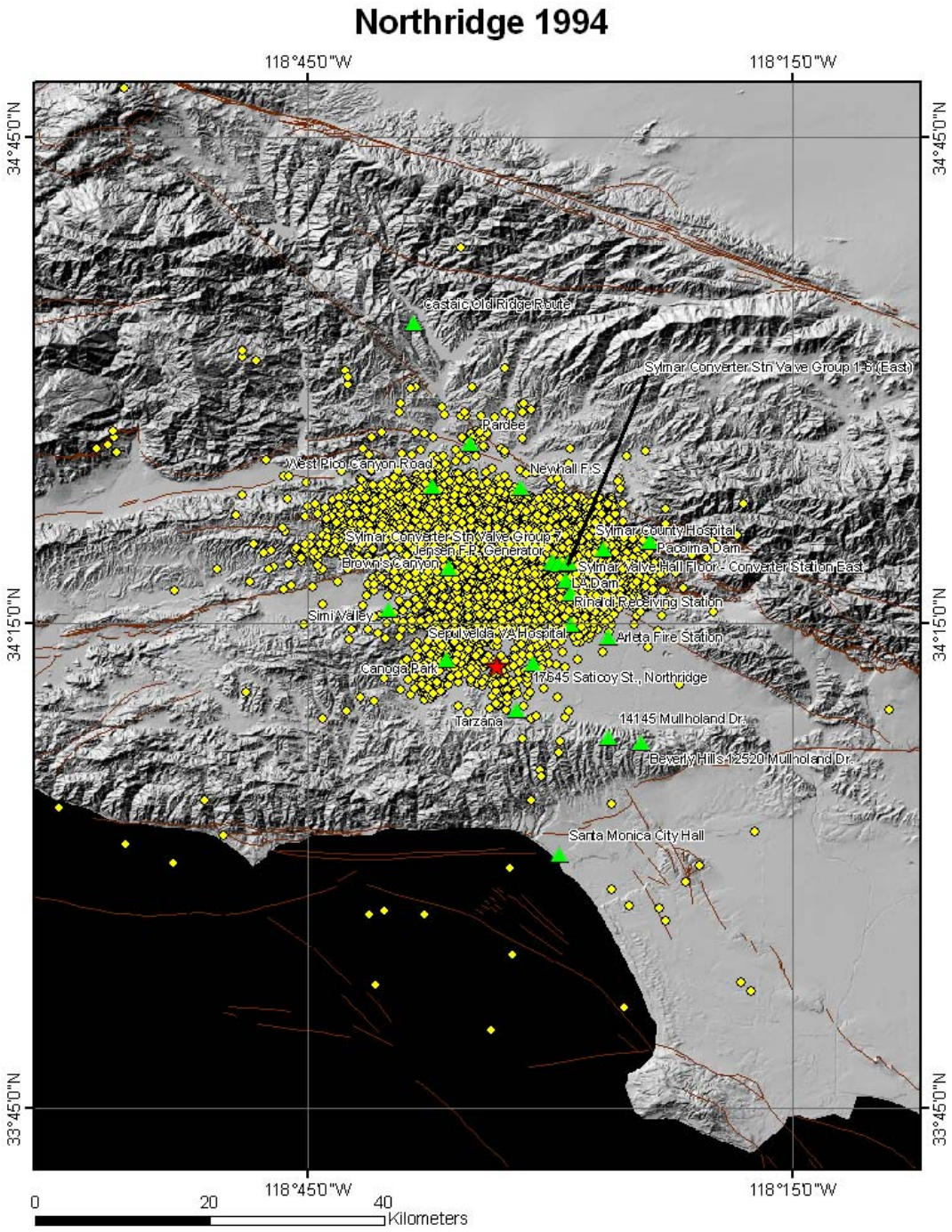

Figure A24. Zanjiran, June 20, 1994, 09:09:02, M_W 5.90

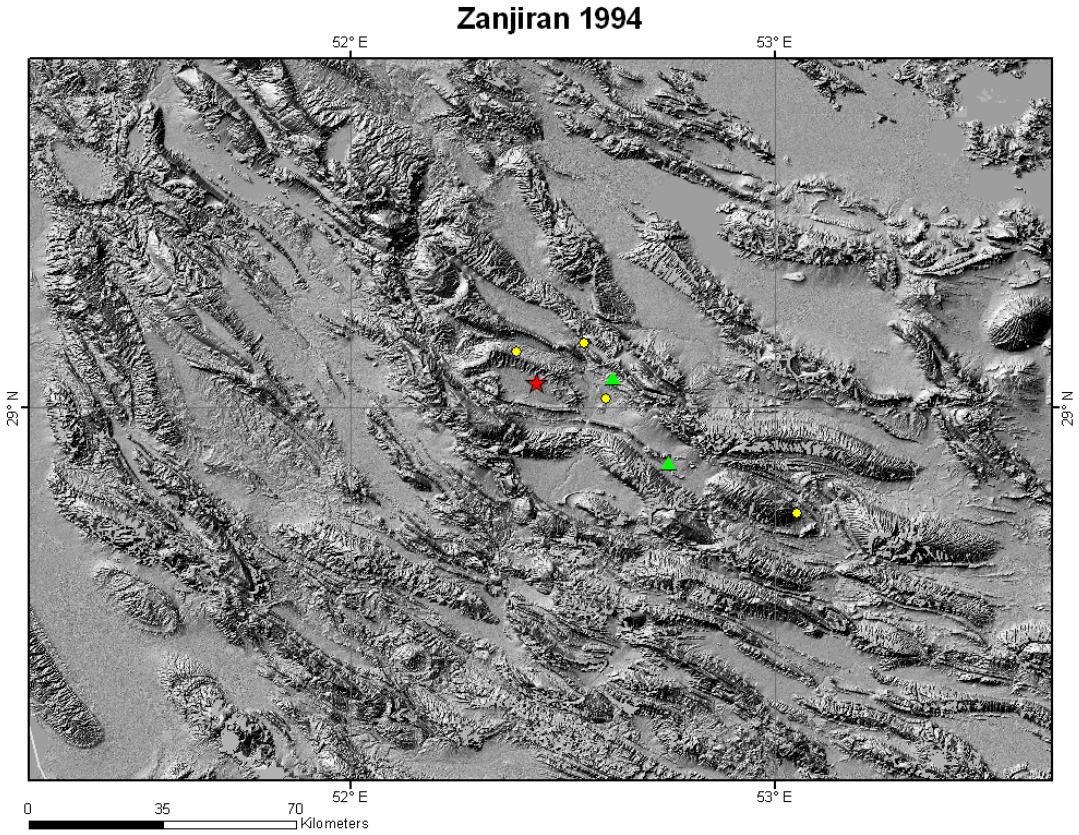

Figure A25. Kobe, January 16, 1995, 20:46:52, M_W 6.90

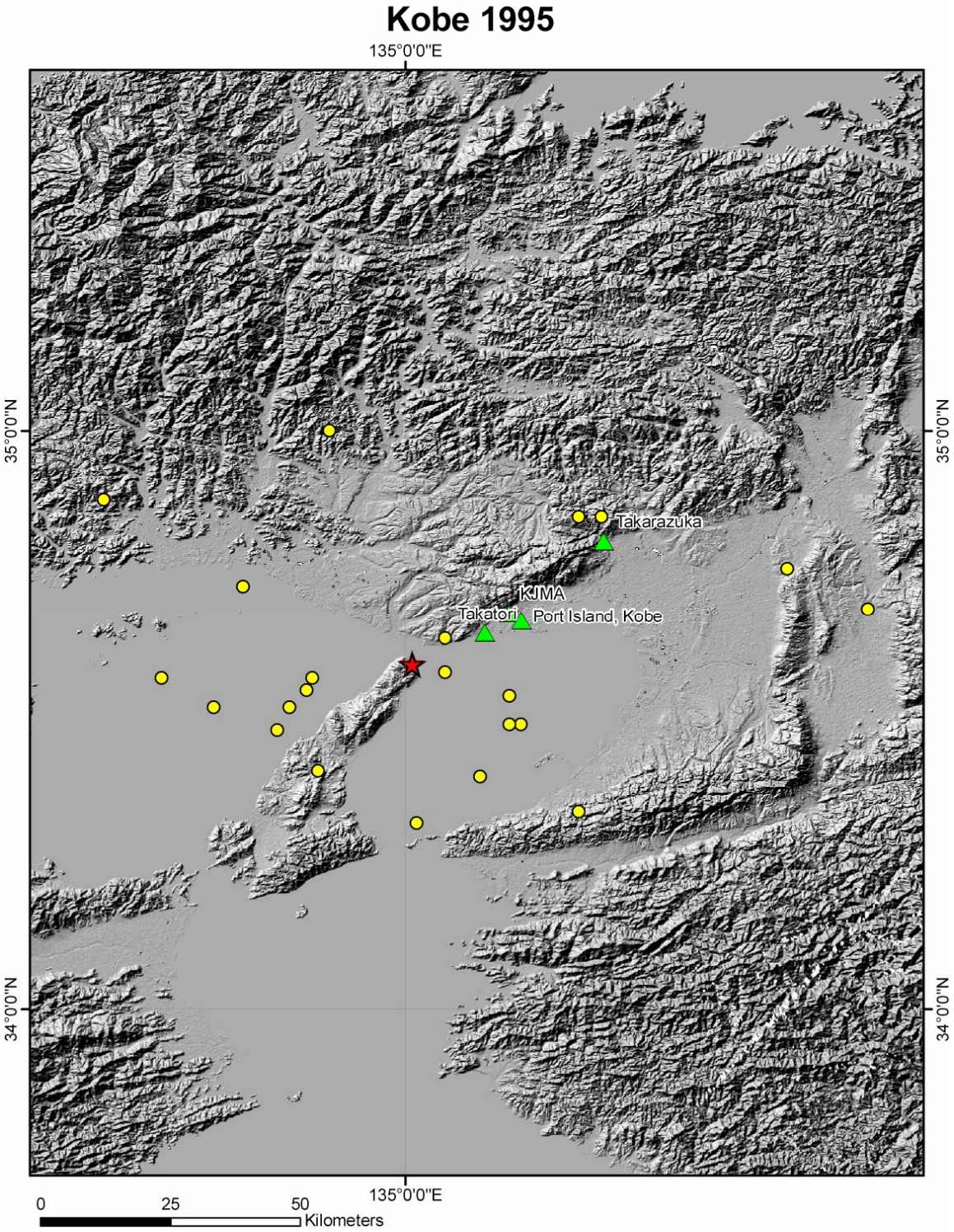

Figure A26. East Coast Honshu, May 23, 1996, 09:36:31, M_W 5.00

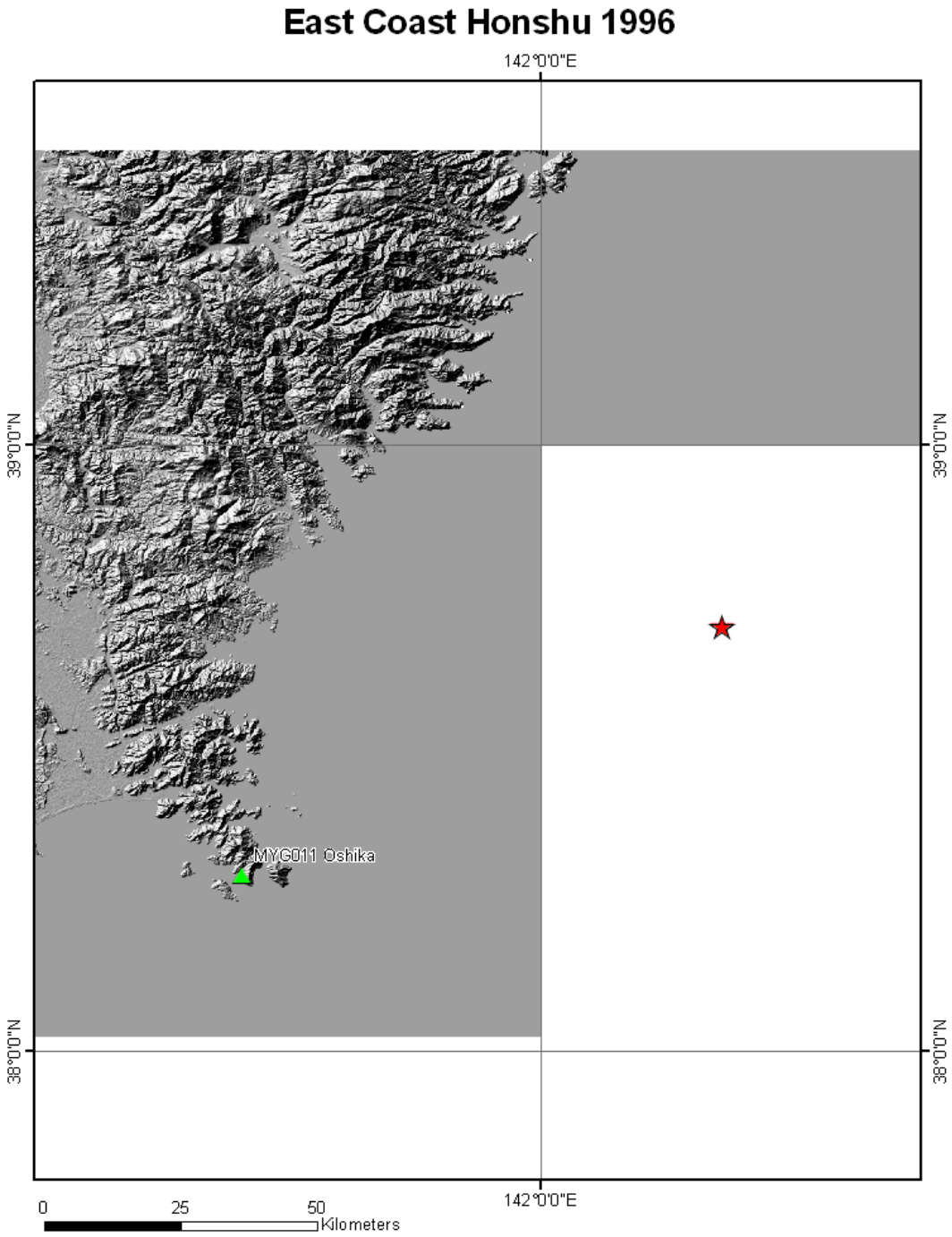

Figure A27. Central Honshu, August 13, 1996, 02:13:00, Mjma 5.00

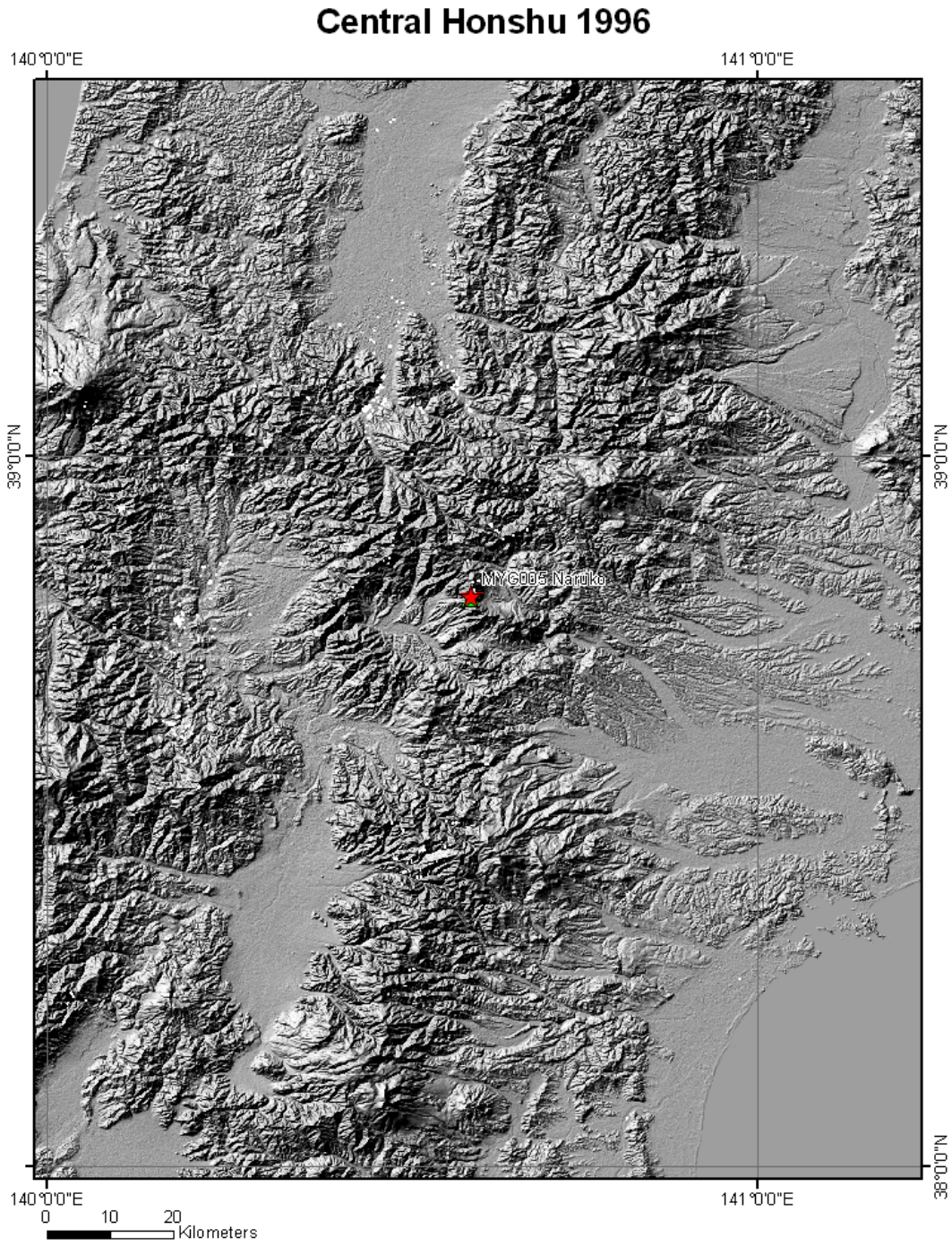

Figure A28. Honshu, December 21, 1996, 01:28:51, mb-GS 5.70

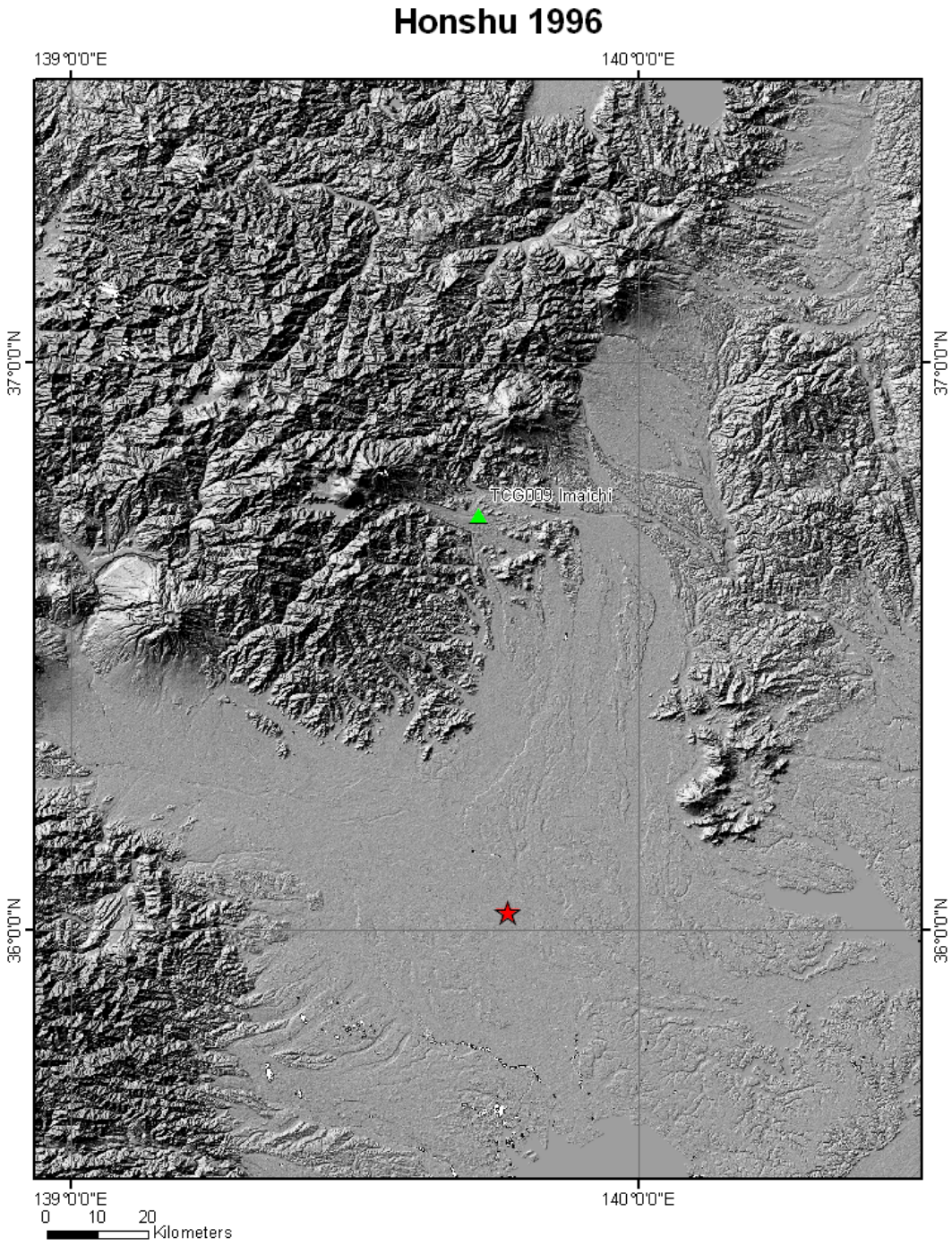

Figure A29. South Coast Honshu, March 3, 1997, 14:09:43, M_W 5.00

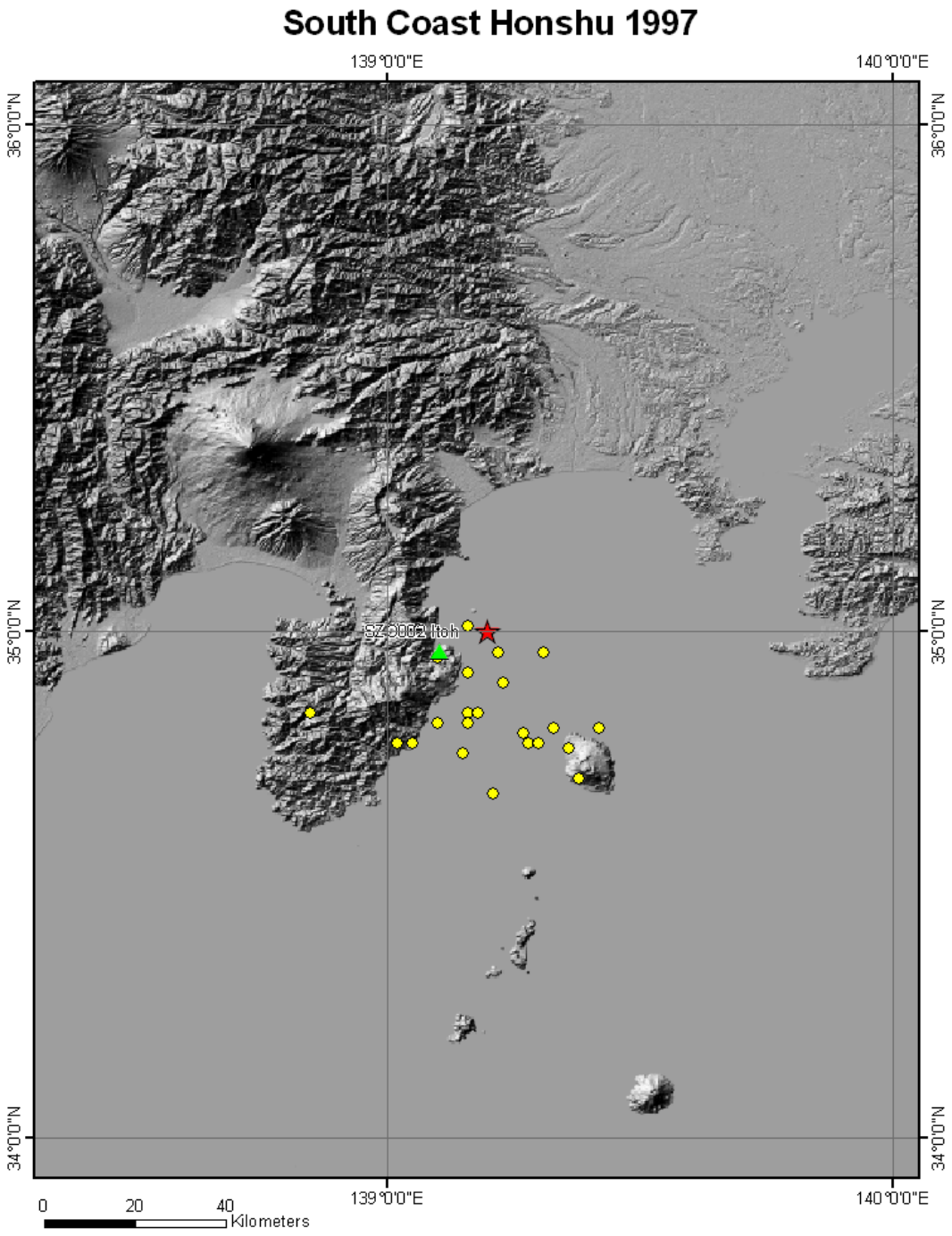

Figure A30. South Coast Honshu, March 16, 1997, 05:51:37, M_W 5.80

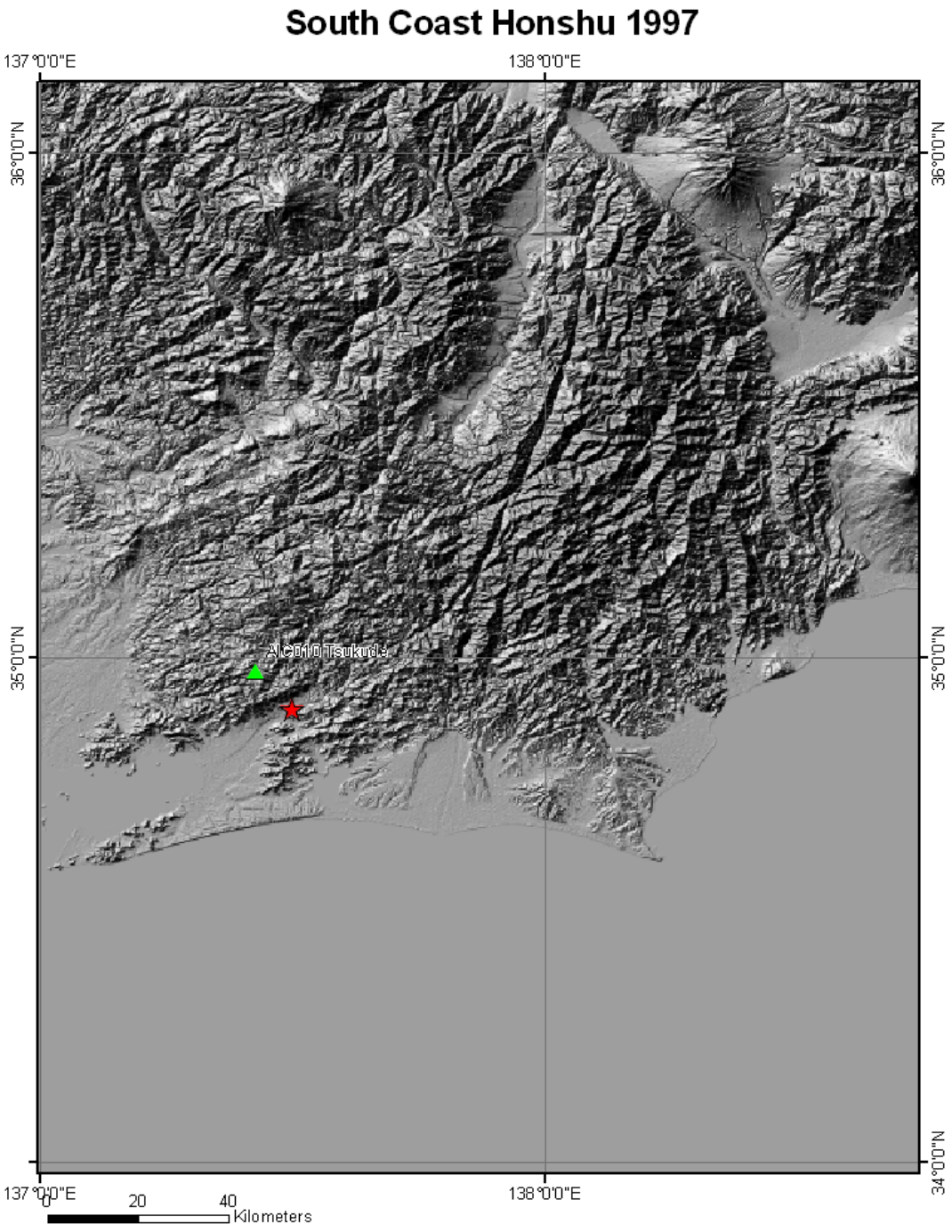

Figure A31. Kyushu, March 26, 1997, 08:31:47, M_W 6.30

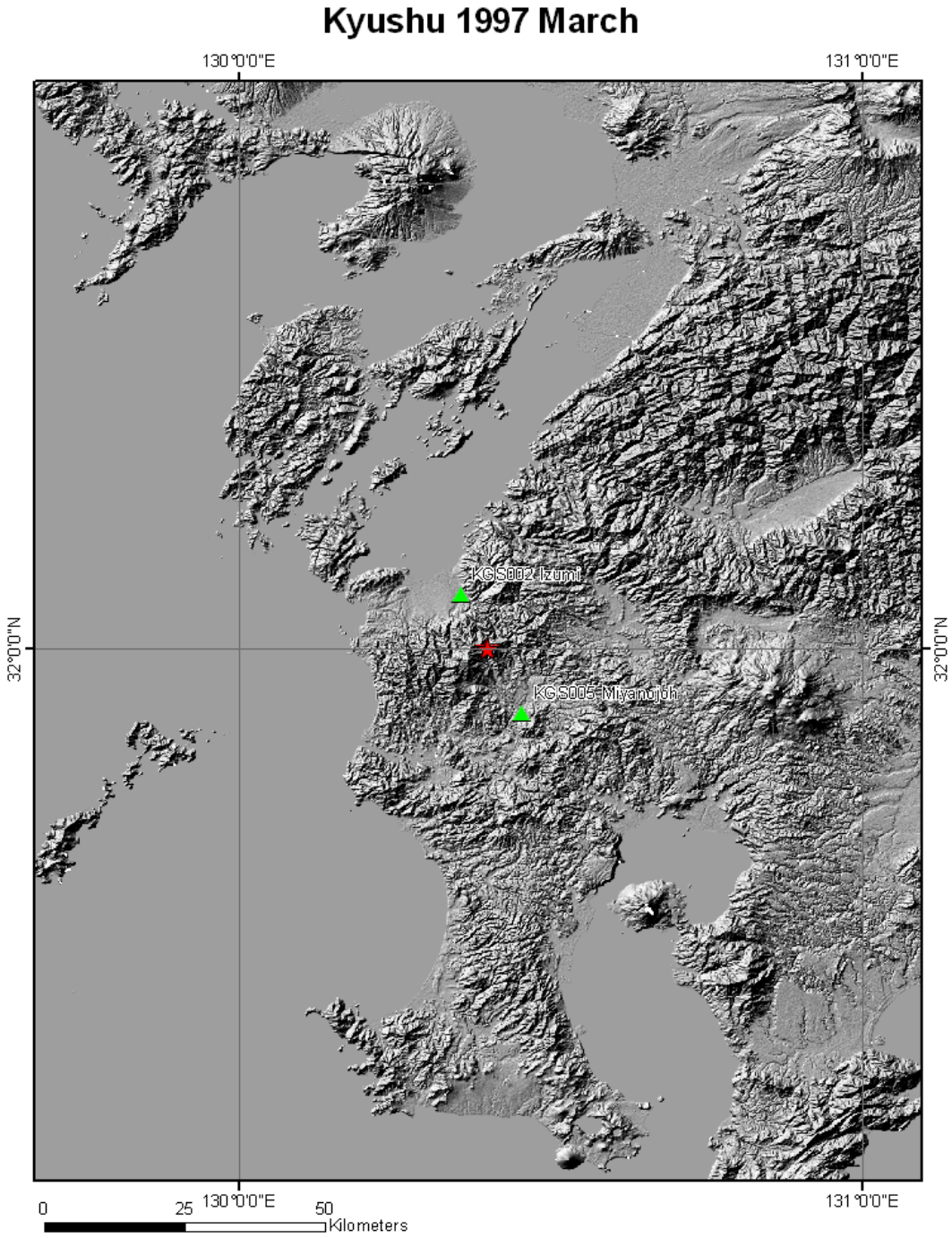

Figure A32. Kyushu, May 13, 1997, 05:38:30, M_W 6.20

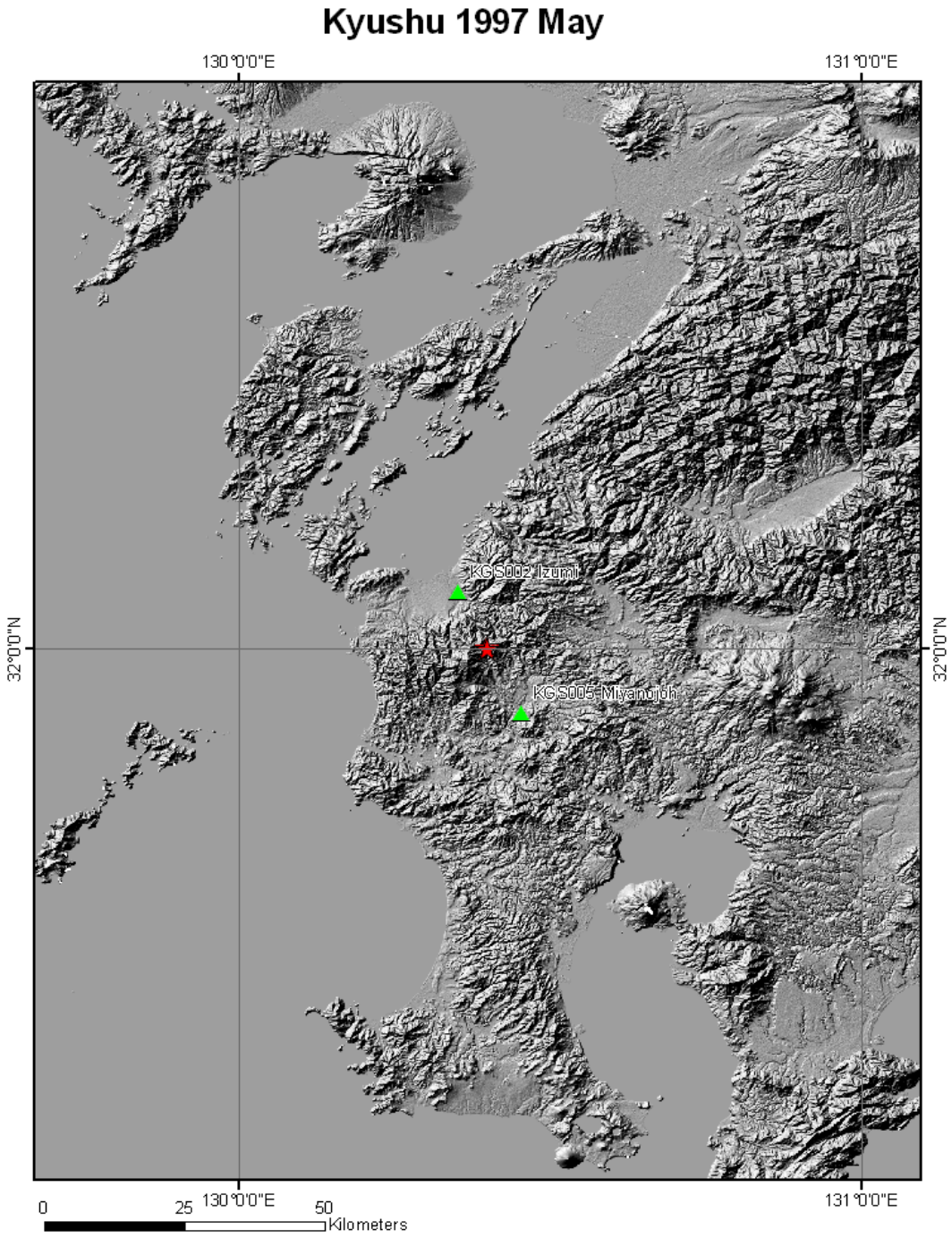

Figure A33. Umbria Marche, Italy foreshock, September 26, 1997, 00:33:16, Mw 5.72 and 09:40:33, Mw 6.04

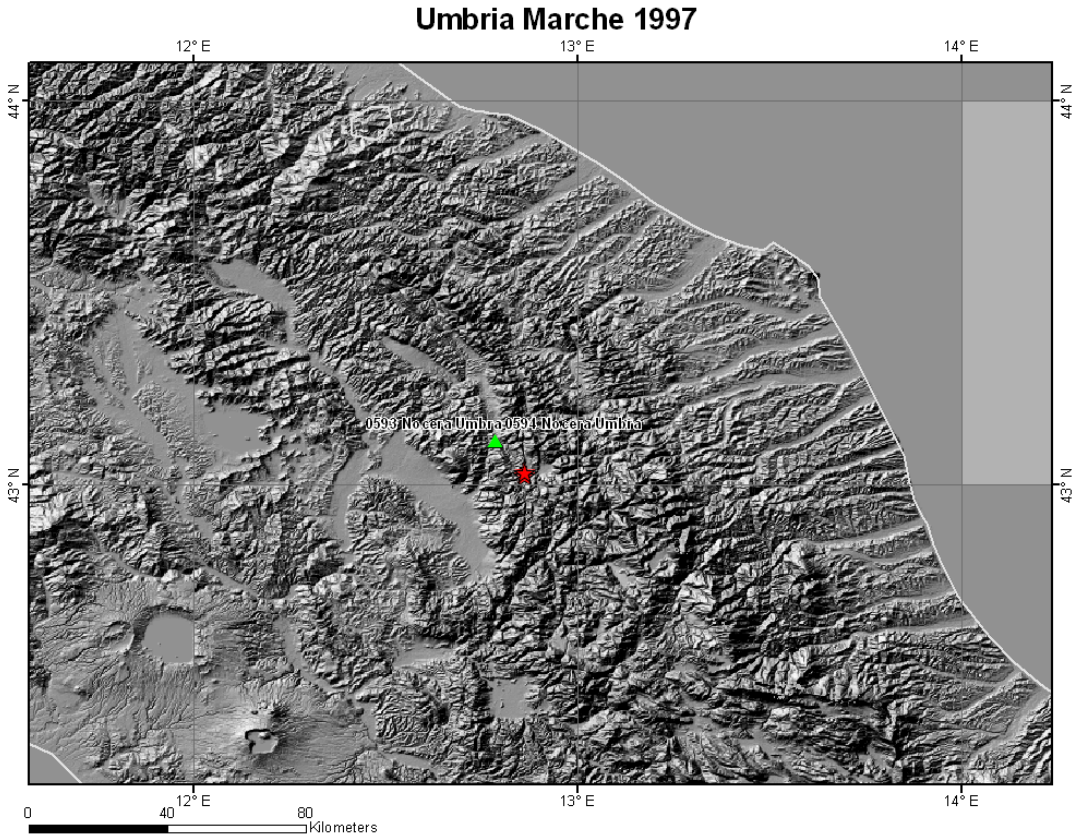

Figure A34. Chamoli, March 28, 1999, 19:05:11, M_W 6.60

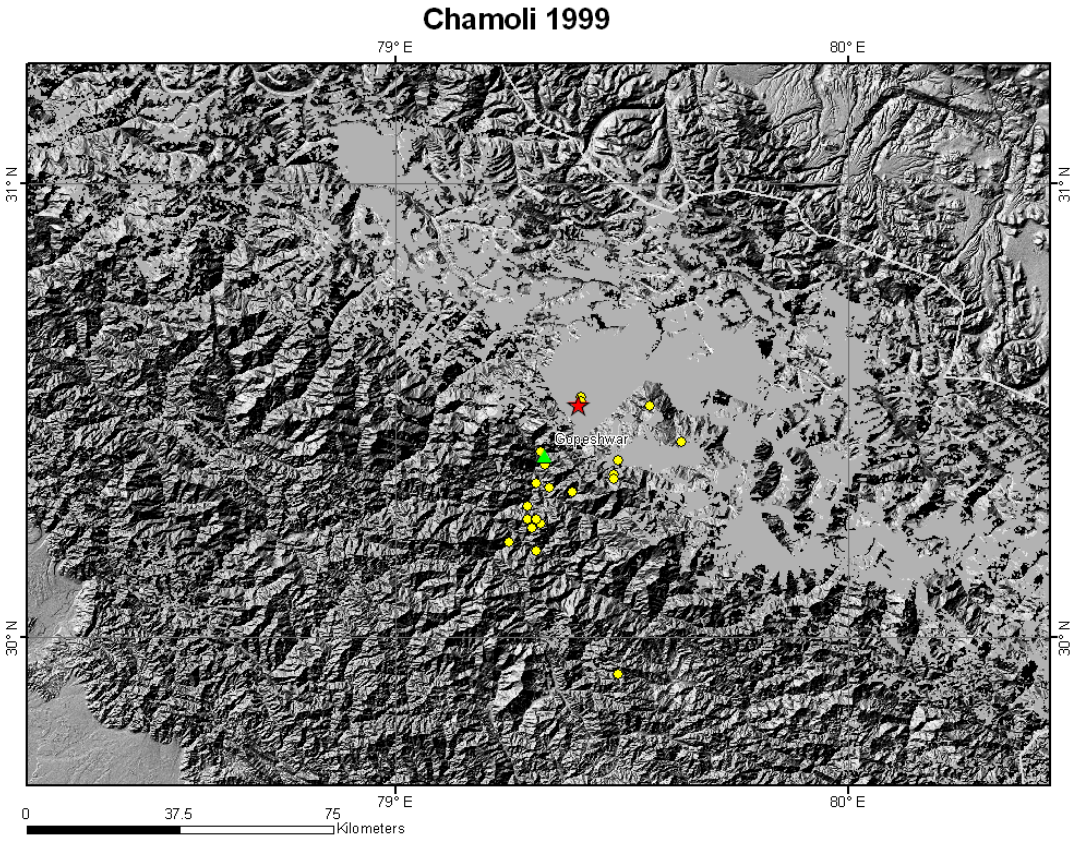

Figure A35. Karehbas, May 6, 1999, 23:00:53, M_W 5.90

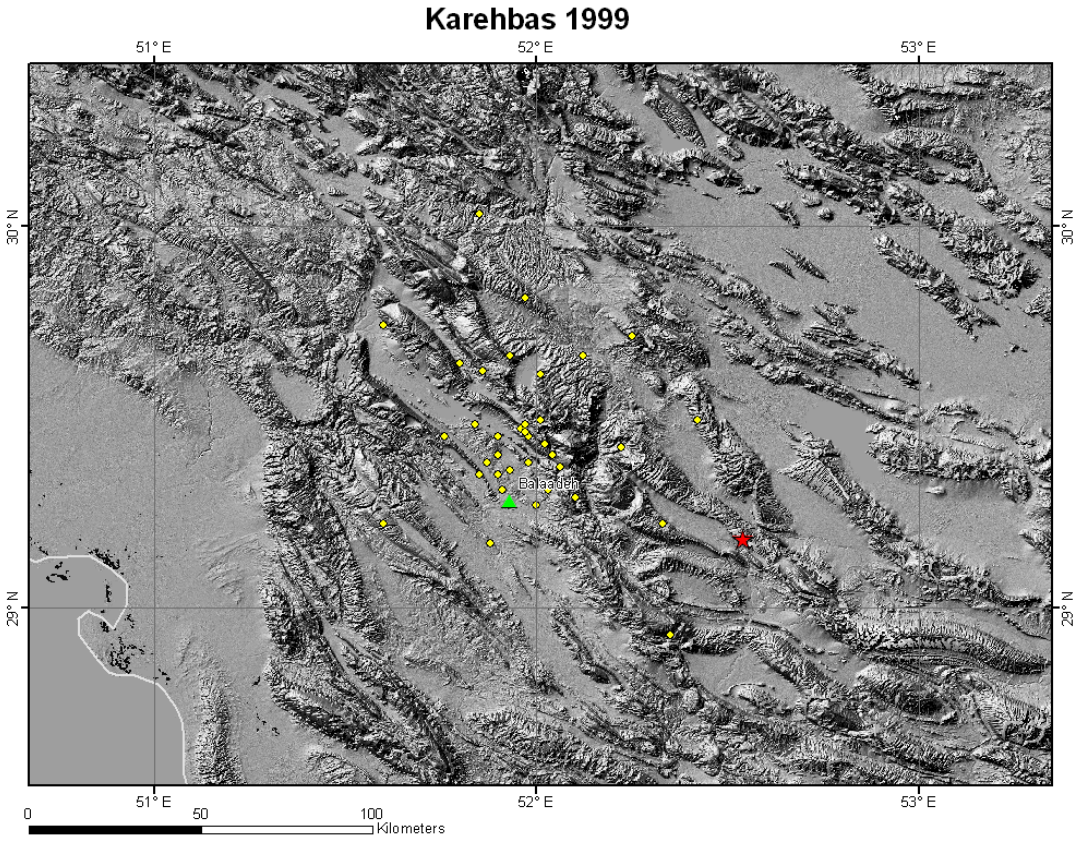

Figure A36. Kocaeli, Turkey, August 17, 1999, 00:01:40, M_w-hrv 7.60

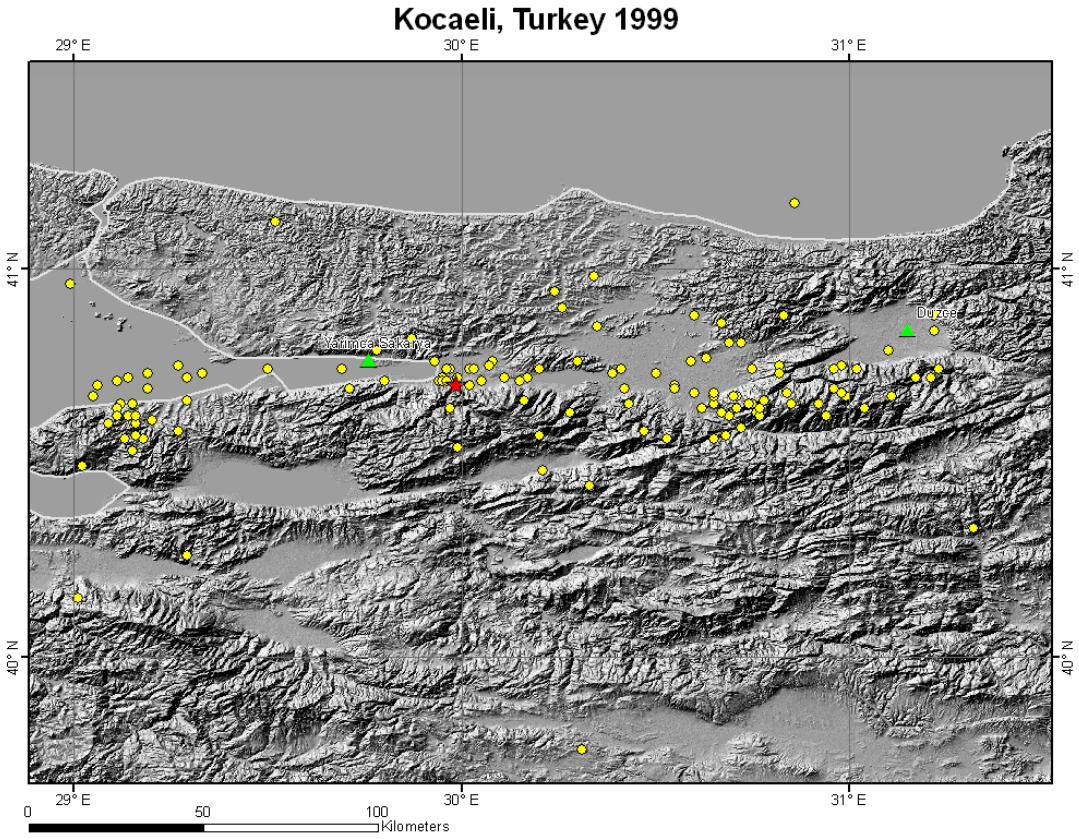

Figure A37. Southern Honshu, August 20, 1999, 20:33:00, Mjma 5.40

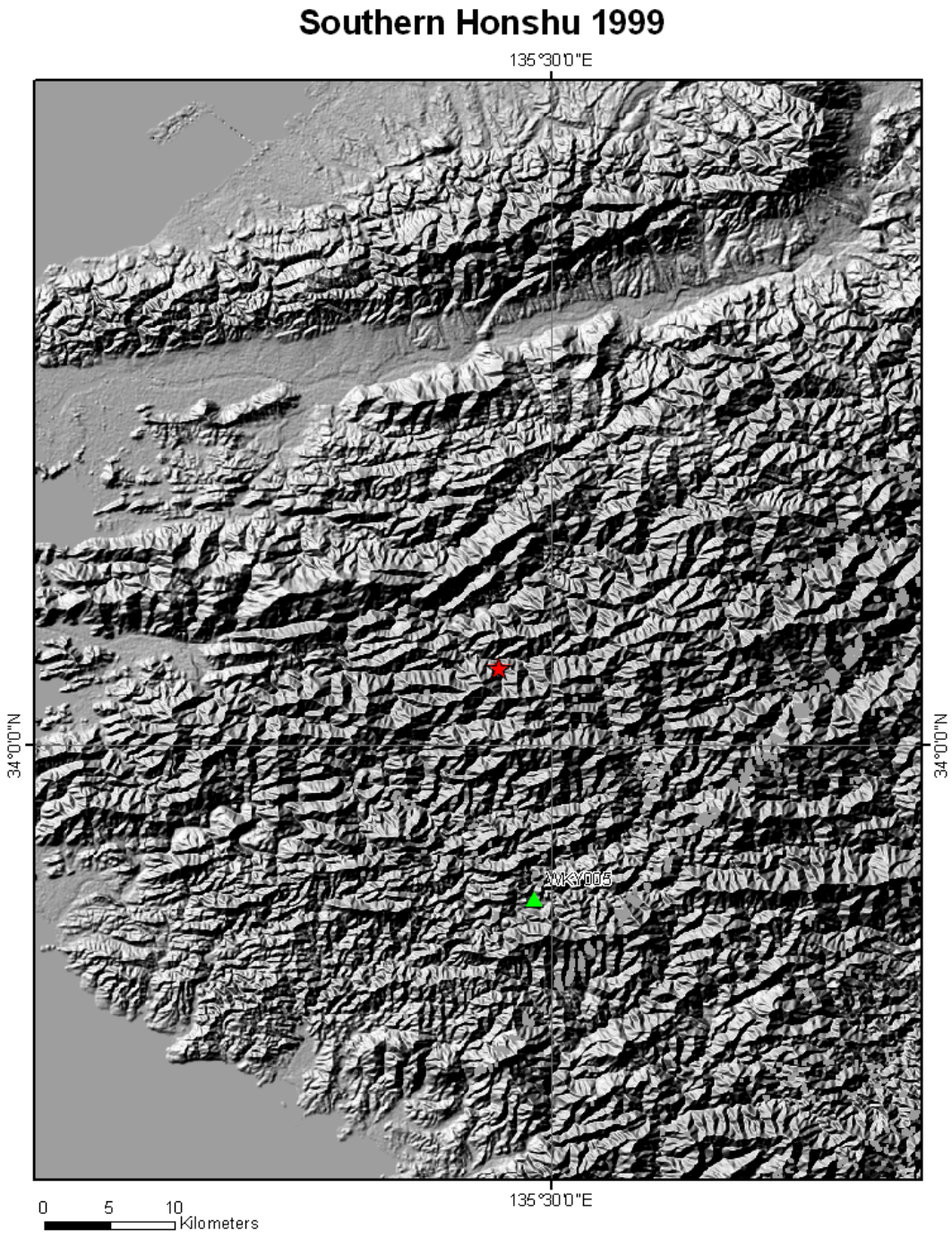

Figure A38. Chi-Chi, September 20, 1999, 17:47:16, M_W 7.60

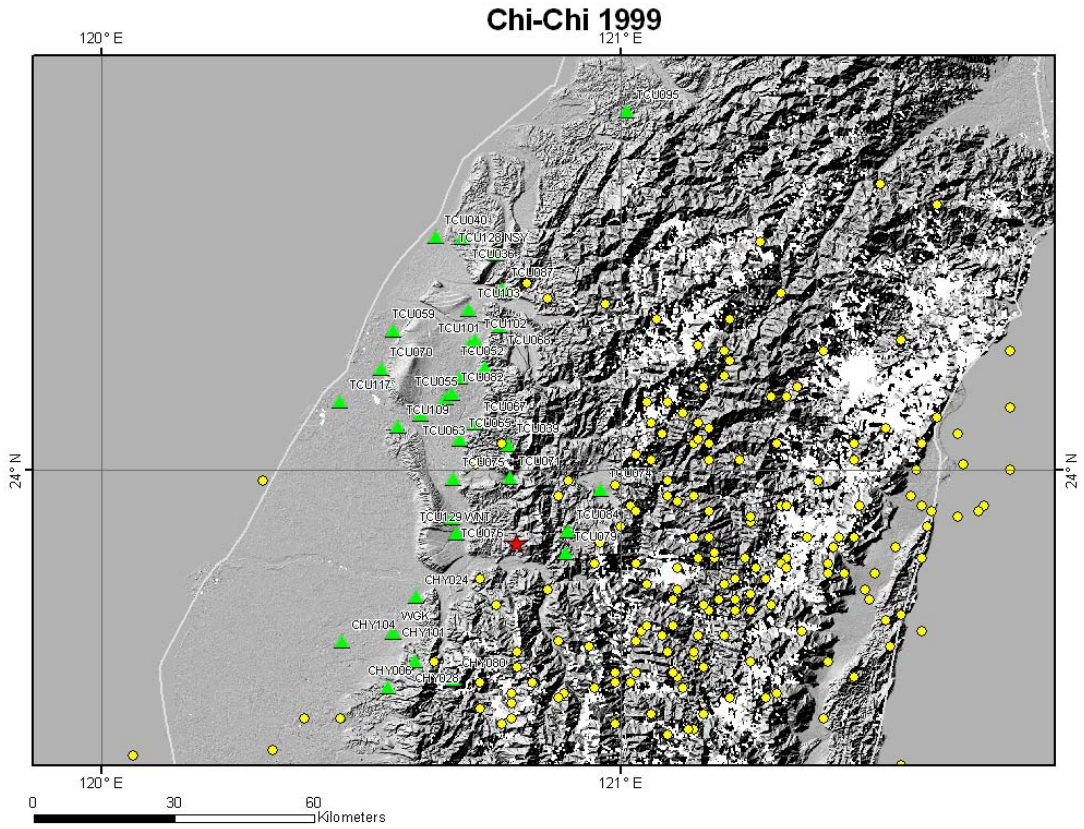

Figure A39. Duzce, November 12, 1999, 16:57:27, M_W 7.10

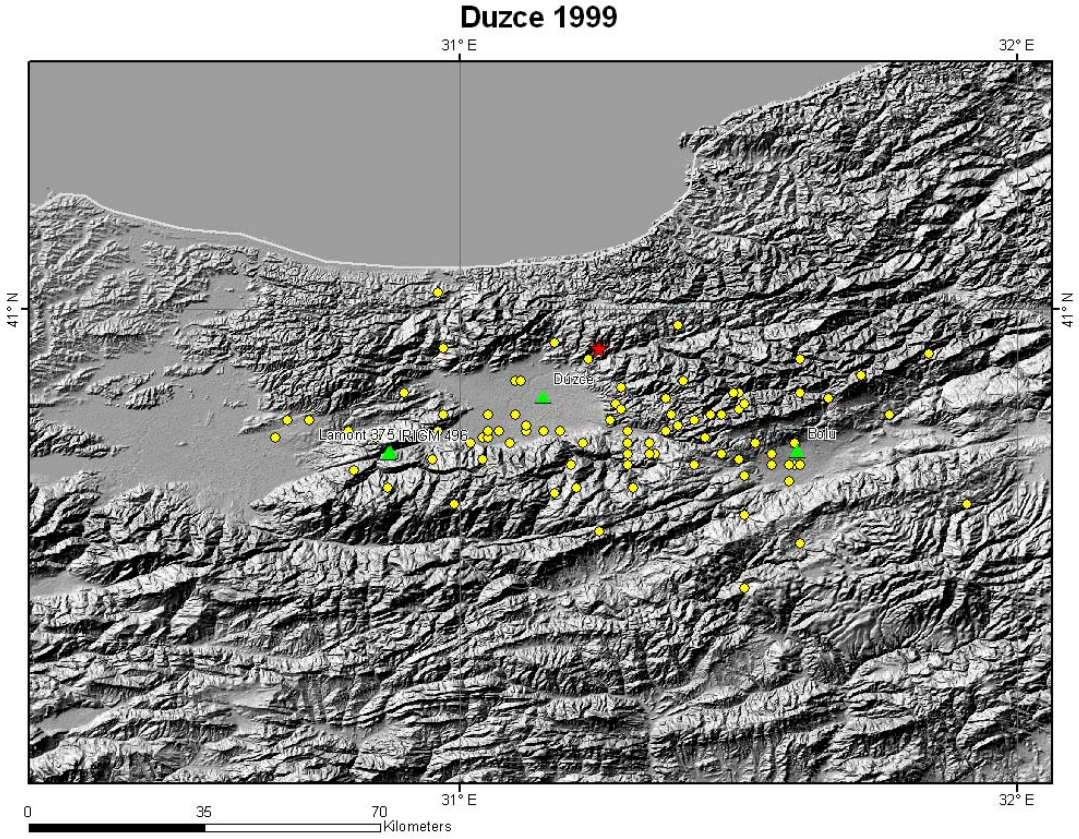

Figure A40. South Iceland, June 17, 2000, 15:40:41, M_W 6.57 and 00:51:48, M_W 6.49

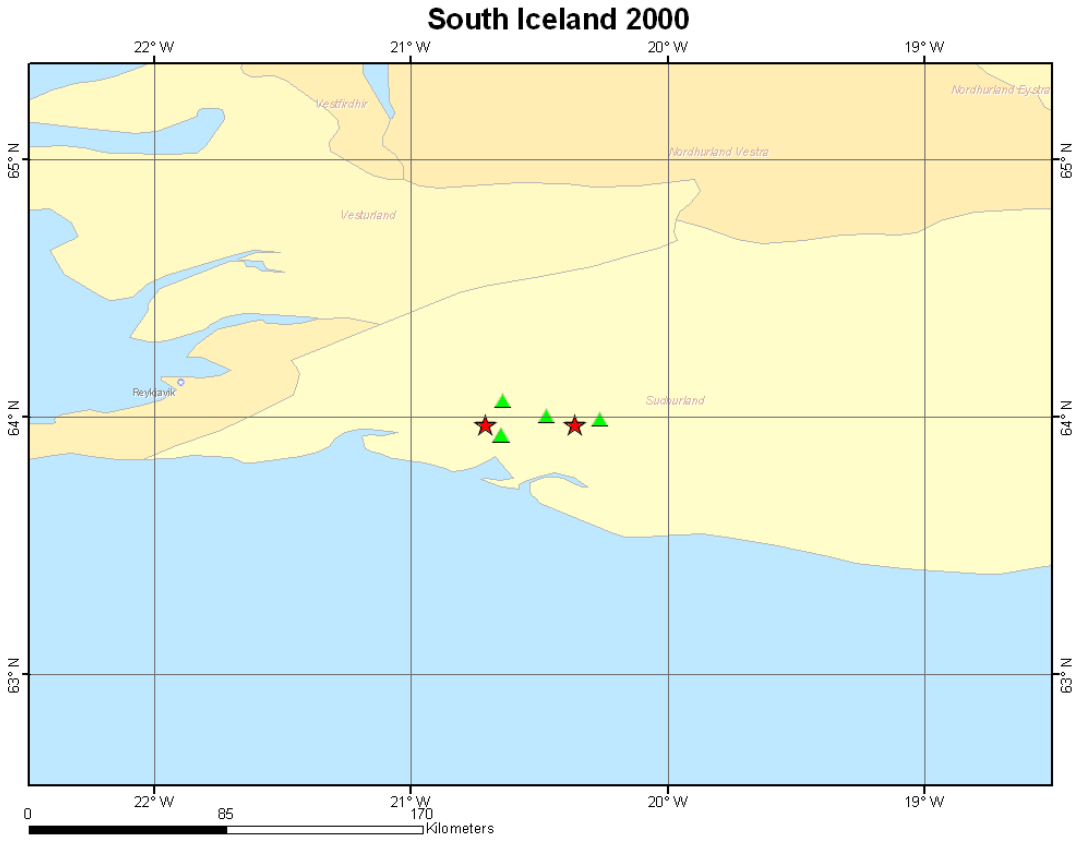

Figure A41. Japan, July 14, 2000, 16:18:00, Mjma 3.90

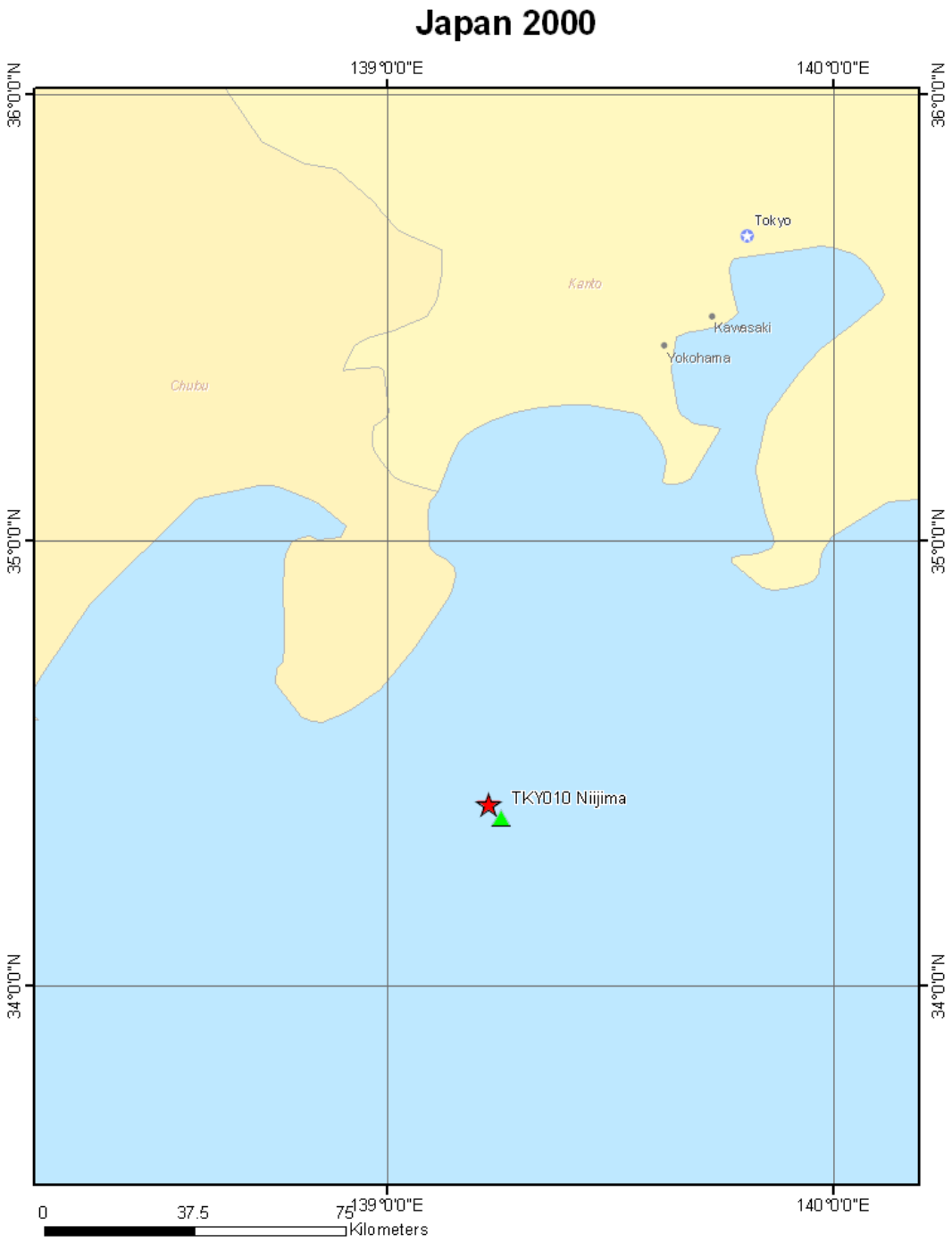

Figure A42. Yountville, September 3, 2000, 08:36:30, M_W 5.00

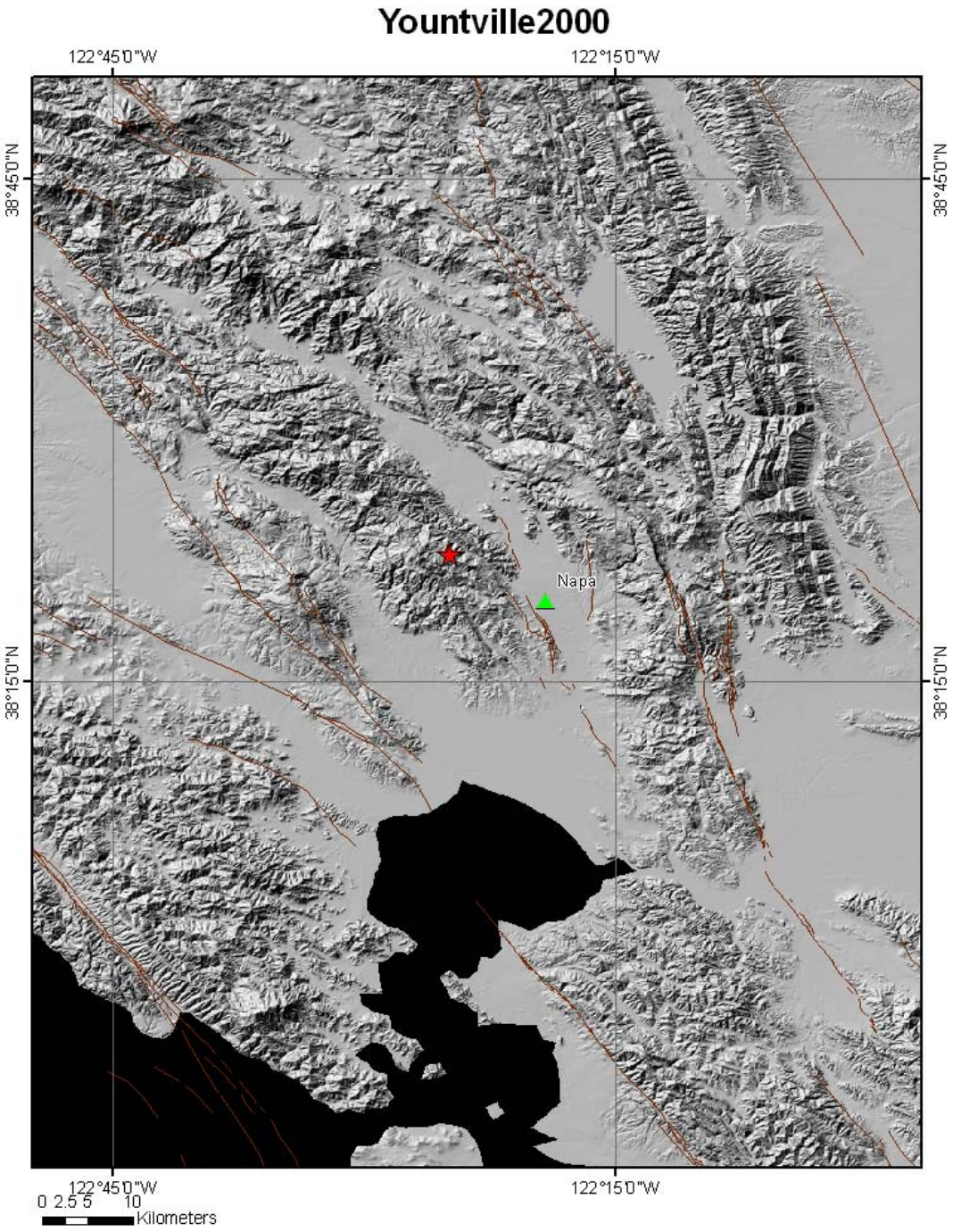

Figure A43. Western Tottori, October 6, 2000, 04:30:19, M_W 7.10

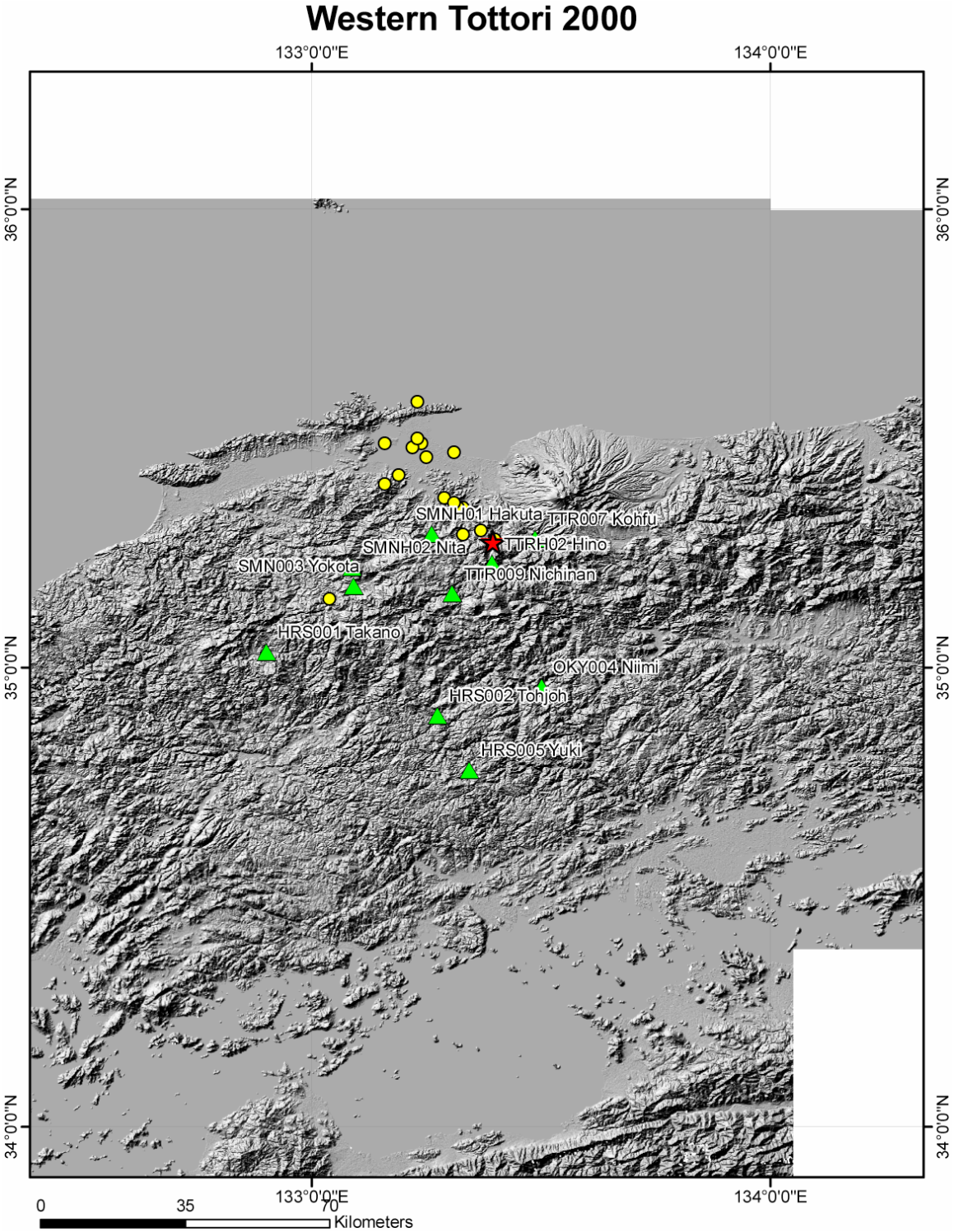

Figure A44. Honshu, October 30, 2000, 16:42:52, Mjma 5.50

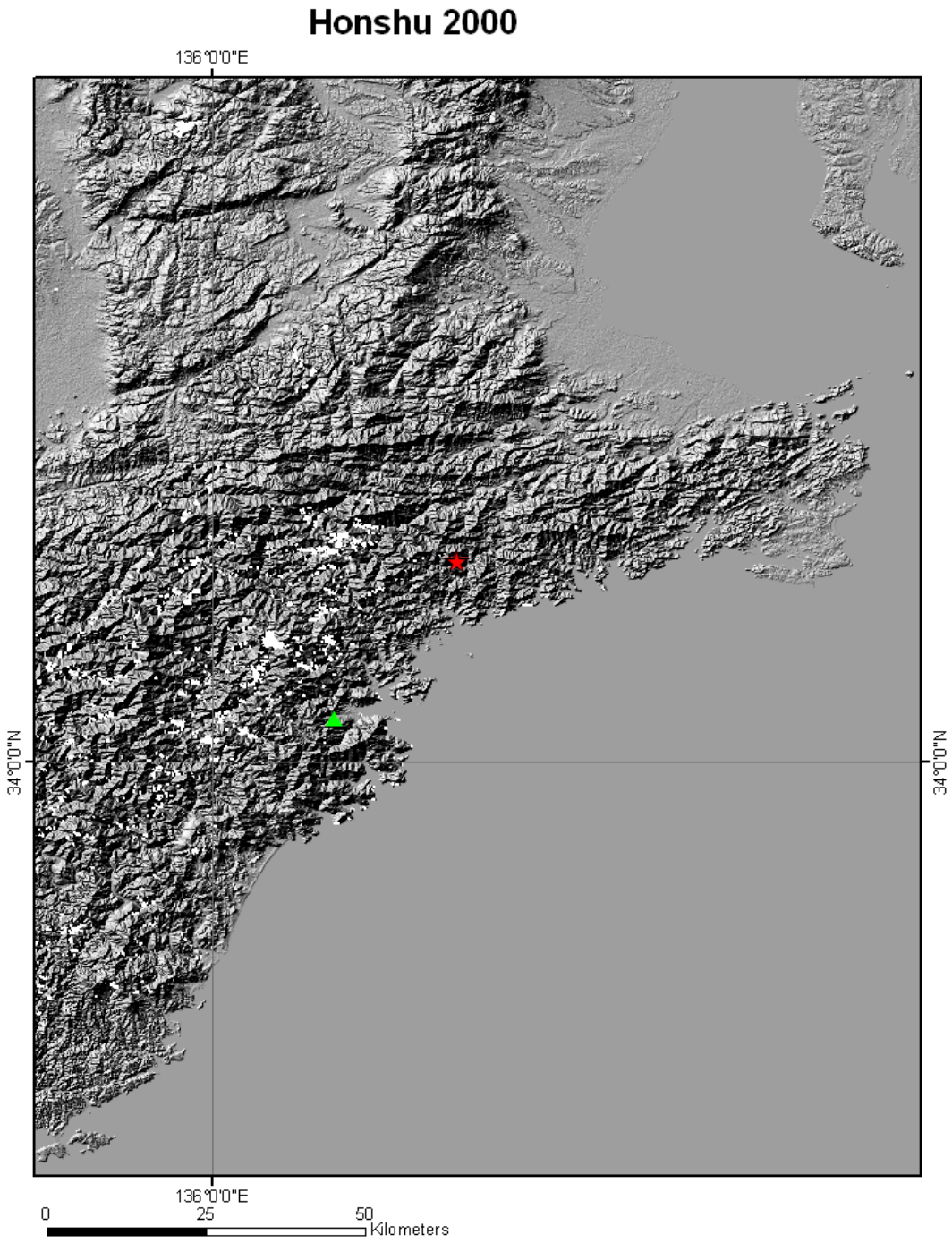

Figure A45. El Salvador, January 13, 2001, 17:33:32, M_W 7.60

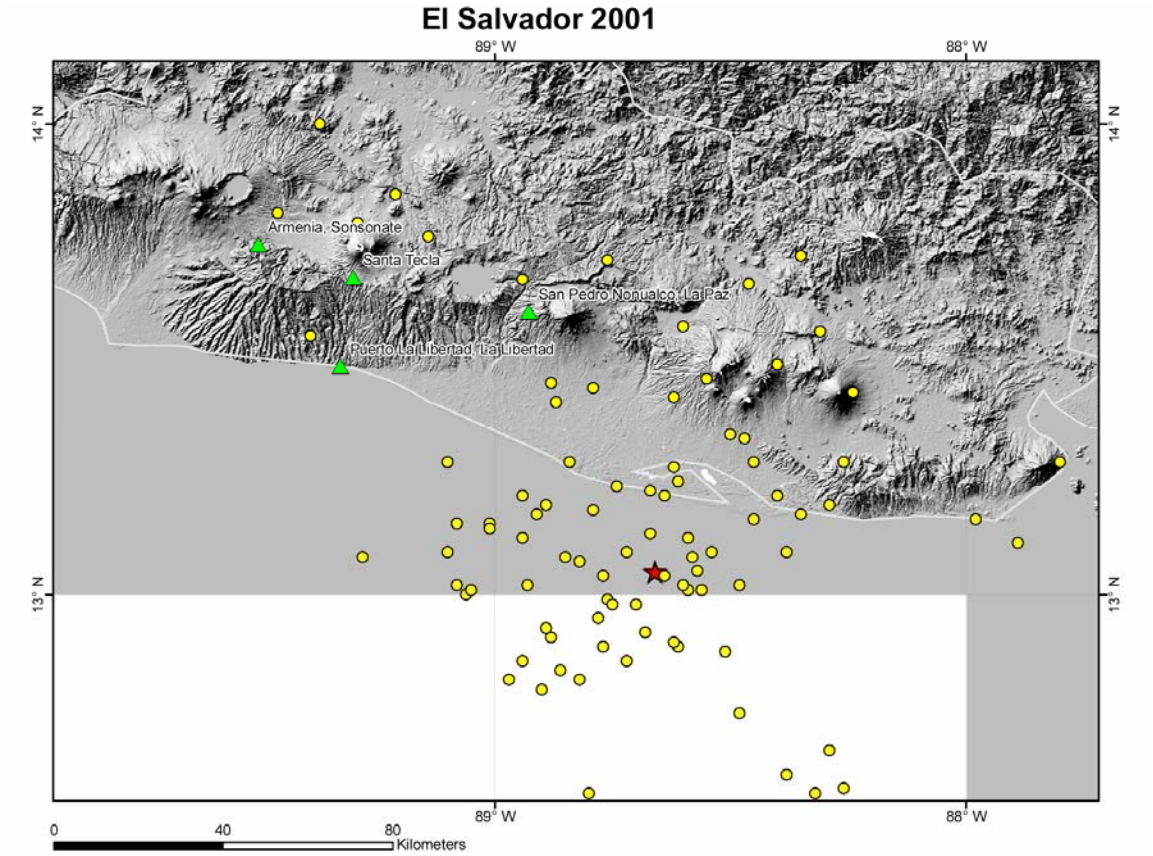

Figure A46. Nisqually, February 28, 2001, 18:54:31, M_W 6.80

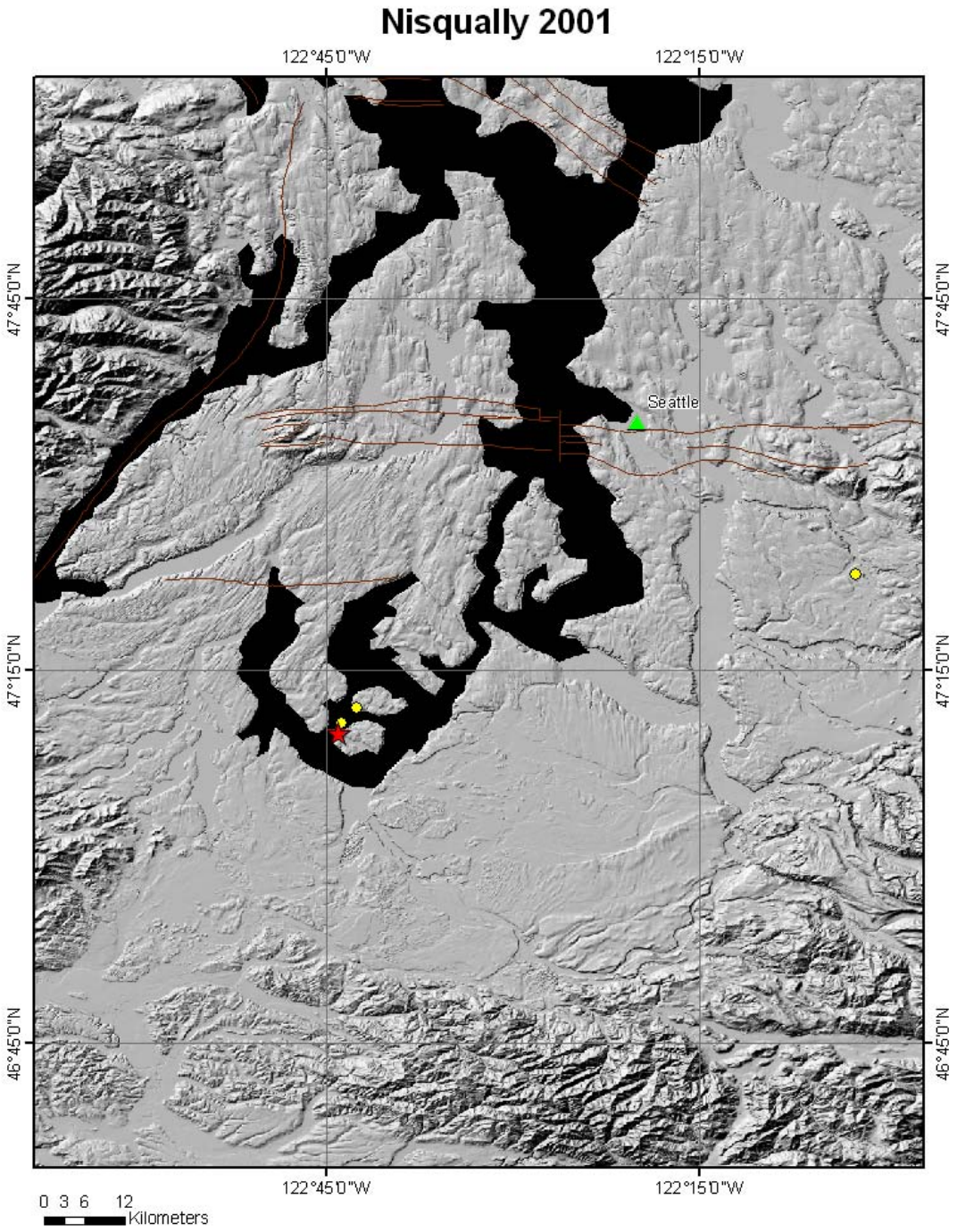

Figure A47. Southern Honshu, March 24, 2001, 06:27:54, M_W 6.40

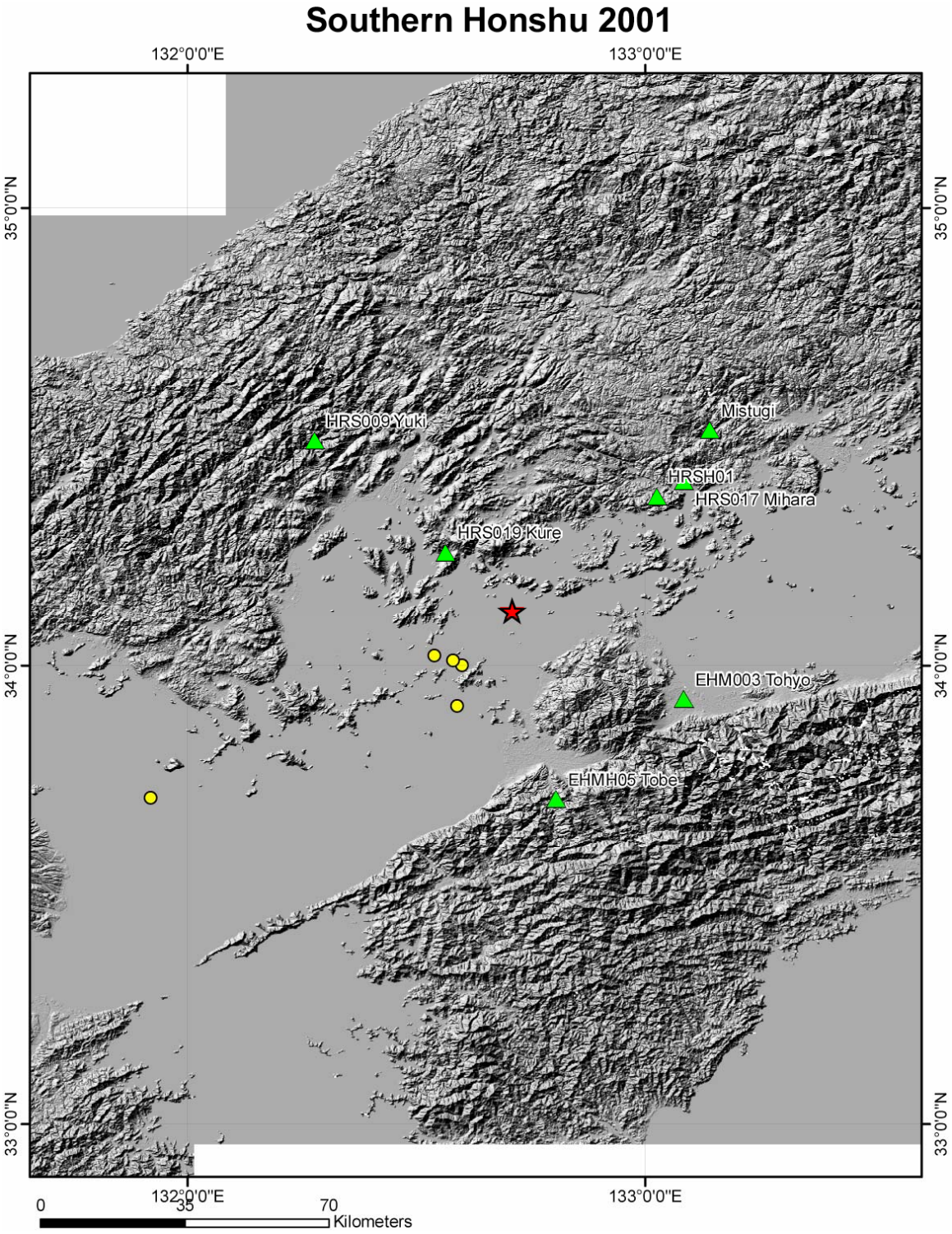

Figure A48. Japan, June 14, 2002, 02:42:00, Mjma 4.90

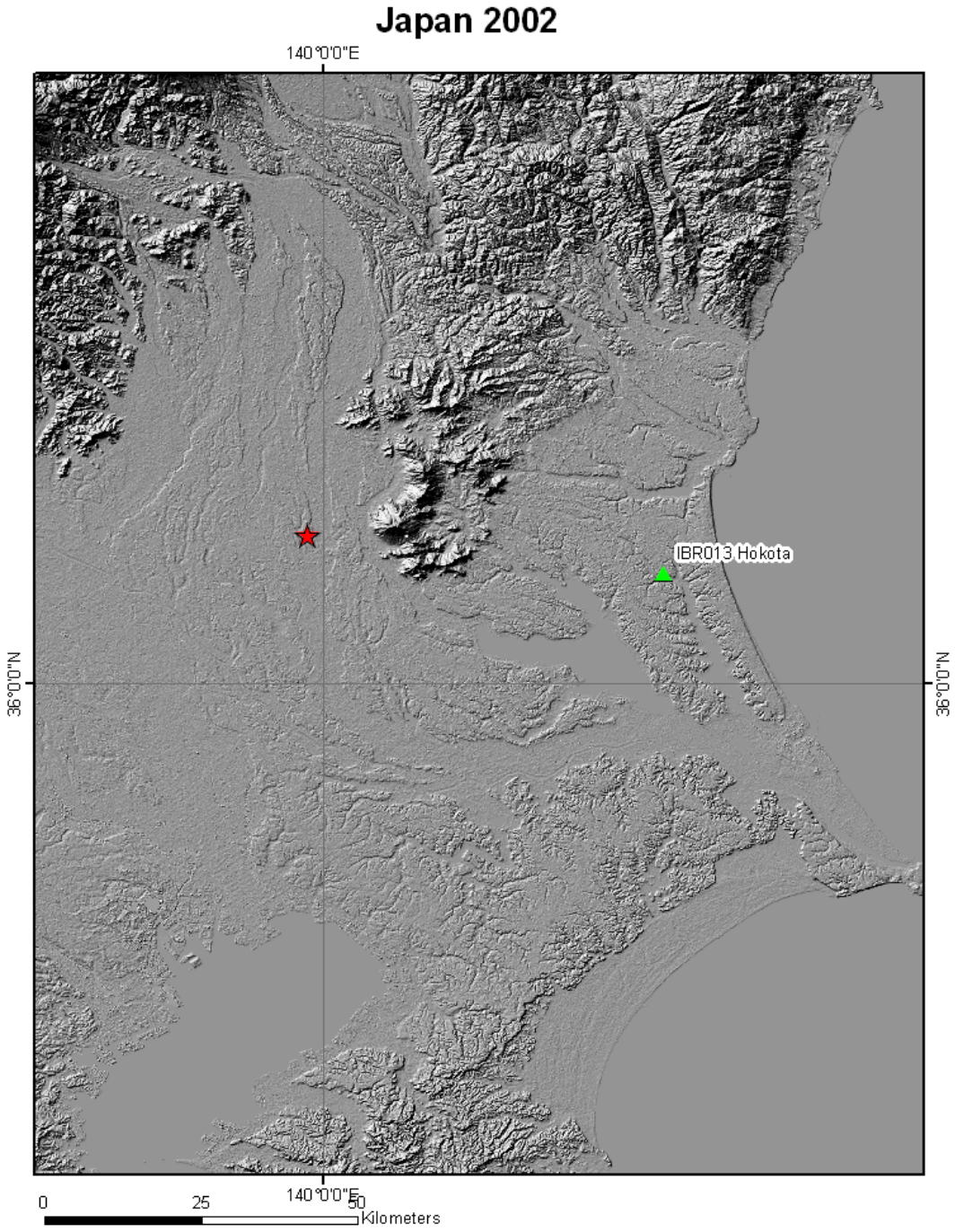

Figure A49. Avaj, Iran, June 22, 2002, 02:58:20, M_W 6.50

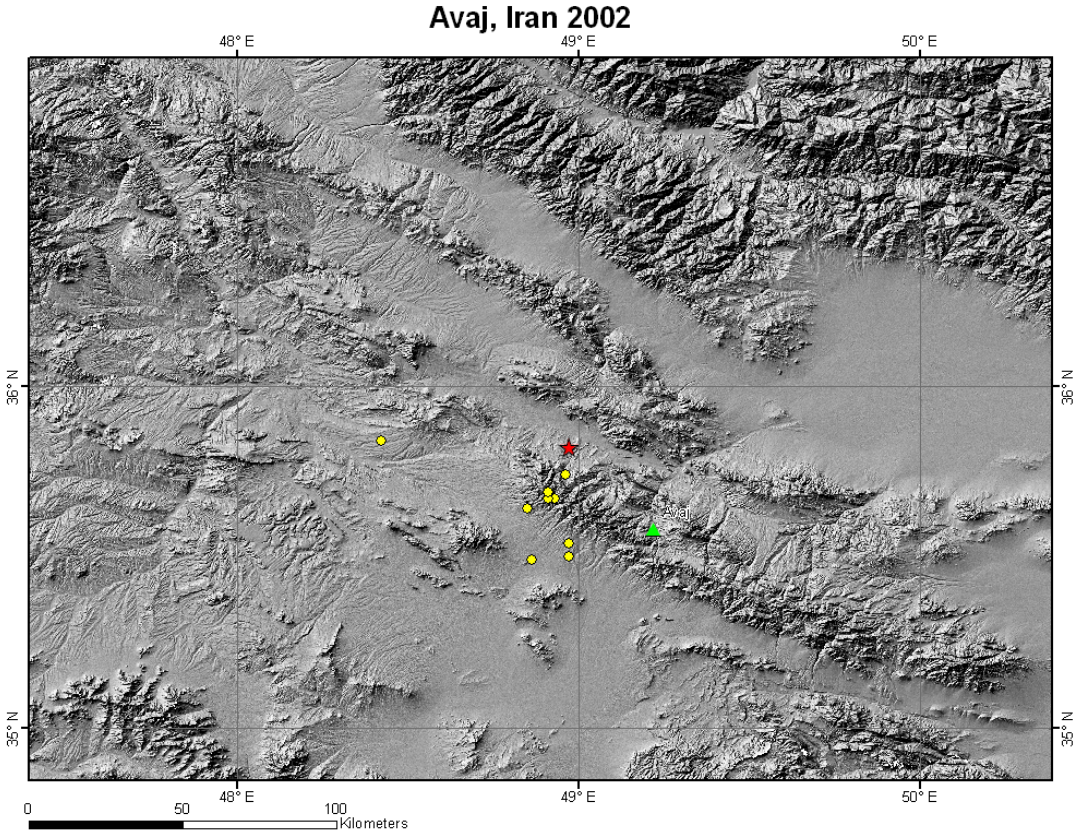

Figure A50. Denali, Alaska, November 3, 2002, 22:13:00, M_S 7.90

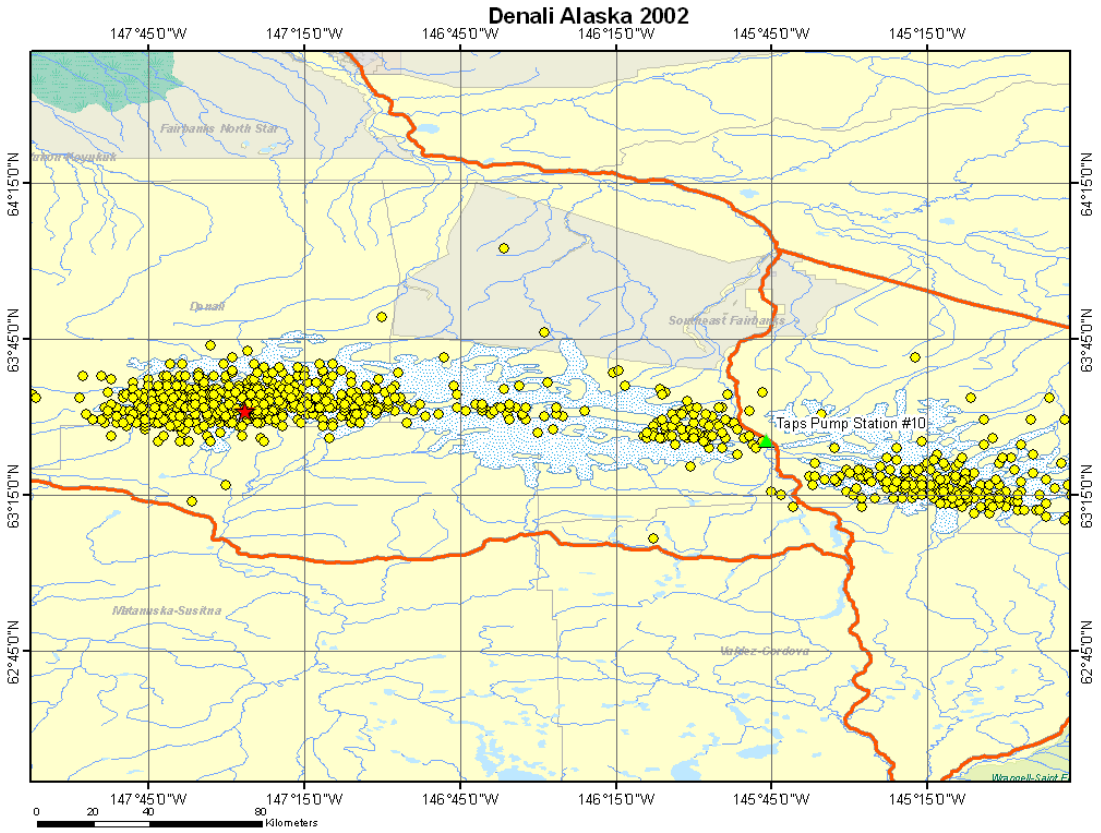

Figure A51. Miyagi-Oki, May 26, 2003, 09:24:33, M_W 7.00

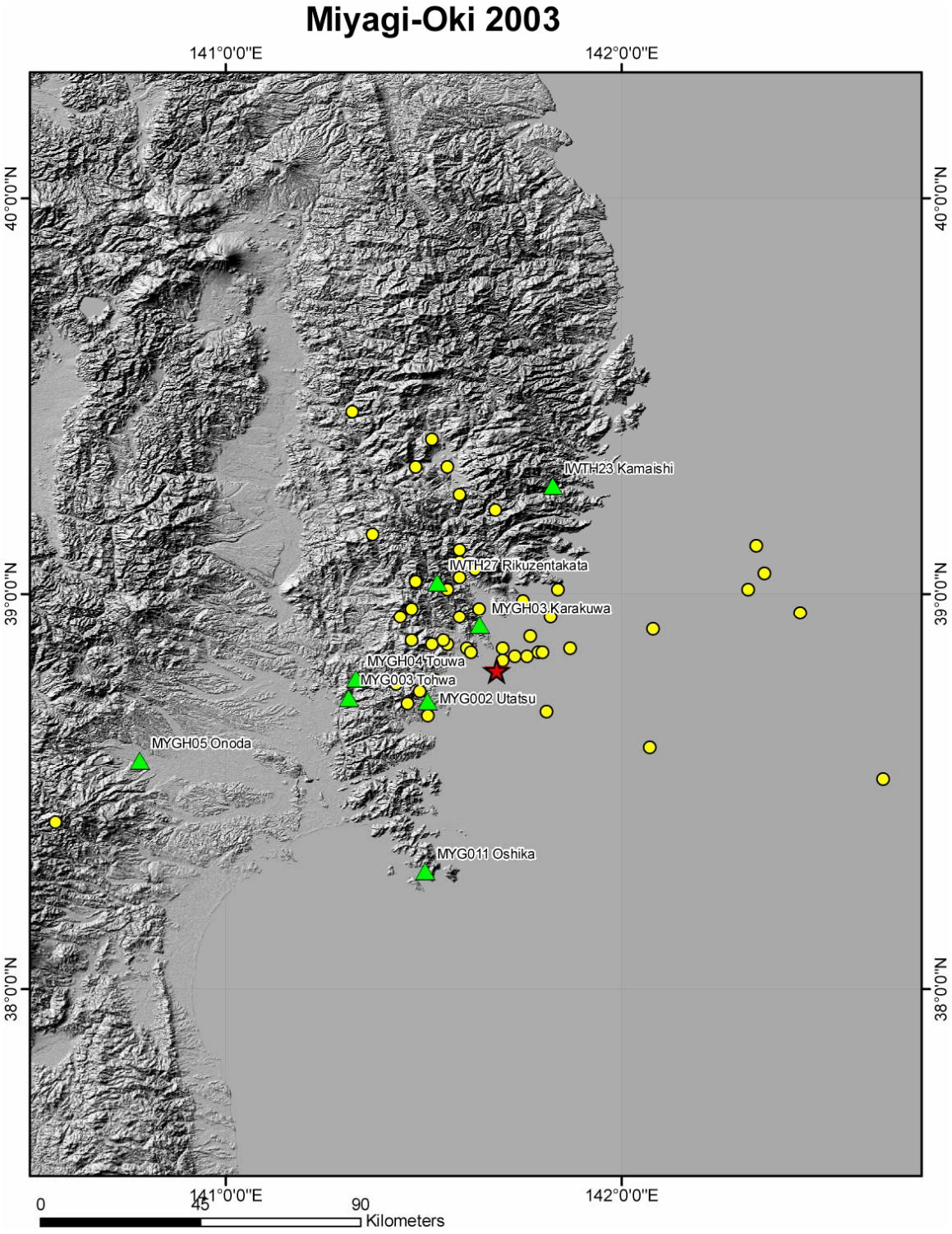

Figure A52. Tokachi-Oki, September 25, 2003, 19:50:07, M_W 8.00

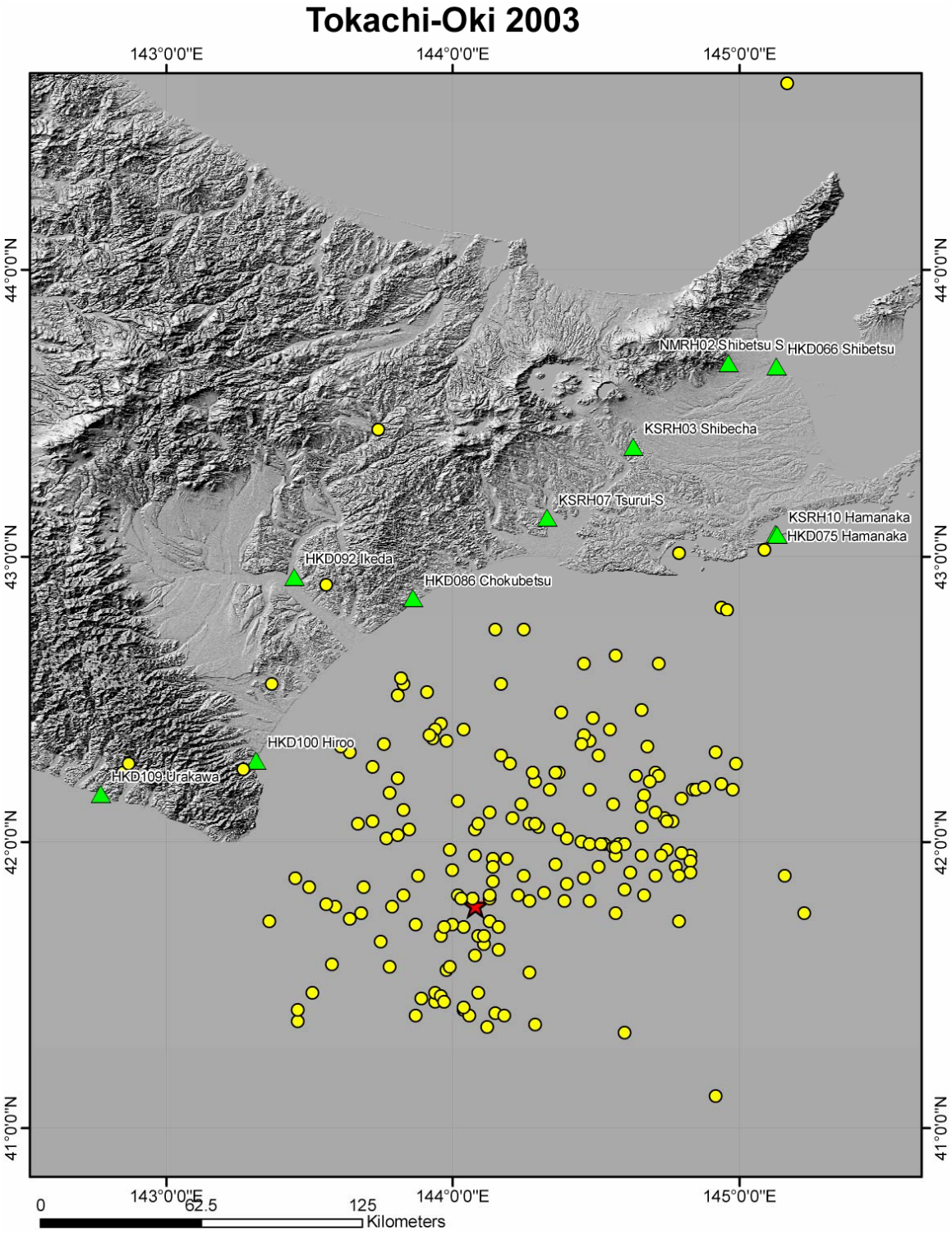

Figure A53. Bam, December 26, 2003, 01:56:56, M_W 6.70

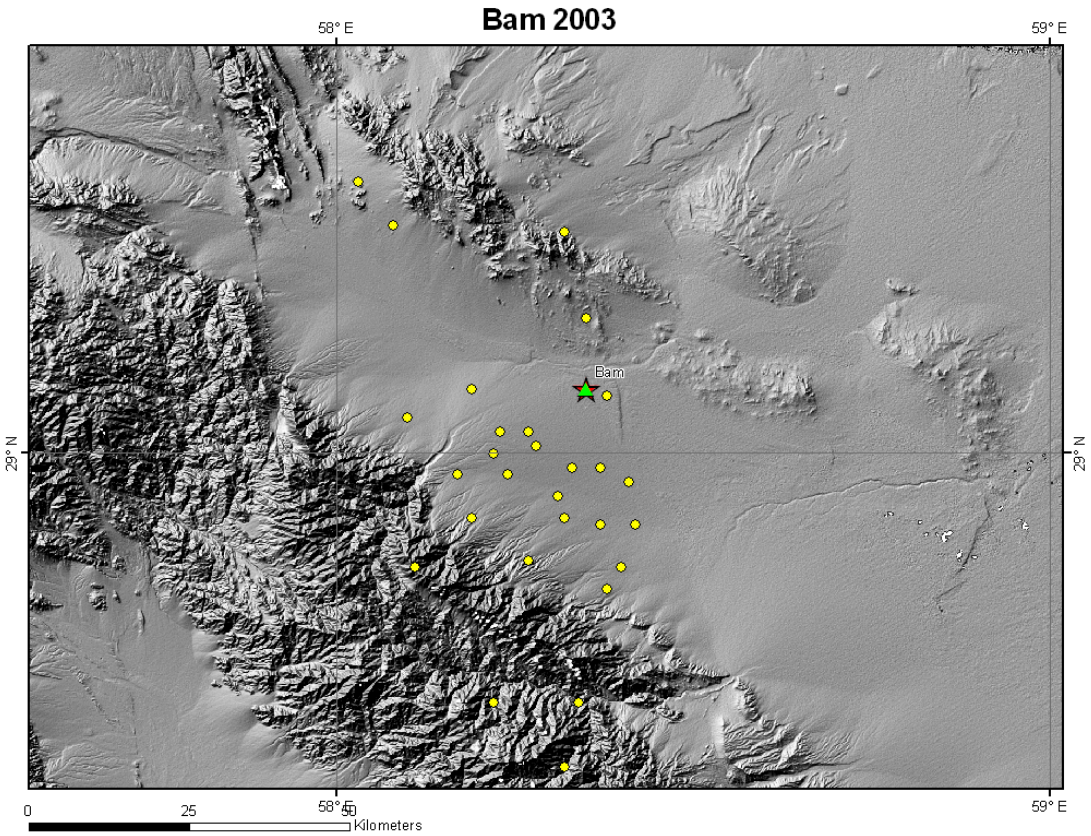

Figure A54. Honshu, July 9, 2004, 10:54:00, Mjma 4.40

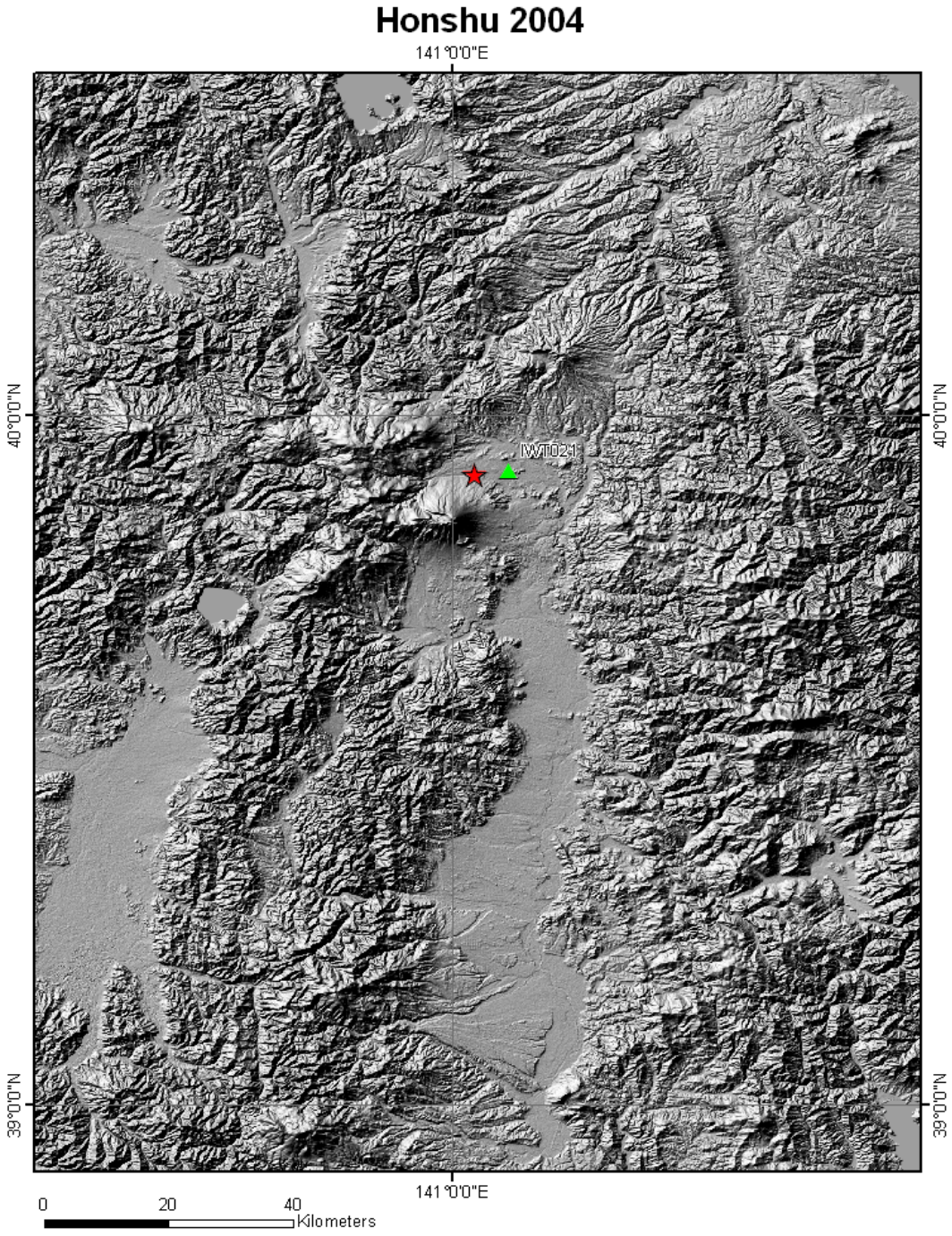

Figure A55. Parkfield, September 28, 2004, 17:15:24, M_W 6.00

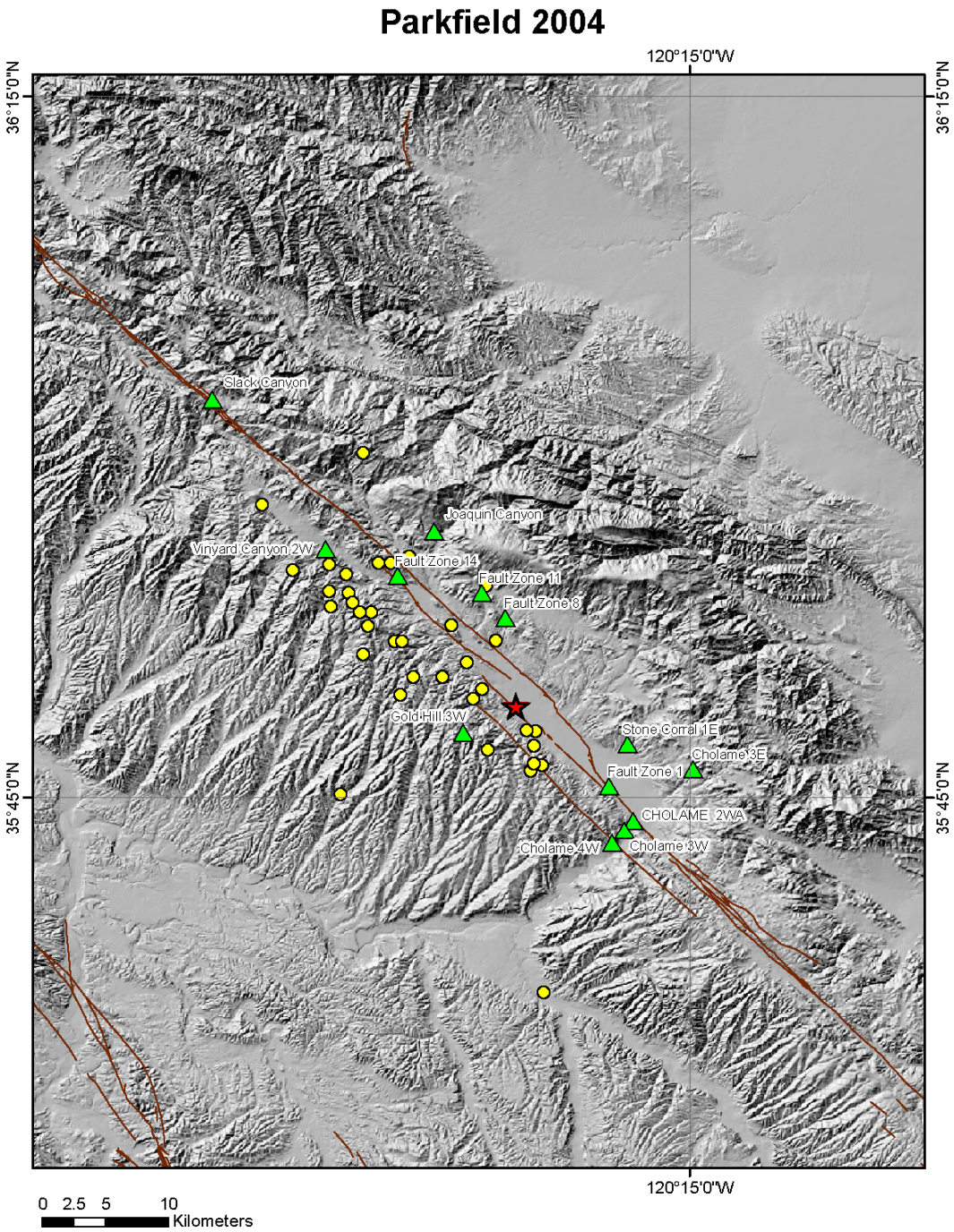

Figure A56. Niigata-Ken Chuetsu, October 23, 2004, 08:56:00, M_W 6.60

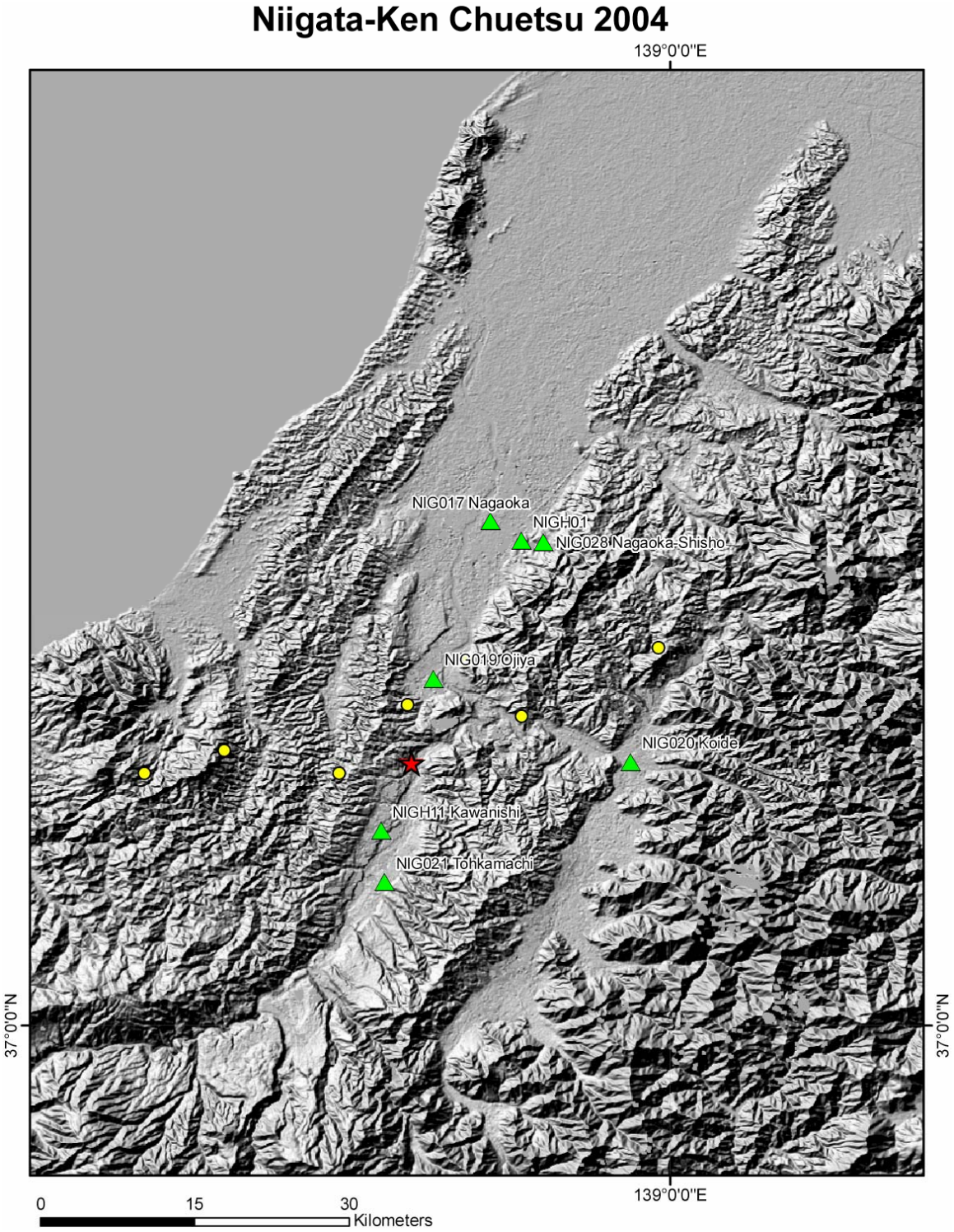

Figure A57. Niigata-Ken Chuetsu, October 23, 2004, 09:34:07 M_W 6.30

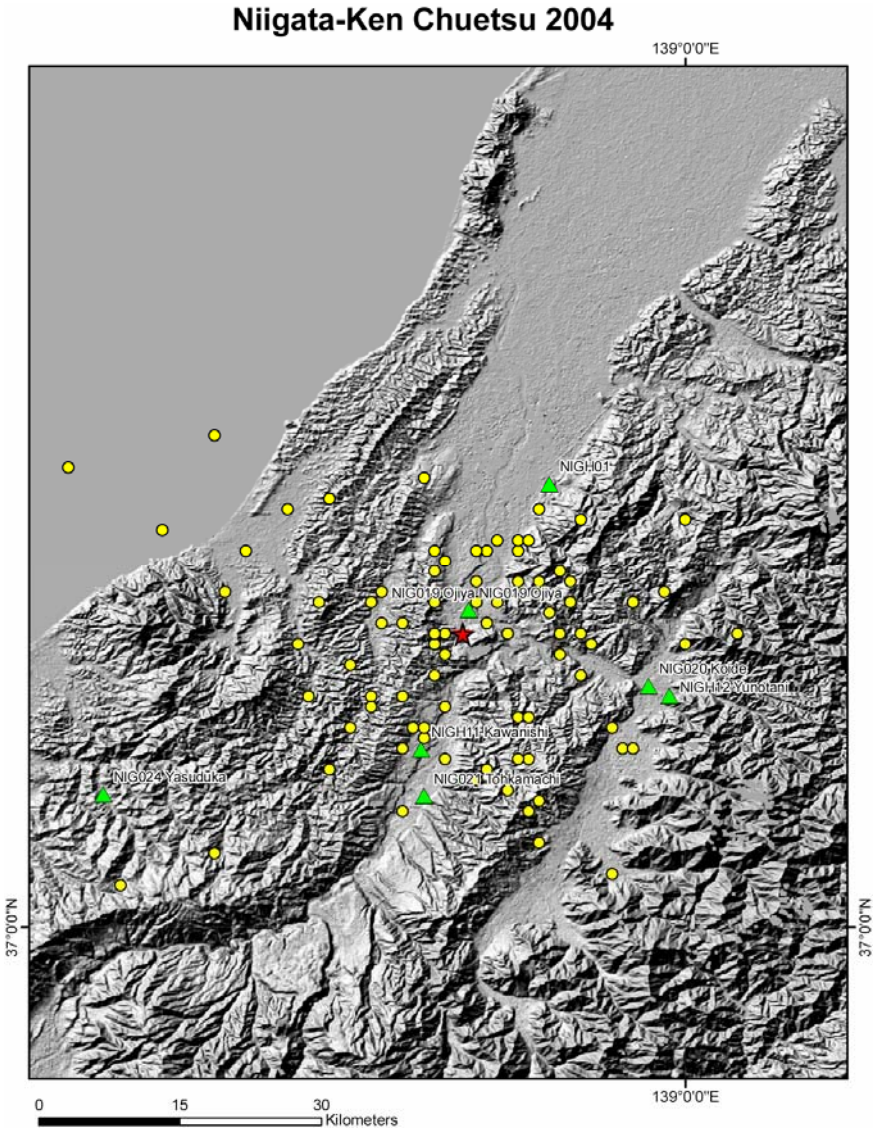

Figure A58. Hokkaido, November 28, 2004, 18:32:00, Mjma 7.10

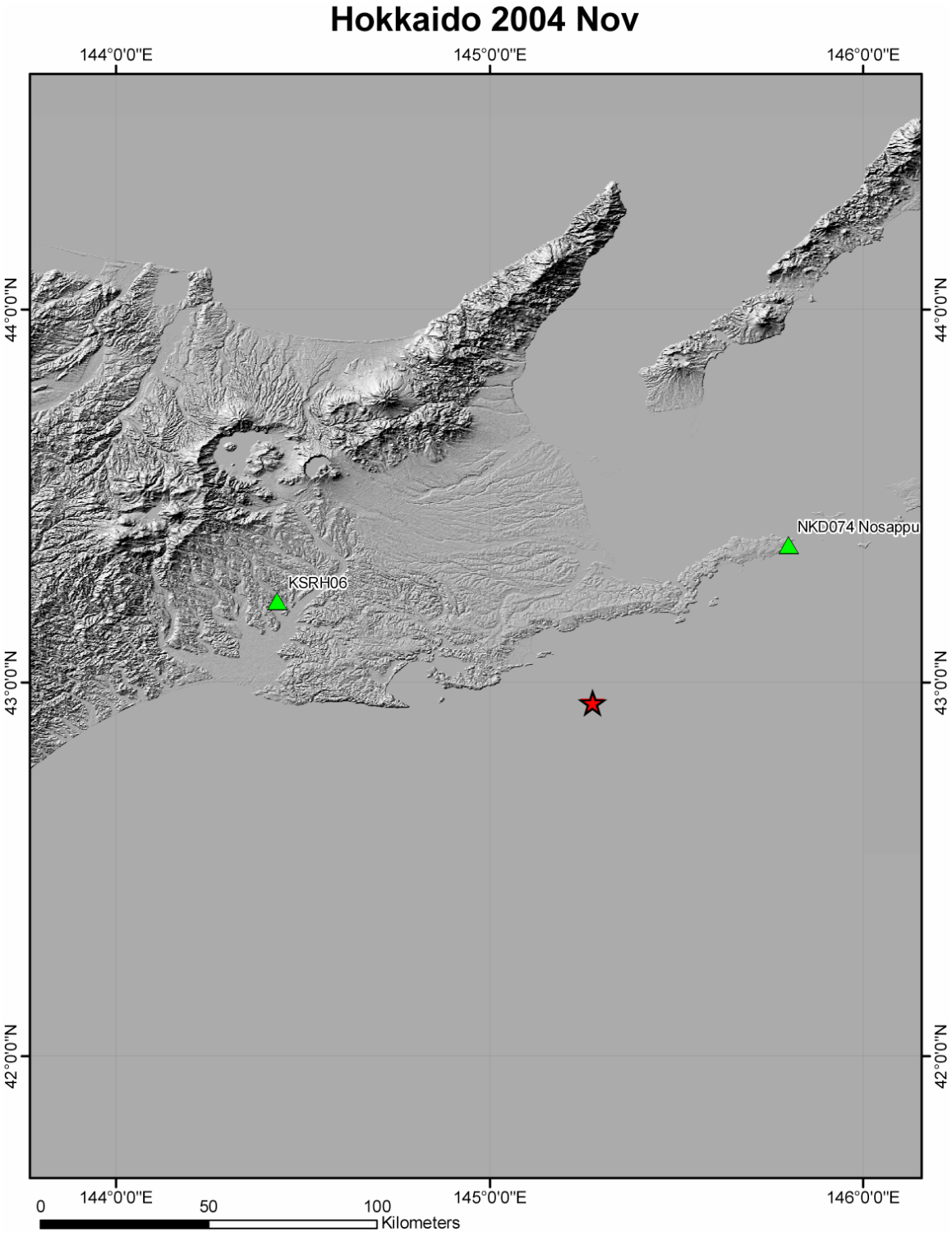

Figure A59. Hokkaido, December 14, 2004, 05:56:09, M_W 5.80

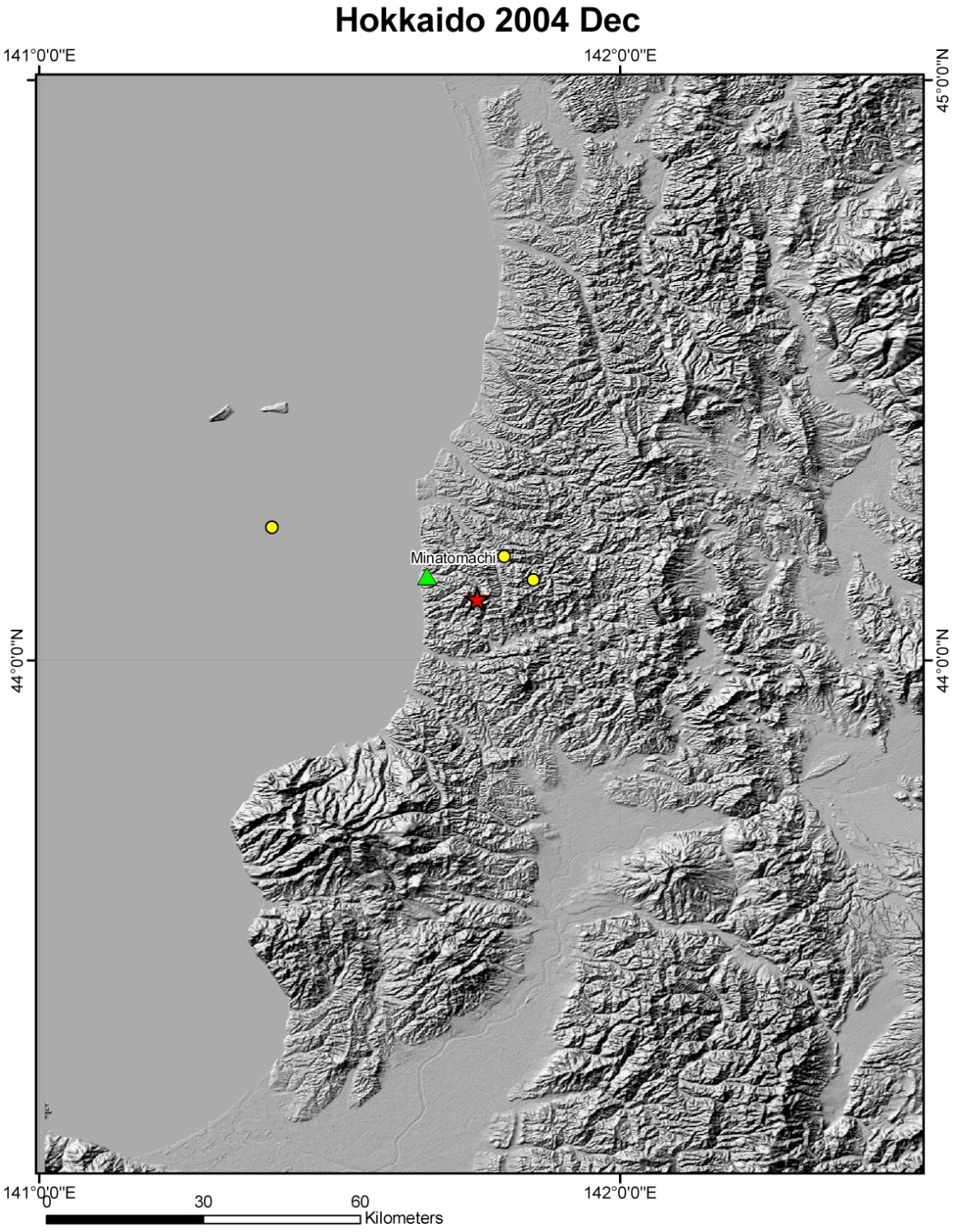

Figure A60. Honshu, August 16, 2005, 02:46:00, Mjma 7.20

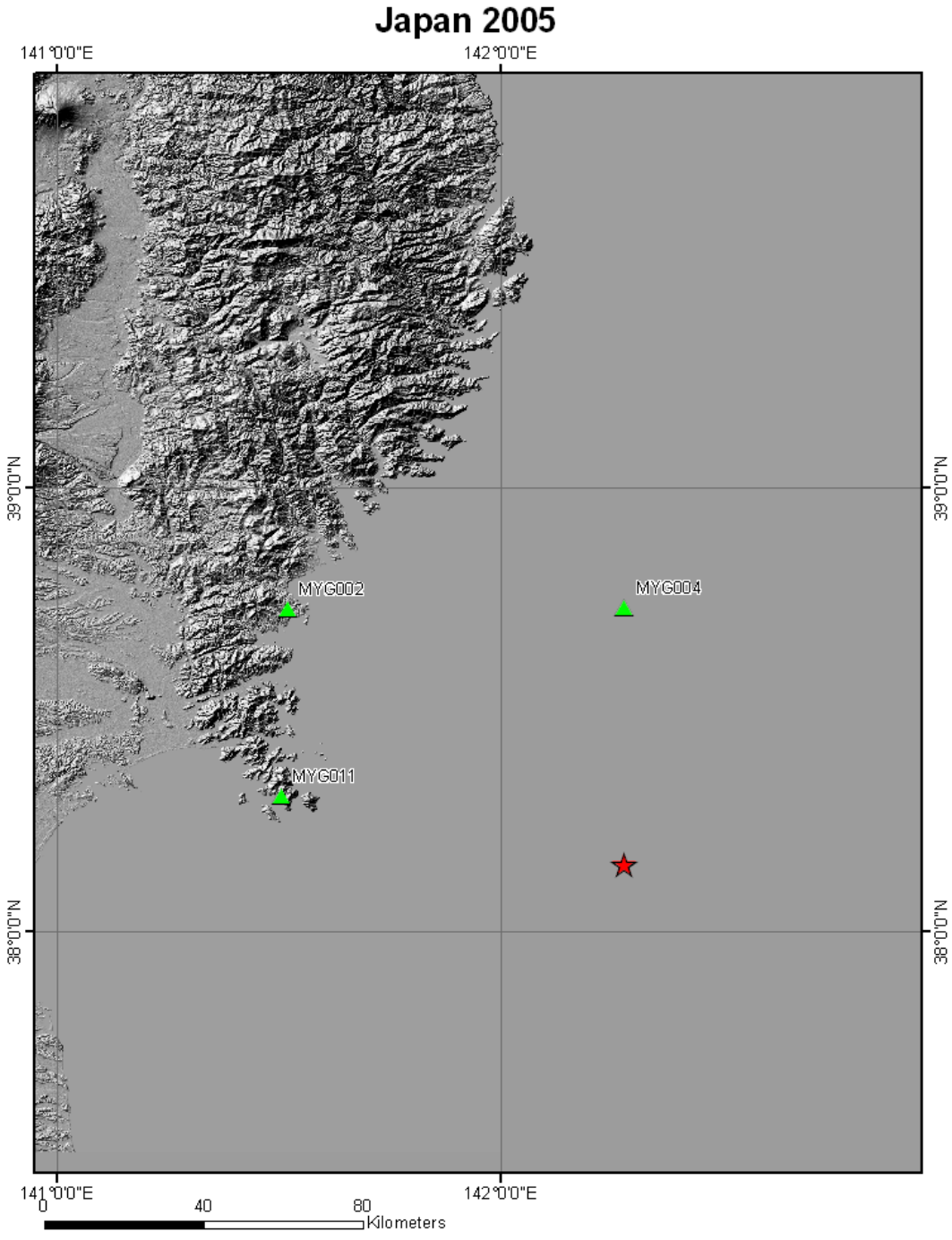

Figure A61. Anza, June 12, 2005, 15:41:46, M_W 5.20

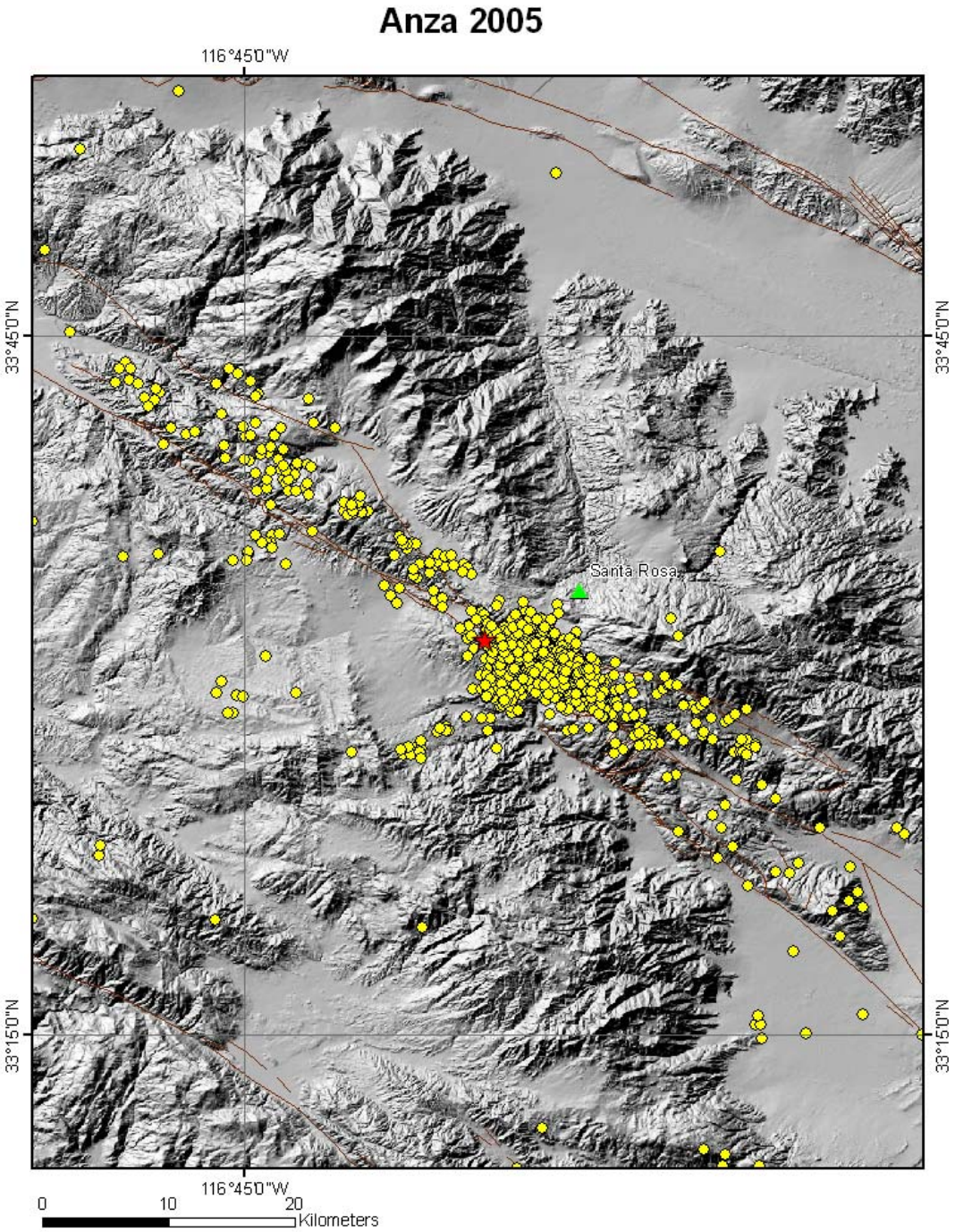

Figure A62. Southern Honshu, March 25, 2007, 00:42:00, Mjma 6.90

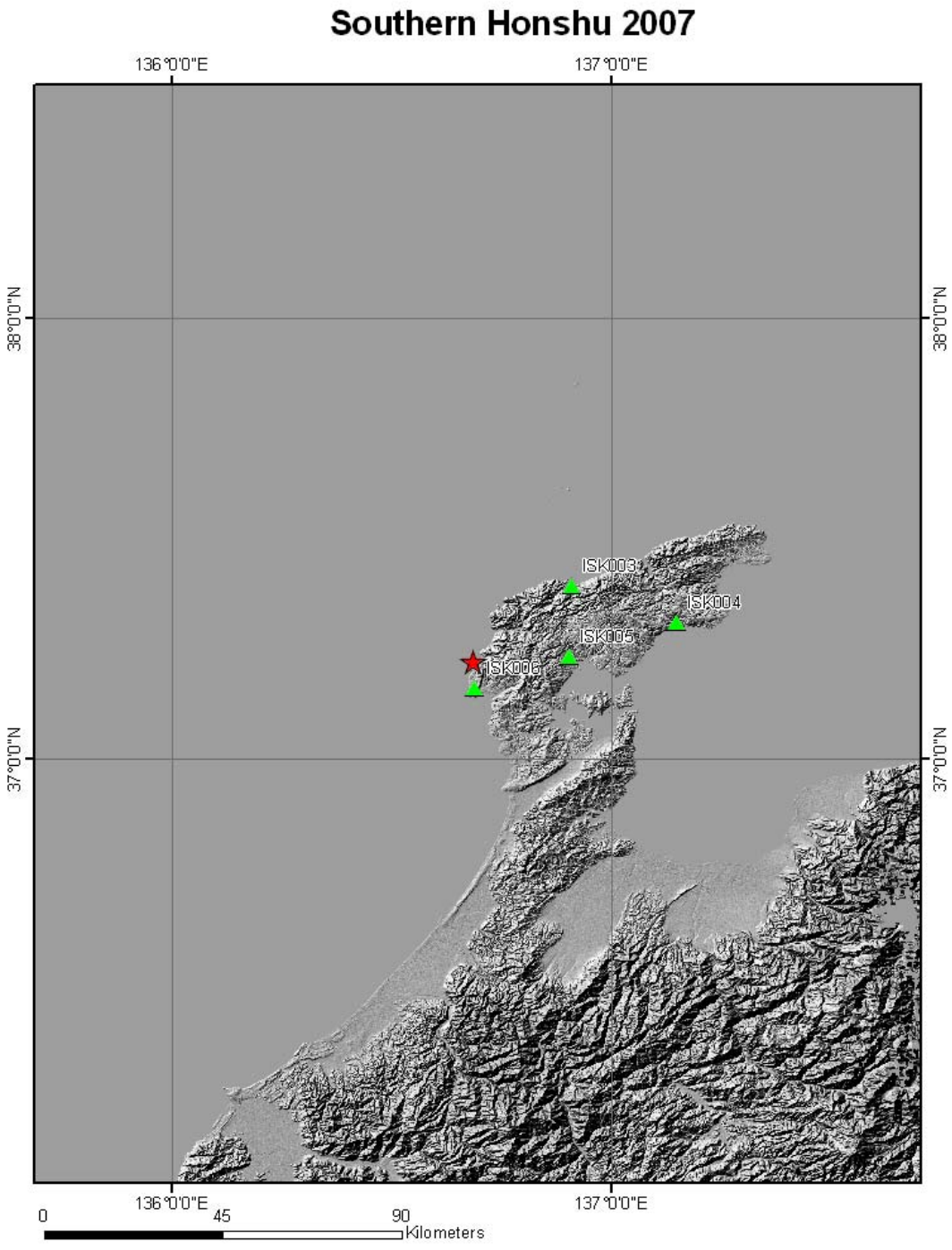

Figure A63. Southern Honshu, April 15, 2007, 03:19:00, Mjma 5.40

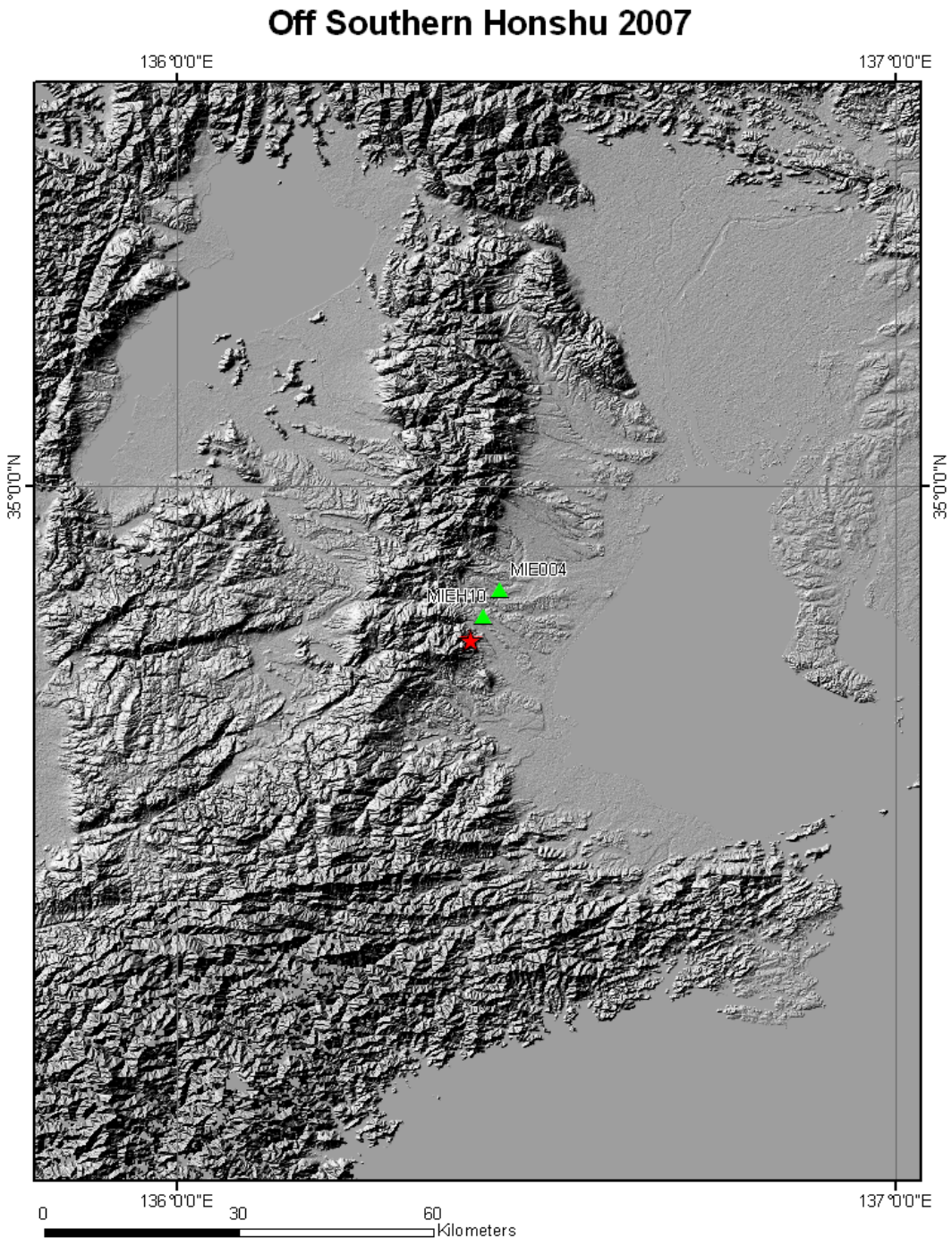

Figure A64. Off Southern Shikoku, April 26, 2007, 00:03:00, Mjma 5.30